A GEOCHEMICAL STUDY OF NEOPROTEROZOIC PALAEO-EVAPORITES AND THEIR POSSIBLE ROLE IN METALLOGENESIS IN THE DAMARA BELT OF NAMIBIA

By

Nevantheran Pillay

Dissertation submitted in fulfilment of the requirements for the degree of Master of Science (Geology) at the University of Cape Town, South Africa.

Department of Geological Sciences
(July 2000)

Abstract

Former evaporite horizons in metamorphic terrains have frequently been referred to as a source for highly saline fluids associated with base metal ore deposits in various parts of the world. Data on the nature of these former evaporites and their associated connate fluids, however, is frequently quite sparse, and the link between the ore deposits and the source evaporites is usually intuitive, at best.

In an attempt to characterise such evaporite-derived fluids and their source evaporites, a study of former evaporites in the Duruchaus Formation in the Southern Marginal Zone (SMZ) of the Damara Belt was carried out. The lithological units that make up the evaporite sequence within the Duruchaus Formation were mapped and sampled, along with discordant quartz-dolomite plugs intruding at various levels in the Duruchaus Formation stratigraphy, and in the overlying Hakos Group. A fluid inclusion study (microthermometry and crush-leach analyses) of the fluid inclusions hosted by these quartz-dolomite plugs showed that the fluids preserved as inclusions in these plugs are highly saline (>40wt% $NaCl_{eq}$) and are characterised by low Na/Br and Cl/Br ratios, indicating that the source fluids were most likely evaporite-derived. The presence of albitite and carbonate xenoliths, within the quartz-dolomite plugs, which are almost identical to the in situ units of the evaporite sequence of the Duruchaus Formation in terms of their trace and rare earth element distributions, suggests that the source of the fluids preserved within these plugs is from within the main evaporite sequence of the Duruchaus Formation.

The whole rock rare earth element distributions in the sampled units from this evaporite sequence are characterised by steep (chondrite-mormalised) light rare earth enrichment trends (seen mainly in the arenaceous units) and positive Ce anomalies (most pronounced in the carbonate). Both these features indicate a strong continental influence on these units, i.e., a continental depositional environment for the evaporite sequence.

An assessment of whether evaporite-derived fluids also occur in the Northern Zone (NZ) of the Damara Belt (and if these fluids played any role in metallogenesis there) was also attempted. Discordant quartz veins and quartz plugs associated with base metal occurrences were sampled in several test localities in the NZ. A fluid inclusion study similar to that carried out in the SMZ, revealed the presence of highly saline fluids (up to 26wt% $NaCl_{eq}$) in some of these test localities. An evaporitic origin for these fluids is suggested, based on the Na-Cl-Br chemistry of fluid inclusion leachates and calculated salinities. The source region for these fluids in the NZ is still contentious, though. The existence of buried (Nosib Group) evaporites in the NZ is supported by the presence of xenoliths characterised by a similar trace element and rare earth element distribution to that seen in comparable in situ units within the Duruchaus Formation evaporite sequence. An alternate source for the NZ fluids may be the Hüttenberg Formation evaporites present in the upper Tsumeb Subgroup.

The fluid inclusion leachates from the quartz samples associated with base metal mineralisation were typically of variable salinity with low Na/Br and Cl/Br ratios. The variation in salinity in these leachates is thought to reflect fluid mixing at the ore localities prior to ore deposition. This fluid signature may potentially be a useful pointer to the presence of base metal mineralisation in prospect areas.

Contents

List of Figures

List of Tables

List of Plates

1. Introduction

1.1 Background :

The Damara Belt of Namibia is host to a wide range of base metal ore deposits. Those of the Mississippi Valley-Type (MVT) are particularly sought after and MVT-style ore deposits occur at two stratigraphic levels within the Damara Supergroup of the Damara Belt. MVT mineralisation is thought to be associated with basinal or orogenic brines. It is commonly of the Pb-Zn type, hosted by carbonates, and is epigenetic in nature, with karsting playing an important role in creating the pathways for fluid flow (Leach and Sangster, 1993). This type of mineralisation is encountered in the Abenab Subgroup (Berg-Aukas Formation) of the Otavi Group within the Damara Supergroup. The mineralisation is hosted in a dolomitic breccia and the ore minerals are predominantly galena and sphalerite which are deposited as open space (karst) fillings (Misiewicz, 1988). A variation of the MVT style of mineralisation (also thought to be related to basinal or orogenic brines) is the more cupiferous Tsumeb-type deposits encountered higher up in the stratigraphy of the Damara Supergroup. These Tsumeb-type deposits are hosted in discordant, brecciated pipe-like features in the carbonates of the upper Tsumeb Subgroup and are characterised by Pb-Zn mineralisation with a significant amount of Cu mineralisation also present (Lombaard *et al.*, 1986). The two types of ore deposits described above are classified on the basis of ore association and stratigraphic level.

While there is generally agreement on the mode of ore deposition in both the Tsumeb-type and Berg-Aukas MVT ore deposits (hydrothermal-replacement, epigenetic and fracture-filling), the source of the fluids responsible for both these types of

mineralisation (and similar deposits in the region) is still a point of contention. The four likely candidates that stand out as probable sources for the mineralising fluids are: magmatic fluids, prograde metamorphic dehydration fluids, retrograde metamorphic fluids and evaporite-derived (connate) fluids. This study focuses on the role these evaporite-derived fluids might have played in mineralisation in the Damara Supergroup, as well as the geochemical nature of the probable source evaporites.

1.2 Previous Work :

1.2.1 Evaporite-derived fluids and metallogenesis

Evaporites have previously been quoted as probable sources for mineralising fluids in the Damara Belt (Miller, 1983a; Schmidt-Mumm and Behr, 1987; Chetty and Frimmel, 2000) due to the high salinity of the fluid inclusions found in association with Berg-Aukas-type and Tsumeb-type ore deposits in the Otavi Mountainland (Chetty and Frimmel, 2000), and minor mineralisation in the Southern Marginal Zone (Schmidt-Mumm and Behr, 1987). The Na-Cl-Br concentrations of leachates derived from fluid inclusions preserved within the gangue minerals associated with MVT mineralisation in the Berg-Aukas Formation and the Tsumeb-type ore deposits within the Tsumeb Subgroup, showed that the high salinity of these fluids was possibly derived from interaction with evaporites *en route* to the locus of deposition (Chetty and Frimmel, 2000).

A microthermometric study of fluid inclusions preserved within quartz-dolomite plugs in the lower Hakos Group in the Southern Marginal Zone (SMZ) of the Damara Belt by Schmidt-Mumm and Behr (1987), led the authors to the conclusion that a highly saline fluid derived by dehydration and leaching of the evaporitic units in the Duruchaus Formation may have been involved in the mineralising events there. This

study also revealed the existence of several phases of fluid activity (preserved as inclusions in the quartz-dolomite plugs) which were subdivided by the authors into the three main phases (on the basis of the data from aqueous fluid inclusions), i.e., a high salinity (up to 38 wt% $NaCl_{eq}$), CO_2-poor first phase with homogenisation temperatures (T_h) between 130-330°C; a high salinity (up to 32 wt% $NaCl_{eq}$), CO_2–rich second phase with T_h between 180 – 230°C; and a low salinity, CO_2-dominated third phase. Xenolithic rock fragments present within the quartz-dolomite plugs in the lower Hakos Group supported an origin for the fluids preserved as inclusions in these plugs, in the Duruchaus Formation of the SMZ (Schmidt-Mumm and Behr, 1987).

1.2.2 Evaporites in Metamorphic terrains

The units of the Damara Supergroup in Nambia have been subject to multiple phases of deformation and attendant metamorphism (Miller, 1983a). The deformation and metamorphic overprinting on the sedimentary units associated with the Damara Orogen has made it difficult to identify possible source evaporites for the Berg-Aukas-type and Tsumeb-type mineralisation which occurs within the Damara Supergroup. Suspected former evaporitic sequences in the Damara stratigraphy have been identified, however, in the Gariep Belt (the Chameis Complex) (Frimmel and Jiang, 2001) and in the Damara Belt, i.e., the Duruchaus Formation in the Nosib Group (Behr *et al.*, 1983a) and the Hüttenberg Formation in the Otavi Group (Chetty and Frimmel, 2000).

The Duruchaus Formation in the Nosib Group has been the subject of several previous studies, one of the most comprehensive of which is reported in Behr *et al.* (1983a). Mineralogical and textural analyses on the existing mineral suites of this formation, along with fluid inclusions studies, suggests the existence of a preserved

palaeo-evaporitic environment; more specifically, a sequence of continental playa-lake deposits capped by a marine sabkha deposit (Behr *et al.*, 1983a). The presence of scapolite-bearing pelitic units within the Duruchaus Formation appears to support the above interpretation of an evaporitic environment of deposition for these units, scapolite commonly being associated with metamorphosed evaporites. However, it should be noted that the presence of scapolite within a sequence does not necessarily indicate the activity of an evaporite-derived fluid, as was demonstrated by Dombrowski *et al.* (1996). These authors studied scapolite-bearing schists within the Kuiseb Formation in the Damara Belt and found evidence for the scapolite having formed from locally derived fluids within the Kuiseb Formation and not from an outside evaporitic source.

Data on the geochemical nature of the Hüttenberg Formation evaporites is sparse. However, Chetty and Frimmel (2000) found that the Na-Cl-Br concentrations of fluid inclusion leachates from minerals within this formation suggests an evaporitic origin for the units preserved there. Former evaporites have also been identified in an oceanic setting in the Mamora Terrane (Gariep Belt) (Frimmel and Jiang, *in press*). The authors conducted a study on an allochthonous sequence of dolomitic and pelitic units which were intercalated with tourmalinite and albitite layers in the Mamora Terrane. They found that the facies relationships as well as the whole rock chemistry of the units pointed to a marine, evaporitive origin for these units. In particular, the B isotopic composition (high $\delta^{11}B$ values) of tourmaline grains within the tourmalinite layers indicated a marine origin for the tourmalinite layers and the units associated with them (Frimmel and Jiang, *in press*).

The mineral tourmaline has been found to be useful as a petrogenetic indicator (Henry and Guidotti, 1985). It provides a record of unusual chemical and palaeogeographical conditions in clastic sedimentary basins, and it is also commonly associated with evaporites and stratabound mineral deposits, usually occurring as tourmalinite layers (Slack *et al.*, 1984; Henry and Guidotti, 1985; Slack *et al.*, 1993). Henry and Guidotti (1985) found that some generalisations can be made in the relationship between tourmaline composition and host rock type, using the aluminium, magnesium, iron and calcium contents of the tourmaline grains. Using this method, Schmidt-Mumm (1989) found that most of tourmaline grains present in the Duruchaus Formation were probably derived from Ca-poor metapelites and metapsammites. An origin from borates previously present within the evaporite sequence in the Duruchaus Formation was thus proposed by Schmidt-Mumm (1989).

Previous studies which document the involvement of evaporites and evaporite-derived fluids in generating base metal ore deposits elsewhere include the copper-gold deposits of the Copper-Canyon area in Cloncurry (Stewart, 1994) and the ore deposits associated with the Olary Block (Willyama Supergroup) in South Australia (Cook and Ashley, 1992). In the Copper-Canyon study, detailed mineralogical and textural analyses of the metasedimentary rocks, along with a study on the sulphur isotopic character of the sulphide ores suggests that the preserved evaporites in the sequence played an important role in providing the transporting brines and the source of sulphur for the ore deposits (Stewart, 1994).

Similar work on the Olary Block, west of the Broken Hill deposit in South Australia, has led to the identification of former evaporitic rocks in the sequence (Cook and Ashley, 1992). These studies focussed on whole rock geochemistry and fluid

inclusion work, and many features consistent with evaporitic units were found, including high salinities in fluid inclusions and daughter crystals of halite and anhydrite present in fluid inclusions. The presence of these evaporites in this region presents a possible source for mineralising fluids in the Olary Block and suggests the possible existence of evaporitic equivalents in the metamorphosed Broken Hill deposit adjacent to it (Cook and Ashley, 1992). Due to the highly metamorphosed nature of the Broken Hill sediments, though, any obvious evidence for the presence of palaeo-evaporites in the sequence (if they did exist) has been obliterated.

1.3 Aims of the Study:

While the geochemical data outlined in the papers in the previous section are consistent with the existence of palaeo-evaporites in each stratigraphy, the link between the ore deposits and the evaporitic sequences in these regions seems to be intuitive. The application of more clear cut criteria linking the source of the mineralising fluids and the ore deposits needs to be examined, as well as the establishment of a geochemical signature (in terms of fluid chemistry and whole rock chemistry) diagnostic of former evaporitic sequences in metamorphic terrains (like the Olary Block and Broken Hill terrain in Australia, and the Damara Belt of Namibia).

Using the Damara Belt as a type area, the following aims were used in this study to attempt to reach this end.

- to determine the geochemical character of suspected former evaporites and their associated connate fluids in the metamorphosed Damara Supergroup, with the aim identifying a geochemical signature diagnostic of palaeo-evaporitic sediments and their associated connate fluids in metamorphic terrains;

- to determine if the depositional environments of the former evaporites can be deduced on the basis of their fluid and whole rock geochemistry (marine vs continental evaporites);

- to determine if the connate fluids derived from these evaporites could be linked to metallogenesis in the Damara Supergroup by comparing the geochemical character of these evaporitic-derived fluids with the geochemistry of fluids seen to be associated with base metal mineralisation within the Damara Supergroup.

This research was carried out in three parts: (i) by establishing a geochemical signature (in terms of whole rock and fluid chemistry) for palaeo-evaporitic units in the Damara Belt using a suitable type locality/formation where the presence of former evaporites and their associated connate fluids has been established; (ii) testing this signature in unknown areas where the presence of evaporitic units and their associated fluids has been suspected but not proven; and (iii) determining the possible role that these fluids played in metallogenesis in the Damara Belt.

1.3.1 Selecting the type locality/formation

The type locality/formation selected for the first part of the study was the Duruchaus Formation within the Nosib Group. This formation is well exposed in the Southern Marginal Zone of the Damara Belt and was chosen for the following reasons. Sedimentological and mineralogical evidence quoted in (Behr *et al.*, 1983a) provides convincing proof that a continental palaeo-evaporitic environment did exist in the Southern Marginal Zone during Nosib times. The presence of distinct, distinguishable sedimentary cycles deposited in different facies domains, i.e., sediments representing a central playa lake associated with sediments of the surrounding mud flats, as well as the presence of silicate pseudomorphs of sodium carbonate and sodium sulphate precursors (shortite, natron, trona and thenardite) within the sequence, seems to suggest that a continental playa lake deposit is preserved in the Duruchaus Formation within the Nosib Group (Behr *et al.*, 1983a). The Duruchaus Formation therefore represented a good starting point for this study on Neo-proterozoic palaeo-evaporites and their associated connate fluids in metamorphic terrains.

In addition to the above, the following should also be noted. The criteria for identifying and classifying evaporites (distinguishing marine and non-marine evaporites) are three-fold, i.e., sedimentological, mineralogical and geochemical (Hardie, 1984). Past studies on the Duruchaus Formation, Behr *et al.* (1983a) being the most prominent among them, have focussed on the first two criteria (sedimentological and mineralogical). Deformation and attendant metamorphism of palaeo-evaporites in such terrains as the Damara Belt makes these criteria the more subjective of the three. This part of the study aimed to add to the above studies from a geochemical perspective, by establishing geochemical criteria for identifying and

classifying suspected palaeo-evaporites in metamorphic terrains on the basis of their whole rock compositions and the compositions of their associated fluids.

1.3.2 Selecting the test localities

The criteria for selecting test localities were two-fold. Firstly, the areas selected needed to be localities where the activity of evaporitic fluids has been suspected but not evaluated. Secondly, the areas selected needed to be associated with epigenetic base metal mineralisation. The field areas that were found to be the best in combining these two criteria were areas which encompassed the upper Swakop Group and upper Otavi Group stratigraphy in the Northern Zone of the Damara Belt, and it was here where test localities were selected.

2. Regional Geological Setting

2.1 Introduction

The geology of Namibia is to a large extent dominated by rocks related to the Damaran Orogen. Units associated with the orogen form part of the system of Upper Proterozoic Pan-African belts of Africa and the Brasiliano belts of South America, which are related to the splitting up of the southern African and South American continents approximately 750 Ma ago (Tankard *et al.*, 1982; Miller, 1983a; Frimmel *et al.*, 1996b; Hoffman *et al.*, 1996). Exposed remnants showing evidence of this and subsequent geological and tectonic events, are preserved within three distinct belts. These comprise a southern coastal arm (the Gariep Belt) which links up with the Saldania Belt along the southern coast of South Africa; a northern coastal arm (the Kaoko Belt) which links up with the West Congolian Belt in Angola; and a north-east trending intra-continental arm (the Damara Belt) which disappears beneath Kalahari cover in the east, but is thought to link up with the Katangan Belt of the Zambian Copper Belt (Tankard *et al.*, 1982; Miller, 1983a) (Figure 2.1).

The geology of the Damara Belt has been the subject of several detailed studies (Miller, 1983a; Hoffmann, 1989). This has led to the unravelling of a complex series of geological events which incorporate sedimentation, deformation, metamorphism and plutonism. Within the Damara Belt one therefore finds a wide variety of preserved sedimentary facies marking the progression from initial rifting and spreading, to subsequent ocean closure and eventual continental collision. This sequence of events has resulted in the complex association of meta-sedimentary facies exposed today.

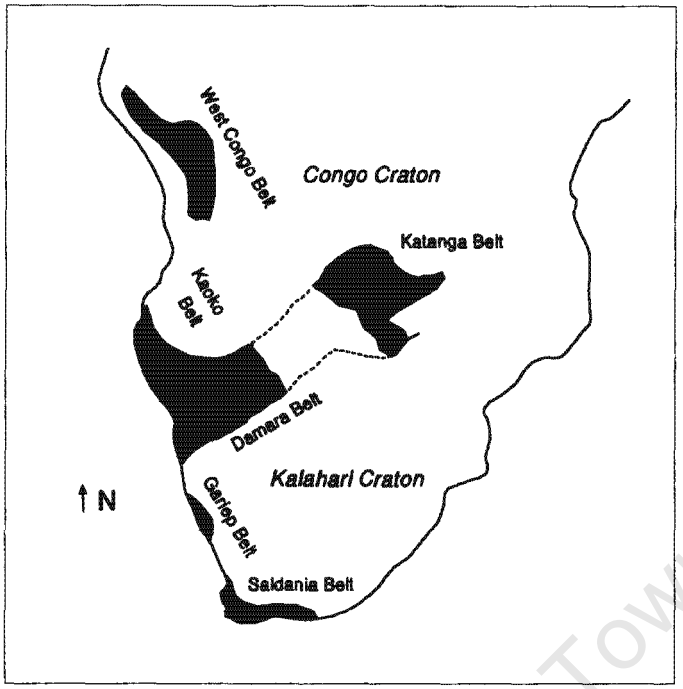

Figure 2.1 Pan-African tectonic belts in the southern part of Africa (after Miller, 1983a).

2.2 Tectono-Stratigraphy

The Damara Belt has been divided into several zones on the basis of stratigraphy, structure, grade of metamorphism, plutonic rocks, geochronology and aeromagnetic characteristics (Miller, 1983a). From north to south they are, the Northern Platform (NP), Northern Zone (NZ), Central Zone (CZ), Okahandja Lineament Zone (OLZ), Southern Zone (SZ), Southern Marginal Zone (SMZ), and Southern Foreland (SF), which passes into the Southern Platform (SP) (Miller, 1983a) (Figure 2.2). The boundaries between these zones are of varied description. Most form linear features and they can be structural boundaries (NZ-CZ, SMZ-SF), lineaments (CZ-OLZ, NZ-NP?), or stratigraphic boundaries (SZ-SMZ). The OLZ-SZ boundary represents a poorly defined tectonic line dividing zones of low pressure metamorphism (OLZ) and high pressure metmorphism (SZ). Together the OLZ and SZ are referred to as the

Khomas Trough (Martin and Porada, 1977). Hoffman (1989) proposed a revision of some of these tectonostratigraphic terms and the revised terms are presented and defined in Table 2.1.

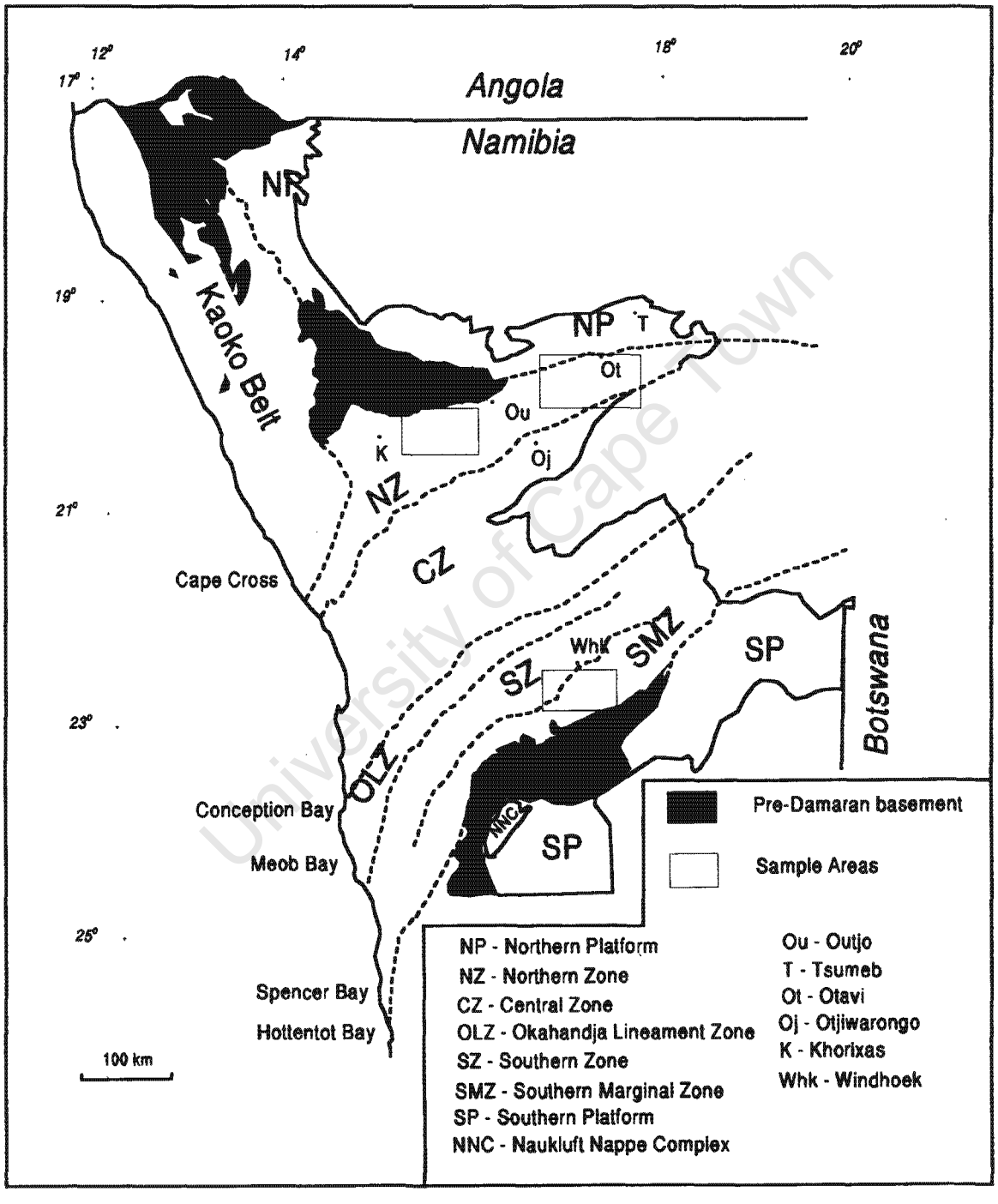

Figure 2.2 Tectonostratigraphic zones of the Damara Belt (after Miller 1983a).

Table 2.1 Stratigraphic table for units of the Damara Supergroup in the northern, central and southern parts of the Damara Belt (from Hoffman, 1989). The Swakop Terrane corresponds to the Central Zone of Miller (1983a); Hakos Terrane = Southern Marginal Zone; Khomas Terrane = Okahandja Lineament Zone. The Chuos Formation of the Otavi Mountains has been renamed the Ghaub Formation (Hoffman and Prave, 1996). The Y-axis represents decreasing age and the shaded areas are missing sequences.

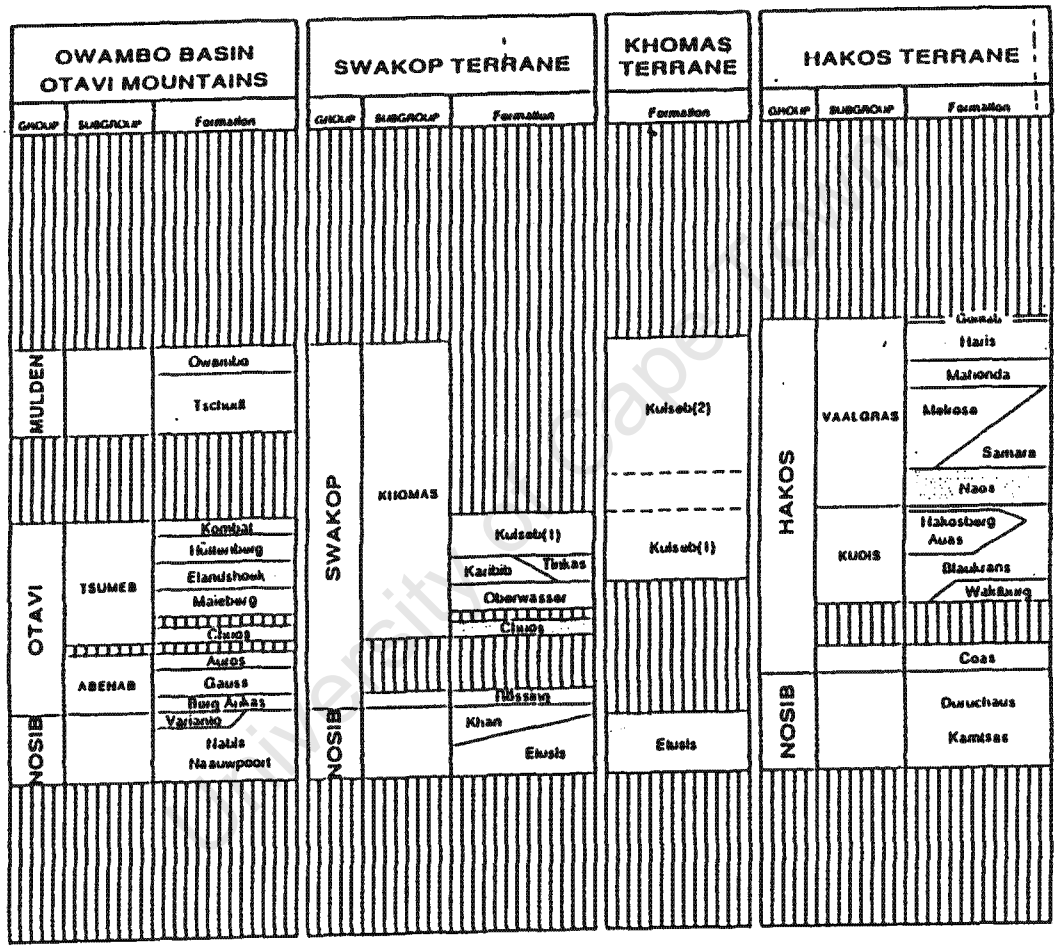

2.3 Geological Evolution of the Damara Belt

The stratigraphic subdivisions of the Damara Supergroup used in the Damara Belt are presented in Table 2.1. The sequence of deposition of these units and the interpreted environments of deposition are outlined in the following geological history of the Damara Belt.

The Damara Supergroup commences with the basal Nosib Group which is comprised of units that are thought to represent basin fill sequences deposited during a period of rifting in the Damara Belt (Miller, 1983a). Rifting is thought to have been initiated approximately 750 Ma years ago (Frimmel *et al.*, 1996b; Hoffman *et al.*, 1996), resulting in the formation of three rift grabens into which the Nosib Group sediments were deposited. These consisted of fluvial and fine-grained shallow water basinal clastic sediments which interfingered with lacustrine (playa lake) carbonates and local evaporites beds (Behr *et al.*, 1983a; Hoffmann, 1987). Significant bimodal volcanism associated with basin edge faults occurred towards the end of Nosib times in the northern rift (between 756 Ma and 746 Ma) (Hoffman *et al.*, 1996), with only minor volcanic activity in the two southern rift grabens (Miller, 1983a).

Widespread subsidence across the Damara Belt followed this period of volcanic activity and led to the development of the Khomas Sea (Miller, 1983a; Hoffmann, 1989). Deposition of the shelf carbonates and massive turbidite sequences of the Hakos and Swakop Groups took place in the southern and central parts of the Damara Belt at this time, and the massive platform carbonates of the Otavi Group were deposited in the north. The turbiditic units and carbonates were no longer confined to rift grabens and were overlapping, extending beyond the shoulders of the rift grabens (Hoffmann, 1989; Miller, 1983a).

This period of massive carbonate and turbidite deposition was interrupted by a period of glaciation at the end of the deposition of the Abenab Subgroup (Otavi Group) and Ugab Subgroup (Swakop Group). The Chuos Formation which overlies the Ugab Subgroup in the central parts of the Damara Belt, and the Ghaub Formation which overlies the Abenab Subgroup in the north, are characterised by units with tillite-like features (Miller, 1983a; Hoffmann and Prave, 1996). These units are thought to be glaciogenic diamictites (Prave and Hoffmann, 1995, Kennedy *et al.*, 1998) that correspond to the Varangian glacial episode (~600 Ma). An equivalent record of this glaciation is not preserved in the Hakos Group possibly due to a discordance seen at the base of the Kudis Subgroup (Hoffmann, 1989). The thickness and continuity of units in the upper parts of the Swakop and Otavi Groups which lie above the Chuos and Ghaub Formations reflects a stable depositional environment for the remainder of Swakop and Otavi times.

The greatest amount of subsidence recorded in the Damara Belt is by far in the Khomas Trough where up to 13km of flysch sediments accumulated (Kuiseb schists of the Swakop Group). Towards the top of this sequence, reflecting its deepest part, a succession of passive margin, deep water fans are preserved (Hoffmann, 1983). Within this sequence one also finds a 350km long belt of metabasic rocks with MORB affinities, called the Matchless Amphibolite Belt. These metabasic units are thought to represent the early stages of continental separation when spreading in the Damara Belt reached its maximum.

The change from spreading to convergence in the Damara Belt commenced with the subduction of the sea floor units of the Khomas Sea below the Congo Craton in the northwest (Miller, 1983a). This subduction and the eventual collision of the Congo

and Kalahari Cratons resulted in widepsread metamorphism, deformation and the large-scale emplacement of granitic bodies (particularly in the CZ), in the intracratonic arm of the Damara Orogen. Miller (1983a) used these syn-tectonic granitic bodies in the CZ to approximate the age of closure of the Khomas Sea at 650 Ma.

The final closure of the Khomas Sea in the Damara Belt was accompanied and followed by uplift and denudation of high-lying areas. The Otavi and Swakop Groups are overlain by continentally derived molasse-type deposits, i.e., the Mulden Group in the north and the Nama Group sedimentary rocks in the south. Deformation of the sequence of units which make up the Mulden Group suggests that the deposition of these units was syn-tectonic. The deposition of the Nama Group metasedimentary units in the southern part of the Damara Belt is also interpreted to have been syn-tectonic due to deformation of these units along the northern edge of the Southern Platform. The Nama Group units further south, though, were less affected by the deformation events described above and are relatively flat-lying (Miller, 1983a).

Three main periods of deformation associated with the orogenesis described above can be recognised in the Damara Belt. The first two, D_1 and D_2, are associated with continental convergence and continent-continent collision, and produced south-east vergent structures related to the north-west subduction described above (Miller, 1983a). The south-east vergent macro- and micro-structures recording these two events are present throughout the orogen, but they may be temporally distinct in different parts of the Damara Belt, i.e., D_1 and D_2 in the northern part of the Damara Belt (NZ, NP, CZ) are generally older than D_1 and D_2 in the SZ and SMZ (although some phases of deformation in the CZ and SZ may be contemporaneous) (Miller,

1983a). A third phase of deformation, D_3, also related to continental collision can be recognised in the CZ. D_3 is associated with isoclinal folding of the structures produced by D_1 and D_2 (Miller, 1983a).

The deformation in the SZ and SMZ culminated in the thrusting of the basal Hakos Group rocks over the relatively undeformed Nosib Group rocks in the SMZ, and, in the final stages of thrusting in the Naukluft Nappe Complex (Behr *et al.*, 1983b). Late stage movement of these thrusts is thought to have been facilitated by the intrusion of a highly saline, fluid dolomitic mush derived from the evaporitic Duruchaus Formation in the SMZ along thrust planes (Behr *et al.*, 1983a, b).

2.4 Geology of the SMZ (Hakos Terrane)

2.4.1 Stratigraphy

The Nosib Group metasedimentary units form the basal units in the SMZ. The dominant rock type within this group is a medium-grained, moderately sorted feldspathic quartzite. Together with basal and intraformational conglomerate, this quartzite makes up the Kamtsas Formation at the base of the Nosib Group. Various fluvial sedimentary features are preserved in these units including cross-bedding, fining upward sequences and wedge-like channel deposits, suggesting a fluvial depositional setting (Hälbich, 1970).

The upper part of the Nosib Group in the SMZ is characterised by a calcareous, pelitic facies, the Duruchaus Formation. The lower part of this formation is dominated by pelitic units with subordinate sandstone and conglomerate (Hoffmann, 1987). The upper part of the sequence is characterised by what is thought to be a metamorphosed playa and sabkha evaporite sequence (Hoffmann, 1987; Behr *et al.*, 1983a). This

upper sequence is also dominated by pelitic units but the subordinate units here are albitite layers, sandy dolomite layers with albite pseudomorphs, and concordant and discordant brecciated dolomitic units.

The Nosib Group is overlain by the Hakos Group in the SMZ (Table 2.1). Hoffmann (1989) recognised a basal dolomitic sequence, with minor marbles, which follows conformably on the Nosib Group units and termed this sequence the Coas Formation. The Kudis Subgroup overlies this formation and its base is marked by a regional discordance. The Kudis Subgroup commences with the Waldburg Formation (Corona Formation of SACS, 1980 and Miller 1983a) and consists of graphitic schist with intercalated quartz-mica schist, quartzite, conglomerate and dark grey dolomitic marble. Towards the top of this formation, the sequence interfingers with the overlying Blaukrans Formation (Hoffmann, 1983). The Blaukrans Formation consists predominantly of schistose units, except in the western part of the SMZ, where it is interbedded with thick quartzite and a turbiditic quartz-graphite schist of the Hakosberg (Hakos Formation of SACS, 1980) and Auas Formations. This sequence is interpreted to reflect a deeper water environment (Miller, 1983a; Hoffmann, 1989).

The overlying Vaalgras Subgroup in the SMZ consists of the basal Naos Formation (formerly the Chuos Formation of SACS, 1980), and the overlying Melrose, Samara, Mahonda, Haris and Gomab (River) Formations. The Naos Formation is characterised by tillite-like features and has been interpreted to represent a glaciogenic diamictite (Hoffmann, 1989). It is overlain by the Melrose Formation which is dominated by green chlorite-garnet schist and a greyish mica schist, and the Samara Formation (present only in the extreme south-western part of the SMZ) which consists predominantly of dolomitic units (Hoffmann, 1989). These formations are overlain by

the quartzite and schist of the Mahonda and Haris Formations, and the amphibolite of the Gomab River Formation. The quartzite of the Mahonda and Haris Formations shows several features which are consistent with deep water fan deposits and indicate a distal, deep water depositional enviroment at this time (Hoffmann, 1983). The Gomab River Formation forms the top of this sequence in the SMZ.

2.4.2 Structure

Four deformation events are distinguished in the SMZ. The first two, D_1 and D_2, produced overturned to recumbant F_1 anf F_2 folds accompanied by intense, south-eastward thrusting (Hoffmann, 1983; Miller, 1983a). The thrusting involved the overriding of highly deformed, deep water facies in the north-western SMZ over the more shallow water facies (less intensely deformed) preserved in the south-east (Hoffmann, 1983).

The D_3 and D_4 events in the SMZ produced open, north-east trending and east-west trending basement domes. These later periods of deformation are also thought to have resulted in the steepening of the thrust planes associated with the D_1 and D_2 events. The SMZ is broadly divided into a northern subzone marked by intense deformation containing thrust sheets of Damaran and pre-Damaran rocks, and a less deformed southern subzone containing thrust sheets of mainly pre-Damaran rocks (Kasch 1983c; Hoffmann, 1983).

2.4.3 Metamorphism

The metamorphic history of the southern Damara Belt has been a source of debate between various authors. Kasch (1983a) provides evidence for polymetamorphism in the southern part of the Damara Belt. Microtextural analysis of a suite of syn-tectonic

and post-tectonic metamorphic minerals from the SMZ and SZ, as well as garnet-biotite geothermometry and garnet-plagioclase geobarometry done on the same mineral suite, suggested the existence of two metamorphic events in these areas (Kasch, 1983a). Geothermometry revealed the existence of two thermal peaks, one reaching 590°C during D_2 (M_1), and the other reaching 570°C post-tectonically (M_2) (Kasch, 1983a). Corresponding pressures were calculated at 9-10 kbar during M_1 and 6-8 kbar during M_2 for the sample areas in the SZ and SMZ .

Hoffer and Hoernes (1979) and Hoffer (1983) suggested that only one prograde metamorphic event accompanied the deformation in the southern part the Damara Belt. Hoffer (1983) examined the mineralogical changes in a quartz muscovite-bearing metapelite which extends over large distances south of Windhoek in the SMZ. He found that the area is defined by a flat temperature gradient and that the isograds are spaced over large distances. The reactions in the pelites which define these isograds were found to form a regular succession of zones (and isograds) defined by univariant and bivariant AKFM-reactions. The evidence presented in these papers therefore indicates that the area under investigation in the SMZ was affected by one metamorphic heating event. Oxygen-isotope studies done on mineral pairs from the sample area indicate a temperature interval of between 480°C and 580°C (Hoernes and Hoffer, 1979). Pressure estimates for the area using a garnet-plagioclase barometer were in the range of 6-9 kbar (Hoffer, 1983).

2.5 Geology of the NZ (Swakop Terrane and Otavi Mountainland)

2.5.1 Stratigraphy

The Nosib Group in the Northern Zone commences with the basal Nabis Formation which consists predominantly of feldspathic quartzite with subordinate polymictic conglomerate (Hedberg, 1979; Miller, 1983a). Fluvial sedimentary features are well preserved within this sequence and suggest a fluvial depositional setting for these units.

Volcanic units form a large part of the sequence in the Northern Zone Nosib Group and the basal Nabis Formation is overlain by, and intercalated with, two volcanic formations. The Naauwpoort Formation in the western NZ is made up predominantly of alkaline to peralkaline ignimbrite with minor felsic volcanic units (Miller, 1980). The Askevold Formation in the eastern NZ is made up of green tuffaceous units with minor green epidotised lavas (Hedberg, 1979). The Nosib Group volcanic rocks are present mainly in this northern graben in the NZ and are thought to be related to basin edge faulting (Miller, 1980; Hedberg, 1979).

Evaporitic units similar to those seen in the Duruchaus Formation in the Nosib Group of the SMZ have not yet been encountered in the Nosib Group of the NZ. However, discordant, brecciated dolomitic units with associated albititic and dolomitic xenoliths bearing a striking resemblance to the units of the Duruchaus Formation have been encountered in the NZ of the Damara Belt (Weber *et al.*, 1983). The presence of these xenoliths in the NZ suggests the presence of buried evaporitic units similar to those seen in the SMZ, in the northern graben as well.

The Nosib Group is overlain by the Ugab Subgroup (Swakop Group) throughout most of the NZ, except in the extreme northeastern part of the NZ where it is overlain by the Abenab Subgroup of the Otavi Group. The Ugab Subgroup in the CZ consists essentially of dolomite, cross-bedded quartzite and quartz-biotite schist of the Rössing Formation. In the NZ, the Ugab Subgroup consists of the siliceous and calcareous turbiditic units of the Okotjize and Okonguarri Formations, respectively (Porada and Wittig, 1983). The Okotjize Formation is thin in the west, and thickens eastward as it becomes intercalated with the Okonguarri Formation.

The Ugab Subgroup is overlain by the Khomas Subgroup which commences with the diamictite of the Chuos Formation. This poorly sorted tillite-like unit has been speculated to have originated by various means, i.e., a glaciogenic origin (Miller, 1980; Kröner and Rankama, 1972), deposition by sedimentary mass flows (Schermerhorn, 1975), or a combination of the two (Hoffman, 1983). Recent chemostratigraphic evidence, however, seems to indicate that the diamictite is of a glaciogenic origin (Kennedy *et al.*, 1998).

The Chuos Formation is overlain by the dolomite and limestone of the Karibib Formation, which, in turn, is overlain by the metapelite and metagreywacke of the Kuiseb Formation. The latter are thought to represent turbiditic sequences deposited in a deep water marine environment (Hoffmann, 1983).

The Abenab Subgroup which overlies the Nosib Group in the northeastern NZ commences with the basal Varianto Formation. This formation is made up of a sequence of poorly sorted units containing angular, matrix-supported clasts. An origin as a sedimentary mass flow for these units has been proposed by Hedberg (1979).

However, the presence of isolated dropstones within these units and the regional correlation of the Varianto Formation with the Chuos Formation of the Eastern Kaokoveld, seems to indicate that a glaciogenic origin for these units is more likely (Hoffmann and Prave, 1996; Botha, 1960 – *in* Martin 1965).

The Varianto Formation is overlain by the Berg-Aukas, Gauss and Auros Formations. The intercalated carbonate and clastic sequence of the Berg-Aukas Formation is thought to represent a transitional succession between the Nosib and Otavi Groups. The overlying Gauss and Auros Formations consist essentially of carbonate (limestone and dolomite) layers with subordinate shales and associated marker stromatolites. These units are indicative of a relatively stable, shallow marine, platform environment.

The Tsumeb Subgroup overlies the Abenab Subgroup and it commences with the basal Ghaub Formation (previously the Chuos Formation; Hoffman and Prave, 1996). The environment of deposition of this diamictite has been similarly ambiguous like the Chuos Formation and Varianto Formation, with both a glaciogenic origin and sedimentary mass flow origin being proposed (Schermerhorn, 1975; Kröner and Rankama, 1972). More recently, Hoffmann and Prave (1996) presented stratigraphic evidence (the correlation of this diamictite with a glaciogenic diamictite horizon in the Eastern Kaokoveld) and morphological evidence (the presence of well preserved dropstones, and bedded dolostones suggesting glaciomarine sedimentation) in support of a glaciogenic origin for these diamictites. The authors have also proposed a revision of the regional correlation of the Chuos Formation advocated by SACS (1980). The relationship between the Ghaub Formation and Chuos Formation of the Swakop Terrane, however, remains unclear.

The Maieberg and Elandshoek Formations which overlie the Ghaub Formation consist essentially of (varied) dolomitic units. The Hüttenberg Formation is also dominated by dolomitic layers (containing silicified stromatolites), with subordinate limestone, chert and shale layers. The thickness of the units within these three formations as well as the continuity of these units over large areas suggests the existence of a stable, shallow marine environment over a large area, throughout the period of deposition (Miller, 1983a). The uppermost Kombat Formation consists essentially of shale and dolomitic lenses and represents a possible deeper water facies equivalent of the Hüttenberg Formation (Hoffmann, 1989).

The Otavi Group is overlain by the continentally derived clastics of the Mulden Group. The basal Tschudi Formation consists of feldspathic sandstone and arkose with minor greywacke. A fining upward sequence is seen as one crosses into the overlying Owambo Formation which consists of siltstone and sandstone units with dolomite layers, shales and minor limestone appearing towards the top of the sequence (Miller, 1983a). Shallow marine conditions are therefore indicated towards the end of Mulden times. The Mulden Group forms the uppermost sequence of units in the NZ.

2.5.2 Structure

D_1 and D_2 are preserved in the northern zone as east-west trending, northward vergent folds. D_1 produced open east-west trending, upright to northward vergent folds which pre-date the deposition of the Mulden Group (Miller, 1980). D_2 was more intense resulting in tighter, northward vergent folds of similar orientation to D_1. The northward thrusting of Swakop Group rocks over the younger rocks in the north is also thought to be associated with this deformation event (Miller, 1983a). The

overlapping of the F_1/F_2 fold structures produced several dome-like interference folds in the NZ (Weber *et al.*, 1983; Miller, 1983a).

Various V-shaped deformation structures like the Mitten fold, Harmonie structure and Omburu East Structure, which occur between Khorixas and Outjo (Figure 2.2), provide evidence for an earlier phase of east-west compression (pre-dating D_1) in the NZ (Weber *et al.*, 1983). This phase of compression is overprinted by the D_1 and D_2 events and results in complicated intererence folds in these areas. The final phase of deformation in the NZ is marked by northeast-southwest trending (post-metamorphic) fracture and crenulation cleavages, and kink folds (Miller, 1980; Weber *et al.*, 1983).

2.5.3 Metamorphism

Metamorphism in the NZ appears to be mainly of low to very low grade (Miller, 1980). Metamorphic temperatures tend to decrease from west to east (Miller, 1980, Ahrendt *et al.*, 1983). Cordierite present in units in the extreme western part of the NZ suggests the influence of slighty higher metamorphic temperatures in this part of the NZ (Gunter, 1970). This corresponds to a high temperature region seen in the western CZ as well (Miller, 1983a). Arendt *et al.* (1983) on examination of a cross-section of units from Kamanjab to Sesfontein in the northern Damara Belt, also found evidence to support this shift from a low metamorphic grade in the east to a higher grade of metamorphism in the west, reaching the sillimanite isograde near the coast.

Chlorite-Biotite-Muscovite-Quartz assemblages in the eastern NZ define an isograde following a thrust contact between the Swakop and Mulden Groups in the NZ (Hoffer, 1977). This assemblage represents an estimated pressure of metamorphism of 2.5 kbar and peak metamorphic temperature of 430-450°C, and is thought to be syn-D_2 in age.

Slightly to the north of this area, the biotite-in isograd is thought to occur within pelitic rocks just south of the Otavi Mountainland (Frimmel *et al.*, 1996a). This corresponds to an estimated peak metamorphic temperature of 300°C to 400°C for this area.

Other than the metamorphic features listed above, thermal aureoles associated with post-tectonic granitoids are also present in the NZ. These aureoles can be up to 12km wide and can locally complicate the regional metamorphic overprint (Miller, 1983a).

(3)The Type Locality

3.1. Sample Selection & Analyses - The Type Locality

3.1.1 Introduction

The Duruchaus Formation stratigraphy is best exposed in the Gurumanus and Geelkop Domes, south of Windhoek, in the SMZ (Figure 2.2). A thick, relatively undisrupted section through the Duruchaus Formation stratigraphy is preserved within a tectonic half-window in this area.

3.1.2 Sample Selection

A complete section through the main evaporite sequence of the Duruchaus Formation, adjacent to the Gurumanus and Geelkop Domes, was initially mapped and sampled (Figure 3.1). Selected samples from lower down in the Duruchaus Formation stratigraphy were also collected at suitable intervals to gain a relatively complete picture of the upper Nosib Group stratigraphy in this part of the Damara Belt (Figure 3.2).

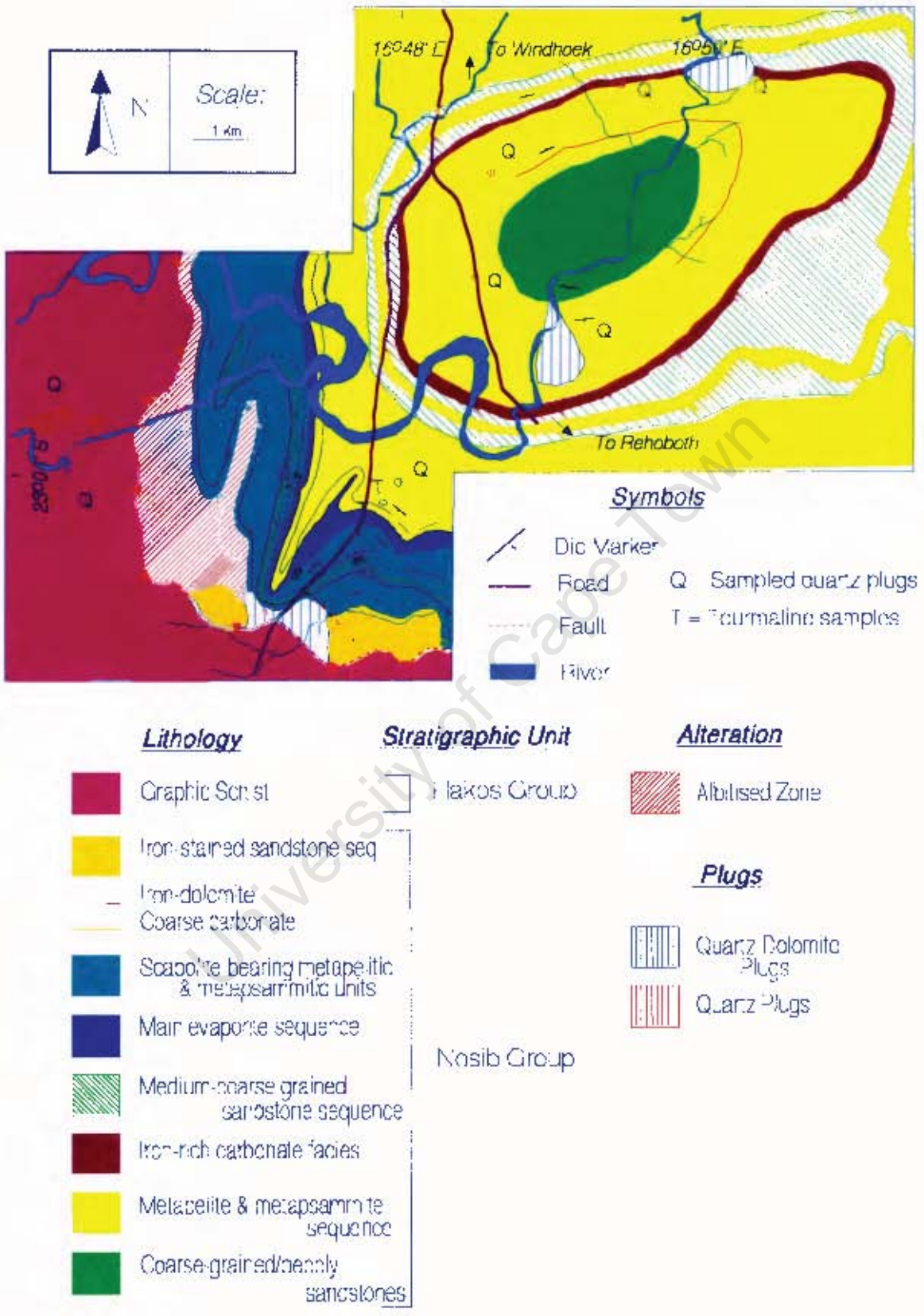

Figure 3.1 Lithological map of the upper part of the Duruchaus Formation showing the main sequences and marker units found in this area. For a complete breakdown of the units found in the main evaporite sequence refer Figure 3.2.

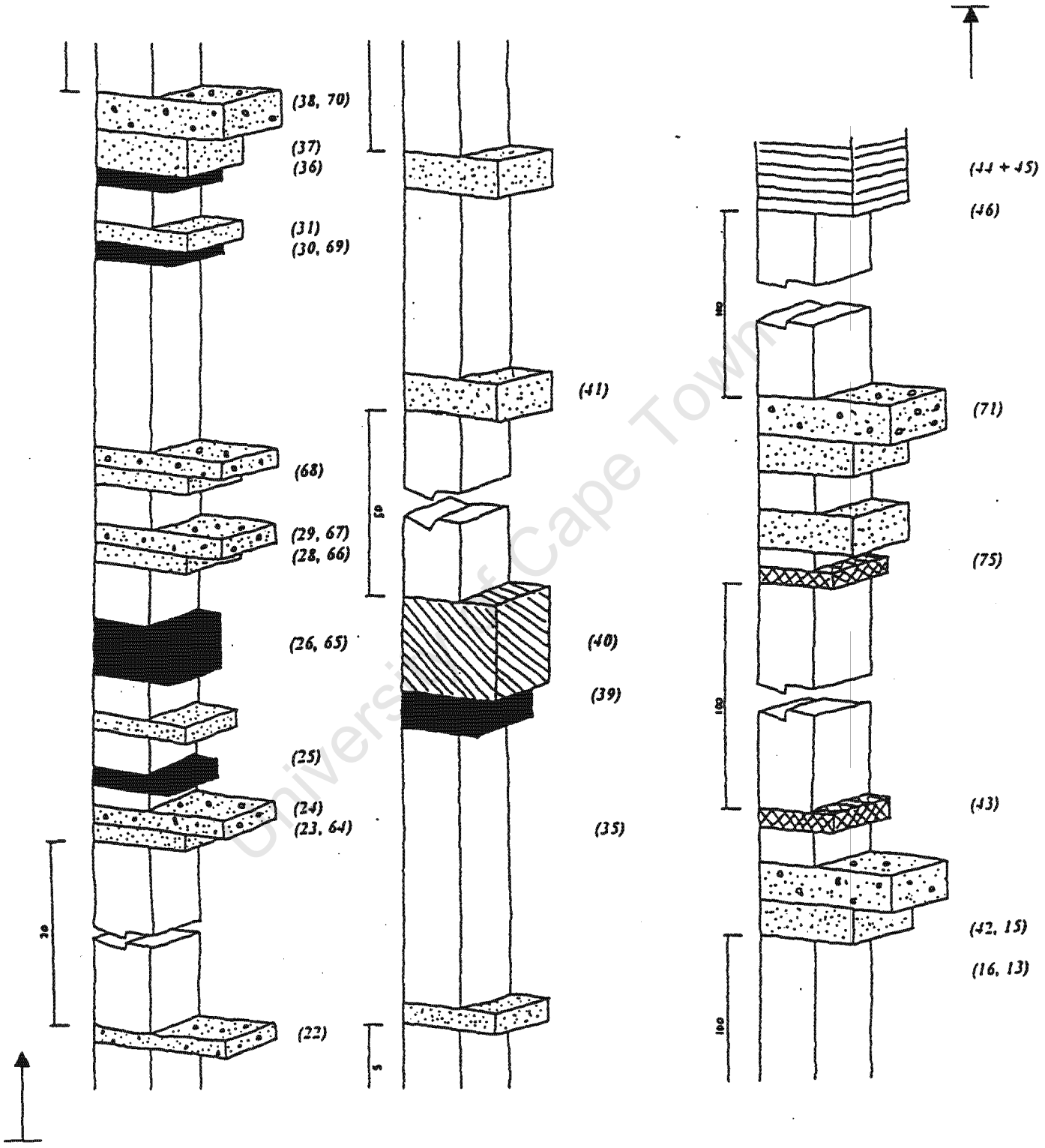

Figure 3.2 Stratigraphic column for units of the main evaporite sequence in the upper Duruchaus Formation. Units are in metres and the scale for this column is 1:300. The numbers in brackets represent sample numbers.

Legend:

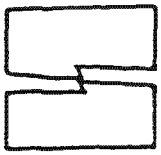

Stratigraphy continues unchanged or with very slight variation.

Coarsely and finely laminated micaceous sandstone; usually soft and weather pink-brown; ripple marks and convolute bedding is common in finer units.

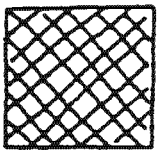

Fe-dolomite units –Weathers brown-black and fresh surfaces are pink-red.

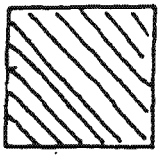

Grey Quartzite – Finely and coarsely laminated grey arenaceous units with well developed ripple surfaces; finer-grained layers rich in K-feldspar.

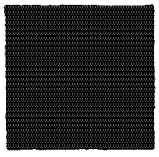

Sandy Dolomite – Finely laminated (recrystallised?) dolomite with albite pseudomorphs; becomes more massive further up the sequence; weathers brown-black, fresh surfaces are pink-red.

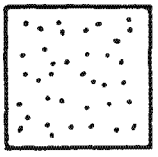

Albitite – Predominantly quartz-albite rock. Appears massive and recrystallised and is commonly overlain by breccias; weathers light brown and fresh surfaces are pink; well developed ripple surfaces are common.

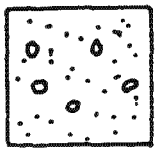

Breccias – Consists of albite fragments in a sparry carbonate matrix; layers are not consistent in thickness (laterally).

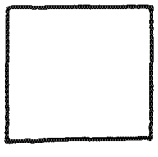

Pelitic/Psammitic Sequence – Finely laminated blue-grey pelite and psammite showing well preserved sedimentary structures (dessication cracks and ripple surfaces); finer- grained units are biotite-rich, and some units show prominent K-feldspar-quartz veining, subordinate carbonate layers and minor concordant breccias.

Figure 3.2 (continued)

3.1.3 Field Relations

The stratigraphy below the main evaporite sequence consists of a monotonous series of pelites intercalated with iron-stained sandstone, pebbly sandstone and carbonate rocks, culminating in a dark iron-rich carbonate facies which outlines the rim of the Gurumanus Dome (Figure 3.1). The main evaporitic sequence which lies above these units consists largely of pelitic units with intercalated massive (recrystallised?) pink albitite and brown-black sandy dolomite which contains albite pseudomorphs. Concordant breccias are encountered on various levels in the stratigraphy typically overlying the albitite, with iron-rich dolomite units present at the top of the sequence. Pelitic units also overlie the main evaporite sequence, being intercalated with occasional carbonates and psammitic units until the top of the sequence is reached (Figure 3.2). Each of these lithotypes were sampled within the main evaporite sequence, and a select number of samples were taken from below the main evaporite sequence.

The lithotypes mentioned above are folded tightly into a disharmonic fold in the area mapped (Figure 3.1). A number of cross-cutting quartz-feldspar veins also occur within the main evaporite sequence (overprinting the stratigraphy). This overprinting is mild in some areas, i.e., veins interfingering with the quartzite, and more extensive in others (the stratigraphy of the extreme western part of the mapped area appears completely obliterated by extensive albitisation of the meta-sedimentary rocks). The western zone consists almost exclusively of massive pink albitite and silicified breccias, and marks the western extent of the mapped and sampled area. An additional set of samples in the form of an albitised and associated unalbitised pelitic unit within the Hakos Group was also collected.

Discordant quartz-dolomite plugs, representing further post-lithification mobilisation of fluids, are present at various levels in the stratigraphy. These plugs vary in size from less than a metre in diameter, to tens of metres across and consist of well formed quartz crystals intergrown with subordinate dolomite and haematite crystals. The plugs, along with discordant and concordant quartz veins present in some units, were sampled within the Duruchaus Formation and the overlying Hakos Group, as representing a possible remobilisation of evaporitic fluids previously trapped within the main evaporite sequence of the Duruchaus Formation. Xenolithic rock fragments commonly occur within these plugs. Sandy dolomite, iron dolomite and breccia similar to the *in situ* units in the Duruchaus Formation stratigraphy were found within these plugs. These xenoliths were sampled along with the quartz-dolomite plugs themselves. Quartz-tourmaline veins are also present in the sampled area, crosscutting the stratigraphy within the main evaporite sequence. These were also sampled along with tourmaline-bearing quartz plugs below the main evaporite sequence.

The metamorphic grade of these units appeared to be quite low (low grade, greenschist facies). The sedimentary character (bedding planes, ripple marks, etc.) of the units described, are well preserved.

3.1.4 Discussion of Field Evidence

A number of initial observations can be made from the field evidence. The first is that late stage albitisation of the main evaporite sequence is indicated, the more porous arenaceous units being replaced/albitised preferentially, when compared with the less porous pelitic units. The timing of the emplacement of the quartz-dolomite plugs appears to be post-albitisation as the xenolithic rocks fragments present within these

plugs appear albitised. Evidence for albitisation further down in the Duruchaus Formation stratigraphy, i.e., below the main evaporite sequence, is not seen.

The xenolithic rock fragments present within these plugs provide strong evidence for an origin within the Duruchaus Formation. All the xenolithic fragments encountered, i.e., sandy dolomite, breccia and iron-dolomite, bear a striking resemblance to the units seen in the Duruchaus Formation stratigraphy. The quartz-dolomite plugs are thought to be related to late stage movement of nappes during the Damaran deformation (Behr *et al.*, 1983b). The south-eastward overriding of nappes derived from the Khomas Trough over Nosib Group sediments is thought to have forced a dolomitic evaporitic mush which included autolithic and xenolithic rock fragments up planes of weaknesses, i.e., fractures, forming discordant units or plugs, like those encountered in the Duruchaus Formation and in the Hakos Group (the most famous of these examples being the Sole Dolomite at the base of the Naukluft Nappe Complex - Behr *et al.*, 1983b). The field evidence supports this contention and argues strongly for a root in the Duruchaus Formation for these plugs. Remobilised connate evaporitic fluids originating from the evaporitic units within the Duruchaus Formation may therefore be preserved as fluid inclusions in the quartz and dolomite crystals which make up these quartz-dolomite plugs.

3.1.5 Analyses

The analytical work for this part of the study was subdivided into three main categories:

(i) Fluid Inclusion Studies :

Microthermometry,

Crush-leach analyses using high performance ion chromatography (HPIC) and inductively-coupled plasma mass spectrometry (ICP-MS)

(ii) Whole Rock Geochemistry:

X-Ray fluorescence spectrometry analyses (XRFS)

Inductively-coupled plasma mass spectrometry analyses (ICP-MS)

(iii) Mineral Chemistry:

Electron microprobe analyses (EMPA)

The analyses listed in (i) were carried out to determine the density, overall salinity and bulk fluid chemistry of the fluids preserved as inclusions within the quartz-dolomite plugs and quartz vein samples. The analyses listed in (ii) were carried out to determine the whole rock geochemical compositions of the units within the Duruchaus Formation. XRFS was used to determine the major element distribution in the sampled units, and ICP-MS was used to determine their trace element and rare earth element concentrations. EMPA analyses were carried out on the tourmaline grains within the quartz-tourmaline veins and quartz-tourmaline plugs sampled in the Duruchaus Formation to determine the chemistry of these grains. Details of the sample preparation, instrumental set-up and lower limits of detection for each of the above techniques are presented in Appendix I.

3.2. Petrography and Mineralogy

3.2.1 Introduction

A brief outline of the pertinent petrographic and mineralogical features of the units encountered in the Duruchaus Formation are presented in the following sections. Complete petrographic descriptions and the complete set of electron microprobe analyses are presented in Appendices II and III.

3.2.2 Petrography

Metapelite and Metapsammite

The mineralogy of the metapelite and metapsammite is quite similar with only the grain size and quartz and mica contents showing some variation in terms of modal proportions. The metapelite is dominated by quartz grains (0.1-0.25mm), with significant amounts of biotite, muscovite and opaques (haematite, ilmenite) also present. Plagioclase and carbonate grains (in the form of dolomite) commonly form a small component of the matrix in the metapelite below the main evaporite sequence. The carbonate content of the metapelite within the main evaporite is slightly higher. Metapelite within the main evaporite sequence also contains quartz-albite aggregates thought to be pseudomorphing primary, syn-sedimentary mineral phases. Tourmaline grains are present within some of these pseudomorphs (Plate 1). The metapelite within the main evaporite sequence is characterised by a polygonal granoblastic texture.

The metapsammite is also dominated by interlocking quartz grains (0.25-0.5mm), with biotite, rare muscovite and dolomite grains also present. The proportions of the mica and carbonate grains are significantly lower than those observed in the pelitic

units. Sphene is a common accessory phase. A polygonal granoblastic texture is also seen in the metapsammite.

Sandy Dolomite

The sandy dolomite units of the main evaporite sequence contain equal proportions of quartz, albite and dolomite. The dolomite grains form the dominant part of the matrix while the quartz and albite grains form porphyroblasts (Plate 2). Minor amounts of talc and haematite are also present in these units. The sandy dolomite units show a porphyroblastic texture. A dolomitic xenolith bearing a physical resemblance to the sandy dolomite units described above was encountered within the quartz-dolomite plugs in the Duruchaus Formation. The xenolith also conforms well to the above petrographic description (Plate 6).

Breccias

The brecciated units consist essentially of dolomite and quartz fragments in an albitised matrix (Plate 3). The quartz and dolomite grains form clasts and matrix components, along with smaller albite grains. Sphene and opaque (haematite) grains also form a minor component of the matrix. The texture observed in all the brecciated units is seriate. A breccia xenolith encountered within the quartz-dolomite plugs in the Duruchaus Formation was also subjected to a similar petrographic study and was found to conform to the above petrographic description (Plate 5).

Albitite

The albitite within the main evaporite sequence consists predominantly of quartz and albite grains (~1mm) (Plate 4). Significant amounts of dolomite are also present within these units with minor sphene and rutile (after ilmenite?), and haematite grains.

Minor muscovite is also present within these units. An equigranular, granoblastic texture is common in these rocks with the quartz and albite grains sometimes forming small porphyroblasts.

Quartzite/Quartz Arenite

Quartzite is present in the stratigraphy below the main evaporite sequence and consists essentially of quartz, microcline and plagioclase grains (0.5-1mm). Biotite and muscovite grains also form a significant part of the matrix, with minor amounts of zircon, sphene and opaque mineral grains (haematite?). A recystallised, granoblastic texture is shown by these units.

Dolomite/Dolostones

The mineralogy of the dolomitic units is quite consistent throughout the sequence. Dolomite is the main mineral component with minor amounts of quartz and talc. Haematite proportions in these carbonates show some degree of variation with the more haematite-rich carbonates being classified as Fe-dolomite. Polygonal granoblastic textures shown by these units suggests that they are recrystallised.

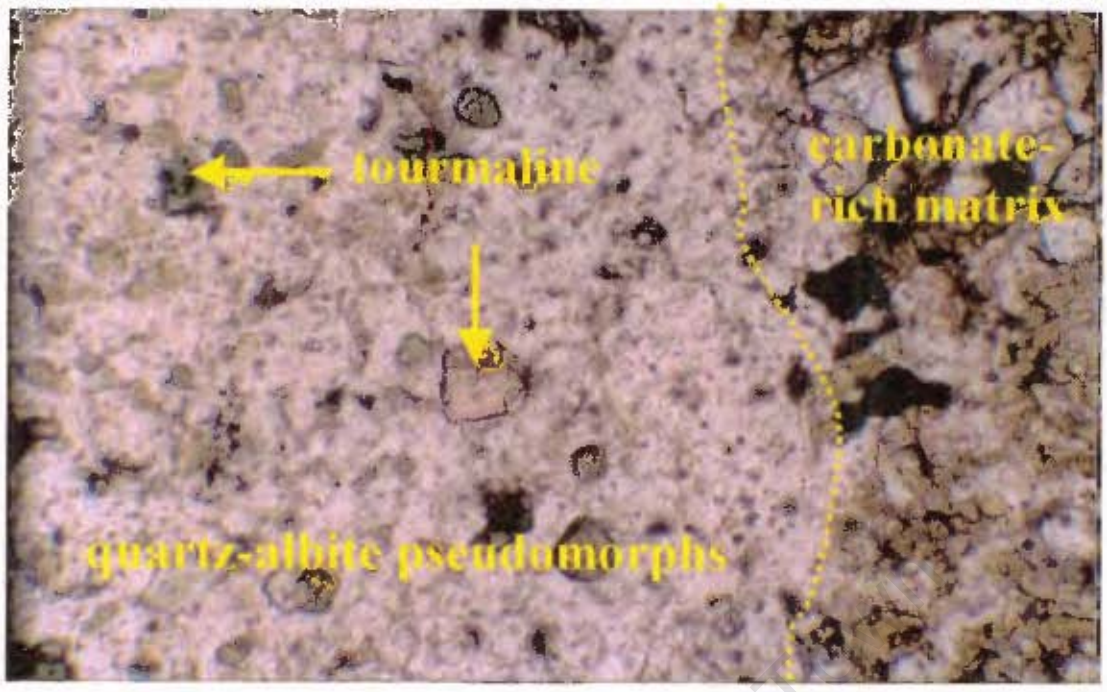

Plate 1. Metapelite within the main evaporite sequence showing quartz-albite pseudomorphs bearing tourmaline grains (field of view : 1mm).

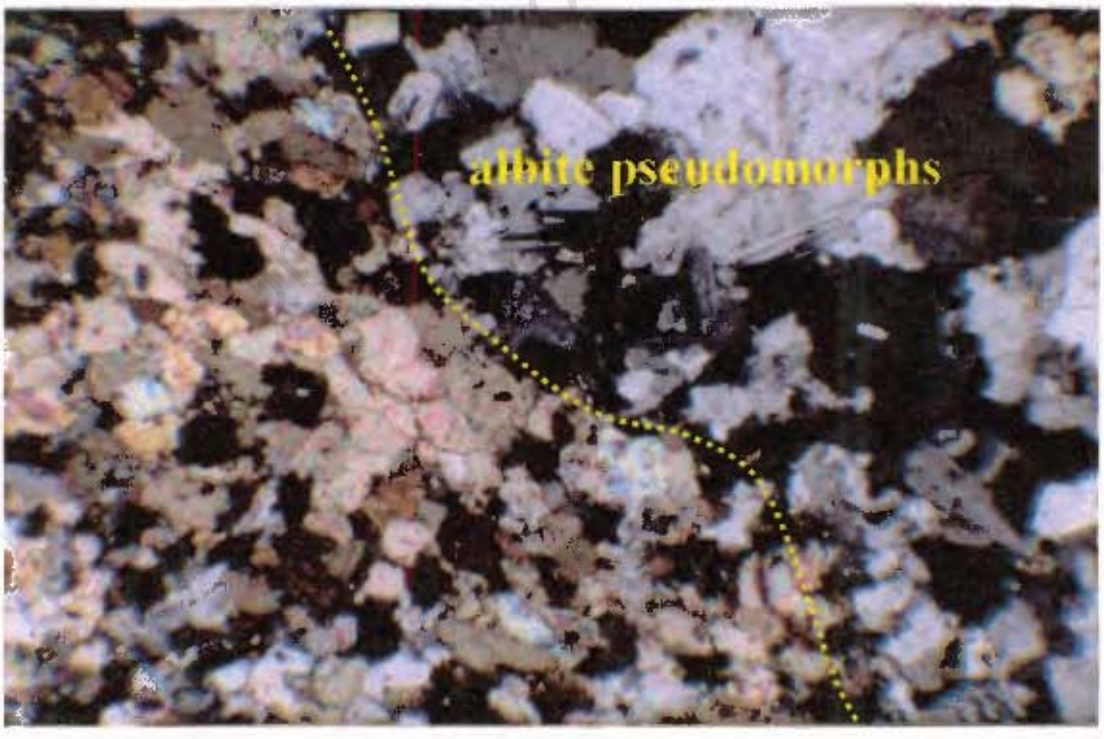

Plate 2. Sandy dolomite showing albite pseudomorphs in fine-grained dolomitic matrix (field of view: 4mm).

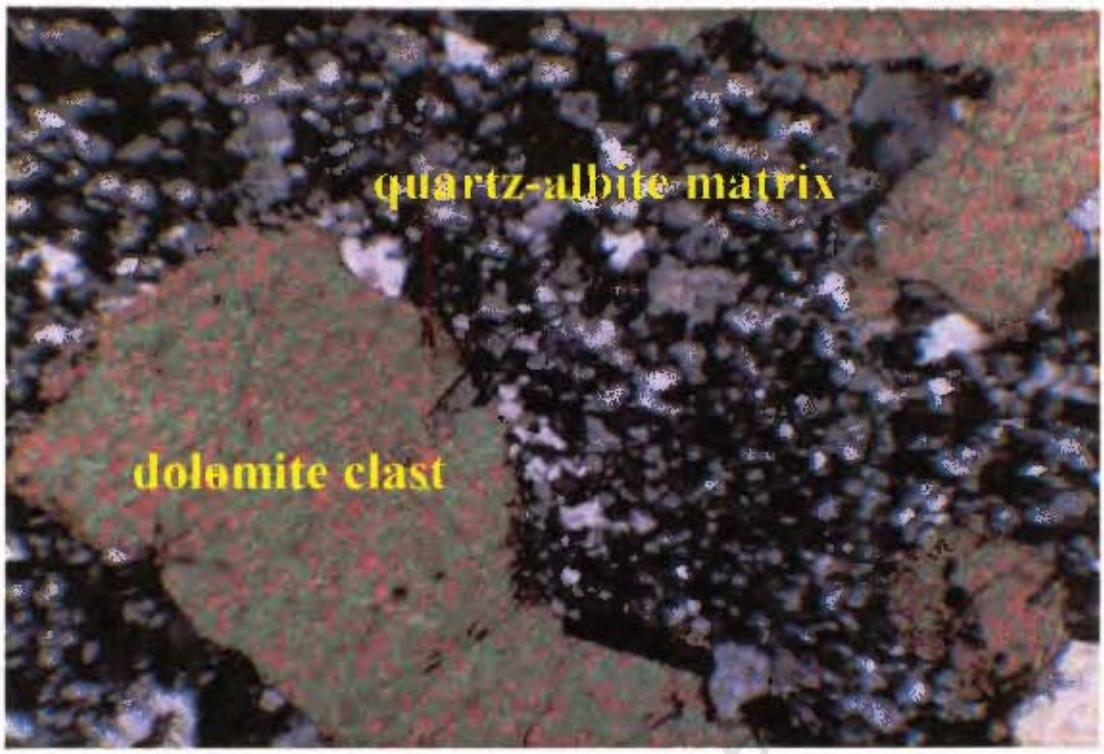

Plate 3. Breccia within the main evaporite sequence showing anhedral dolomite clasts in a fine grained quartz-albite matrix (field of view: 4mm).

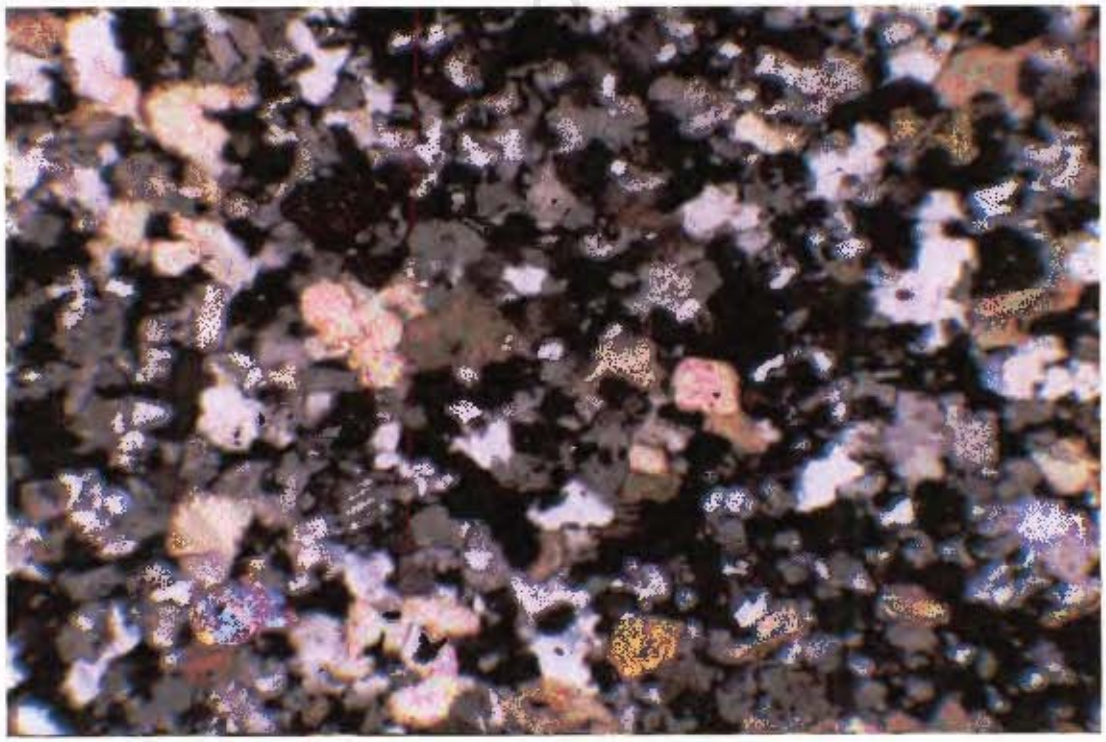

Plate 4. Equigranular matrix of albitite containing equal proportions of albite, dolomite and quartz, with significant amounts of rutile and sphene also present (field of view: 4mm).

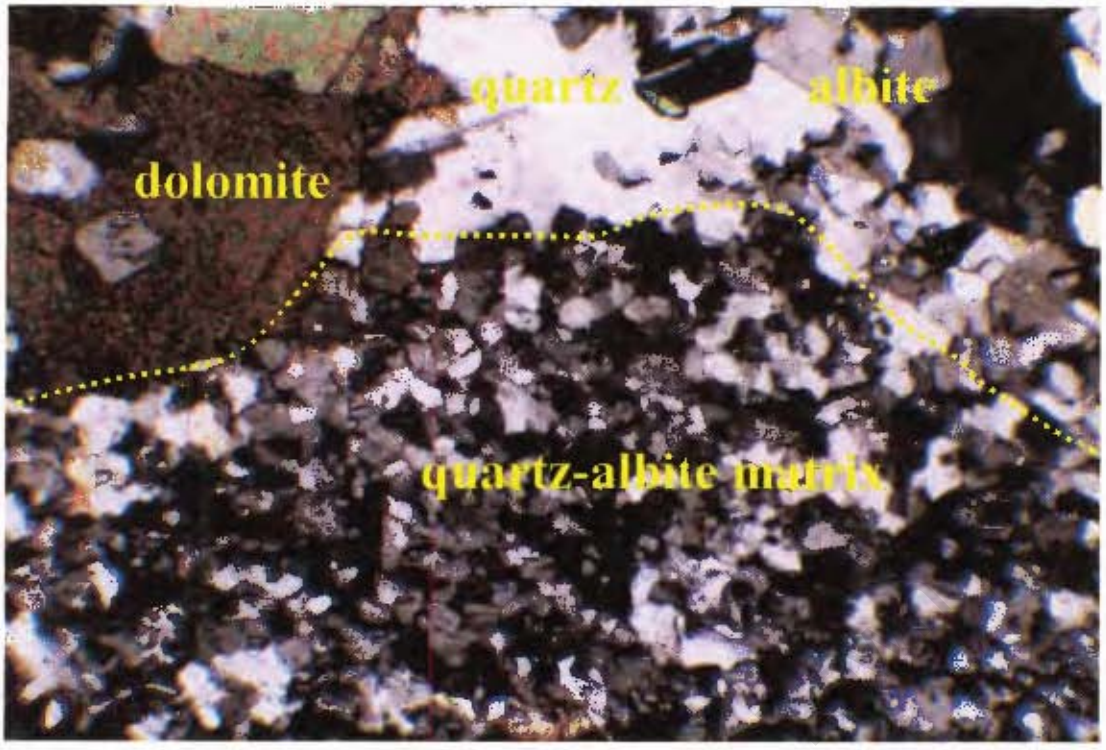

Plate 5. Xenolithic breccia from a quartz-dolomite plug within the Duruchaus Formation showing quartz, albite and dolomitic clasts in a fine grained albite-quartz matrix (field of view: 4mm).

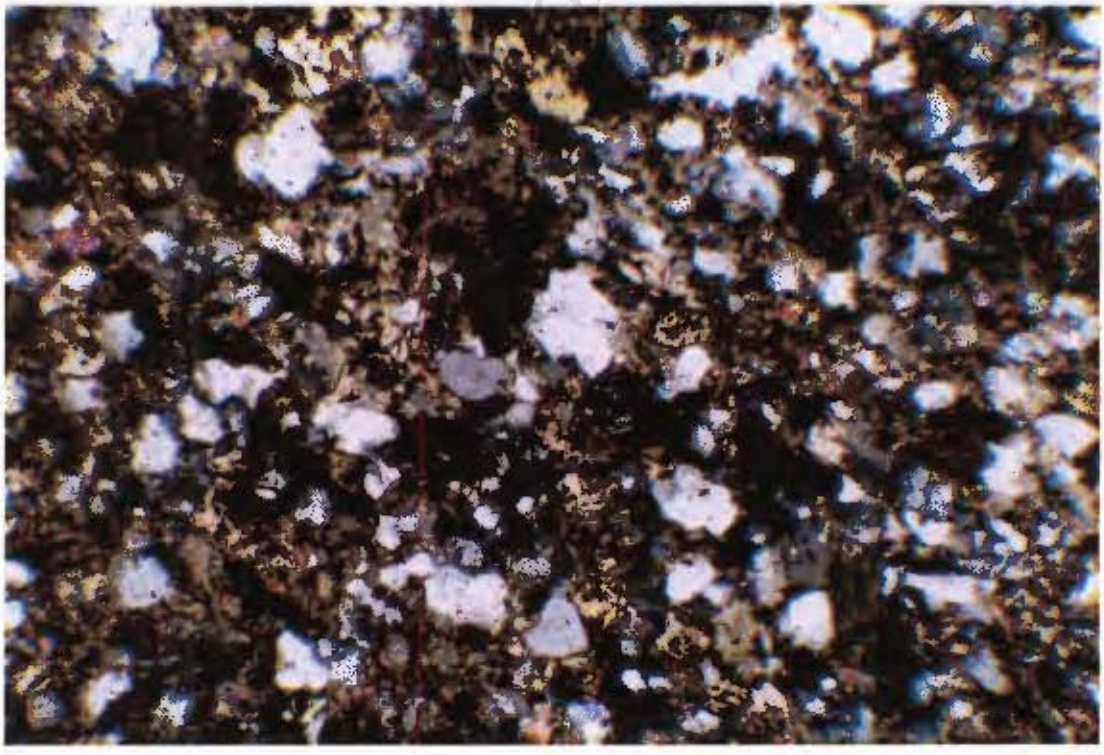

Plate 6. Sandy dolomite xenolith sampled with a quartz-dolomite plug in the Duruchaus Formation showing equal proportions of quartz, albite and slightly altered dolomite grains (field of view: 4mm).

3.2.3 Mineralogy – Tourmaline Chemistry

3.2.3.1 Sample Selection and Analyses

Three tourmaline samples from within the Duruchaus Formation were selected for electron microprobe analyses. The first sample originates from a quartz plug near the bottom of the Duruchaus Formation (NP059). These tourmaline crystals are associated with the quartz crystals in the plug and appear co-genetic. The second sample is from a quartz-tourmaline vein below the main evaporite sequence (NP021; see Figure 3.1). The third sample originates from a metapelite within the main evaporite sequence (NP035). The tourmaline grains were only discovered after petrographic examination of quartz-albite pseudomorphs present in the metapelite layer within the main evaporite sequence. Microscopic tourmaline grains were found to be associated with some of the pseudomorphs within this layer, which suggests that these pseudomorphs may represent former boron-rich diagenetic phases.

The tourmaline grains in the above samples were subjected to an EMPA study (Appendix I.3a) and the Al, Mg, Fe and Ca contents of these grains were plotted on ternary diagrams after Henry and Guidotti (1985). The general formula for tourmaline is $XY_3Z_6(BO3)_3Si_6O_{18}(OH)_4$ (Henry and Guidotti, 1985). The amount of Fe present in the Y and Z sites was calculated assuming a full occupancy of the $(BO3)_3$ site. Assuming that all the Fe in the Y site was Fe^{2+} and all Fe in the Z site was Fe^{3+}, the total Fe was recalculated to Fe^{2+} and Fe^{3+}, and then iteratively adjusted until full occupancy of the Z site was achieved.

3.2.3.2 Results

The samples NP059 and NP021 plot within two fields, the field representing metapsammite/metapelite host rocks and the field representing quartz-tourmaline and metapelite host rocks (Figure 3.3). The sample NP035 plots only within the quartz-tourmaline/metapelite field (as defined by Henry and Guidotti, 1985) extending toward a more Mg-rich composition than the other two samples. In Figure 3.4, all samples plot within field 4 (Ca-poor metapelite/metapsammites), with sample NP035 again trending towards more Mg-rich compositions. The compositions of these tourmalines are intermediate between schorl and dravite, with sample NP035 being more dravitic than the other two. There is little core-rim variation in all the tourmaline grains analysed.

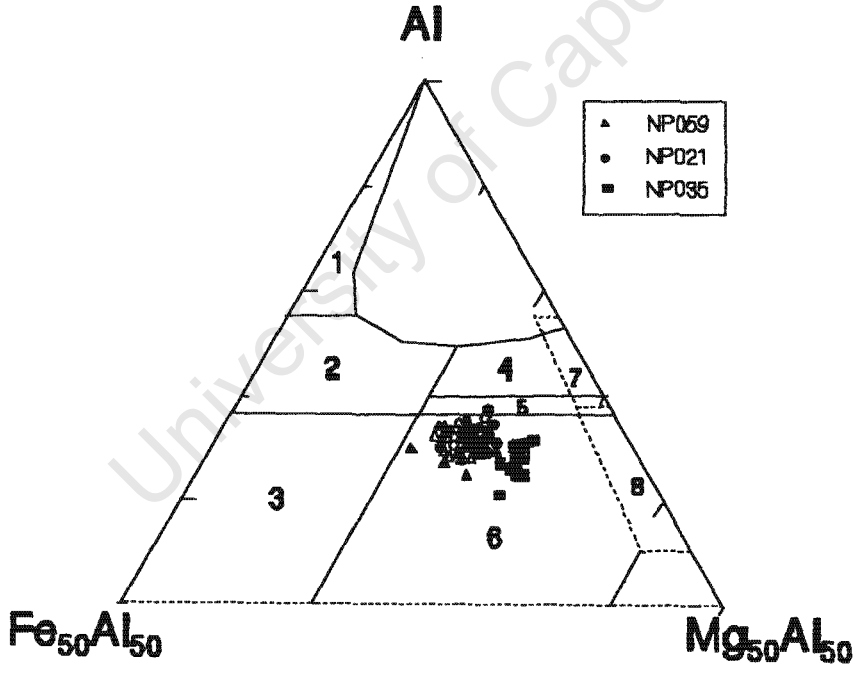

Figure 3.3 Al-Fe(tot)-Mg diagram for tourmaline grains from the Duruchaus Formation in the SMZ (after Henry and Guidotti, 1985). Values are in molecular proportions; open symbols = rims, closed symbols = cores. Fields: 1-Li-rich granitoids; 2–Li-poor granitoids; 3-Fe^{3+}-rich quartz tourmaline rocks; 4-metapelites and metapsammites (+Al-saturating phase); 5-metapelites and metapsammites (no Al-saturating phase); 6-Fe^{3+}-rich quartz-tourmaline rocks, calc-silicates, metapelites; 7-low Ca meta-ultramafics, Cr-V rich sediments; 8-metacarbonates, metapyroxenites.

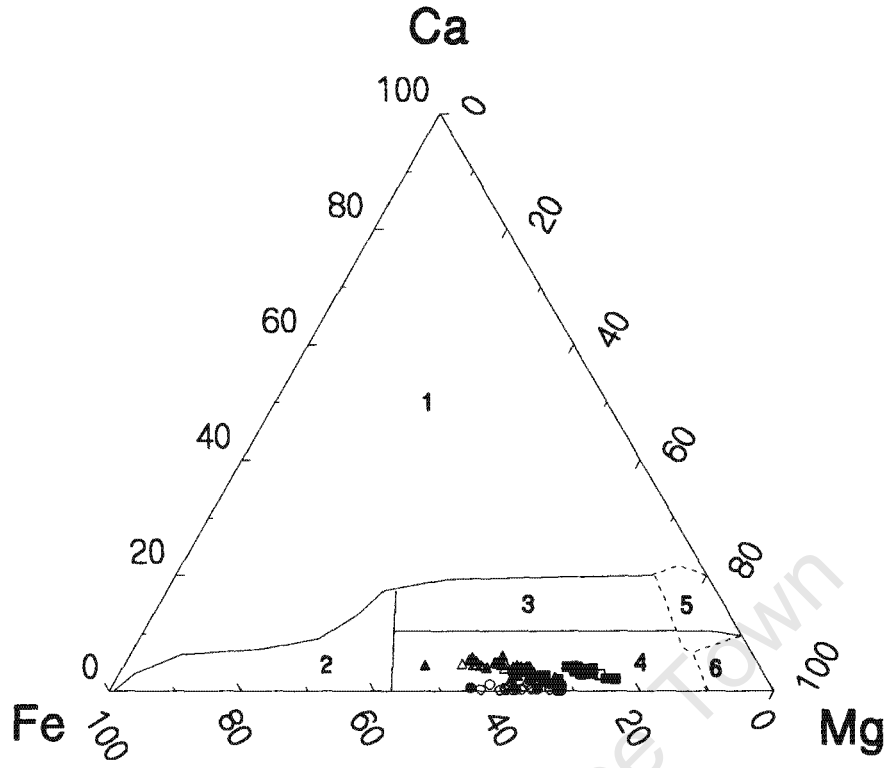

Figure 3.4 Ca-Fe(tot)-Mg diagram for tourmaline grains from the Duruchaus Formation in the SMZ (after Henry and Guidotti, 1985). Values are in molecular proportions (symbols used are the same as Figure 3.3). Fields: 1 and 2 (as in Figure 3.3); 3-Ca-rich metapelites, metapsammites, calc-silicate rocks; 4-Ca-poor metapelites, metapsammites, calc-silicates rocks; 5-metacarbonates; 6-meta-ultramafics.

3.3. Whole Rock Chemistry

3.3.1 Major Element Distribution

The major element distribution in the units from the Duruchaus Formation was used to ascertain the degree of chemical weathering and alteration experienced by the various metasedimentary rock types in the Duruchaus Formation. Using the chemical index of alteration (CIA) as defined by Nesbitt and Young (1982), it is possible to evaluate the degree of pre-metamorphic chemical weathering experienced by sedimentary rocks as well as determine the effect of any late stage metasomatic processes on the geochemistry of a unit. The procedure involves examining the effect that the chemical weathering process has on more mobile cations (e.g., Ca^{2+}, K^{+}, Na^{+}) relative to less mobile constituents, e.g., Al^{3+}, Ti^{4+}. The CIA of a unit can be graphically represented in a ternary plot of Al_2O_3 vs $CaO+Na_2O$ vs K_2O (Figure 3.5). This figure also illustrates the trend generated by the chemical weathering process (using an average Upper Archaean upper crust value as a starting point) and the effect of K-metasomatism on these trends.

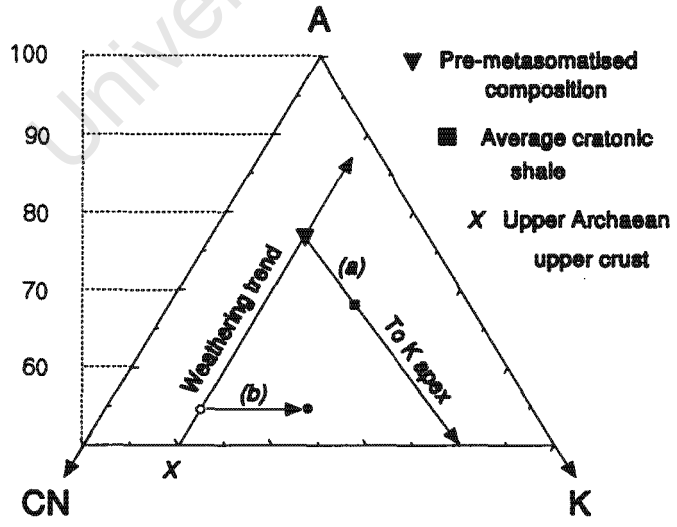

Figure 3.5 Ternary plot of Al_2O_3 (A), $CaO+Na_2O$ (CN) and K_2O (K), showing the trends created by weathering of Upper Archaean upper crust (Condie, 1993) and the addition of K to the feldspars (a: K-metasomatism; b: subsitution of K for Ca,Na in plagioclase) (after Young *et al.*, 1995). All values are in molar proportions and CaO represents the amount of CaO in the silicate fraction of the rock only.

3.3.1.1 Sample Selection and Analysis

The lithotypes present within the Duruchaus Formation stratigraphy include Fe-dolomite, sandy dolomite, albitite, breccia, feldspathic arenite and pelitic units. However, only the arenaceous units (albitite and arenite) and pelitic units were considered in the CIA study due to the heterolithic nature of the breccias and the high CaO contents of the carbonates. Samples showing the least amount of (modern) alteration were selected (degree of alteration determined by a detailed petrographic study of the samples – Appendix II). These samples were subjected to X-Ray fluorescence analyses to determine their major element chemistry (Appendix I.2a). CIA plots for the units of the Duruchaus Formation were produced and are presented in Figure 3.6 and 3.7. It should be noted that the CaO values have not been corrected for the amount of calcium that is present in the form of carbonates in these units. Additional data in the form of the albitised and associated unalbitised pelitic unit sampled within the Hakos Group is also represented on these diagrams. The compositon of the Upper Archaean upper crust quoted in Condie (1993) is quite similar to the average upper continental crust quoted in Taylor and Mclennan (1985) and was therefore used as a reference point for the units of the Duruchaus Formation rocks as well.

3.3.1.2 Results

An examination of Figures 3.6 and 3.7 with regard to the relative positions of these units in the stratigraphy has revealed the following. It was found that samples at the bottom of the sampled sequence appeared to be the least altered, i.e., they plot closest to the composition of the average Upper Archaean upper crust (Figure 3.6). The units higher up in the stratigraphy plot toward progressively higher Al_2O_3 and K_2O values until the bottom of the main evaporite sequence is reached. The units within the main

evaporite sequence in Figure 3.7 plot closer to the $CaO+Na_2O$ (CN) apex, with the units at the top of the main evaporite sequence having little or no K. The CIA plots therefore show a shift toward more Ca- and Na-rich chemistry as one goes from the below the main evaporite sequence into the main evaporite sequence (Figure 3.7).

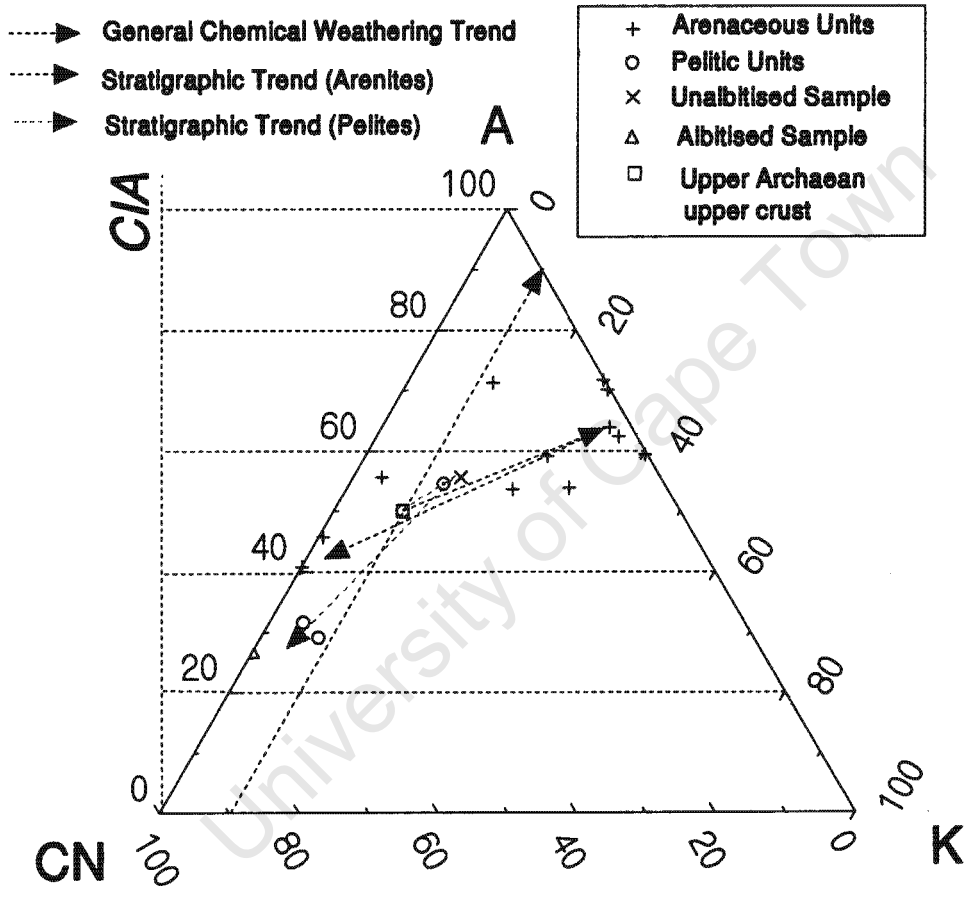

Figure 3.6 CIA plot showing the distribution of data for the lithological units from the Duruchaus Formation in $A(Al_2O_3)$-$CN(CaO+Na_2O)$-$K(K_2O)$ space. The average Upper Archaean upper crust composition is from Condie (1993).

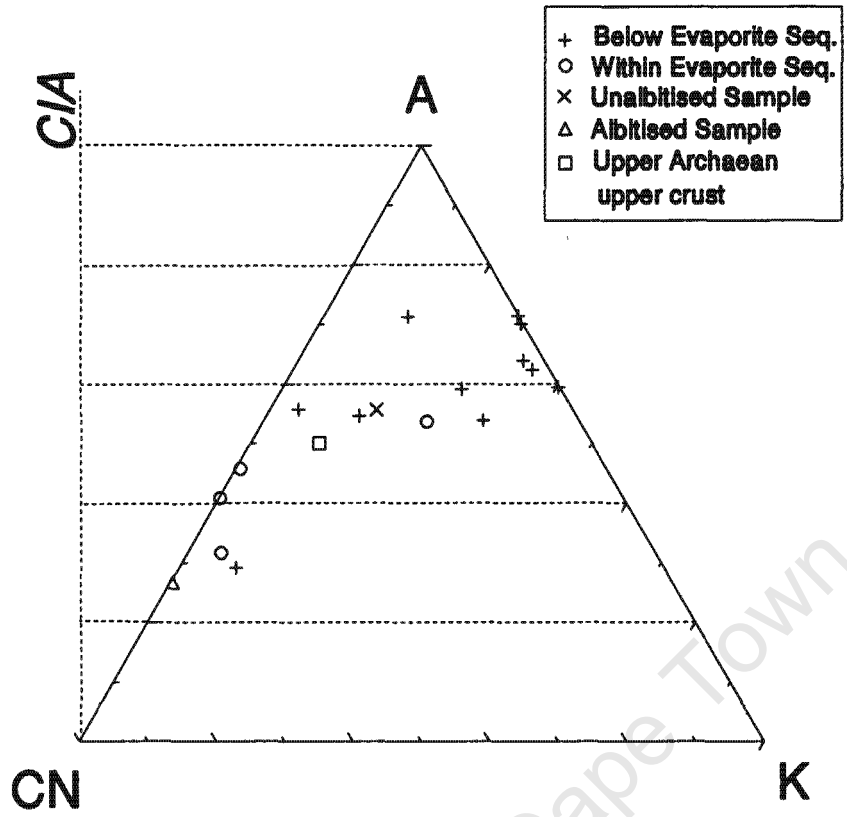

Figure 3.7 CIA plot showing the distribution of data for the units from the Duruchaus Formation in $A(Al_2O_3)$-$CN(CaO+Na_2O)$-$K(K_2O)$ space according to their positions in the stratigraphy. The average Upper Archaean upper crust composition is from Condie (1993).

3.3.2 Trace Element and Rare Earth Element Distribution

The rare earth element (REE) distributions and trace element distributions (to a lesser extent) in rocks are not as susceptable to alteration as that of the major element species, as the REE and certain trace elements (e.g. Th, Sc, Cs, Rb, Ba) are relatively immobile in the secondary environment (Rollinson, 1993). The aim of this part of the study was to characterise the units of the Duruchaus Formation with regard to their REE and trace element distributions and investigate their depositional environments and probable provenance. In particular, the effect of albitisation on the trace element and rare earth element concentrations of these samples was considered.

3.3.2.1 Sample Selection and Analyses

Selected whole rock samples collected from throughout the Duruchaus Formation stratigraphy (all rock types) were subjected to ICP-MS analyses to determine their trace element and rare earth element distributions (Appendix I.2b). Again, samples showing the least amount of (modern) alteration were initially selected (determined from petrographic character of the samples). A suitable spread of samples throughout the Duruchaus Formation stratigraphy were then analysed to give an indication of the geochemical variation in the sequence. Xenolithic units sampled within the quartz and quartz-dolomite plugs within the Duruchaus Formation and the overlying Hakos Group were also included in this analysis.

3.3.2.2 Rare Earth Element Distribution

The different lithological units in the Duruchaus Formation stratigraphy show a number of consistent features with regard to their chondrite-normalised rare earth element abundances, i.e., a strong light rare earth enrichment pattern (very steep pattern in the arenaceous units, less so in the carbonates and pelites), a negative Eu

anomaly, and Ce anomalies (positive within the main evaporite sequence and negative below the main evaporite sequence) (Figure 3.8).

Upper continental crust-normalised plots yield flat REE patterns for all lithotypes (Figures 3.9). In addition to a flattening of the light rare earth enrichment trend, it is also seen that the negative Eu anomalies all but disappear, suggesting that both these features are inherited from a source lithology of similar rare earth element chemistry to the upper continental crust, i.e., the clasts and sedimentary grains which make up the metasedimentary units of the Duruchaus Formation originated from a source lithology which was characterised by a light rare earth enrichment trend and a negative europium anomaly.

The Ce (and sometimes Eu anomalies) persist in the upper continental crust-normalised plots of some of the carbonate units within the main evaporite sequence (Figure 3.9). It is also noted that the Ce anomalies are either absent or negative in the carbonates below the main evaporite sequence, and positive in some of the carbonates within the main evaporite sequence (Figure 3.9). This feature is seen in all the lithological units but is more evident in the carbonate units. The Eu anomaly in one of the carbonates within the main evaporite sequence has also shifted from a negative anomaly in the chondrite- normalised plots to a positive one in the upper continental crust-normalised plots (Figure 3.9). A significant light rare earth element depletion is also seen in all the carbonate and arenaceous units within the main evaporite sequence in the upper continental crust- normalised plots.

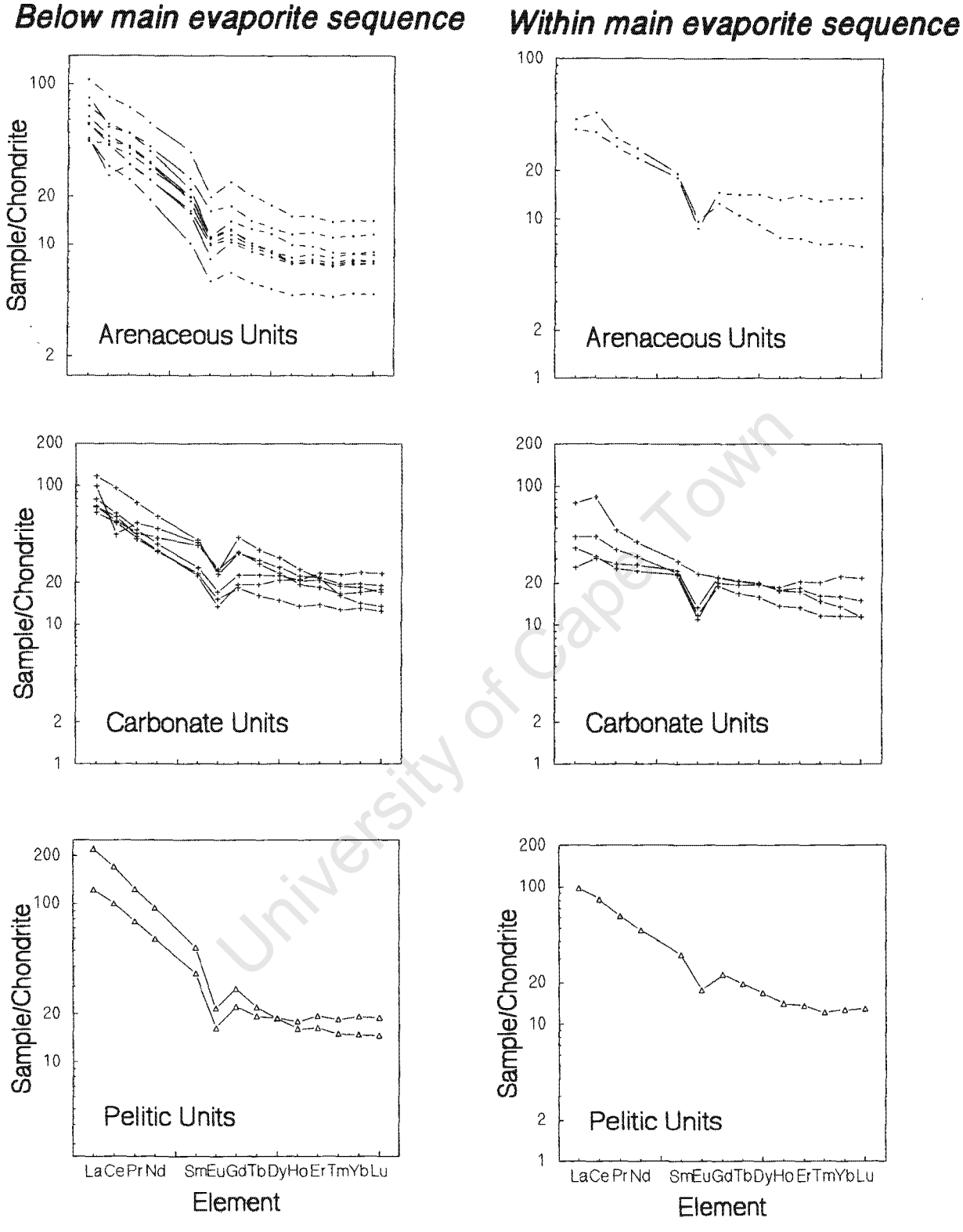

Figure 3.8 Chondrite-normalised rare earth element plot for all the sampled lithologies from below and within the main evaporite sequence in the Duruchaus Formation. Chondrite normalising values are from Sun and McDonough (1989).

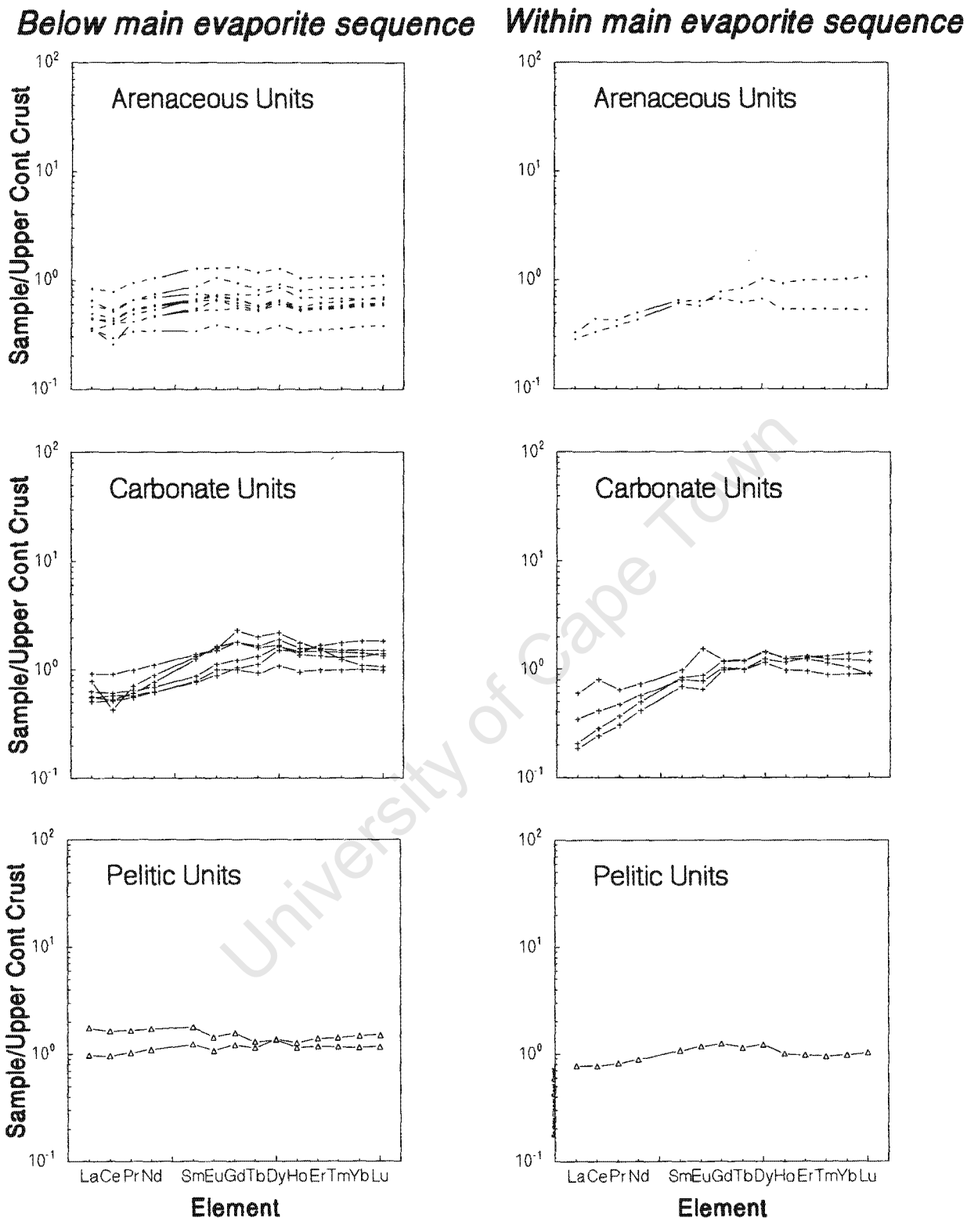

Figure 3.9 Upper continental crust-normalised rare earth element plots for all the sampled lithological units from the Duruchaus Formation below and within the main evaporite sequence. Upper continental crust crust normalising values are from Taylor and Mclennan (1981).

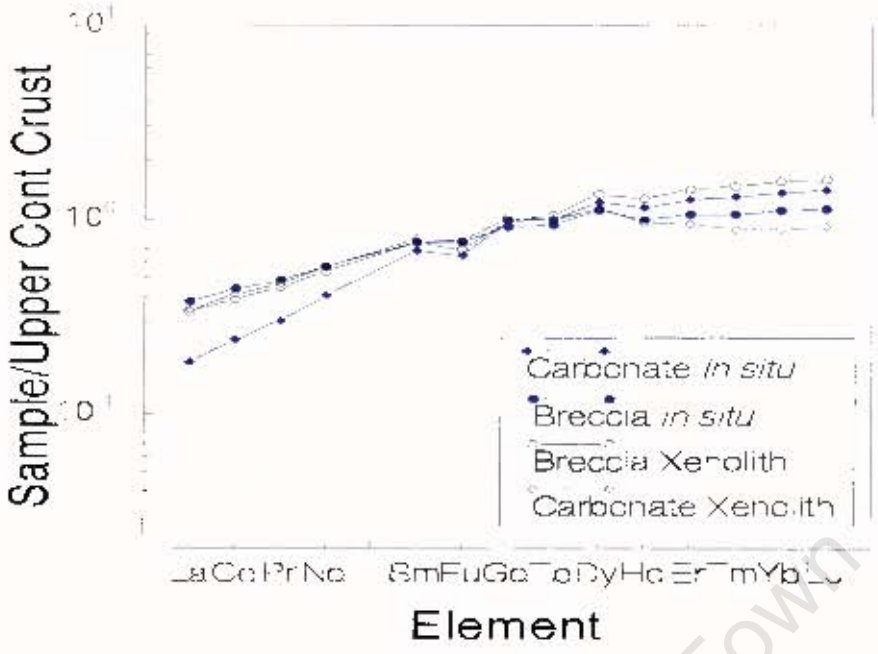

Figure 3.10 Upper continental crust-normalised rare earth element distributions of xenoliths from discordant quartz and quartz-dolomite plugs in the Hakos Group and in the Duruchaus Formation, compared with lithologically similar units within the Duruchaus Formation.

Finally, the xenolithic units sampled in the quartz-dolomite plugs do not only bear a physical resemblance to the *in situ* units within the Duruchaus Formation but also show very similar (upper continental crust-normalised) rare earth element patterns to comparable, *in situ* units within the Duruchaus Formation (Figure 3.10).

3.3.2.3 Trace Element Distribution

Arenaceous and pelitic units below the main evaporite sequence are enriched in all trace elements relative to the upper continental crust (Figure 3.11). Carbonate units below the main evaporite sequence, and carbonate and arenaceous units within the main evaporite sequence are also enriched with respect to most trace elements relative to the upper continental crust, except for the elements Rb, Cs and Ba. All units,

irrespective of lithology, show marked enrichments in Y, Yb and Th (Figure 3.11). A negative Nb anomaly is also evident in all the lithological units.

In addition to the features described above, there is some variation especially in the more incompatible elements, between the different lithotypes. The arenaceous units below the main evaporite sequence show marked negative Sr anomalies (Figure 3.11). Moderate V and Zr anomalies are seen in some samples, with moderate positive Cr and Ba anomalies also seen. The arenaceous units within the main evaporite sequence do not follow the trends shown by the arenceous units below the main evaporite sequence but mirror the trends of the carbonates and pelitic units found within the main evaporite sequence (Figure 3.11).

The carbonates below the main evaporite sequence show a marked depletion in Rb, Cs and Ba, along with negative Hf and Zr anomalies (Figure 3.11). A slight variation is also noted between the carbonate units below the main evaporite sequence and those within the main evaporite sequence. Those units within the main evaporite sequence show less marked Cs and Nb anomalies, and small negative La and Ce anomalies, which are not evident in the carbonates below it. The pelitic units within the main evaporite sequence show a combination of features of the lithological trends described above. Negative Sr and Ba anomalies are the most obvious features of this trend (Figure 3.11).

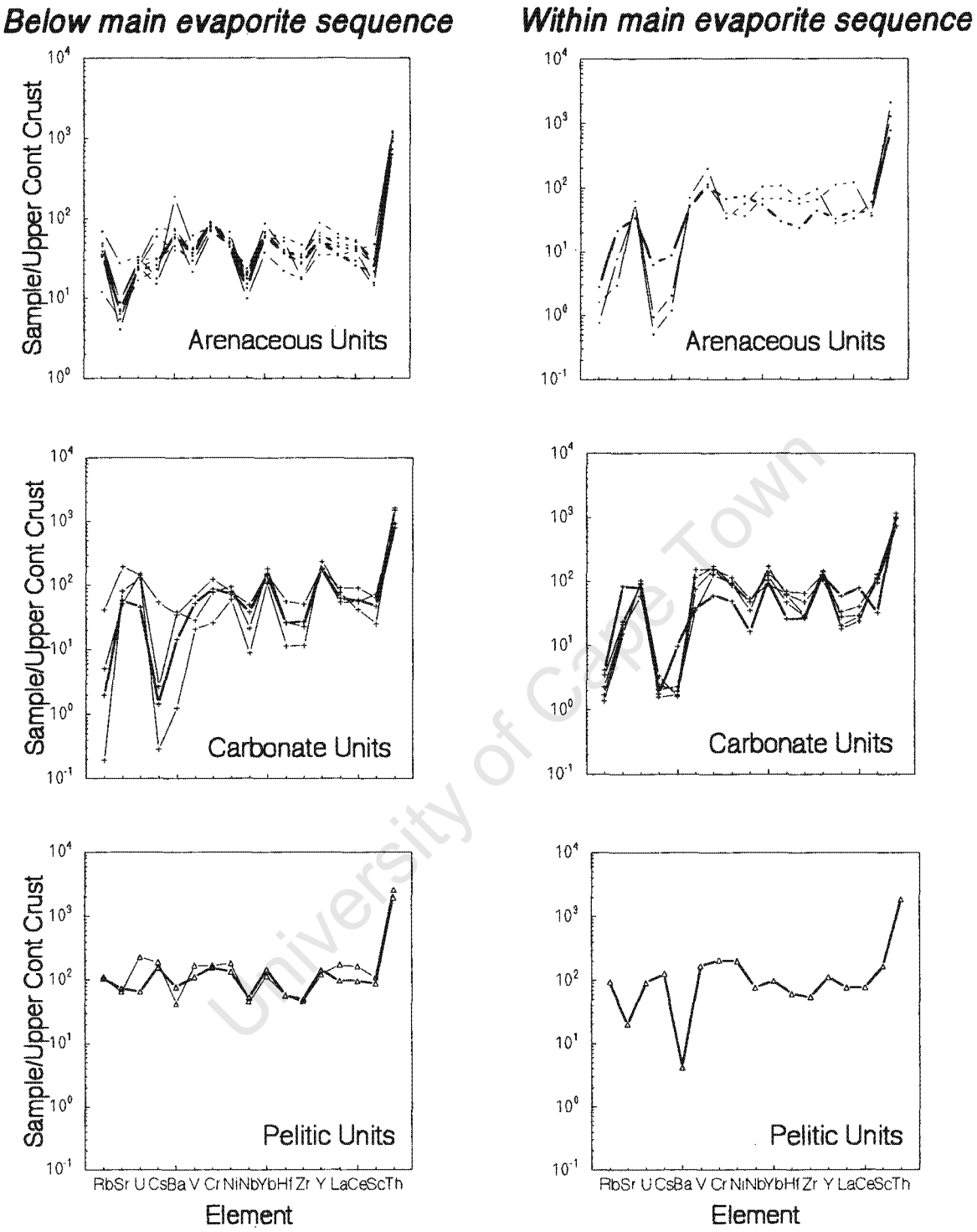

Figure 3.11 Multi-element variation diagrams for units from each of the lithological groupings present in the stratigraphy of the Duruchuas Formation below and within the main evaporite sequence. Upper continental crust normalising values are from Taylor and Mclennan (1981).

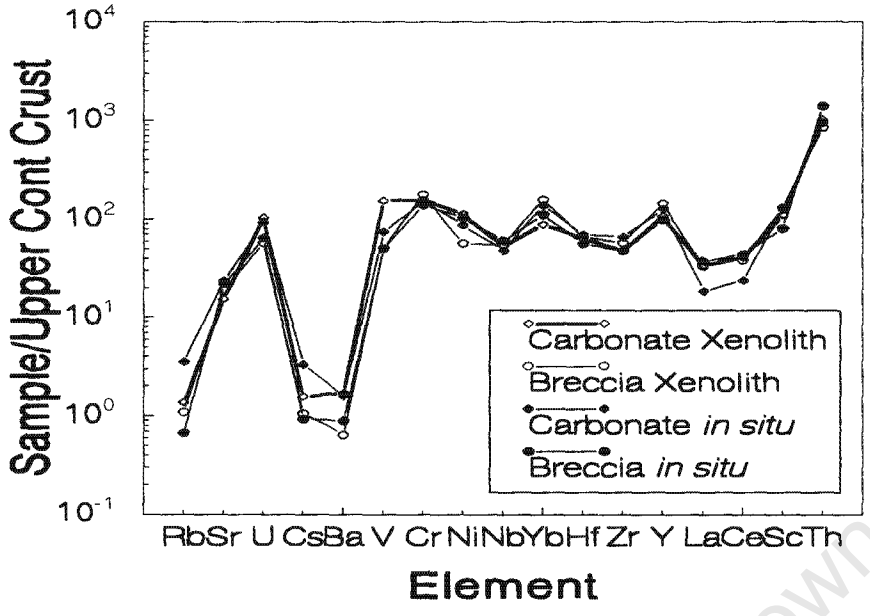

Figure 3.12 Upper continental crust-normalised trace element plots of xenoliths from the discordant quartz and quartz-dolomite plugs in the Hakos Group and in the Duruchaus Formation, compared with lithologically similar *in situ* units from the Duruchaus Formation.

The xenolithic units sampled within the quartz and quartz–dolomite plugs of the Hakos Group and Duruchaus Formation show very similar trace element patterns to comparable *in situ* units in the Duruchaus Formation (Figure 3.12). The xenoliths are also enriched in all trace elements except Rb, Cs and Ba, relative to the continental crust, and are characterised by a trend almost identical to that displayed by the units of the main evaporite sequence.

3.4. Fluid Inclusion Study

3.4.1 Microthermometry

3.4.1.1 Sample Selection, Petrography and Analyses

Eleven quartz samples were selected for fluid inclusion microthermometry (details of the sample preparation and instrumental set-up are presented in Appendix I.1a). Three samples originate from the Hakos Group quartz-dolomite plugs, six samples from quartz plugs within the Duruchaus Formation and two samples from quartz veins within the Duruchaus Formation. Plug and vein samples intruding various levels in the Duruchaus Formation stratigraphy were selected to investigate a similar origin for the fluids preserved (as inclusions) at various levels in the stratigraphy. Quartz samples were analysed in preference to other potential fluid inclusion host minerals due to the fact that quartz-hosted inclusions were more easily optically resolvable and because the mineral quartz is a relatively strong mineral host which has the potential to preserve fluid inclusions under varying conditions better than most other mineral hosts, e.g., calcite. A petrographic and preliminary microthermometric study of the samples mentioned above revealed the existence of four main types of fluid inclusions within them (aq=aqueous, carb=carbonic),

(i) Clathrate-bearing aqueous 3 phase inclusions ($L_{carb;aq}+V_{aq}+S_{salt}$) *(Type I)*

(ii) Aqueous 3 phase inclusions ($L_{aq} + V_{aq} + S_{salt}$) *(Type II)*

(iii) Aqueous 2 phase inclusions ($L_{aq} + V_{aq}$) *(Type III)*

(iv) Rare 2 phase CO_2 inclusions ($L_{carb} + V_{carb}$) *(Type IV)*

The solids present within the Type I and II inclusions were found to be cubic in shape with a refractive index similar to that of quartz. The solids were also isotropic under

crossed polarised light (observed where solids were large enough) and were characterised by dissolution temperatures of above 150°C. These characteristics indicated that the solids present within Type I and II inclusions were halite crystals (Roedder, 1984). The halite crystals are most likely daughter crystals as they consistently occupy similar volumetric proportions in their host inclusions (Roedder, 1984).

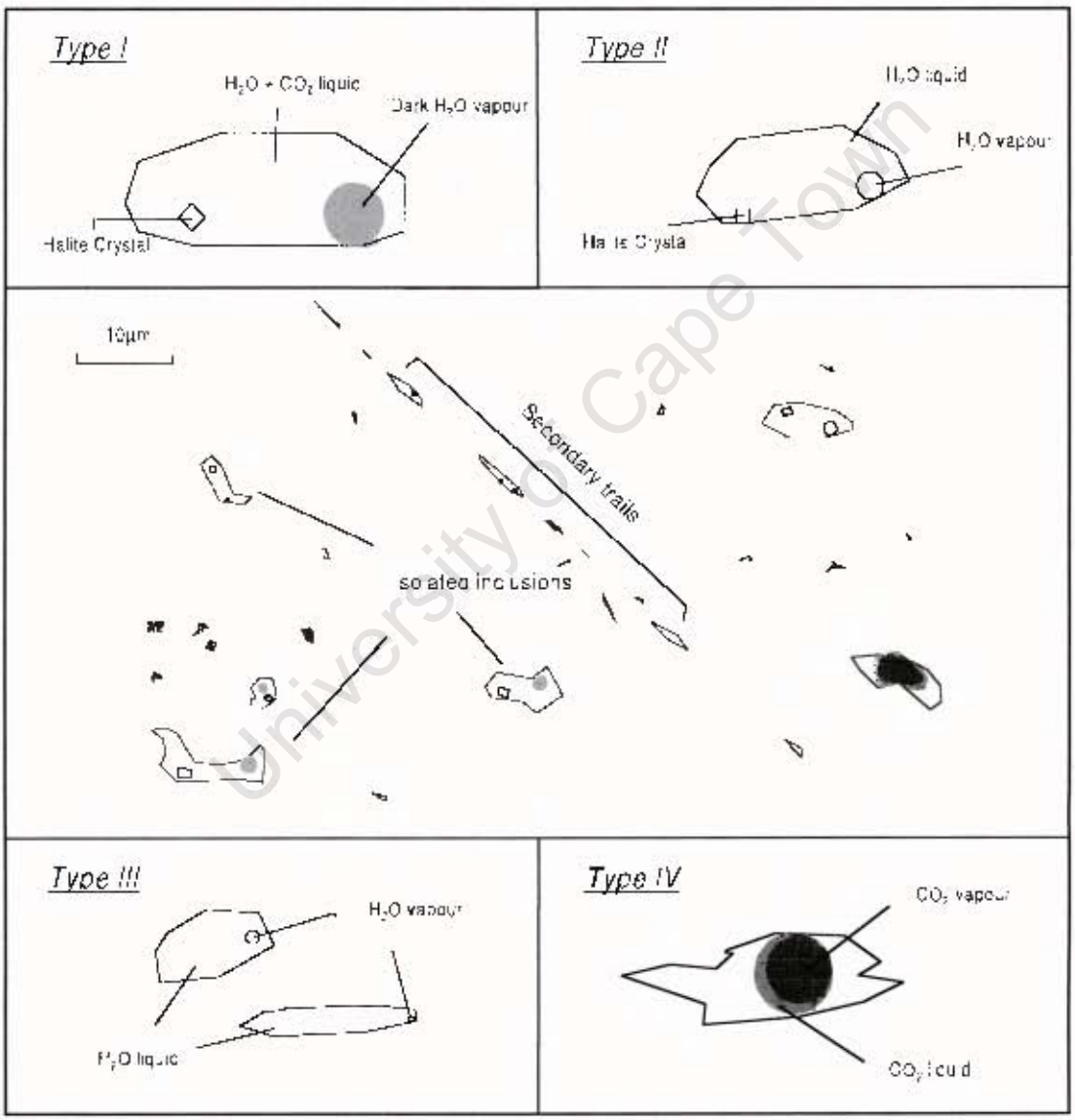

Figure 3.13 Sketch diagram showing the four types of fluid inclusions encountered in the samples from the Type Locality as well as the distribution of these inclusions in one of the sample chips.

Type I and II inclusions commonly form large (up to 15μm), isolated inclusions in the samples analysed (Figure 3.13). The large, isolated inclusions seem to be the oldest fluid generation in the samples analysed showing little or no relationship to later trails unless overprinted by them. Type II, III and IV inclusions form predominantly smaller (5μm or less) secondary (and pseudosecondary?) inclusions. Type IV inclusions do form isolated inclusions in one sample (NP060) but it remains unclear whether this fluid was cogenetic with the fluid preserved in the Type I and II isolated inclusions.

The secondary inclusion trails represent annealed fractures in the host minerals. Those inclusion trails selected for analysis showed consistent liquid/vapour and liquid/vapour/daughter ratios in each inclusion. The effect of necking of these inclusions on the microthermometric data produced was minimised by averaging out the measured eutectic temperatures, melting temperatures and homogenisation temperatures in each secondary trail.

Eutectic temperatures, melting temperatures and homogenisation temperatures were measured for each of the phases (CO_2, H_2O) present in the isolated and secondary inclusions. In the Type II inclusions, salinities were calculated from halite dissolution temperatures as most of the aqueous inclusions appeared over-saturated with respect to halite, i.e., halite daughter crystals were present in the inclusions. The equations used are from Sterner *et al.* (1988). The salinities quoted for Type III inclusions were calculated using the equation of Bodnar (1993). The salinities quoted represent averaged salinities for each sample.

3.4.1.2 Results

Table 3.1 presents a summary of the microthermometric data described below (Inclusion Types I-III). The results of the microthermometric study of Type II and III inclusions within the Hakos Group quartz-dolomite plugs and the discordant plugs and veins in the Duruchaus Formation are presented together in Figures 3.14 to 3.17.

Type I inclusions which form isolated inclusions in the Hakos Group plugs show eutectic temperatures (T_e) of down to –20.5 °C. Clathrate melting temperatures (Tm_{clath}) values lie in the range 5.4 °C to 11.0 °C, with some values up to 29.3 °C also recorded. A large range of homogenisation temperatures were observed in these inclusions extending from low values of around 130 °C, to higher values of up to 382 °C (Table 3.1). Homogenisation was to the liquid phase. (Salinities:38-40wt% $NaCl_{eq}$)

Similar results were observed for the Type I isolated inclusions within Duruchaus Formation plugs and veins with T_e values as low as –28.1 °C, final ice melting temperatures (Tm_{ice}) of between –2.1 °C and –27.1 °C and Tm_{clath} values of between 1 °C to 10.2 °C (with some higher values of up to 29.9 °C also recorded). A large range of homogenisation temperatures of between 136°C and 313°C were also recorded for the Duruchaus Formation plugs. Type I inclusions which form secondary inclusions in the Duruchaus Formation plugs fall into similar ranges as the isolated inclusions described above but show a more restricted range of T_e and Tm_{clath} values, with a generally lower homgenisation temperature range of between 160 °C and 229 °C (Table 3.1). Homogenisation was to the liquid phase. (Salinities: 33-47wt% $NaCl_{eq}$)

The Type I isolated inclusions in the Duruchaus Formation vein samples analysed also lie within the T_e, Tm_{ice} and Tm_{clath} ranges showed by the Hakos Group plugs with

a generally higher homogenisation temperature range of 235 °C to 366 °C. Homogenisation was always to the liquid phase. (Salinities: 33-38wt% $NaCl_{eq}$)

Type II inclusions and Type III inclusions are considered together in the following discussion, Type II inclusions present as both isolated and secondary inclusions, and Type III inclusions present as predominantly secondary inclusions in the sampled plugs and veins. The Type II and Type III secondary inclusions are commonly found together in fluid inclusion trails and are hence regarded as co-genetic.

T_e values for the Type II and III, isolated inclusions in the Hakos Group plugs lie in the range -22.2 °C and –27.4 °C, with Tm_{ice} values between –8.1 °C and –25.6 °C, and a range of homogenisation temperatures (T_hH_2O) of between 263 °C and 390 °C. The secondary Type II and III inclusions show a wider range of values for T_e and Tm_{ice} with a generally lower T_hH_2O range of 114 °C to 236 °C. Salinities calculated for these sets of inclusions in the Hakos Group plugs are between 38 to 40 wt% $NaCl_{eq}$ for the isolated inclusions and approximately 31 wt% $NaCl_{eq}$ for the secondary inclusions.

T_e values for the Type II and III, isolated inclusions in the Duruchaus Formation plugs show a similar overlapping range with the Hakos Group plugs of between –21.7 °C and –30.0 °C, with Tm_{ice} values between –1.5 °C and –35.5 °C. T_hH_2O values, though, show a much wider distribution but overlap with the range showed by the Hakos Group plugs (133 °C to 334 °C). The secondary Type II and III inclusions show a similar temperature distribution to the isolated inclusions with respect to T_e (with some lower values), and Tm_{ice}. The observed T_hH_2O values shown by the secondary inclusions is again slightly lower than that seen in the isolated inclusions (127 °C to 287 °C). Calculated salinities for the isolated and secondary inclusions show a general

agreement with that than shown by the Type II and III inclusions in the Hakos Group plugs, i.e., between 32-34 wt% $NaCl_{eq}$ for the secondary inclusions and higher salinites of between 33-47 wt% $NaCl_{eq}$ for the isolated inclusions.

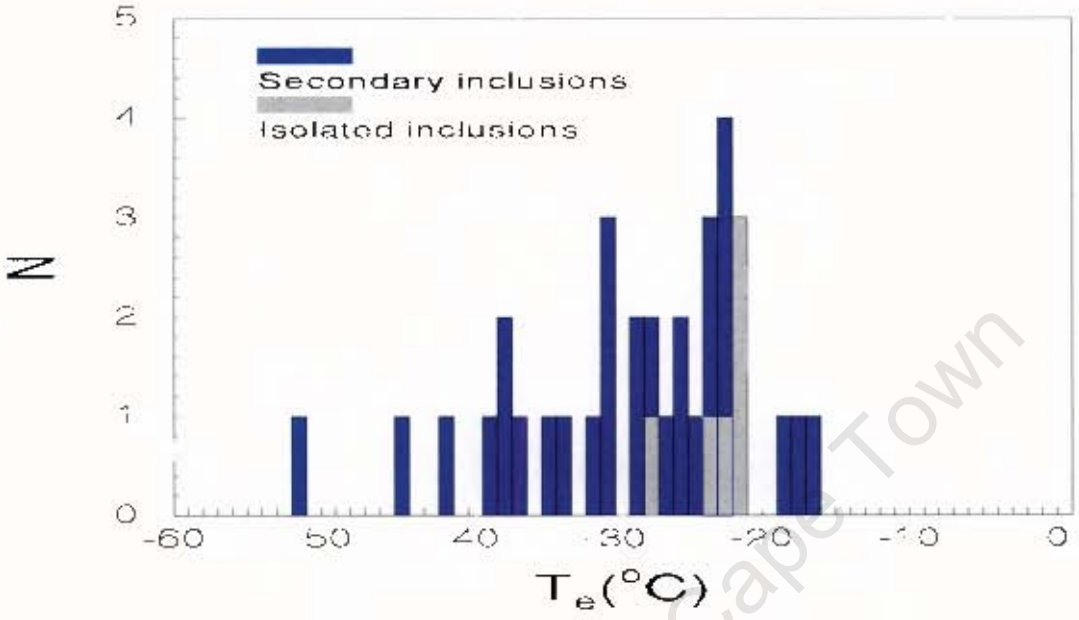

Figure 3.14 Frequency histogram of eutectic temperatures observed in the aqueous inclusions preserved in the quartz and quartz-dolomite plugs of the Duruchaus Formation and Hakos Group.

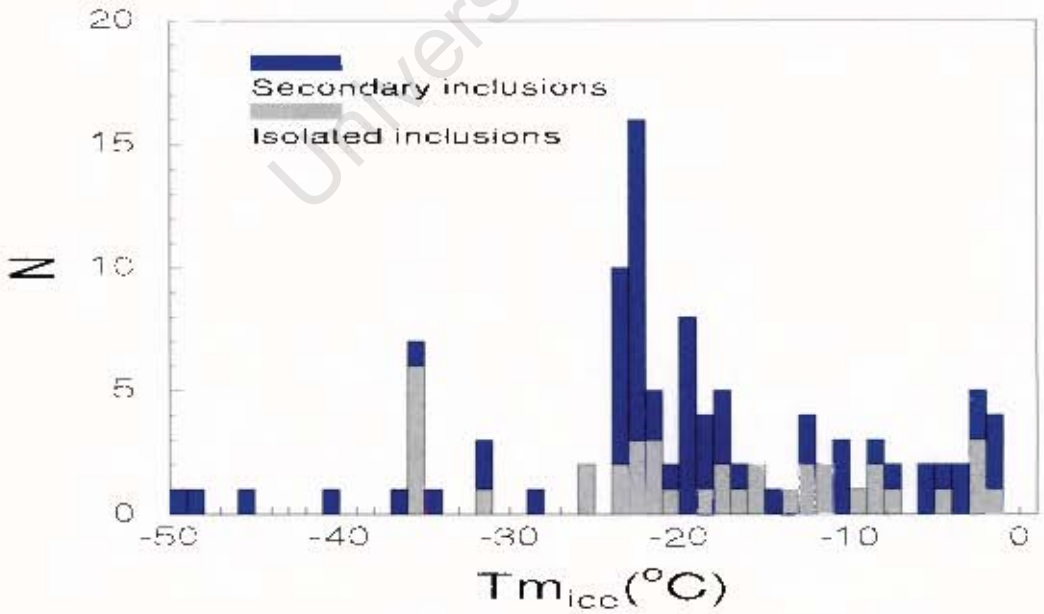

Figure 3.15 Frequency histograms of melting temperatures (Tm_{ice}) values observed in aqueous inclusions preserved in the quartz and quartz-dolomite plugs from the Duruchaus Formation and Hakos Group.

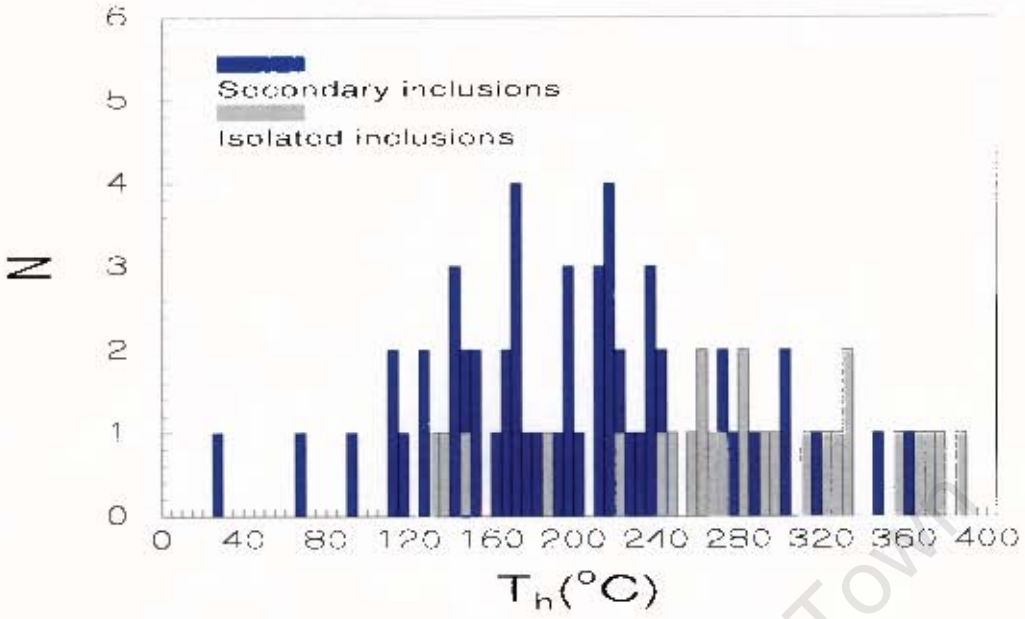

Figure 3.16 Frequency histograms of homogenisation temperatures (vapour to liquid) observed in aqueous inclusions from the quartz and quartz-dolomite plugs of the Duruchaus Formation and Hakos Group.

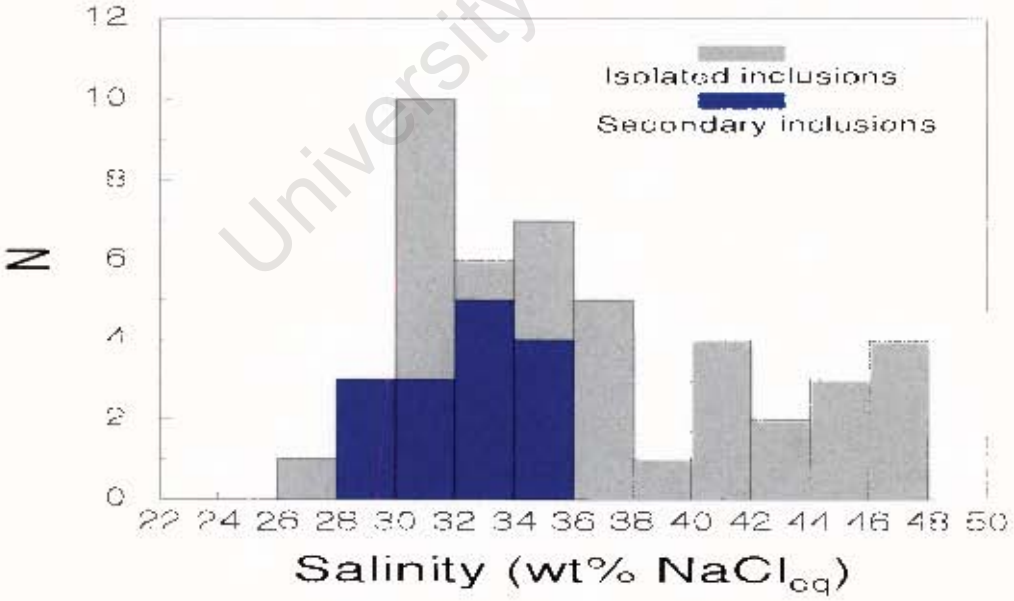

Figure 3.17 Frequency histogram of calculated salinities from halite dissolution temperatures observed in Type I and II inclusions in the Duruchaus Formation plugs and Hakos Group plugs.

The T_e, Tm_{ice} and T_hH_2O values observed in the isolated and secondary inclusions in the Duruchaus Formation vein samples generally conform to that observed in both the Hakos Group plugs and Duruchaus Formation plugs. The data is consistent other than an anomalous sample NP060, which shows secondary Type II inclusions with anomalously low T_e and Tm_{ice} values. Other than that, T_e values of down to –21.3 °C, Tm_{ice} values of between -2.2 °C and 23.4 °C, and T_hH_2O values of 221 °C to 371 °C were observed. Salinities calculated for the isolated inclusions are in the range 34-38 wt% $NaCl_{eq}$.

Rare Type IV isolated inclusions were encountered in samples from the Hakos Group plugs and exhibited homogenisation temperatures (T_hCO_2) of between 6.9 °C and 14.5 °C. Homogenisation was to the vapour phase. Type IV isolated inclusions in the Duruchaus Formation plugs and veins showed a similar (overlapping) range of 3.5 °C to 19.5 °C, and 8.4 °C to 17.3°C, respectively. Secondary Type IV inclusions yielded a similar range of values with an outlier at -20.7°C. Homogenisation was always to the vapour phase.

The T_hH_2O versus Tm_{ice} plot for the aqueous inclusions described shows that the isolated fluid inclusions generally form a higher temperature dataset with the secondary fluid inclusions being more variable in terms of T_hH_2O values (Figure 3.18). The Tm_{ice} values for both these fluid generations lies predominantly in the range -18°C to -24°C. There is a large degree of overlap between the types of fluid inclusions (isolated and secondary) in this plot. The salinities calculated for these inclusion types on the basis of halite dissolution temperatures, though, indicate a variation in salinity between these two fluid generations, the isolated inclusions

showing a range of salinities extending to higher salinities and the secondary inclusions showing a more restricted, lower salinity range (Figure 3.17).

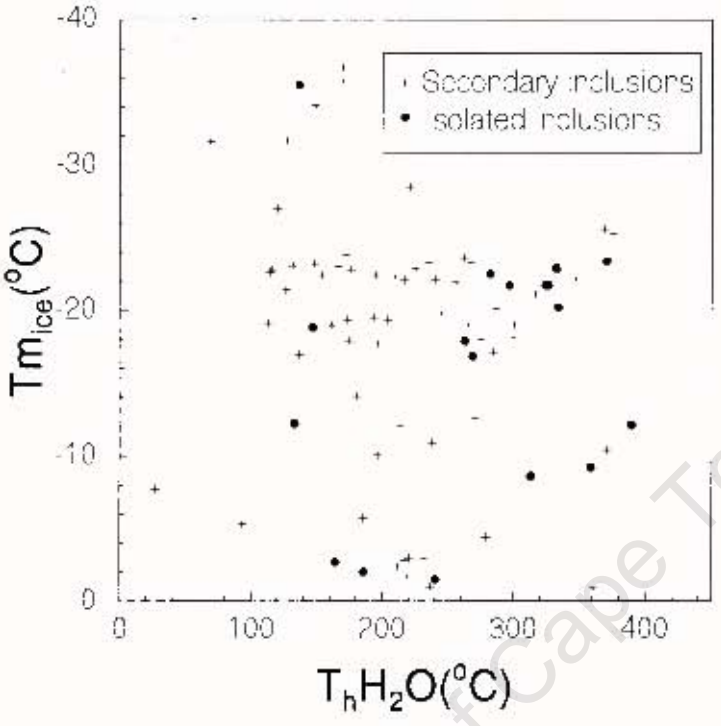

Figure 3.18 Tm_{ice} vs T_hH_2O plot for halite undersaturated aqueous inclusions from the quartz and quartz-dolomite plugs from the Hakos Group and Duruchaus Formation.

Table 3.1 Fluid inclusion results subdivided according to the area of origin in the Duruchaus Formation stratigraphy. T_e values represent the temperature at which melting is first observed and is assumed to be close to the true eutectic temperature for each inclusion.

	$Te(^{o}C)$	$Tm_{ice}(^{o}C)$	$Tm_{clath}(^{o}C)$	$ThH_2O(^{o}C)$	Salinity (wt% NaCl eq.)
Hakos Group					
Type I					
Isolated incl.	-20.0		5.4 to 11.0 (29.3)	130 – 382	38-40wt%
Type II & III					
Isolated incl.	27.4	-8.1 to - 25.6		203 - 390	38-40wt%
Secondary Incl.	36.2	-1.0 to - 22.8		114 - 236	31wt%
Duruchaus Plugs (Duruchaus Formation)					
Type I					
Isolated incl.	28.1	2.1 to - 27.1	1.0 to 10.2 (29.9)	136 - 313	33-17wt%
Secondary incl.	23.2		7.4 to 11.0	160 – 229	32-34wt%
Type II & III					
Isolated incl.	30.0	-1.5 to - 35.5		123 - 334	33-47wt%
Secondary incl.	44.7	-1.5 to - 36.7		127 - 287	32-34wt%
Duruchaus Veins (Duruchaus Formation)					
Type I					
Isolated incl.	26.0		0.4 to 9.7 (19.8)	235 - 366	33-38wt%
Type II & III					
Isolated incl.	-21.3	-2.2 to -23.4		221 - 371	33-38wt%
Secondary incl.	-51.8	-1.0 to - 49.8		144 - 360	

3.4.2 Crush Leach Analyses :

3.4.2.1 Sample Selection and Analysis

Crush leach anaylses of leachates from quartz, dolomite and tourmaline subsamples from the quartz-dolomite plugs and quartz veins from the Duruchaus Formation and Hakos Group were carried out. Leachates from the selected samples were analysed using HPIC (for anionic and cationic concentrations) and ICP-MS (exclusively for determining the Br^- concentration of these fluids) (Appendix I.1b). A combination of these two analytical techniques was used due to the low concentrations of Br^- in the samples analysed (below the detection limits of HPIC). The ICP-MS technique was therefore employed to determine the Br^- concentrations of the fluid inclusion leachates as it has a significantly lower detection limit than the HPIC. Analyses of Na^+ and Cl^- concentrations poses some problems using the ICP-MS technique due to interference effects and high concentrations of these elements in the fluids analysed. A combination of both these techniques was therefore employed to determine the desired anionic and cationic character of the fluid inclusion leachates.

3.4.2.2 Results

The quartz-hosted fluid inclusion leachates were subdivided into those which originate from samples which were halite-oversaturated and halite-undersaturated (from the petrography of the samples and calculated salinities). Na^+ is the dominant cation in both the halite under-saturated and halite over-saturated sample leachates from the Duruchaus Formation plugs and veins, and Hakos Group plugs, with only small amounts of K^+ and Mg^{2+} detected (Figure 3.19). There is a degree of overlap in terms of cationic proportions between the halite-oversaturated and halite-undersaturated fluids but the halite under-saturated fluids show a slight variation extending towards more Ca^{2+}-rich compositions (and Mg^{2+}-rich compositions to a

lesser extent) than the halite-oversaturated fluids (Figure 3.19). The halite-undersaturated fluids are present mainly in the Duruchaus Formation plug samples which therefore show a more Ca^{2+}-rich composition than the Hakos Group plug samples (Figure 3.20).

The tourmaline-hosted fluid inclusion leachates show a marked variation, K^+-rich and Ca^{2+}-rich samples from within the main evaporite sequence, and K^+-poor and Ca^{2+}-poor samples from below the main evaporite sequence. Compositions are extremely variable for these three samples, though. Inclusion leachates extracted from a single dolomite sample, show a distinct chemical character, being dominated by Mg^{2+} and Ca^{2+} ions as would be expected.

Cl^- is by far the dominant anion in the halite-oversaturated fluids (Figure 3.21 and 3.23). Although the halite-undersaturated fluids do contain significant amounts of Cl^-, these fluids tend to be dominated by CO_3^{2-} ions, with significantly greater amounts of Br^- than that seen in the halite oversaturated inclusions (Figure 3.23). Only minor amounts of SO_4^{2-} and $NO3^-$ were detected in both the halite-oversaturated and halite-undersaturated fluid inlcusion leachates.

The CO_3^{2-} value used in Figure 3.23 represents a calculated value on the basis of a charge imbalance which was found to exist in these leachates. Roedder (1984) found that large errors in charge balances can result from the presence of CO_2 in a solution, forming species such as HCO_3^-, H_2CO_3 and CO_3^{2-}. The presence of CO_2 inclusions in the samples analysed and the presence of co-genetic carbonate minerals associated with the sampled quartz plugs, supports the contention that the charge imbalance which is seen in the inclusion leachates reflects a carbonic species. The actual CO_3^{2-}

contents of these leachates was not determined during the analytical runs on the HPIC due to the fact that the eluent used was a $Na_2CO_3/NaHCO_3$ mixture. The calculated values are used to only give an indication of the CO_3^{2-} content of the leachates with the assumption that CO_3^{2-} ions are the only possible remaining anions in solution.

Tourmaline-hosted inclusions from samples from the main evaporite sequence do not contain significant amounts of Cl^- (also seen in Figure 3.25), and are correspondingly more CO_3^{2-}-, NO_3^-- and Br^--rich than their quartz-hosted counterparts. The dolomite-hosted inclusion leachates appear to have a similar character to the quartz-hosted inclusion leachates with respect to their anionic composition. In terms of their area of origin, the fluid inclusion leachates from the Duruchaus Formation samples show higher Br^- and CO_3^{2-} proportions than those from the Hakos Group (Figure 3.22).

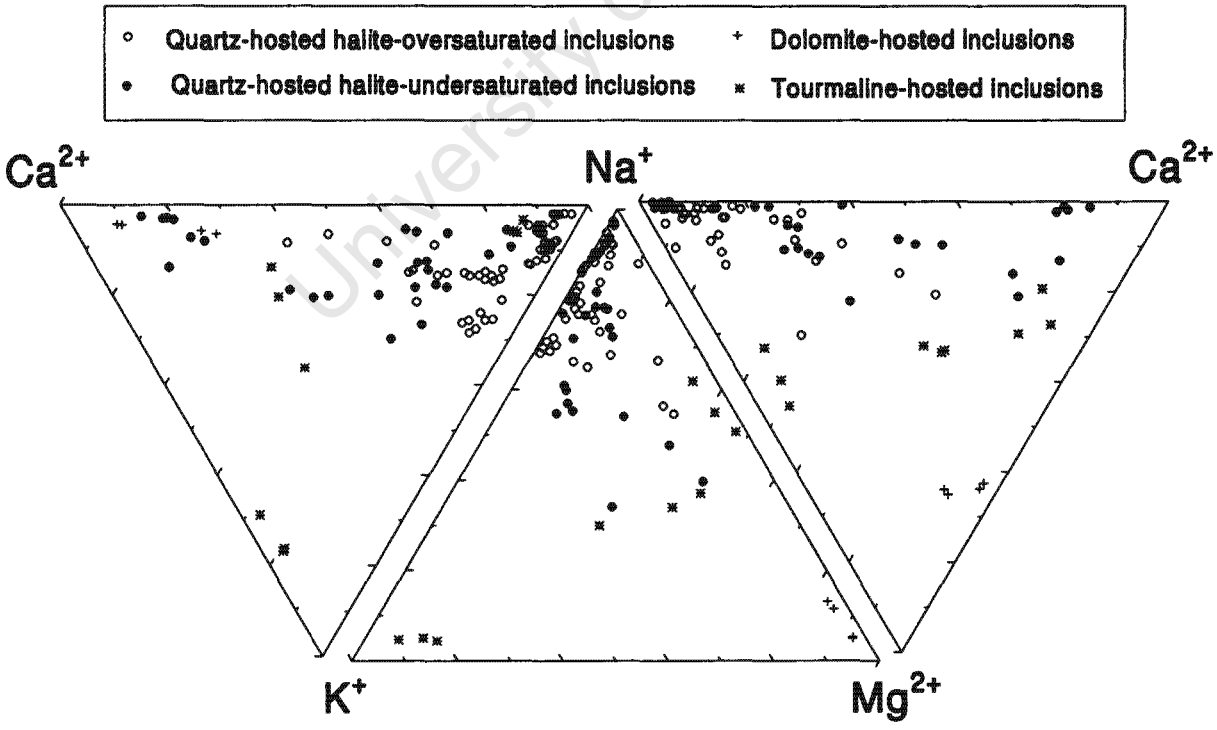

Figure 3.19 Molar proportions of cations in the fluid inclusion leachates from the quartz-dolomite plugs within the Duruchaus Formation and Hakos Group as a function of their mineral hosts.

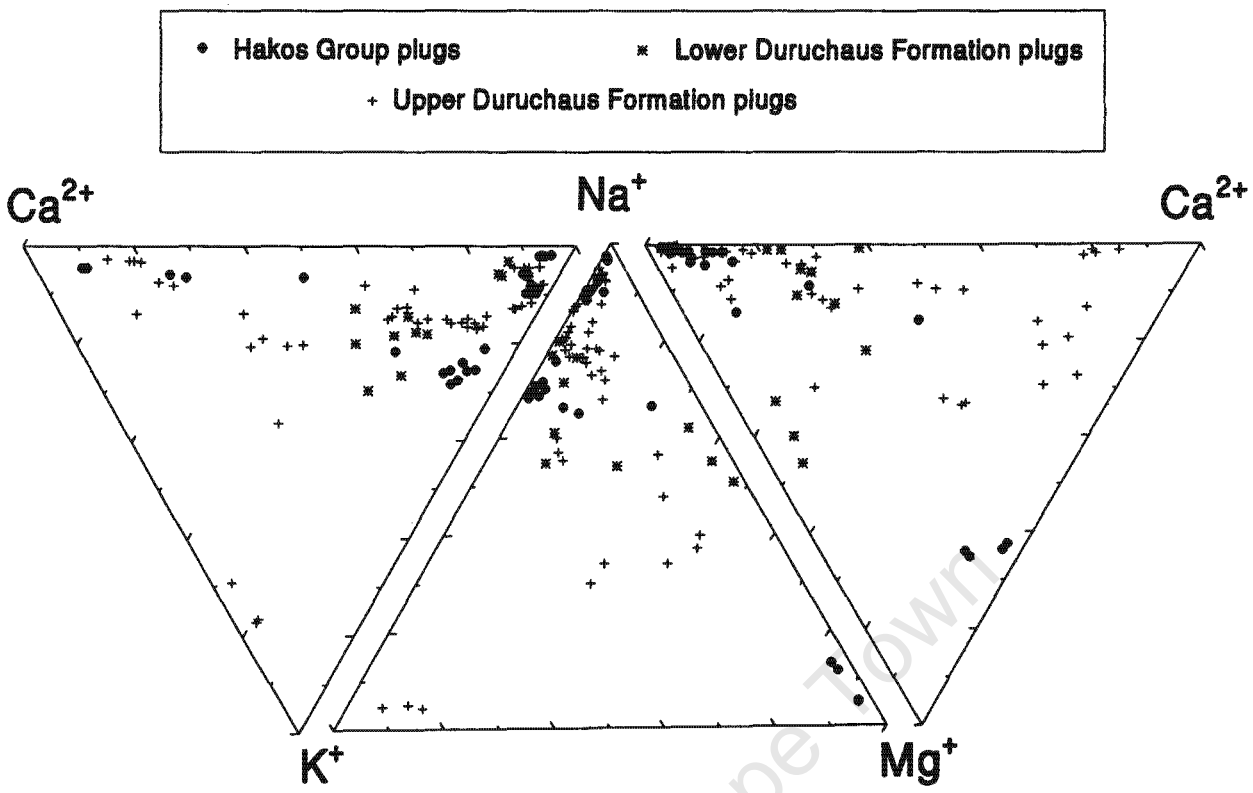

Figure 3.20 Molar proportions of cations in the fluid inclusion leachates from the quartz-dolomite plugs within the Duruchaus Formation and Hakos Group. Subdivisions are on the basis of area of origin within the Damaran stratigraphy.

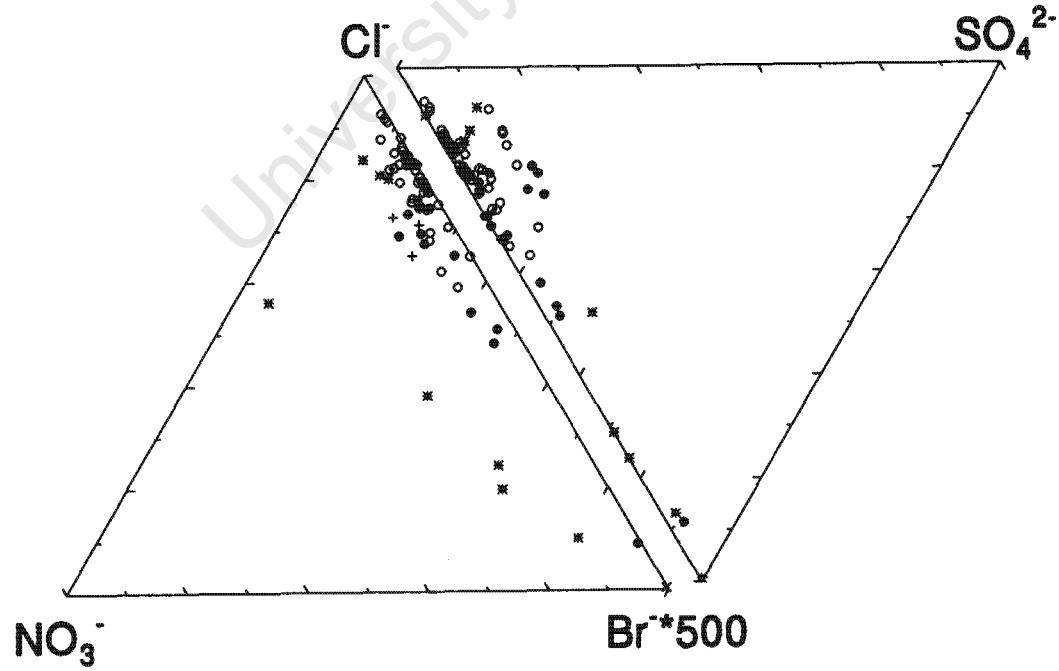

Figure 3.21 Ternary plots showing the molar proportions of anions in fluid inclusion leachates from the Duruchaus Formation and Hakos Group as a function of their mineral hosts; for legend see Figure 3.19.

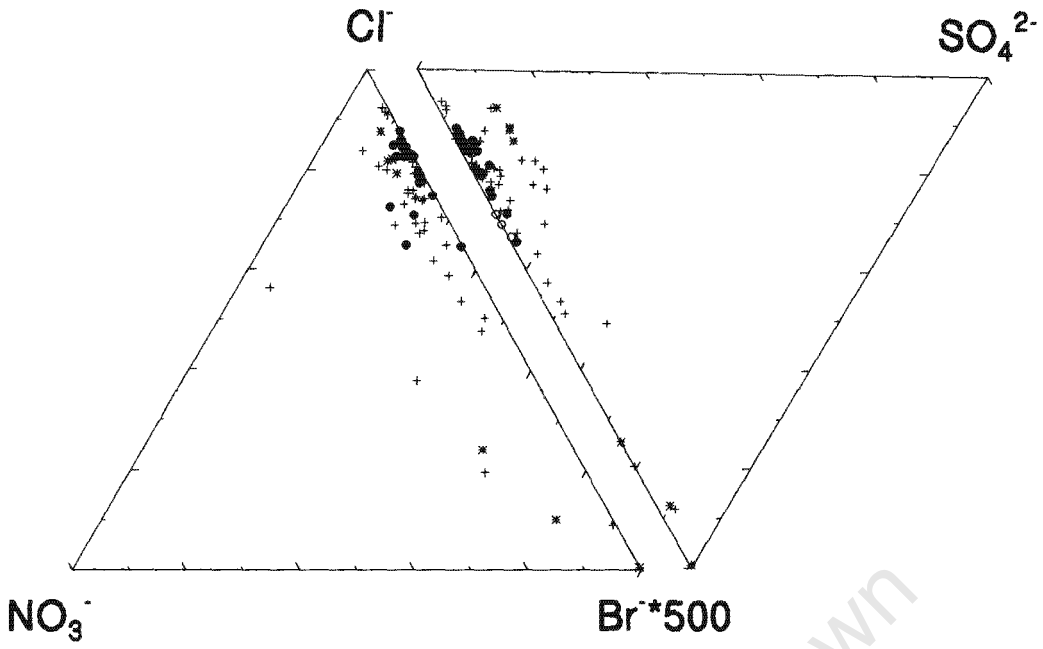

Figure 3.22 Ternary plots showing the molar proportions of anions in the fluid inclusion leachates as a function of their areas of origin in the stratigraphy; for legend see Figure 3.20.

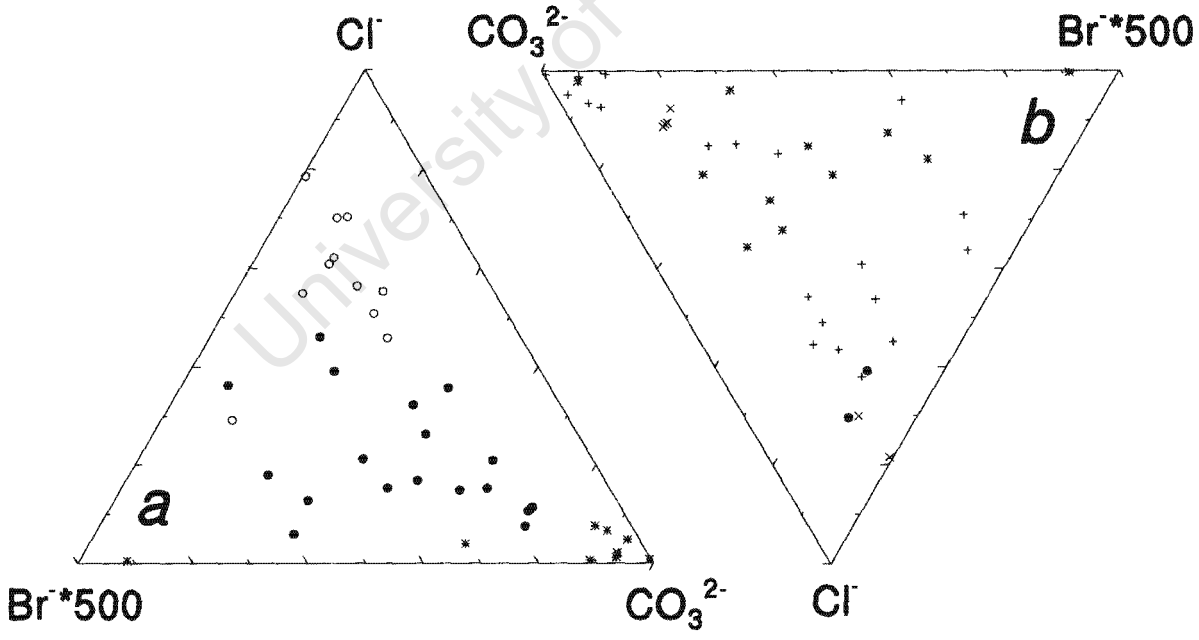

Figure 3.23 Plot of fluid compositional variation of the fluid inclusion leachates from the Duruchaus Formation and Hakos Group using a calculated CO_3^{2-} composition (determined by charge balance calculations). These leachates are plotted as a function of (a) their mineral hosts and (b) their area of origin in the stratigraphy; for legend see Figures 3.19 and 3.20. Points represent molar proportions of each element.

3.4.2.3 Na-Br-Cl systematics of fluid inclusion leachates

The Na-Br-Cl concentrations of fluids has been found to be a useful tool in discriminating between different solute sources for mineralising fluids as well as characterising the source of the mineralising brines (Kesler *et al.*, 1995; Walter *et al.*, 1990). Bromine functions as an effective monitor of the degree of evaporation due to the fact that during the evaporation of seawater, into and beyond halite facies, Br becomes progressively more concentrated in the residual brine (Siemann and Schramm, 2000; Glynn *et al.*, 1992). As seawater evaporates, the Cl/Br ratio of the residual brine remains similar to that of seawater until halite saturation is reached. Further evaporation leads to the precipitation of halite and both the Cl/Br and Na/Br ratios in the residual brine become progressively lower than that of seawater. Residual brines that are separated from the precipitated evaporite minerals will therefore reflect this degree of evaporation. However, brines which remain in contact with the precipitated evaporite minerals can experience the dissolution of halite and other previously precipitated evaporitic minerals, which would enrich the brine in Na^+ and Cl^- relative to Br^-. This results in a brine with Cl/Br and Na/Br ratios which are considerably higher than that of seawater (Figure 3.24). The molar ratios therefore allow one to distinguish brines which derive their salinity from simple halite dissolution and those which derive their salinity from the evaporation of seawater.

Ratios rather than absolute concentrations are used due to the fact that the absolute concentrations of Na, Cl and Br are dependant on the amount of dilution that the fluids were subjected to during sample preparation, and in the case of fluid inclusion analyses, the amount of fluid present in the fluid inclusions, both of which are not constant. The ratios therefore allow the comparison of fluids from different areas in

terms of their Na, Cl, and Br contents regardless of the variation in fluid volume or dilution.

Na/Br versus Cl/Br ratios of the absolute Na, Br, Cl concentrations of the leachates from the quartz, tourmaline and dolomite subsamples mentioned earlier, are presented in Figures 3.25 and 3.26. A large number of samples from the Duruchaus Formation and Hakos Group plugs follow the halite dissolution trend (Figure 3.25). Petrographic examination of the fluid inclusions in these samples as well as calculated salinities (previous section) showed that these samples are generally saturated with respect to halite and it is thus likely that they experienced some halite dissolution during their fluid evolution. The Cl/Br ratios seen in these samples also support this contention, generally falling within the range expected for evaporitic fluids which have experienced halite dissolution, i.e., Cl/Br ratios in the thousands (Holser *et al.*, 1979).

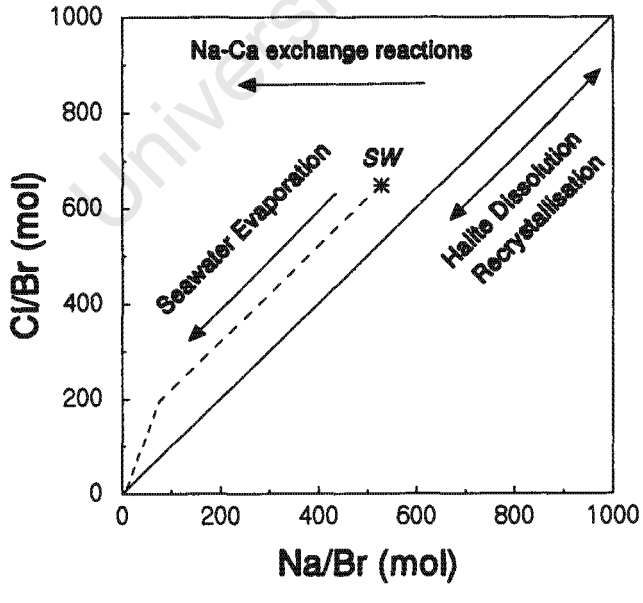

Figure 3.24 Schematic plot showing Na-Br-Cl systematics for sea water and associated evaporitic brines (after Kesler *et al.*, 1995).

In contrast, fluid inclusions in the leachate samples which lie below the sea water marker, are conspicuously lacking in halite daughter crystals and are thought to be representative of the initial character of the evaporitic (connate) fluid. The plots therefore show samples that are divided into those which are halite under-saturated and halite over-saturated. The tourmaline samples are presented separately as no petrographic or fluid inclusion data are available for them. However, from their positions in Figure 3.25, and their generally lower Na^+ concentrations in Figure 3.19, it can be inferred that they are under-saturated with respect to halite. These tourmaline samples show no relationship with the sea water evaporation line, though.

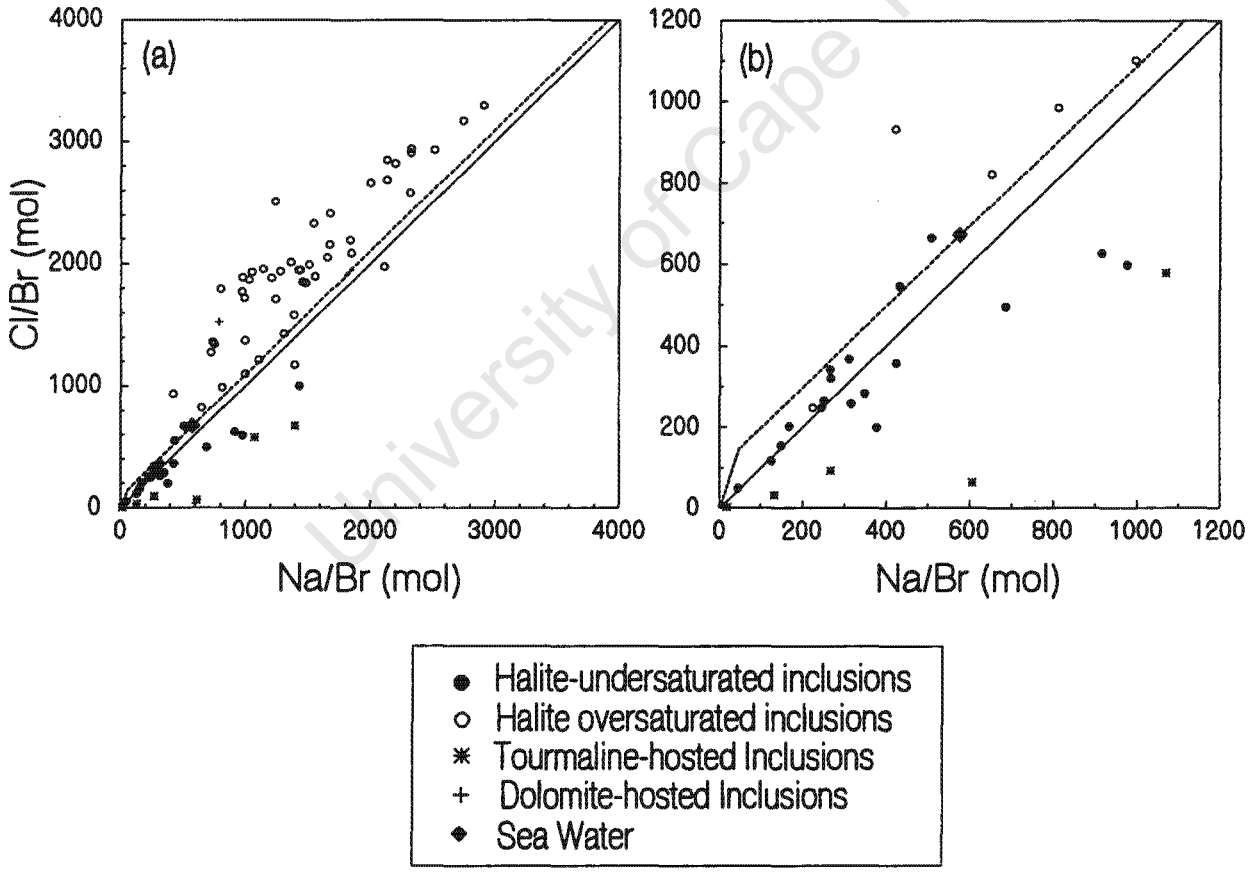

Figure 3.25 (a) Na-Br-Cl systematics of fluid inclusion leachates from selected plug samples from the Duruchaus Formation and Swakop Group using the composition of sea water as a reference. The halite under-saturated and over-saturated inclusions are hosted in quartz. Sea water composition is quoted from Horita *et al* (1991). (b) Enlargement of (a) showing the distribution of halite under-saturated inclusions more clearly.

The leachates from the Hakos Group plugs tend to be oversaturated with respect to halite while the leachates from the Duruchaus Formation plugs and veins are more variable, some samples being halite-oversaturated and others halite-undersaturated. This explains the distribution of data in Figure 3.26, whichs shows that the Hakos Group plugs generally have higher Cl/Br and Na/Br ratios than sea water, while the Duruchaus Formation plugs and veins show a variable character, extending from below the sea water marker to above the sea water marker along the halite dissolution trend.

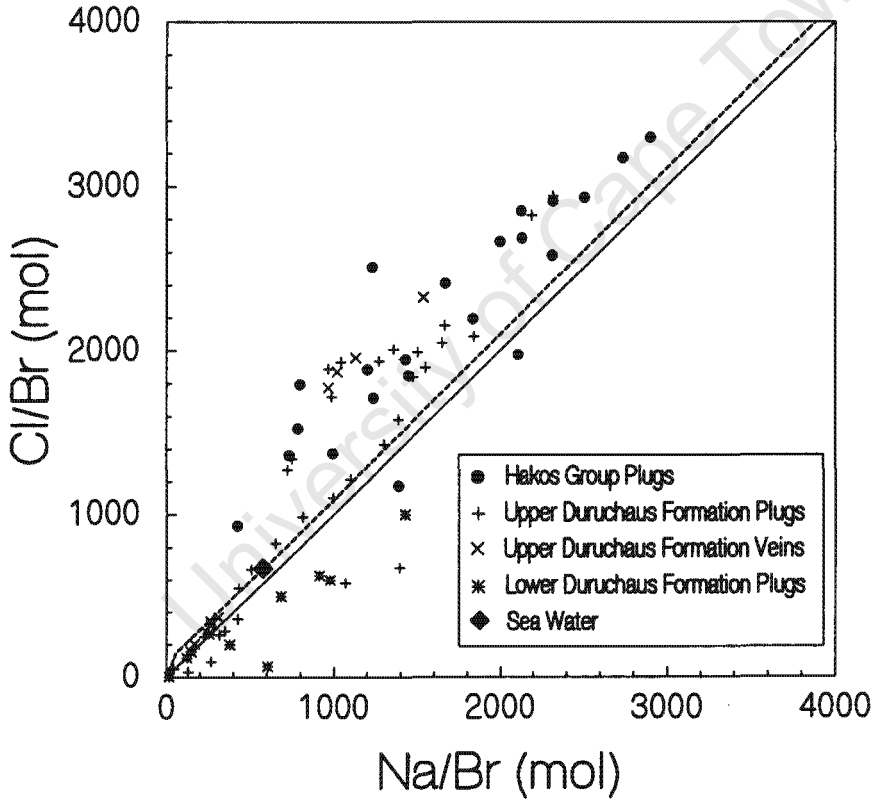

Figure 3.26 Plot showing the distribution of leachates in Na-Br-Cl space, subdivided according to their positions in the Damaran stratigraphy.

3.5 Discussion – The Type Locality

3.5.1 Depositional Environment

On the basis of the whole rock chemistry of the units which make up the Duruchaus Formation, it was possible to make some judgements on their probable environment of deposition. It was first necessary, however, to assess to what the degree the original chemistry of the units had been altered.

Alteration

The chemical index of alteration (CIA) of the units within the Duruchaus Formation shown graphically in Figure 3.6, indicates that a combination of three geochemical processes produced the CIA trends shown by the units today (see section 3.3.1.2). A chemical weathering trend combined with some K^+–Na^+ exchange (most likely in the feldspar grains present in these units) is indicated in the units below the main evaporite sequence. The K^+–Na^+ exchange process is supported by the petrography of these samples as it is found that most samples that plot on the right hand side of the ternary diagram (mainly arenites) with low CN (CaO +Na_2O) values, contain significant amounts of K feldspar, with little or no plagioclase (Appendix II). Late stage albitisation of the units within the main evaporite sequence, observed in the field, is thought to have resulted in a more Na-rich chemistry of these units (Figure 3.7). The degree of albitisation was variable resulting in a spread of samples extending towards the CN (CaO+Na_2O) apex, mirroring the trend of the unalbitised pelite sample towards the albitised pelite sample (Figure 3.6).

The arenite shows a shallow weathering trend, with a small increase in CN values after albitisation, while the pelite shows a much steeper change in CIA values with a

more pronounced increase in CN values after albitisation. An examination of the independant variation of Na and Ca in the pelitic and arenaceous units, revealed that the change in Na concentrations from below to within the main evaporite sequence is much more pronounced in the arenaceous units. The steep change in CN values seen in the pelitic units is thought to be due to the effect of Ca in the form of carbonates present in these units.

The dominant process that seems to have affected the major element chemistry of the evaporitic units within the main evaporite sequence in the Duruchaus Formation is therefore albitisation which overprints the original geochemistry of these units. The effect of this process on the whole rock chemistry therefore needed to be evaluated in order to characterise the original geochemistry of the protoliths. This was attempted using the rare earth element and trace element trends of the units from the main evaporite sequence.

The trace and rare earth element trends in all the units within the main evaporite sequence show a large degree of overlap, irrespective of lithology (Figure 3.11). The units below the main evaporite sequence show varied trends, normally consistent within each lithotype (carbonates, pelites, arenites), and different between lithotypes. Late stage albitisation of the main evaporite sequence is thought to have affected the trace element and rare earth element concentrations of the units of the main evaporite sequence and is thought to account for the large degree of overlap between the upper continental crust normalised-trace element trends of all lithological units preserved there (Figure 3.11). This is borne out by Figure 3.27 which shows the trace element distribution of an albitised pelite unit and an associated unalbitised pelite from the Hakos Group.

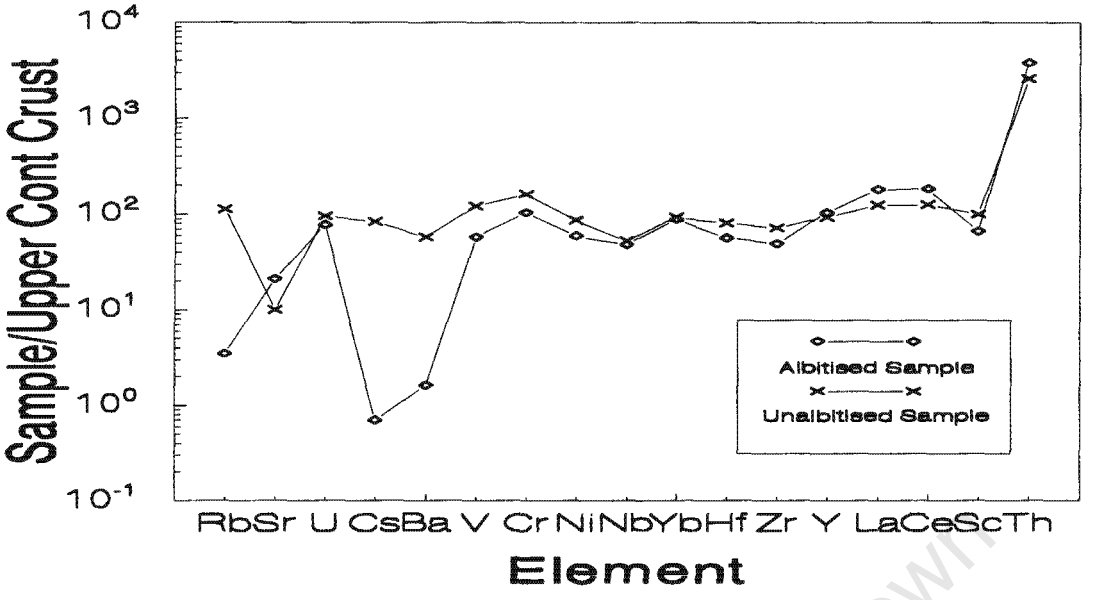

Figure 3.27 Multi-element variation diagram for an albitised and associated unalbitised pelitic unit within the Hakos Group. Upper continental crust values are from Taylor and Mclennan (1981).

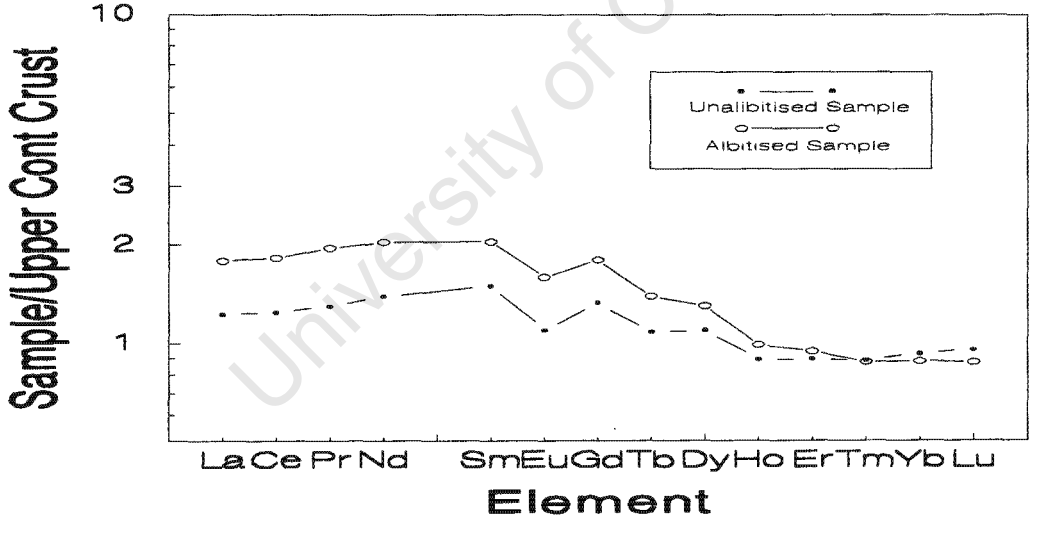

Figure 3.28 Rare earth element plot for the albitised and unalbitised pelitic unit in Figure 3.27. Upper continental crust values are from Taylor and Mclennan (1981).

The albitised pelite in Figure 3.27 shows a trace element pattern consistent with that displayed by the units within the main evaporite sequence suggesting that the process of albitisation has overprinted the original geochemical signatures of the all

lithological units found there. The rare earth element trend shown by the albitised pelitic unit, though, seems relatively unaffected by the albitisation, other than a slight enrichment in the light rare earth elements (Figure 3.28). The rare earth element trends of the arenaceous and carbonate units within the main evaporite sequence, however, are characterised by a light rare earth element depletion. From the field evidence, it was observed that the more porous units were being albitised preferentially when compared to the less porous pelitic units. The effect of the albitisation on rare earth element trends is therefore thought to be variable depending on the lithology of the units. The trace element trends shown by these units provide a more clear indication of albitisation in these units, the albitisation trend being characterised by negative Rb, Cs and Ba anomalies. Furthermore, the albitisation is observed only in the main evaporite sequence. The preferential albitisation of these units argues for a local source of Na which is most likely derived from halite dissolution.

Depositional Environment

The steep light rare earth enrichment patterns in the chondrite-normalised plots and flattening of all these patterns in the upper continental crust-normalised diagrams, argues for a continental provenance for the units of the Duruchaus Formation (Figures 3.8 and 3.9).. The positive Yb, Y and Th anomalies exhibited by all lithological units (Figure 3.11) suggests a consistent source area for the units of the Duruchaus Formation throughout the period of deposition. The variation in the more incompatible elements (Figure 3.11) are clearly due to a lithological control as the

trends described are consistent within each lithological grouping, i.e., arenaceous units, carbonate and pelite.

The positive Ce and Eu anomalies within the carbonate units in the main evaporite sequence are interpreted as diagenetic features (see section 3.3.2.2). Although there is a slight rare earth element depletion seen in the upper continental crust-normalised plots of the albitised main evaporite sequence, the Ce and Eu anomalies in these units are still evident (Figure 3.9). Positive Ce anomalies have been recorded previously in continental alkaline, carbonate-rich, aerobic lake waters (Möller & Bau, 1993). Positive Ce anomalies are thought to result from the oxidation of Ce^{III} to Ce^{IV} and the stabilisation of these ions by higher order solution complexation with CO_3^{2-} in solution. CO_3^{2-} is one of the dominant anions in continental waters and is thus available for complexation with the Ce ions present in solution. Marine carbonates, in contrast to this, are characterised by negative Ce anomalies (Rollinson, 1993). The Ce^{IV} once formed in marine waters precipitates out as CeO_2. The appearance of positive Ce anomalies in the carbonates within the main evaporite sequence therefore argues for a continental setting for these evaporites. The crush-leach data supports this interpretation as the calculated CO_3^{2-} concentration in the fluids preserved within the quart-dolomite plugs in the Type Locality is comparable to that seen in non-marine (continental) waters. The presence of a negative Ce anomaly in one of the carbonates below the main evaporite sequence suggests a slight marine influence on the lower Duruchaus Formation before the deposition of the main evaporite sequence (Figure 3.9).

The formation Eu^{2+} in reducing environments may result in the preferential partitioning of the Eu^{2+} into the precipitating mineral phases, e.g., carbonates, oxides,

etc (Rollinson, 1993). The residual fluid is may thus characterised by a negative Eu anomaly. Oxidising depositional environments are reflected by positive Eu anomalies. The positive Eu anomalies seen in the upper continental crust-normalised plots of some of the carbonate units in the main evaporite sequence (Figure 3.9), therefore suggests an oxidising environment of deposition for the units. This is supported by the presence of sphene/rutile after ilmenite in all of the sampled units (Petrography – Appendix II).

To summarise, the whole rock geochemical data suggests a strong continental influence on the Duruchaus Formation sediments. The positive Ce anomalies and strong light rare earth enrichment patterns seen in the main evaporite sequence seem to indicate a continental origin for these evaporites, possibly in an oxidising, continental playa lake-type environment. The source region for these sediments appears to be consistent being characterised by a marked Th enrichment (with moderate positive Y and Yb anomalies and negative Nb anomalies).

The presence of tourmaline within an sequence of units can potentially be a useful indicator for the presence of former evaporitic beds (Slack *et al.*, 1984). The chemistry of the tourmaline grains sampled within the Duruchaus Formation indicates that a Ca-poor metapelitic or metapsammitic unit was the original host rock for these tourmaline grains (Figures 3.3 and 3.4). As a more dravitic composition may be indicative of an *in situ* evaporitic tourmaline (Henry aand Dutrow, 1996), it is speculated that tourmaline grains from the main evaporite sequence (NP035) originate from former evaporitic borates within the main evaporite sequence of the Duruchaus Formation. Remobilisation of the tourmaline in the vein samples (NP059 and NP021) could possibly account for the more Fe-rich character of these grains.

3.5.2 Fluid Character

With regards to the fluid inclusions in the quartz and quartz-dolomite plugs and veins sampled from different parts of the stratigraphy, the following can be observed. The overlap of T_e, Tm_{ice} and T_hH_2O values observed in the fluid inclusions from the different plugs sampled (Figures 3.14 to 3.16) points to a similar history with respect to the fluid generations for all the sampled areas. This indicates that the fluids preserved in these plugs originate from a similar source and can thus be regarded as one dataset for the objectives of this study. Although there is a overlap of the T_hH_2O, Tm_{ice}, T_e values and salinities for both the isolated and secondary inclusions in Figures 3.14 to 3.17, it may be speculated on their respective mean values that two genetically related fluid generations exist, one extending to T_hH_2O values (and higher salinities) and the other to slightly lower T_hH_2O values (with similar but slightly lower salinities) (Figures 3.16 and 3.17).

There are some very high T_hH_2O values observed in the both the isolated and secondary inclusion datasets. Necking of fluid inclusions occurs to varying extents in some samples. This along with the presence of small amounts of CO_2 which seems to be present in various quantities in these inclusions (indicated by the presence of CO_2 inclusions and clathrate-bearing inclusions in the samples analysed), can explain the large range of T_hH_2O values observed and potential outliers seen. The possibility exists that some of the interpreted aqueous inclusions contain small but undetectable amounts of CO_2. These inclusions should be classified clathrate-bearing but because of the small amounts of CO_2 in these inclusions, no Tm_{clath} values could be observed. An assessment of the amount of CO_2 present in these inferred clathrate-bearing inclusions was carried out as follows. Assuming that the Type I, II and IV isolated inclusions are co-genetic, and that the $X(CO_2)$ values observed at T_hCO_2 are

reasonably accurate, an estimate of the amount of CO_2 in the inferred clathrate-bearing inclusions in the samples can be made using the phase relations in the NaCl-CO_2-H_2O system (Bowers and Helgeson, 1983) (Figure 3.29). The solid lines in this figure represent an unmixing path of a NaCl-CO_2-H_2O fluid into its CO_2-rich and NaCl-H_2O-rich end members during cooling. Using an X(CO_2) value of between 60 and 80% (observed in the Type IV inclusions in this study) for the CO_2-rich end member, an estimated 5% CO_2 is indicated to be present in related NaCl-H_2O-rich end member (Figure 3.29). Predicted total homogenisation temperatures for such a fluid are in the range 400°C to 550°C which conforms well to the high T_hH_2O ranges observed in the Type I and II inclusions inclusions from the Duruchaus Formation and Hakos Group Plugs. This suggests that the Type I (+ some Type II) and Type IV inclusions in the Duruchaus Formation and Hakos Group plugs could represent carbonic-bearing and carbonic-rich end-members of fluids that were formed by H_2O-NaCl-CO_2 fluid unmixing prior to entrapment.

The range of T_hH_2O values below 400°C, however, cannot wholly be ascribed to variable CO_2 contents. The effect of necking in the secondary inclusions was minimised by selecting secondary inclusion trails which showed consistent liquid/vapour and liquid/vapour/solid ratios for microthermometric study, and then averaging out the Tm_{ice} and T_hH_2O values of the inclusions in each trail. An alternative explanation for the wide range in T_hH_2O observed in the samples from the Type Locality could be entrapment under varying pressure conditions. This is examined further in the next section (geothermobarometry).

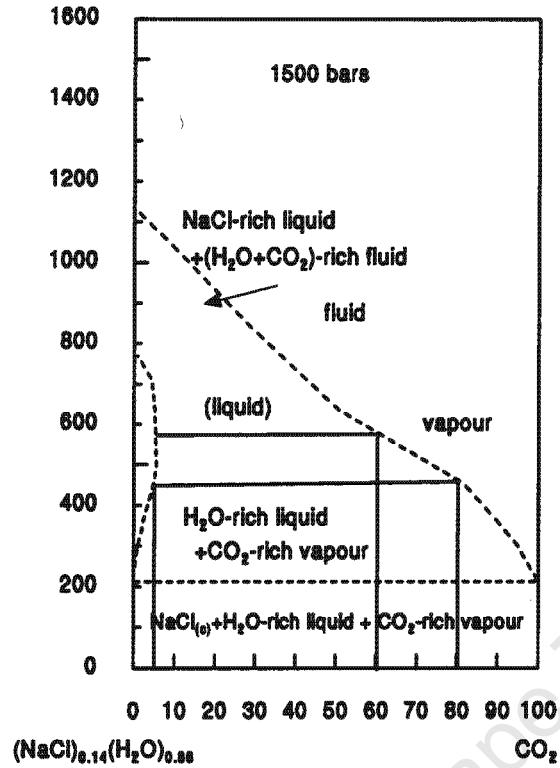

Figure 3.29 Temperature-Composition diagram for the system NaCl-H_2O-CO_2, assuming a salinity of 35 wt% $NaCl_{eq}$ (after Bowers and Helgeson, 1983).

The low T_e values (down to –44°C) observed in the inclusions from the Duruchaus Formation and Hakos Group plugs suggests the presence of divalent cations (Ca^{2+} and Mg^{2+}) in these fluids, in addition to NaCl (Goldstein and Reynolds, 1994). Eutectic temperatures of between –40°C and –30°C are regarded as difficult to interpret due to the appearance of intermediate phases and metastable assemblages during freezing and heating of multi-component fluid inclusions (Goldstein and Reynolds, 1994). Observed T_e values for the system KCl-NaCl-H_2O, $CaCl_2$-NaCl-H_2O and $MgCl_2$-NaCl-H_2O are presented in Table 3.2. The range of T_e values observed in the samples from the Duruchaus Formation and Hakos Group are consistent with a combined T_e value representing a mixture of these three components (KCl, $CaCl_2$, $MgCl_2$) in addition to NaCl and H_2O.

Table 3.2 Summary of predicted stable eutectic, predicted metastable eutectic and observed eutectuc temperatures (T_e) from various aqueous systems (after Davis *et al.*, 1990).

System		*Te(°C)*	
$NaCl-H_2O$	stable	-21.2	
	metastable	-28	
	observed	-21.1 to –21.2	
$NaCl-CaCl_2-H_2O$	stable	-52	
	metastable	-70	
	observed	-47 to –53	
$NaCl-MgCl_2-H_20$	stable	-35	
	metastable	(-37 to –55)	-80
	observed	(-33 to –40), (-45 to –50)	(-70 to –80)
$NaCl-KCl-H_2O$	stable	-22.9	
	metastable	-28	
	observed	(-23.0 to 23.4)	

The fluid compositions of the leachates in the crush-leach study confirm the observations made on the microthermometric data. Ca^{2+}, Mg^{2+} and K^+ are indeed present in solution (resulting in the range of eutectic temperatures observed in the fluid inclusion study). The cations are thought to be present as dissolved chloride complexes, sulphuric or carbonic compounds. The dominance of Cl^- and CO_3^{2-} ions in these fluids suggests that most of the cations are present as dissolved salts of chloride and/or carbonic compounds.

A plot of Cl^-/CO_3^{2-} versus $Na^+/(Ca^{2+}+Mg^{2+})$, for the fluid inclusion leachates from the Type Locality (Figure 3.30), shows that the halite-oversaturated fluids and some of the halite-undersaturated fluids are characterised by a predominance of Cl^- over CO_3^{2-}, exhibiting Cl^-/CO_3^{2-} values of >1 (Figure 3.30). This indicates that Mg^{2+} and Ca^{2+} in

these fluids are (at least in part) present as dissolved salts of $MgCl_2$ and $CaCl_2$. The halite-undersaturated fluids which plot on the 1:1 in Figure 3.30 are probably characterised by Mg^{2+} and Ca^{2+} in the form of dissolved carbonates, with Na^+ as a dissolved salt of NaCl (Figure 3.30). The Ca^{2+} and Mg^{2+} as well as some Na^+ in the tourmaline-hosted inclusions and the halite-undersaturated inclusions (which lie below the 1:1 line), are thought to be present as dissolved carbonates.

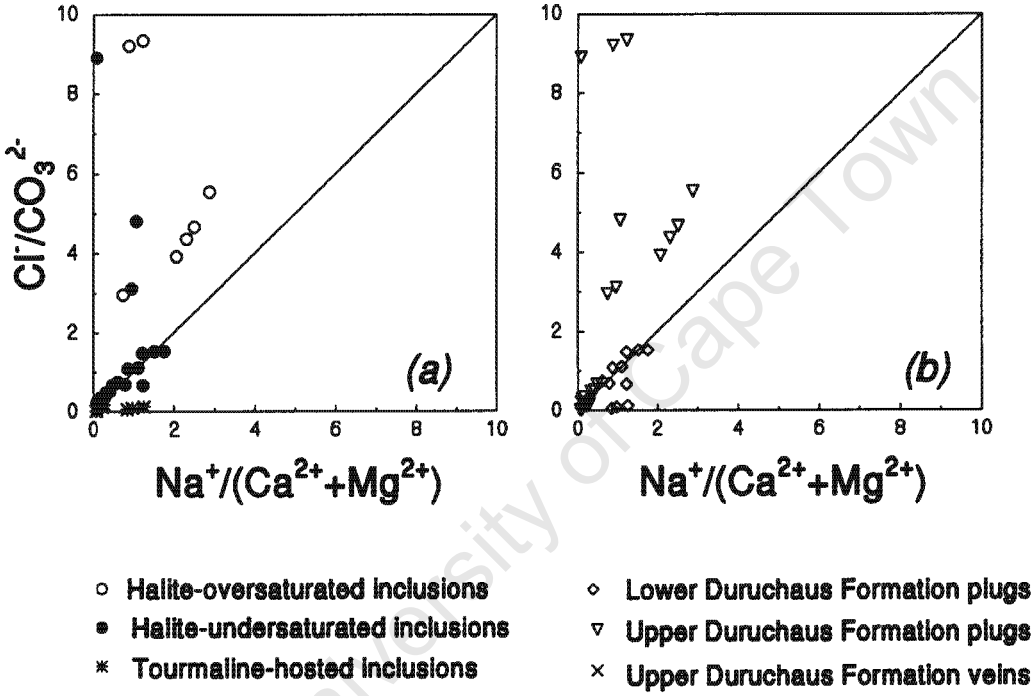

Figure 3.30 $Na^+/(Ca^{2+}+Mg^{2+})$ versus Cl^-/CO_3^{2-} diagram for fluid inclusion leachates originating from the Duruchaus Formation quartz and quartz-dolomite plugs on the basis of (a) mineral hosts and (b) area of origin. CO_3^{2-} represents a calculated composition on the basis of an existing charge imbalance in these leachates.

3.5.3 Geothermobarometry

Using the microthermometric data described in section 3.5.2, it is possible to derive the trapping conditions of the fluids preserved in the Duruchaus Formation and Hakos Group plugs. Using the FLINCOR software (Brown, 1989), an estimated composition of $NaCl-H_2O$, and the Brown and Lamb (1989) equation of state, the densities of the fluids in the isolated and secondary fluid inclusions were calculated. The fluids preserved as inclusions in the Type Locality are clearly multi-component, containing significant amounts of Na^+ and Ca^{2+}, and Mg^{2+} to a lesser extent. The $NaCl-H_2O$ system was used as a model system, nevertheless, as cotectic surfaces where ice melts for the systems $NaCl-H_2O$, $NaCl-CaCl_2-H_2O$, and $NaCl-MgCl_2-H_2O$ lie essentially on top of each other, with <2% deviation (Oakes *et al.*, 1990; Davis *et al.*, 1990).

The calculated isochores (Figure 3.31) are based on the lowest and highest T_hH_2O values observed in the isolated and secondary inclusions in the Duruchaus Formation plugs and veins, and Hakos Group plugs. The fluid densities calculated for the Hakos Group fluids lie in the range 0.77 to 0.93 g/cm^3 for the isolated inclusions and between 0.83 and 1.19 g/cm^3 for the secondary inclusions. Fluid densities for the Duruchaus Formation fluids are between 0.87 and 1.05 g/cm^3 for the isolated inclusions, and between 0.95 and 1.1 g/cm^3 for the secondary inclusions.

In the previous section it was found that the range of T_hH_2O observed in the inclusions preserved in the Hakos Group plugs and Duruchaus Formation plugs and veins cannot be explained by CO_2 contamination alone. An alternate explanation that is proposed for this range of T_hH_2O values is a fluctuation between the influence of hydrostatic and lithostatic pressure during the trapping of the fluids preserved in these inclusions. Henderson and McCaig (1996) found on examination of quartz veins associated with normal and reverse movement of faults within a shear zone in the

French Pyrenees, that the range of T_hH_2O observed in these inclusions could possibly be explained by a fluctuation between lithostatic and hydrostatic pressure during the trapping of the preserved fluids. The plugs and veins in the Hakos Group and Duruchaus Formation are speculated to have been emplaced during thrusting in the SMZ. Such a fluctuation between hydrostatic and lithostatic pressure in this environment is therefore possible. The lines representing the maximum lithostatic and hydrostatic pressures in Figure 3.31 were produced using an average rock density of 2.7 g/cm^{-3}, and a geothermal gradient of 30°C/km. An independent estimate of a peak metamorphic temperature and pressure of between 560°C to 580°C, and 6-8 kbar from Hoffer (1983), Hoernes and Hoffer (1979), and Kasch (1983a) for the SMZ are presented as a field in Figure 3.31.

If peak metamorphic temperatures of 560-580°C are assumed then the data presented in Figure 3.31 suggests that the higher temperature isolated inclusions were trapped under lower (hydrostatic) pressures whereas the lower temperature isolated inclusions and the secondary inclusions were trapped under higher (lithostatic) pressures. The range of lithostatic pressures indicated to be in operation at peak metamorphic temperatures (560-580°C) during the trapping of the fluids preserved in the inclusions in the SMZ (4.2 to 9 kbar) overlaps with the pressures calculated on the basis of garnet-plagioclase barometry (6-9 kbar) for units in the SMZ from Kasch (1983a) and Hoffer (1983). A possible explanation of this fluctuation in pressure recorded by these inclusions, is the entrapment of the higher temperature isolated fluid inclusions during thrusting in the SMZ, when fracturing created pathways for fluid flow (to the surface) resulting in a hydrostatic pressure during this time. Sealing of the fractures by crystallisation of mineral phases or by the weight of the overburden, resulted in a

higher lithostatic pressure being in operation during the trapping of the lower temperature isolated fluid inclusions, and the secondary fluid inclusions.

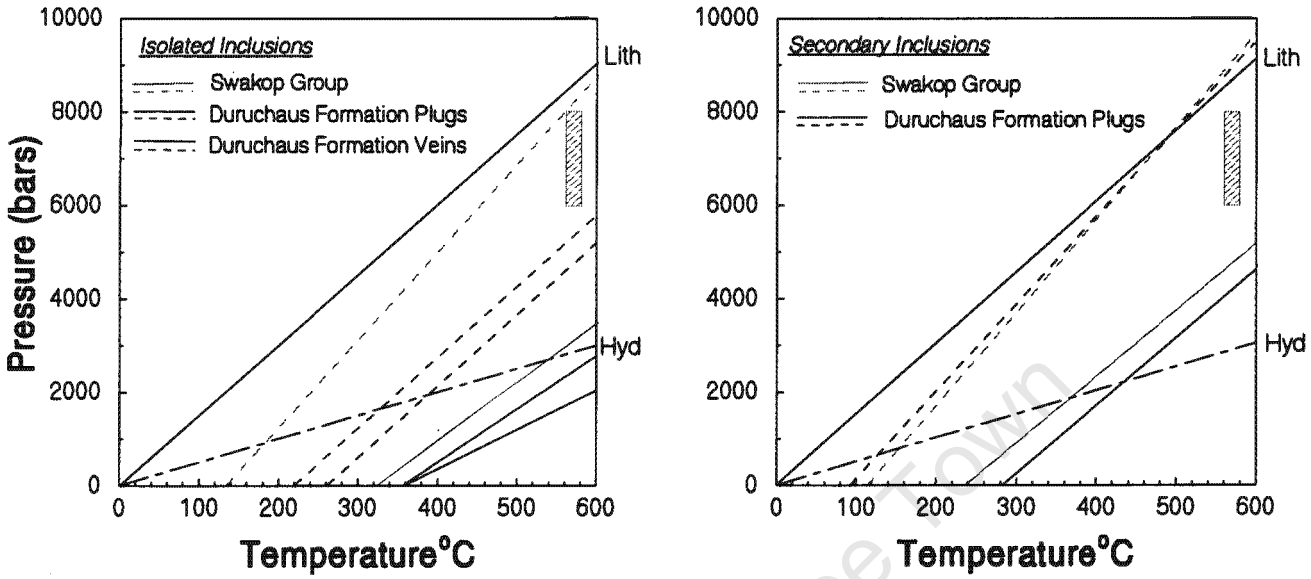

Figure 3.31 Geothermobarometry results based on the fluid inclusion data from the Duruchaus Formation Plugs and Veins, and Hakos Group Plugs. The dashed lines represent isochores for the lowest homogenisation temperatures and the solid lines represent the highest homogenisation temperatures recorded in the isolated and secondary inclusions. The green field represents an estimated peak metamorphic pressure and temperature from Kasch (1983a) and Hoernes and Hoffer (1979). (Lith=lithostatic pressure; Hyd=hydrostatic pressure).

A combination of variable CO_2 content in the aqeuous inclusions and fluctuation of the pressure of entrapment of the fluid inclusions is thus thought to have caused the range of T_hH_2O values observed in the inclusions from the Duruchaus Formation and Hakos Group plugs.

3.5.4 Fluid Source

The likely candidates that represent a possible source for the highly saline fluids preserved in the Duruchaus Formation plugs and Hakos Group plugs are retrograde metamorphic fluids and evaporite-derived connate fluids. Magmatic fluids were eliminated from consideration due to the lack of suitable intrusives in the area examined which could have represented a possible late-stage magmatic fluid source. Prograde metamorphic dehydration fluids were eliminated due to the high salinities of fluids in the Type Locality.

Retrograde metamorphism involving the rapid rehydration of earlier higher grade metamorphic assemblages have been found to produce fluids of high salinity (Bennett and Barker, 1992). However, the evidence presented thus far seems to be inconsistent with such an origin for the fluids from the Duruchaus Formation. Retrograde features, e.g., chloritisation of units and minerals or sericitisation of feldspars, are not seen in the sampled units from the SMZ or the associated plug and vein samples. This along with the low grade of metamorphism associated with the sample area argues against a locally derived retrograde metamorphic fluid. Retrograde fluids originating from higher grade metamorphic terrains in the vicinity of the sample area, e.g., from the Hakos or Swakop Group, can also be a likely fluid source, infiltrating the Duruchaus Formation along thrust zones or the basement contact. The relatively high Br^- contents of the fluids preserved in the Type Locality is, however, difficult to reconcile with a retrograde metamorphic origin but may be readily explained by an evaporitic origin.

The Na-Br-Cl concentrations in the quartz-hosted fluid inclusion leachates from the Duruchaus Formation plugs and Hakos Group plugs clearly supports an evaporitic origin, at least in part, for the halite-undersaturated fluids as the data plot on an

evaporation trend below the sea water marker (Figure 3.25). Halite dissolution has, however, altered the initial geochemical signature of the connate evaporitic fluids in some samples, resulting in halite-oversaturated fluids which plot on a trend above the sea water marker. The halite dissolution was not pervasive, though, and the initial character of the evaporitic fluid is thought to be preserved as halite undersaturated-inclusions. This would indicate a formation brine that is more Ca^{2+}, CO_3^{2-} and Br^--rich than that observed in the halite-oversaturated inclusions.

Alternatively, the leachates which plot on the halite dissolution trend could represent metamorphic fluids which derived their salinities purely from dissolution of evaporitic salts. The presence of fluids which plot below the sea water marker, though, indicates that the salinities calculated for these fluids are, at least in part, derived from connate evaporitic fluids.

The xenoliths sampled within the quartz and quartz-dolomite plugs show trace element and rare earth element distributions very similar to that of comparable *in situ* units in the Duruchaus Formation (Figures 3.10 and 3.12) suggesting an origin for these units in that formation. By implication, an origin of the evaporitic fluids preserved within the quartz and quartz-dolomite plugs, within the Duruchaus Formation of the SMZ is also indicated.

In Figure 3.25 it can be seen that the halite-oversaturated fluids do not lie on a clear trend above the sea water marker. There are two possible explanations for this. One is that early precipitation of halite and sodium carbonate minerals, e.g., natron and trona, thought to be associated with the Duruchaus Formation evaporites (Behr *et al.*, 1983a), removed Na^+ preferentially from solution with respect to Cl^-, and resulted in

the data being shifted off the sea water dissolution/evaporation trend. An alternative explanation is that due to the late stage albitisation of the main evaporite sequence, the Na-rich character of the lithological units as well as the fluid inclusions present in the sequence, resulted from albitisation. An attempt to assess the extent to which the albitisation might have altered the original chemistry of the fluid is based on an approach by Davisson *et al.* (1994) (Figure 3.32). These authors found that using a mathematical transformation of the concentrations of Na, Ca and Cl, in basinal fluids, a slope of 2:1 between the milliequivalenices of Na and Ca is produced, regardless of the area of origin of the fluids. The slope is termed the Basinal Fluid Line (BFL) and it was found to remain consistent for basinal fluids irrespective of host lithology or fluid source (Davisson and Criss, 1996; Davisson *et al.*, 1994). The Ca-excess and Na-deficit are defined mathematically as follows:

$$Ca_{Excess} = [Ca_{meas} - (Ca/Cl)_{SW}\, Cl_{meas}]2/40.08$$

$$Na_{Deficit} = [(Na/Cl)_{SW}\, Cl_{meas} - Na_{meas}]1/22.99$$

The slope of the BFL represents a net cation exchange ratio of 2 Na for 1 Ca in feldspars (albitisation of plagioclase) and is defined mathematically as follows:

$$Ca_{Excess} = 0.967(Na_{Deficit}) + 140.3 \qquad R = 0.981$$

Further examination of the Ca-excess Na-deficit plot led Davisson and Criss (1996) to believe that the trace of various processes involved in basinal fluid evolution can be followed on this diagram. These processes are outlined in Figure 3.32.

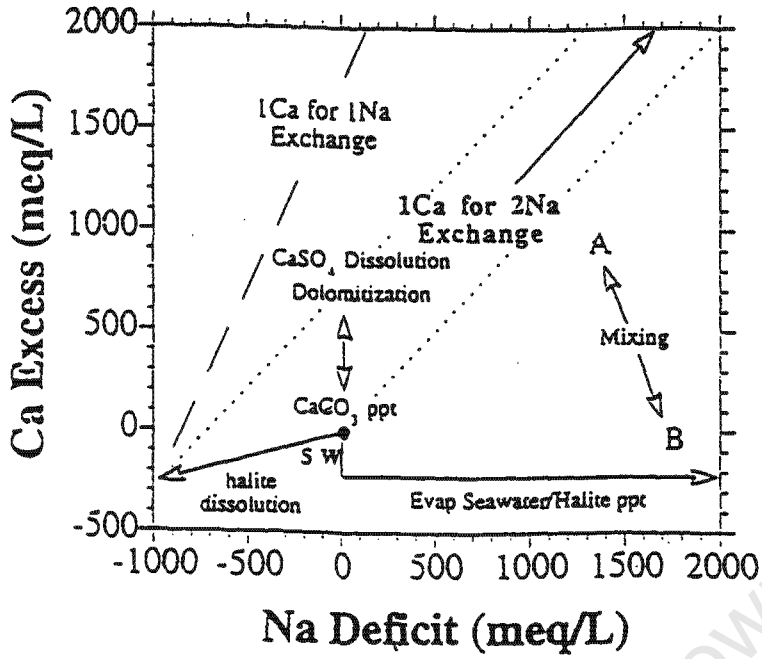

Figure 3.32 Ca Excess – Na Deficit plot showing model predictions for different processes (after Davisson and Criss, 1996).

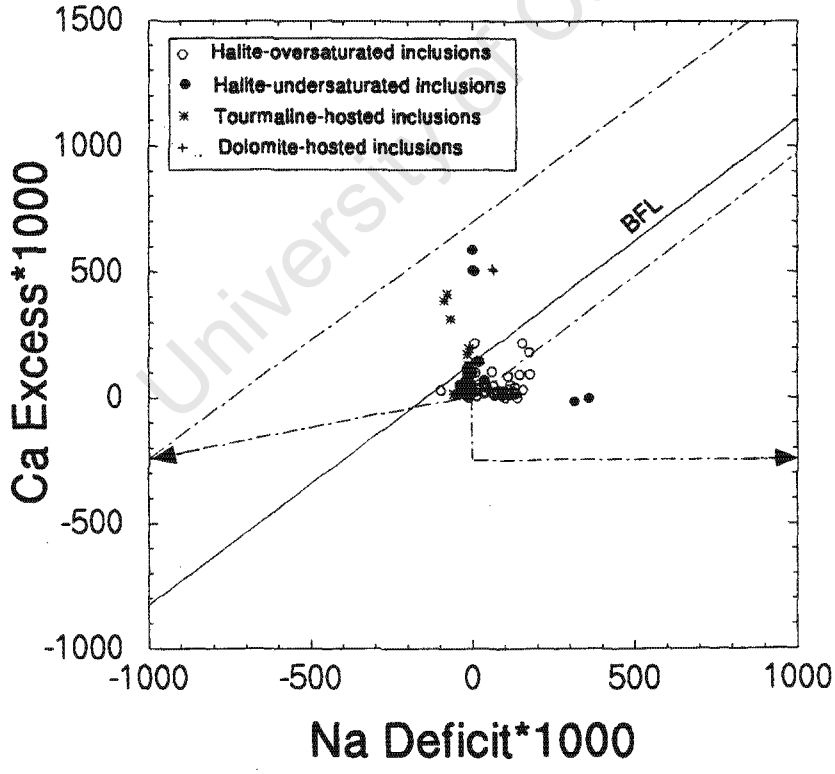

Figure 3.33 Ca-Excess Na-Deficit plot for leachate data from fluid inclusions within the Duruchaus Formation plugs and veins, and Hakos Group plugs. BFL = Basinal Fluid Line.

Other then one anomalous sample (NP060), which contains predominantly CO_2 inclusions, all of the halite-undersaturated fluids plot below the BFL close to the origin, with only a slight Ca-excess seen (Figure 3.33) (*Note:* In an attempt to correct for the effect of dilution on the absolute concentrations of Na^+, Cl^- and Ca^{2+} during the sample preparation of the fluid inclusion leachates, both the Na-deficit and Ca-excess values were multiplied by 1000). The halite-oversaturated inclusions also generally plot below the BFL but extend to higher Na-deficit values (and do not follow the halite dissolution trend as would be expected). This trend could possibly have resulted from the precipitation of halite and sodium carbonates from these fluids, resulting in a shift to the right of the diagram, followed by halite dissolution which would have then resulted in a partial shift back to the left of the diagram to lower Na-deficits. All the leachates also plot above the trend generated by sea water evaporation and halite precipitation suggesting the passage of more calcium-rich fluid through the host minerals. The dolomite-hosted inclusions show a trend consistent with the process of dolomitisation (an increase of Ca-excess in the residual fluids). The tourmaline-hosted inclusions show a similar trend.

The effect of Ca-Na exchange on these fluids therefore appears to be minimal. The dominant factor controlling the distribution of the halite-oversaturated inclusions in Figure 3.25 is therefore more likely to be the early precipitation of halite and sodium carbonates thought to be associated with these evaporites.

In summary then, the fluids are most likely of evaporitic origin. During the process of evaporation, some fluids remained in contact with their mineral precipitates resulting in some halite dissolution which produced a halite-oversaturated fluid. The early precipitation of sodium carbonates combined with the halite dissolution described

above has resulted in a spread of data in Na-Br-Cl space (late stage albitisation of the sequence appears to have had little affect on the trapped fluids). Halite dissolution was therefore not pervasive and some evaporitic brines remained more or less unaffected, or were removed from contact with their evaporite mineral precipitates. These fluids are preserved as halite-undersaturated inclusions and are regarded as indicative of the composition of the initial evaporitic brine. A relatively CO_3^{2-}-rich and bromine-rich fluid composition for the formation brine is indicated.

3.5.5 Brine Evolution

The geochemical data presented thus far suggests a multi-stage evolution for the evaporitic Duruchaus Formation and its associated fluids. This evolution can be outlined as follows.

The deposition of the more clastic units within the Duruchaus Formation took place in an enclosed basinal setting, a rift basin. A short transport distance is indicated by the large amounts of feldspar in the units below the main evaporite sequence (Petrography-Appendix II). These sediments were of continental derivation and continued to accumulate until late Nosib times. The presence a negative cerium anomaly in one of the rare carbonate units below the main evaporite sequence suggests a slight marine influence on these sediments prior to the deposition of the main evaporite sequence.

During late Nosib times carbonate units were deposited in a continental playa lake under relatively oxidising conditions. The continental waters were dominated by significant amounts of Na^+, Ca^{2+}, $CO_3^{2-}$and Cl^-, with minor K^+, Mg^{2+}, SO_4^{2-} and BO_3^-. Precipitation of sodium carbonate minerals, sodium sulphates, sodium chloride along

with minor borates, and magnesian and calcium carbonates, took place during the evaporative phases in the evolution of the playa lake.

The continentally-derived clastic sediments continued to accumulate becoming intercalated with these continental carbonate units until the end of Nosib times. Lithification of these units resulted in the trapping of some of the fluids associated with the formation of the continental carbonates in pore spaces. Partial dissolution of the salts previously precipitated resulted in the alteration of the composition of some of the pore fluids.

Albitisation of the evaporite sequence then took place, altering the whole rock compositions of the units within the evaporite sequence, mainly affecting the Rb, Cs, Ba and light rare earth element concentrations, and most significantly the sodic character of the units. Primary evaporitic minerals that had precipiated early in this sequence of events were pseudomorphed by albite during this albitisation. The compositions of the trapped pore fluids, though, appear to have been relatively unaffected by this event.

Metamorphism and deformation of these units then followed, culminating in late stage thrusting of the units of the Hakos Group from the north over the Duruchaus Formation units in the south. This phase of thrusting resulted in the remobilsation of the pore fluids trapped within the main evaporite sequence into the thrust planes and fractures associated with this event. During the remobilisation of this fluid, dissolution of some of the previously precipitated silicates and borates took place resulting in a more complex fluid composition. Quartz plugs and veins crystallised under low (hydrostatic) pressures and were emplaced within the Duruchaus Formation

and the overlying Hakos Group. Co-genetic crystallisation of haematite and dolomite crystals also took place during this time as the fluid cooled and crystallised. The Ca-rich character of the fluid possibly resulted due to the late stage passage of a Ca-rich fluid, mosty likely as a result of dolomitisation.

Progressive thrusting resulted in repeated fracturing of the crystallised quartz veins and plugs and a renewed input of fluid from the same source (of slightly lower salinity than the earlier fluid).

3.5.6 Characterising evaporites and their associated fluids in metamorphic terrains

The geochemical character of a basinal fluid may therefore reflect a multi-stage evolution. The methods outlined in Chapter 3 proved useful in assessing the degree to which the original chemistry of the preserved fluids in the Type Locality has been altered and similarly, the degree to which the original whole rock chemistry of evaporitic units preserved within the SMZ has been overprinted by metamorphic and metasomatic processes. The extent to which the original chemistry of these units and their associated fluids has been altered needed to be assessed before any conclusions could be made about whether the units (and their associated fluids) were originally evaporitic, and thereafter whether the environment of formation was marine or continental.

Once the degree of alteration was assessed, it was found that two methods proved the most useful in characterising the evaporites and their associated fluids in the Type Locality. The rare earth element trends of the evaporitic units, in particular, proved useful in identifying a possible depositional setting for the carbonate units within the evaporite sequence (LREE enrichment trends; Ce, Eu anomalies). The Na-Br-Cl

systematics of the fluids preserved in the Type Locality proved valuable in characterising the fluid source (along with the complete cationic and anionic compositions of the leachates). The evaporitic trends (or lack thereof) outlined by samples in Na-Cl-Br space (along with the fluid salinity) can therefore be used to assess whether fluids of evaporitic origin, even in metamorphic terrains where the original geochemistry of the fluid may be slightly altered.

The techniques outlined in the previous sections are now applied to initially assess the effects of late stage alteration on suspected evaporitic fluids and evaporitic units in the Test Localities, and then to determine whether the fluids preserved there are indeed of evaporitic origin (Chapter 4).

(4)

The Test Localities

4.1 Sample Selection and Analyses –The Test Localities

4.1.1 Sample Selection

The test localities selected lie in the Northern Zone of the Damara Belt and represent areas where discordant features, i.e., quartz plugs and discordant veins associated with base metal mineral occurrances have been recorded in the upper Swakop Group and upper Otavi Group (Schneider and Seeger, 1992). Sampling took place in two main areas forming an eastern and a western dataset.

The western dataset consists of samples from the farms Karachas, Moselle, Bothashof and Omburu East (Figure 4.1B). The eastern dataset consists of samples originating from the farms Okorusu/Gaidus, Hartbeespoort, Elefantenberg and Kupferberg (with an additional sample from the farm Neuwerk) (Figure 4.1C).

4.1.1.1 Western Dataset (Omburu East, Moselle, Bothashof, Karacahas)

The lithological units on the farms Moselle and Omburu East are made up of a complexly folded sequence of the upper Swakop Group stratigraphy consisting of intercalated dolomites and limestones termed the Omburu East Structure. A siliceous dolomitic unit with associated quartz veins forms outcrops along the northwestern margin of this structure. This unit along with associated quartz veins were sampled on the farm Omburu East. Albitite and breccia xenoliths were also encountered within the siliceous dolomite in this area and these units were sampled as well.

Discordant quartz plugs and veins in the upper Swakop Group stratigraphy (still within the Omburu East Structure), encountered on the adjacent farm Moselle, were also sampled. Xenolithic rock fragments present within these plugs, consisting mainly of arkosic quartzite and silicified quartzite with rare dolomitic fragments, were also collected.

The other sample area which forms part of this dataset, the farm Bothashof, lies slightly to the north of Moselle and Omburu East (Figure 4.1B). The stratigraphy in this area is dominated by grey cherty limestone and dolomite of the upper Tsumeb Subgroup. Mineralisation in the form of copper and lead ore minerals (chalcocite, azurite, chalcopyrite) hosted in a brecciated massive dolomite of the Elandshoek Formation, has been reported on this farm (Schneider and Seeger, 1992). Discordant quartz veins were encountered in this area, and both the quartz veins and host rocks were sampled to give an indication of the nature of the mineralising fluids active in this area.

An additional sample locality in the Western Dataset was the farm Karachas. Although the Nosib Group is generally poorly exposed in the northern part of the Damara Belt, an *in situ* sequence of Nosib Group stratigraphy is exposed on the farm Karachas, and consists predominantly of quartzite and arkosic quartzite. These units are characteristic of the lower Nosib Group (Nabis Formation) in the northern part of the Damara Belt and were sampled along with *in situ* quartz veins to give an indication of the geochemical character of the Nosib Group in the northern part of the Damara Belt.

4.1.1.2 Eastern Dataset (Okorusu/Gaidus, Kupferberg, Elefantenberg, Hartbeespoort)

The stratigraphy in these areas also falls within the upper Swakop Group and upper Tsumeb Subgroup. Minor mineralisation was encountered in the field on the border between the farms Okorusu and Gaidus, within the carbonates of the upper Swakop Group. The mineralisation is in the form of malachite and chrysocolla with minor azurite hosted within a calcitic marble which partially replaces the blue-grey dolomitic units in the area. The quartz-calcite veins associated with this unit were sampled along with the host rocks.

A larger prospect was examined on the farm Kupferberg. A discordant copper-bearing, calcitised, pipe-like breccia body occurs there, within carbonates of the Hüttenberg Formation (Tsumeb Subgroup). This prospect was developed and worked in the early part of the 20th century (Schneider and Seeger, 1992) and remains exposed as a series of adits on the slopes of the mountains in this area. Samples of the quartz and calcite float on the scree slopes of these adits were taken, along with samples of the host carbonate.

Copper, lead and zinc occurrences on the farms Elefantenberg and Hartbeespoort have also been reported by Schneider and Seeger (1992). Carbonates from the upper Otavi Group also cover a large part of these farms. Although mineralisation of the Cu and Pb-Zn type was not encountered in the field, discordant quartz-calcite veins within carbonates of the Maieberg Formation were sampled to give an indication of the types of fluids that were active in this area.

An additional sample locality in this dataset is the farm Neuwerk. On this farm small scale mineralisation was encountered in the Abenab Subgroup/Nosib Group transition

zone. Mineralisation seen at this locality was mainly in the form of chalcopyrite and pyrite, hosted by a chlorite phyllite, which is intercalated with carbonates of the Abenab Subgroup. Samples of discordant quartz veins were taken in this area to give an indication of the nature of the mineralising fluids that were active lower down in the stratigraphy. These samples form a subset of the eastern dataset.

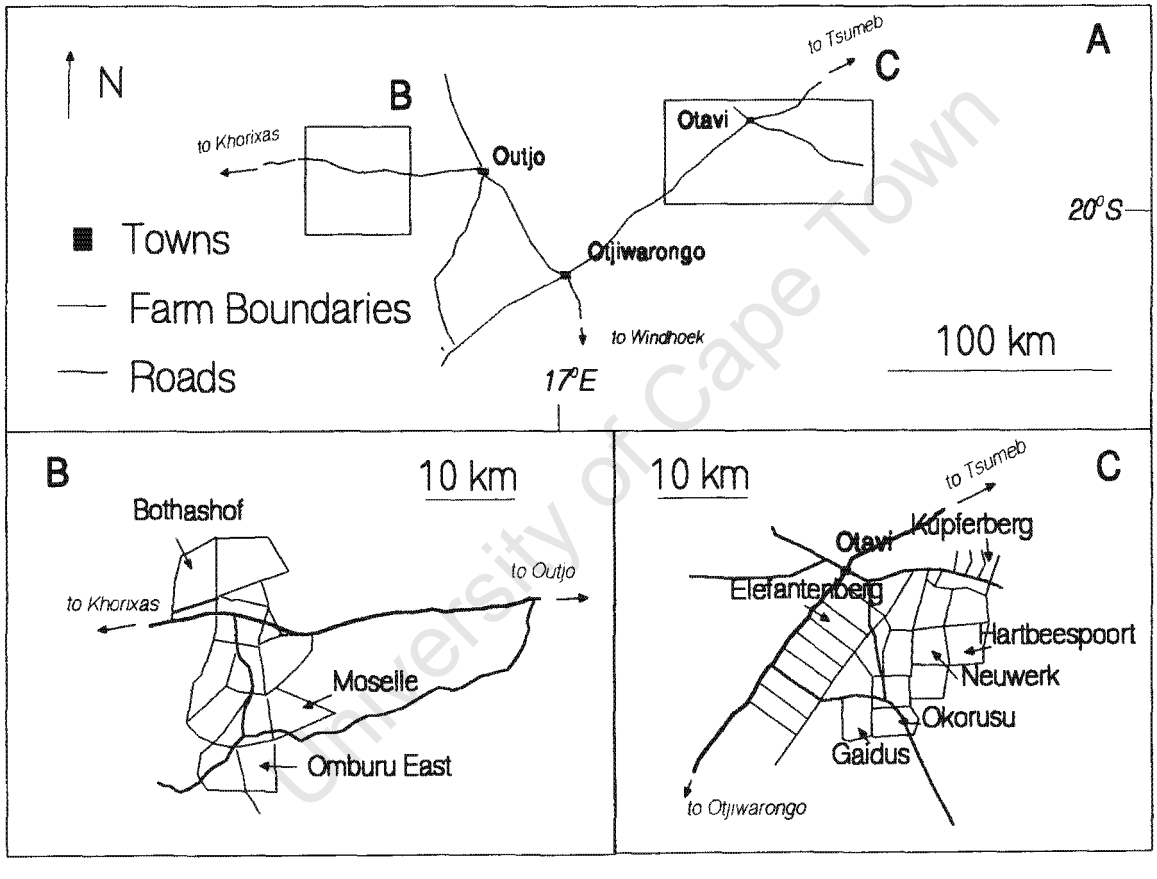

Figure 4.1 Sketch map of the sample localities in the NZ of the Damara Belt.

4.1.2 Field Observations:

The discordant quartz-calcite and quartz veins sampled in the northern part of the Damara Belt are thought to represent post-lithification remobilisation of fluids possibly derived from evaporitic units further down in the sequence. In the sample areas which make up the western dataset, the xenolithic rock fragments present within the siliceous dolomitic unit and the quartz plugs in the Omburu East Structure suggest an origin within an equivalent of the Duruchaus Formation in the northern part of the Damara Belt. All the xenolithic fragments encountered, i.e., the quartzite, albitite, siliceous breccias and arkosic quartzite, bear a striking resemblance to the units seen in the Duruchaus Formation in the SMZ and the *in situ* Nosib units sampled on the farm Karachas. The siliceous dolomite unit along the north western margin of the Omburu East Structure, like the quartz-dolomite plugs in the Duruchaus Formation and the Sole Dolomite, are thought to be related to late stage movement of nappes during the Damaran deformation (Behr *et al.*, 1983b; Weber *et al.*, 1983), forming discordant units or plugs. The fluids preserved as inclusions within these quartz veins and plugs therefore contain a possible record of the nature of the pore fluids trapped within the Duruchaus Formation or its equivalent further north and can be used to determine the nature of the Nosib Group fluids in this part of the Damara Belt.

The source of the mineralising fluids in the sample areas of the eastern dataset is less clear, as similar xenolithic rock fragments were not encountered in the areas sampled there. A clue to the nature of the source rocks for these fluids was determined by their geochemical character. This was considered in the next stage of analytical work which is described in the following sections.

4.1.3 *Analytical Work*

The analytical work for the test localities was subdivided as follows:

(i) *Fluid Inclusion Studies :* Microthermometric analyses
Crush Leach Analyses (using HPIC and ICP-MS)

(ii) *Whole Rock Chemistry :* ICP-MS analyses

The analyses listed in (i) were carried out to determine the density, overall salinity and fluid chemistry of the fluid inclusions present within the quartz plugs and quartz vein samples from the sample areas which form the western and eastern datasets. The sample areas were treated separately to determine whether there is any variation in the fluid character within and between these the two datasets.

The analyses listed in (ii) were carried out to determine the whole rock, trace element compositions of the xenoliths sampled in the quartz plugs from the sample areas of the western dataset with the aim of determining whether the source of these units and thus by implication the source of the fluids in these plugs, is in the Nosib Group (and possibly an equivalent of the Duruchaus Formation in the north).

4.2 Analytical Results

4.2.1 Whole Rock Chemistry

4.2.1.1 Sample Selection, Petrography and Analyses

Xenolith samples from the margin of the Omburu East Structure and the xenoliths from the quartz plugs on the farm Moselle were of the following lithological types: albitite, breccias and dolomite. The breccias and dolomitic units were eliminated from this study due to the heterolithic nature of the breccias and due to the uncertainty in the original stratigraphic position of the dolomite (as dolomite occurs at various levels in the Damaran stratigraphy). A second sample set is formed by the Nosib Group units from the farm Karachas. The dominant rock types in this area is feldspathic quartzite which is thought to form part of the Nabis Formation in the NZ of the Damara Belt.

A petrographic study of the albitic xenolith from the Omburu East Structure revealed that this unit consists predominantly of quartz and albite grains (0.25-0.5mm), with minor sphene and rutile grains. Trace amounts of zircon and muscovite are also present. The xenolith has a granoblastic texture and the petrography of the sample conforms well to that seen in the albitite in the SMZ.

The feldspathic quartzite xenoliths from the farm Moselle consists predominantly of large quartz grains (0.5-4mm) with significant amounts of albite, biotite and dolomite. Sphene, rutile and zircon form accessory phases in these xenoliths and these units are characterised by a seriate texture.

The *in situ* Nosib Group feldspathic quartzite is also dominanted by quartz grains (~1mm) but this rock contains microcline and muscovite as well. Sphene and zircon form the accessory phases in these units. The feldspathic quartzite is characterised by a polygonal, recrystallised texture.

4.2.1.2 ICP-MS Results

4.2.1.2.1 Trace Element Distribution

The trace element distribution in the samples from the three localities are presented in Figures 4.2 to 4.4. The trace element distribution in the albitised and unalbitised pelitic units from the Hakos Group in the SMZ are also presented in these diagrams to assess the degree of albitisation experienced by the xenoliths present in the NZ sample areas.

The albitite from Omburu East is characterised by a distinct depletion in Rb, Cs and Ba relative to the continental crust, as well as a slight La and Ce anomaly and a distinct positive Th anomaly (Figure 4.2). The xenoliths from the farm Moselle show a similar trend to the albitite from Omburu East (distinct Rb, Cs and Ba depletion and positive Th anomaly) with a slightly more variable signature (Figure 4.3). The trends outlined by the Moselle and Omburu East xenoliths conform well to that exhibited by the albitised pelitic unit from the SMZ.

The samples from the Nosib Group, in contrast, do not show the distinct depletion in Rb, Cs and Ba of the albitic units (Figure 4.4). The Nosib Group samples are characterised by a moderate depletion with respect to all trace elements (except Ba, Rb and Th) relative to the continental crust, and significant depletions in Sr, V, Nb and Sc.

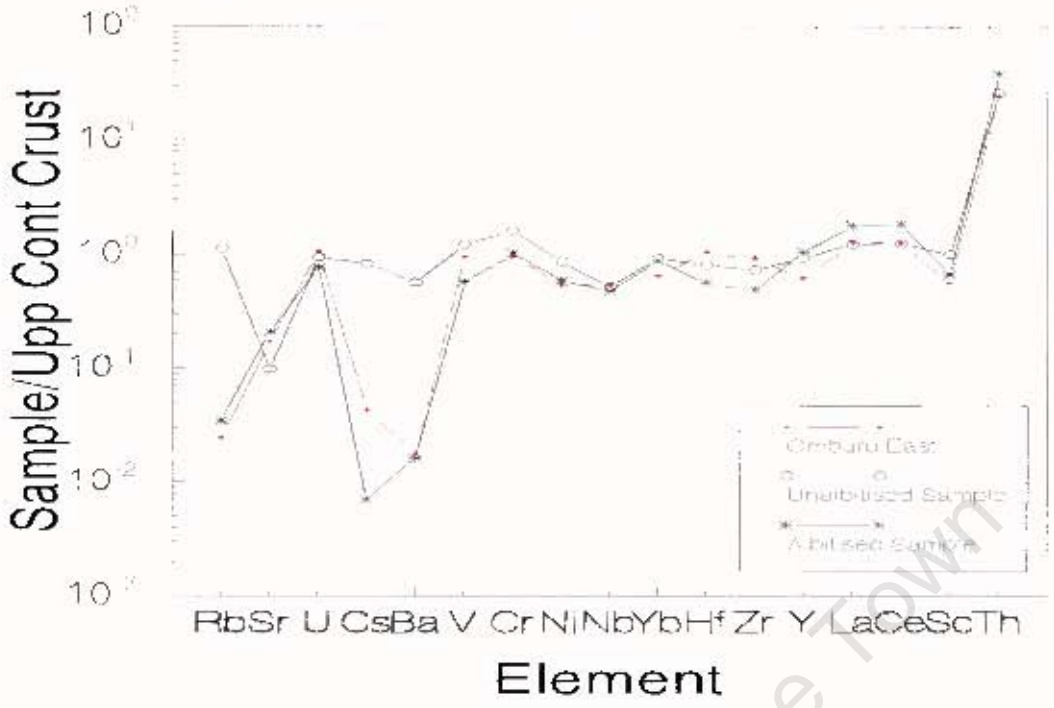

Figure 4.2 Upper continental crust-normalised multi-element diagram for xenolith samples from the Omburu East Structure. Upper continental crust normalising values are from Taylor and McLennan (1981).

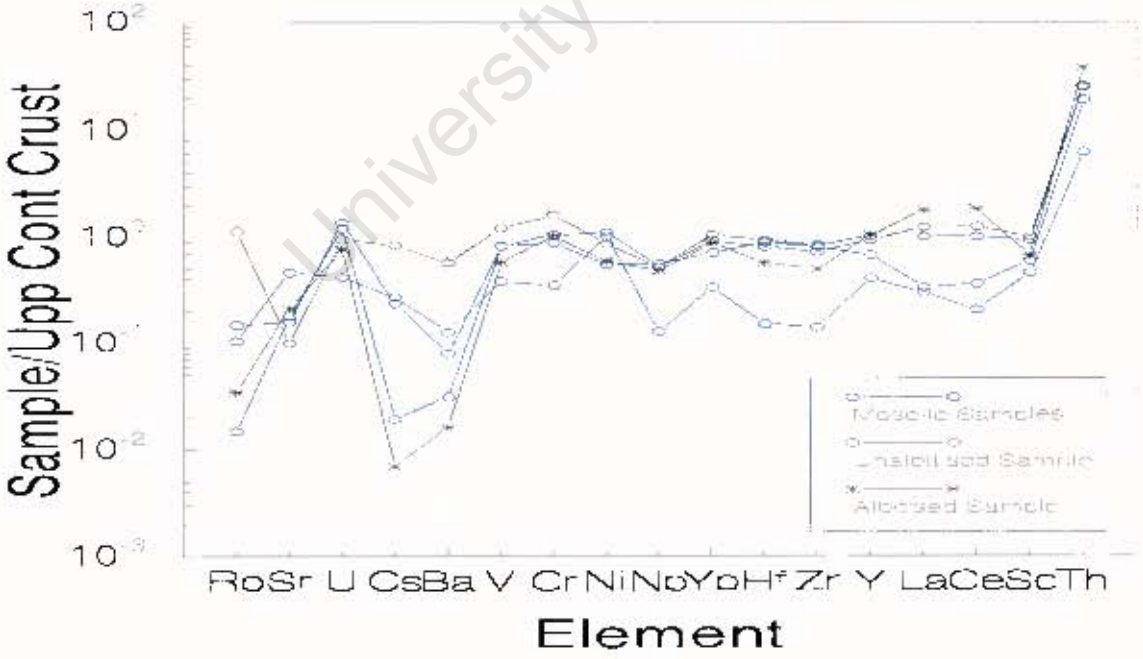

Figure 4.3 Upper continental crust-normalised multi-element diagram for xenolith samples from the farm Moselle. Upper continental crust normalising values are from Taylor and McLennan (1981).

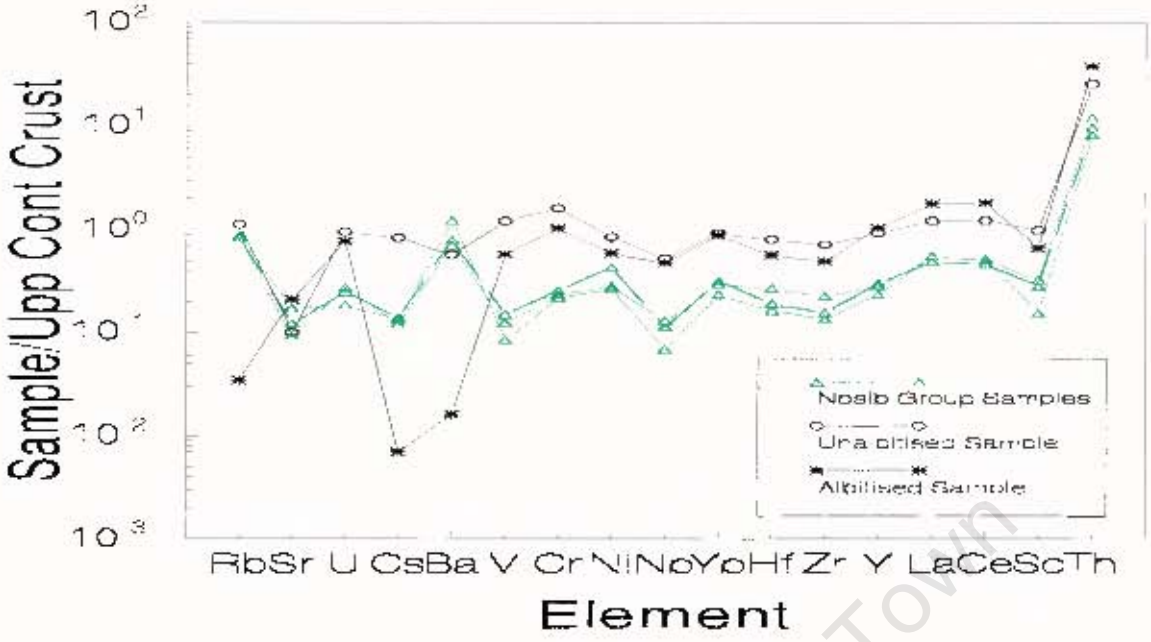

Figure 4.4 Upper continental crust-normalised multi-element diagram for xenolith samples from the Nosib Group. Upper continental crust normalising values are from Taylor and McLennan (1981).

4.2.1.2.2 Rare Earth Element Distribution

The chondrite-normalised rare earth element plots for the xenolith samples from Omburu East and Moselle, as well as the Nosib Group feldspathic quartzites, are characterised by a strong light rare earth enrichment trend and a negative europium anomaly (Figure 4.5).

The rare earth element distribution in the xenoliths conforms well to that of the upper continental crust (Figure 4.6). A flattening of the light rare earth enrichment trend of the chondrite-normalised plots in the upper continental crust-normalised plots is seen in these samples, with the negative europium anomalies either disappearing or becoming less pronounced.

The Omburu East albititic xenolith shows a trend which mirrors that of the albitised pelitic sample from the SMZ, albeit at lower concentrations of rare earth elements (Figure 4.6). The feldspathic quartzite xenoliths from Moselle are characterised by a slight light rare earth depletion (Figure 4.7), whereas the xenolith samples from the NZ Nosib Group are characterised by a distinct depletion with respect to all rare earth elements relative to the upper continental crust (Figure 4.8). A slight negative cerium anomaly is also evident in these units.

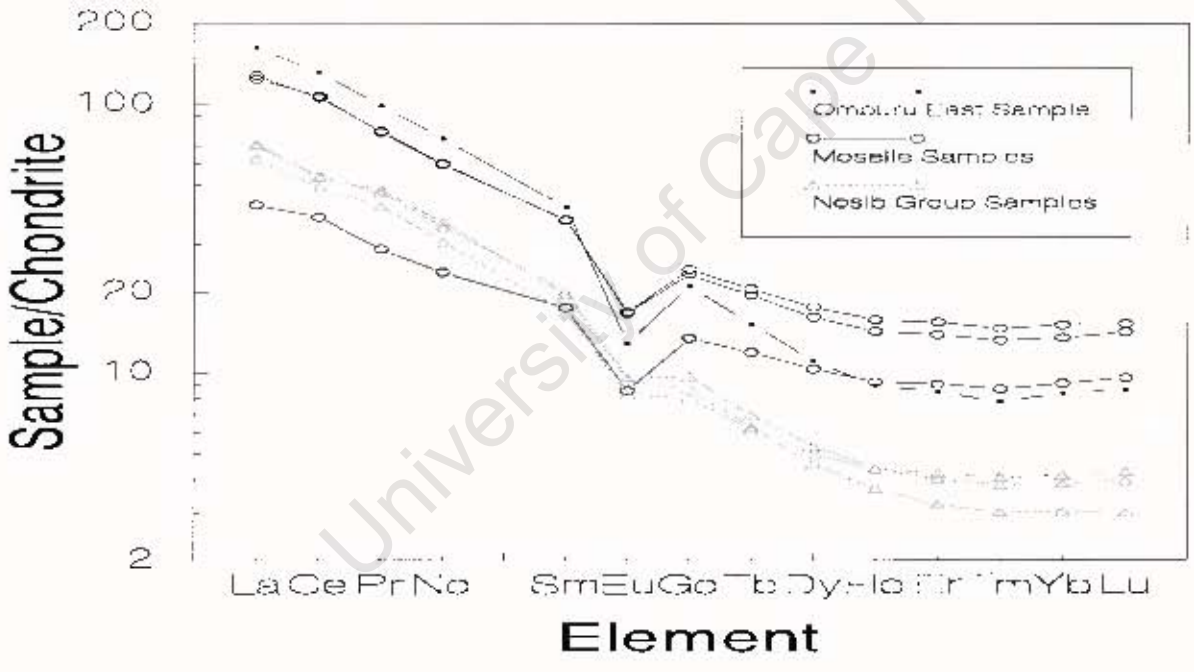

Figure 4.5 Chondrite normalised rare earth element plots for selected xenolith samples from Omburu East annd Moselle, and Nosib Group samples from the NZ. Chondrite normalising values are from Sun and Mcdonough (1989).

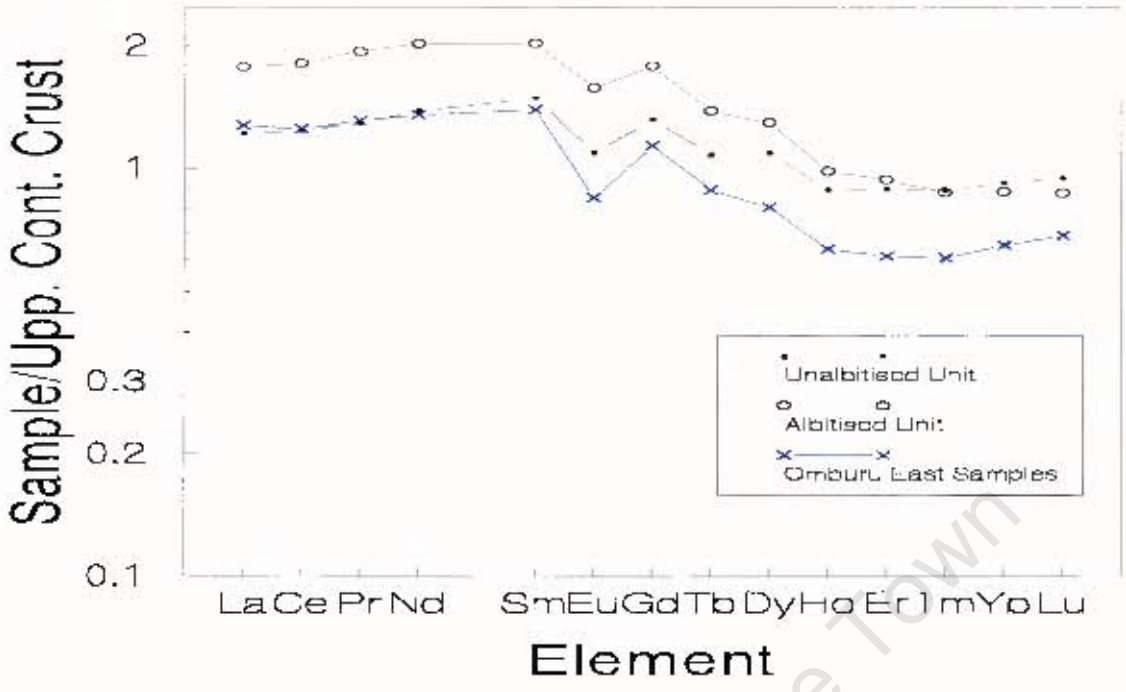

Figure 4.6 Upper continental crust normalised rare earth element plots for selected xenolith samples from the Omburu East Structure. Upper continental crust normalising values are from Taylor and Mclennan (1981).

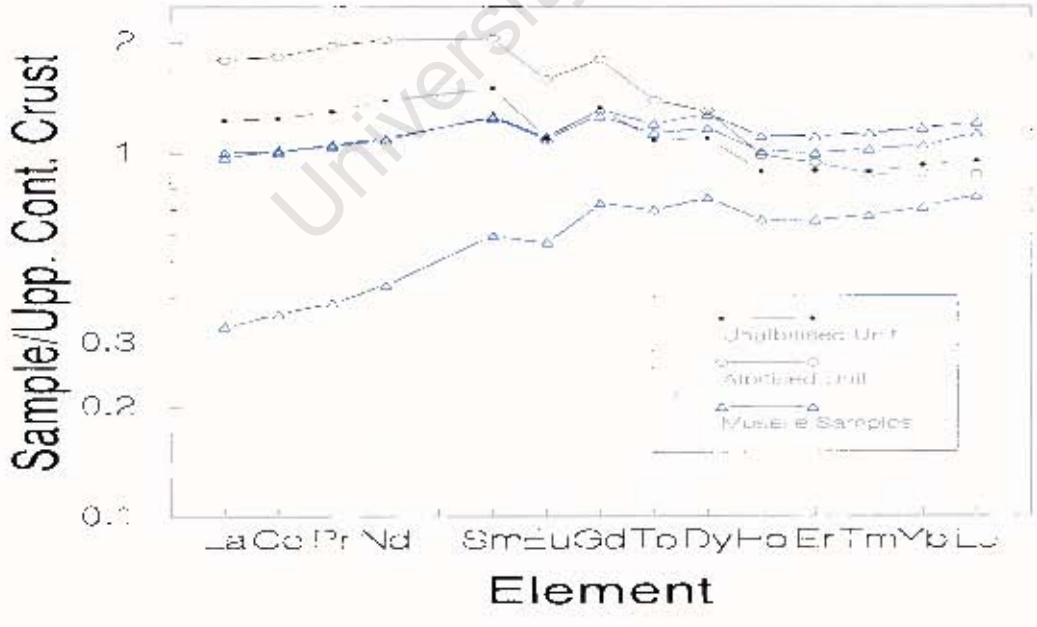

Figure 4.7 Upper continental crust normalised rare earth element plots for selected xenolith samples from quartz plugs on the farm Moselle. Upper continental crust normalising values are from Taylor and Mclennan (1981).

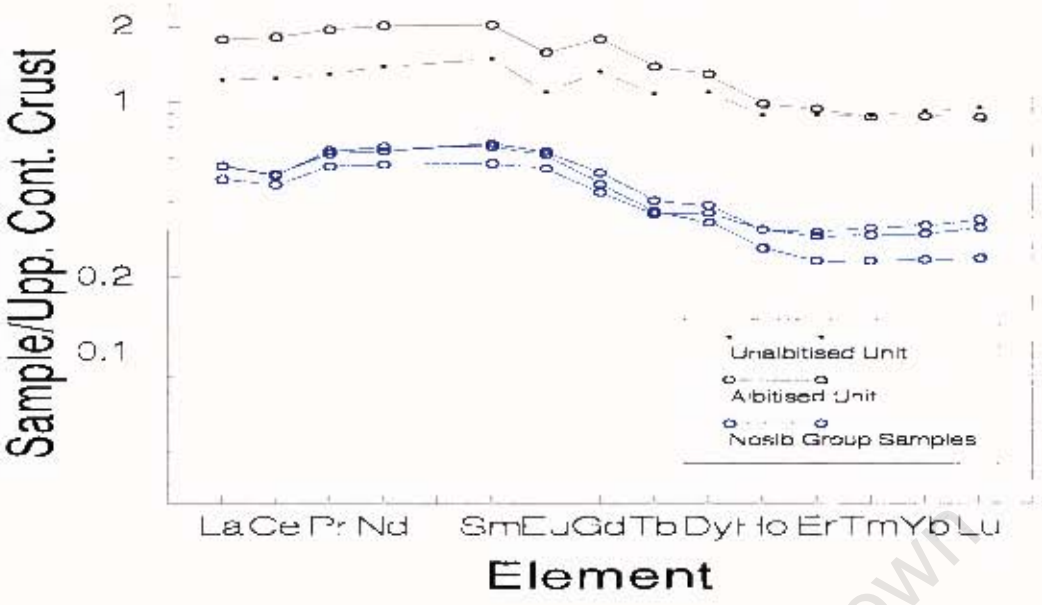

Figure 4.8 Upper continental crust normalised rare earth element plots for selected Nosib Group samples from the farm Karachas. Upper continental crust normalising values are from Taylor and Mclennan (1981).

4.2.2 Microthermometry

4.2.2.1 Sample Selection, Petrography and Analyses

Twelve samples in total were selected for microthermometric analysis. Seven of these samples were from localities which form part of the western dataset and five from localities which form part of the eastern dataset. Samples from different parts of the NZ and different parts of the stratigraphy (in the case of the samples from the Nosib Group and Nosib-Abenab transition zone) were analysed to give an indication of the different types of fluids that were active in this part of the Damara Belt. Quartz samples were again analysed in preference to other potential fluid inclusion mineral hosts due to the fact that the inclusions in these samples were more optically resolvable, and due to the strength of quartz as a host mineral. A petrographic and preliminary microthermometric study of the samples mentioned revealed the existence of four main types of fluid inclusions within them, i.e.,

(i) Clathrate-bearing 2 phase aqueous inclusions ($L_{aq,carb} + V_{aq}$) *(Type I)*

(ii) Aqueous 3 phase inclusions ($L_{aq} + V_{aq} + S_{salt}$) *(Type II)*

(iii) Aqueous 2 phase inclusions ($L_{aq} + V_{aq}$) *(Type III)*

(iv) Rare 2 phase CO_2 inclusions ($L_{carb} + V_{carb}$) *(Type IV)*

In the sample localities from the western dataset, all four inclusion types (Type I-IV) form isolated fluid inclusions, except in the sample from the Nosib Group on the farm Karachas. Isolated fluid inclusions in the Karachas sample are predominantly of the Type III. Type IV inclusions are rare in all these samples and do not occur at all in the sample from the Nosib Group (Karachas). The isolated inclusions generally are between 5-15μm in size.

In the samples from farms Moselle, Omburu East and Karachas a younger overprinting generation is also present, as secondary inclusion trails. This younger generation consists of inclusions of the Type II and III, and the inclusions are typically being between 5-10μm.

The quartz samples from the localities which form part of the eastern dataset are characterised by the presence of randomly distributed, isolated fluid inclusions, i.e., the separation of different, distinguishable phases of fluid activity was not possible on the basis of the distribution of these inclusions. These inclusions were therefore grouped as one fluid generation for the eastern dataset sample areas (inclusion sizes range from 5-20μm). The fluid inclusions in the eastern dataset test localities are predominantly of the Type II and III, with Type I and IV inclusions being quite rare. The sample from the Nosib-Abenab transition zone on the farm Neuwerk contains Type III and rare Type II inclusions only. Samples from the farm Kupferberg did not yield any measurable inclusions.

Eutectic temperatures, melting temperatures and homogenisation temperatures were measured for each of the phases (CO_2, H_2O) present in the isolated and secondary inclusions. The salinities quoted are calculated from the equation of Bodnar (1993).

4.2.2.2 Results

A summary of the analytical results for both the eastern and western datasets is presented in Tables 4.1 and 4.2. The analytical results for the aqueous inclusions from each of the datasets are presented in Figures 4.9 to 4.14. In all these diagrams it should be noted that while all the data is presented, only the ranges into which the majority of data falls (barring outliers) are considered to be representative of the

fluids in each area (these restricted ranges are presented in tables 4.1 and 4.2). The data can be outlined as follows.

Western Dataset

The Type II and III isolated inclusions within the samples from Omburu East and Bothashof show a similar character with regard to eutectic temperatures (T_e) (Figure 4.9). The lowest T_e temperatures measured in the samples from Omburu East are in the vicinity of -40.0°C, while T_e values as low as –44°C were observed in the samples from Bothashof. The samples from Moselle and Karachas are characterised by slightly higher minimum T_e values of –29.4°C and -22.8°C, respectively. The Type II and III secondary inclusions show a similar range of T_e values when compared with the isolated inclusions in each sample area, except in the samples from Omburu East where the lowest T_e value observed was –28.5°C (Figure 4.9).

A large range of final melting temperatures (Tm_{ice}) values were observed in the Type II and III isolated inclusions in the samples from Bothashof, Omburu East and Moselle (Figure 4.10). A large number of the inclusions in these samples have Tm_{ice} values in the range –24.2°C to –11.1°C, with a few outliers extending up to -0.1°C in the Omburu East and Bothashof samples. The isolated Type II and III inclusions in the Omburu East samples seem to form a bimodal Tm_{ice} distribution, the mean values for the two populations being -23°C and -2°C. The isolated inclusions in the Moselle samples show a tighter range of Tm_{ice} values of between –24.2°C to –14.1°C, while the isolated aqueous inclusions in the Karachas samples show a higher temperature Tm_{ice} range of -7.4°C to -0.6°C (Figure 4.10). The Type II and III secondary inclusions in the four areas essentially mirror the Tm_{ice} ranges of the isolated Type II

and III aqueous inclusions, with the exception of the secondary aqueous inclusions in the Moselle samples which show a broader range of -25.6°C to -6.0°C.

The homogenisation temperatures (T_hH_2O) of the Type II and III isolated inclusions in Omburu East, Bothashof and Moselle show a wide range extending from values of 191°C up to 364°C (Figure 4.10). Homogenisation is to the liquid phase. In the samples from Bothashof most of the inclusions lie in the range 180°C to 280°C whereas in Omburu East and Moselle, most inclusions lie in the range 220°C to 360°C, and 240°C to 400°C, respectively. Higher temperatures have been recorded in all these areas, sometimes greater than 400°C, but the largest number of the measured inclusions lie in the ranges mentioned above. Lower temperature inclusions are also sometimes present and these are thought to represent outliers of the dataset. The isolated aqueous inclusions in the samples from the farm Karachas show a much lower T_hH_2O range than those from the other three sample areas, with T_hH_2O values of between 108°C and 178°C (Figure 4.10).

The T_hH_2O values observed in the Type II and III secondary inclusions in the samples from Omburu East and Moselle overlap with the T_hH_2O ranges of the isolated inclusions (Table 4.1). The samples from the farm Karacahas, however, show a clear distinction in terms of T_hH_2O values between the isolated and secondary fluid inclusions. The secondary aqueous inclusions in these samples show a higher T_hH_2O range of 203°C to 315°C (Figure 4.10).

The calculated salinities for the Type II and III isolated inclusions show similar ranges in the samples from Moselle, Omburu East and Bothashof (17-29wt% $NaCl_{eq}$). The isolated Type II and III inclusions in the samples from Karachas show a much

lower salinity range of between 1 and 11wt% $NaCl_{eq}$. The secondary Type II and III inclusions generally lie in the same salinity range as the isolated inclusions in all sample areas in the western dataset.

The clathrate-bearing isolated inclusions show a similar character to the isolated aqueous inclusions with regard to T_e and Tm_{ice} values (where observed). The melting temperatures of the clathrates (Tm_{clath}) observed in isolated inclusions in the samples from Omburu East and Moselle lie in the range of 0.1°C to 11.4°C. The total homogenisation temperatures observed in these inclusions show a large range from 254°C up to 450°C. Clathrate-bearing secondary inclusions show a similar overlapping range with the isolated clathrate-bearing inclusions in terms of Tm_{clath} values and homogenisation temperatures (Table 4.1).

Rare CO_2 inclusions are also encountered in samples from Moselle and Omburu East. Isolated CO_2 inclusions in these samples show a melting temperature range of 59.7°C to –56.9°C, and T_hCO_2 range of -9.1°C to 29.6°C, with most values lying between 28.5°C and 29.6°C.

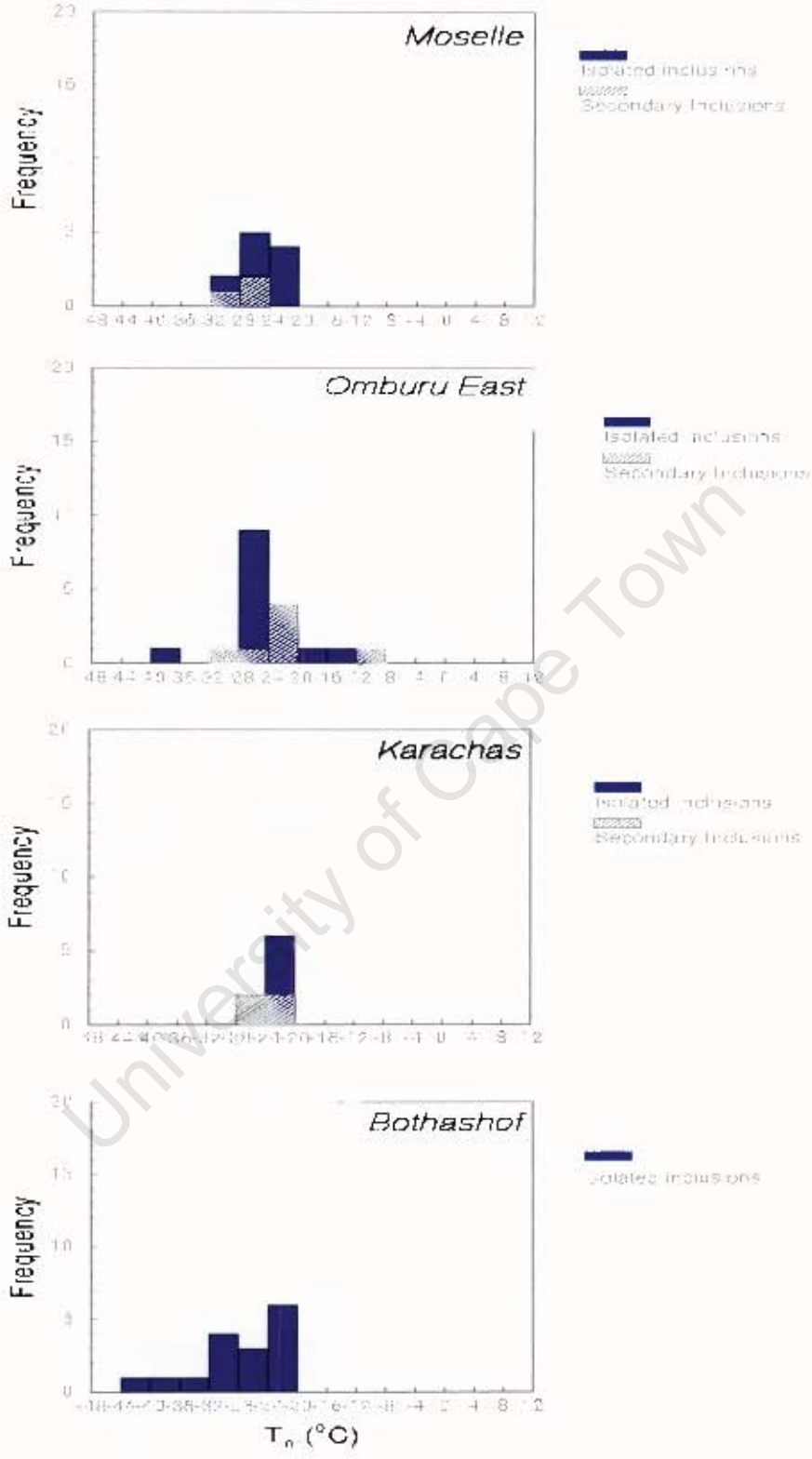

Figure 4.9 Frequency histograms of eutectic temperatures (T_e) observed in aqueous inclusions in samples from the western dataset.

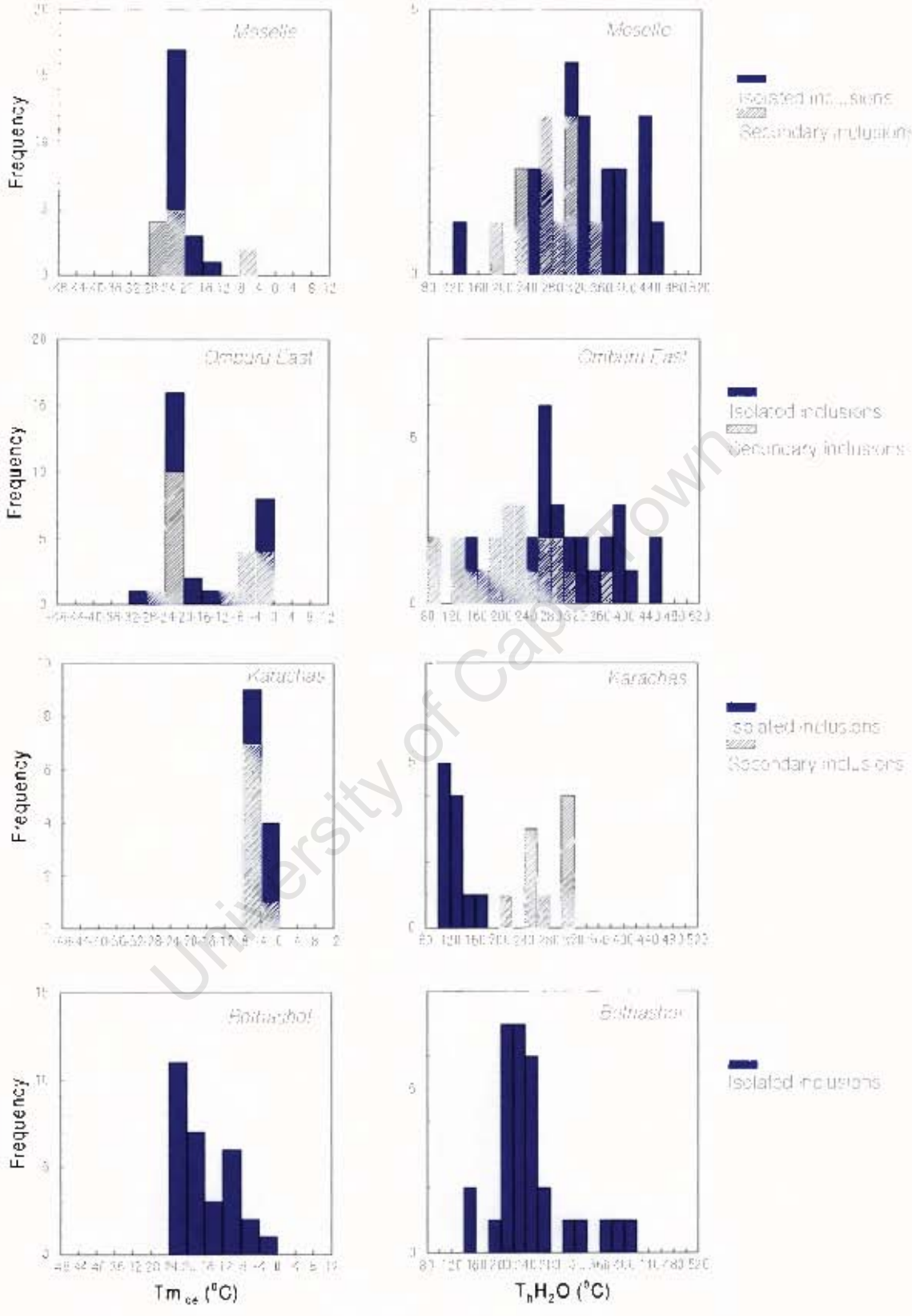

Figure 4.10 Frequency histograms of melting temperatures (Tm_{ice}) and homogenisation temperatures (T_hH_2O) observed in aqueous inclusions in samples from the western dataset.

Table 4.1 Fluid inclusion results subdivided according to the area of origin in the NZ and NZ stratigraphy (Western Dataset). Values in brackets are considered representative ranges for each dataset. T_e values represent the minimum observed T_e in each sample area.

	T_e(°C)	Tm_{ice}(°C)	Tm_{clath}(°C)	T_h(°C)	Salinity (wt% $NaCl_{eq}$)
Omhuru East (Swakop Group)					
Type II & III					
Isolated incl.	-40.0	-30.4 to 0.2 (-24.1 to –0.2)		152 to 456 (191 to 356)	1-29wt% (20-29)
Secondary incl.	-28.5	-24.6 to –2.2		98 to 369 (130 to 306)	4-25wt% (14-25)
Type I					
Isolated incl.			0.1 to 0.4	320 to 356	15-16wt%
Secondary incl.			0.4 to .09	140 to 371	14-15wt%
Moselle Plugs (Swakop Group)					
Type II & III					
Isolated incl.	-29.4	-24.2 to 14.1		129 to 455 (249 to 364)	17-25 wt%
Secondary incl.	-29.1	-25.6 to –6.0 (-25.6 to –21.4)		184 to 357 (232 to 312)	9-26wt% (23-26)
Type I					
Isolated incl.	-28.7	-23.7 to –15.4	0.1 to 11.4	254 – 450	
Bothashof (Otavi Group)					
Type II & III					
Isolated incl.	-44.0	-23.8 to 0.1 (-23.8 to 11.1)		152 to 401 (193 to 276)	1-25wt% (15-25)
Karachas (Nosib Group)					
Type II & III					
Isolated incl.	-22.8	-7.4 to –0.6		108 to 178	1-11wt%
Secondary incl.	-26.5	-6.9 to –1.0		203 to 315	5-10wt%

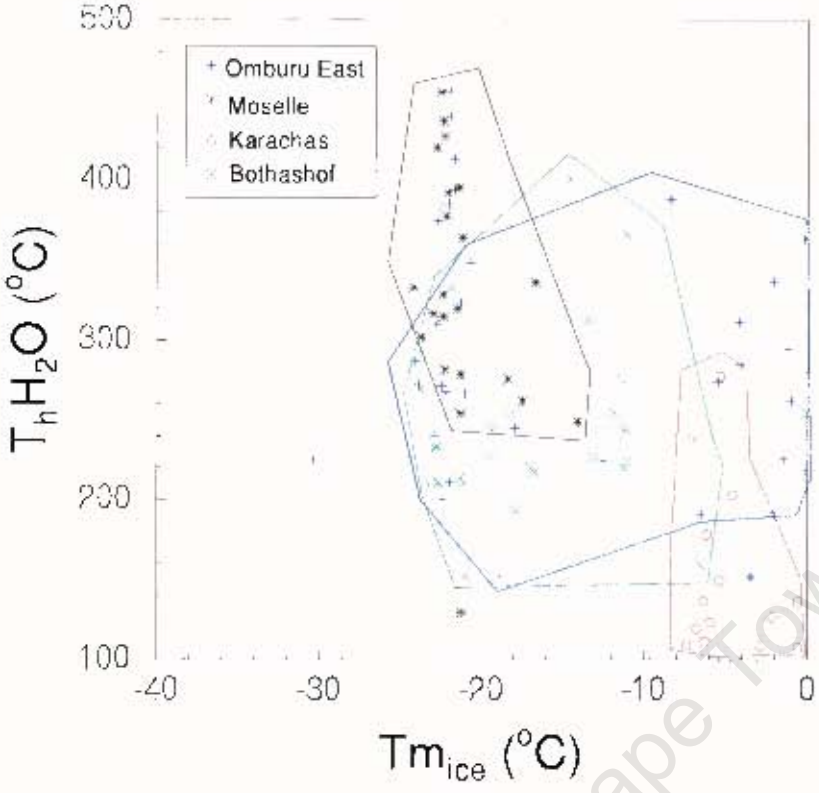

Figure 4.11 T_hH_2O versus Tm_{ice} plot for isolated aqueous inclusions from the western dataset.

The fields of distribution for T_hH_2O and Tm_{ice} values for each sample area from the western dataset are quite different (Figure 4.11). The Moselle samples form a well defined high T_hH_2O, low Tm_{ice} field, while the samples from the farm Karachas are characterised by a low T_hH_2O, high Tm_{ice} field. The samples from the farms Bothashof and Omburu East occupy fields which stretch between these two fields, both areas being characterised by a range of T_hH_2O and corresponding Tm_{ice} values.

Eastern Dataset

The minimum T_e values observed in Type II and III isolated inclusions in the samples from the border of Okorusu/Gaidus and Elefantenberg are –31.2°C and –31.0°C, respectively. The samples from Neuwerk and Hartbeespoort are characterised by slightly higher minimum T_e values of -24.4°C and –25.2°C, respectively (Figure 4.12).

The Tm_{ice} values observed in Type II and III isolated inclusions from the four sample areas in the eastern dataset show a degree of overlap with respect to the actual ranges of values observed. However, the distribution of data within these ranges is quite variable (Figure 4.13). The samples from Okorusu/Gaidus show a wide Tm_{ice} range from –19.2°C to -0.2°C seemingly forming two populations, a lower temperature population of between 19.4°C and 8.0°C and a second population of between 7.0°C and 0.0°C. The isolated inclusions in the samples from the other three sample areas show a more restricted range of Tm_{ice} values, i.e., Hartbeespoort between -16.8°C and 0.2°C (most values between 6.5°C and 0.2°C), Elefantenberg between –10.9°C and –0.1°C, and Neuwerk between -12.3°C and -0.8°C.

The homogenisation temperatures measured in Type II and III isolated inclusions in the four sample areas show some degree of variation. Inclusions in samples from Okorusu/Gaidus show T_hH_2O values between 178°C and 479°C with most of the values falling in the range 280°C to 380°C (Figure 4.13). Type II and III isolated inclusions in samples from Hartbeespoort and Elefantenberg generally fall into a similar range, i.e., 240°C to 380°C, with some values extending above 450°C in these areas as well. In contrast to this, Type II and III isolated inclusions in samples from

Neuwerk show a lower T_hH_2O range of between 102°C and 168°C. Homogenisation was always to the liquid phase.

The calculated salinities for the Type II and III isolated inclusions in Neuwwerk, Elefantenberg and Hartbeeespoort are quite similar (1-15 wt% $NaCl_{eq}$) (Table 4.2). The samples from Okorusu/Gaidus show a range of salinities of up to 26wt% $NaCl_{eq}$.

Clathrate-bearing isolated inclusions are rare in this dataset and are present in the samples from Hartbeeespoort, Elefantenberg and Okorusu/Gaidus. These inclusions show a Tm_{clath} range of between 8.7°C and 15.2°C in the Okorusu/Gaidus samples, and a range of 3.7°C to 8.8°C in the Elefantenberg and Hartbeespoort samples. The total homogenisation temperature ranges observed in these samples are 223°C to 462°C for the Okorusu/Gaidus samples and 367°C to 375°C in Elefantenberg and Hartbeespoort.

Isolated CO_2 inclusions are rare in the eastern dataset as well, and are present mainly in samples from Hartbeespoort. These inclusions show a T_mCO_2 range of –58.6°C to 57.4°C, and T_hCO_2 of between –11.1°C and 29.8°C. Homogenisation was to the vapour phase.

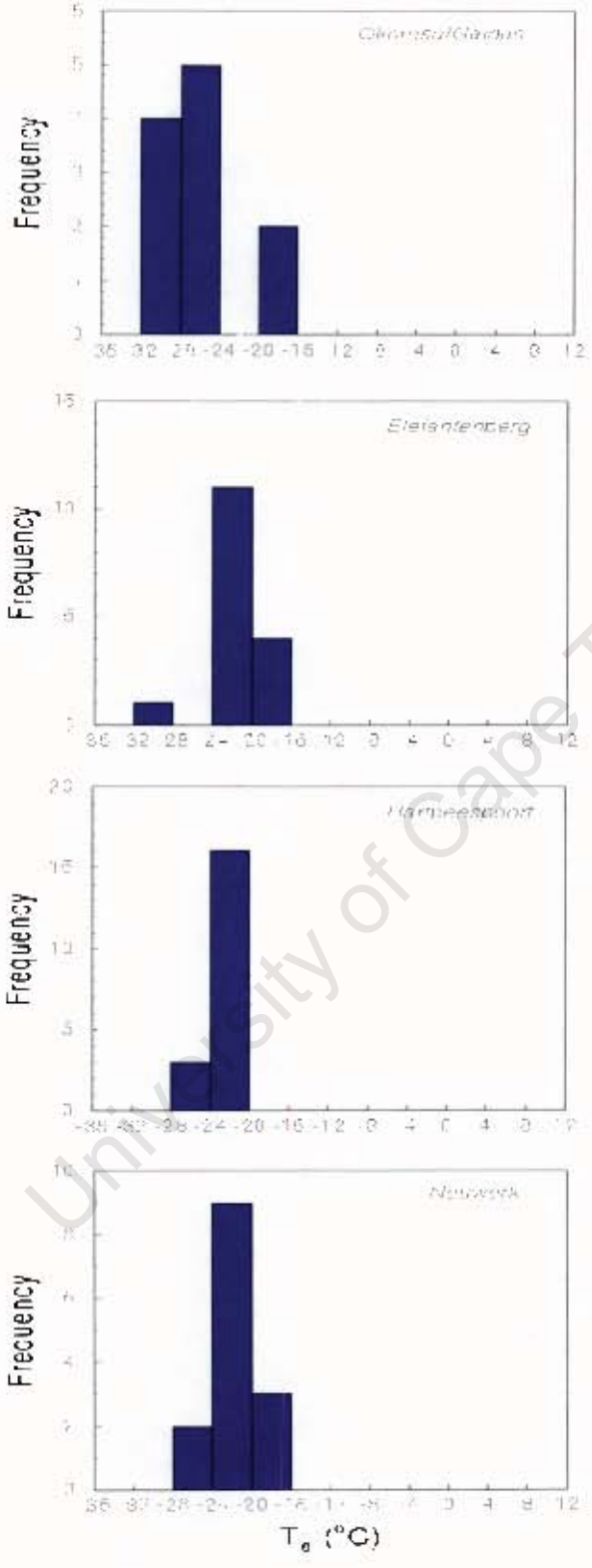

Figure 4.12 Frequency histograms of eutectic temperatures (T_e) observed in aqueous inclusions in samples from the eastern dataset.

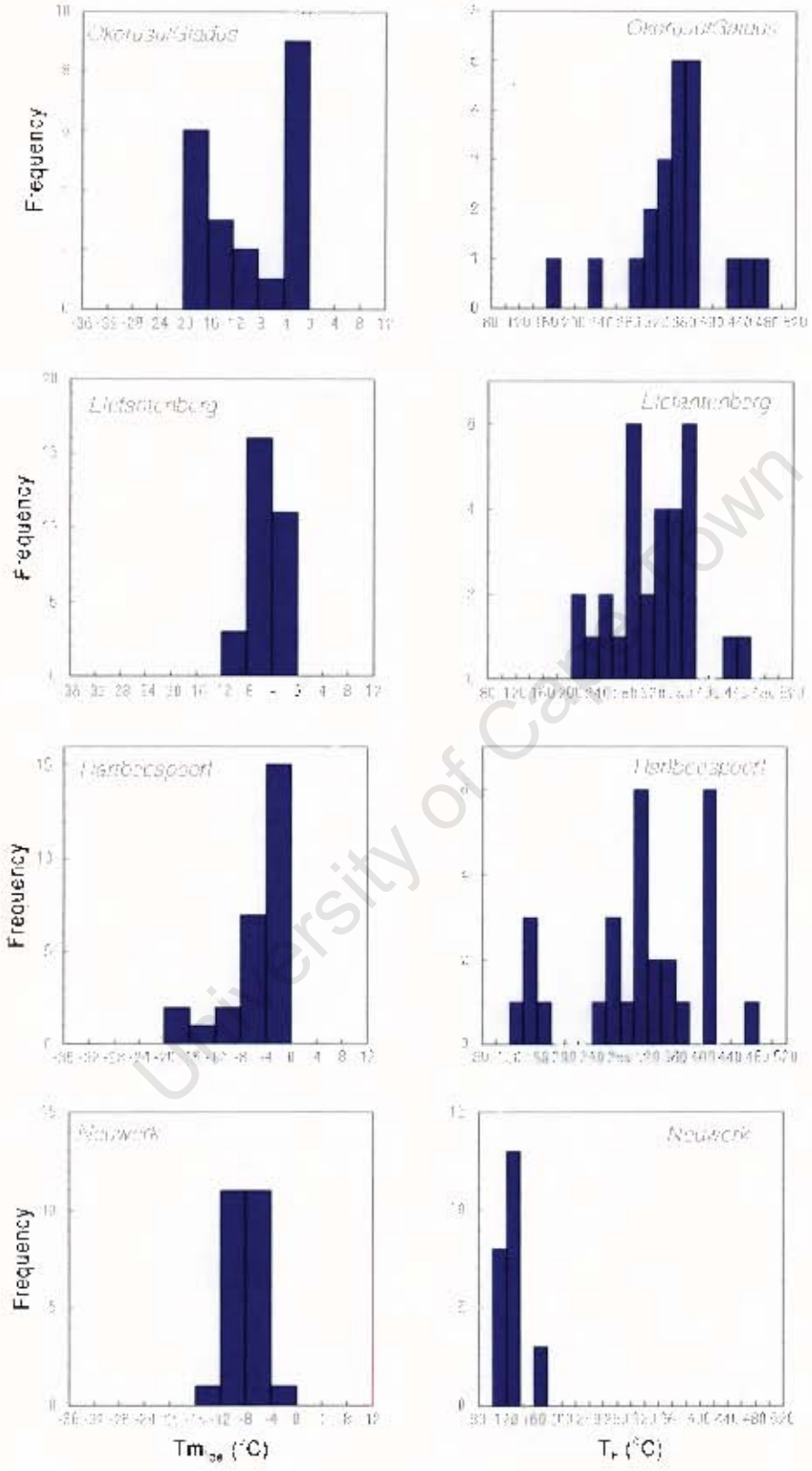

Figure 4.13 Frequency histograms of melting temperatures (Tm_{ice}) and homogenisation temperatures (T_hH_2O) observed for aqueous inclusions in sample areas from the eastern dataset.

Table 4.2 Fluid inclusion results subdivided according to the area of origin in the NZ stratigraphy (eastern dataset). Values in brackets are representative ranges for each sample area. T_e values represent the minimum T_e values observed in each sample area.

	Te(°C)	Tm_{ice}(°C)	Tm_{clath}(°C)	T_h(°C)	Salinity (wt% $NaCl_{eq}$)
Okorusu/Gaidus (Swakop Group)					
Type II & III					
Isolated incl.	-31.2	-19.4 to -0.2		178 to 479	1-26 wt%
Type I					
Isolated incl.	-27.4	-25.2 to –13.5	8.7 to 15.2	223 to 462	
Hartbeespoort (Otavi Group)					
Type II & III					
Isolated incl.	-25.2	-16.8 to –0.2 (-6.5 to –0.2)		173 to 477 (173 to 366)	1-20 wt% (1-10)
Type I					
Phase One	-22.3		8.8	367	2 wt%
Elefantenberg (Otavi Group)					
Type II & III					
Isolated incl.	-31.0	-10.9 to –0.1		209 to 445 (209 to 374)	1-15 wt% (3-15)
Type I					
Isolated incl.			3.7	375	11 wt%
Neuwerk (Nosib-Abenab Transition Zone)					
Type II & III					
Isolated incl.	-24.4 to –9.5	-12.3 to –0.8 (-12.3 to –4.4)		102 to 168	1-16 wt% (7-16)

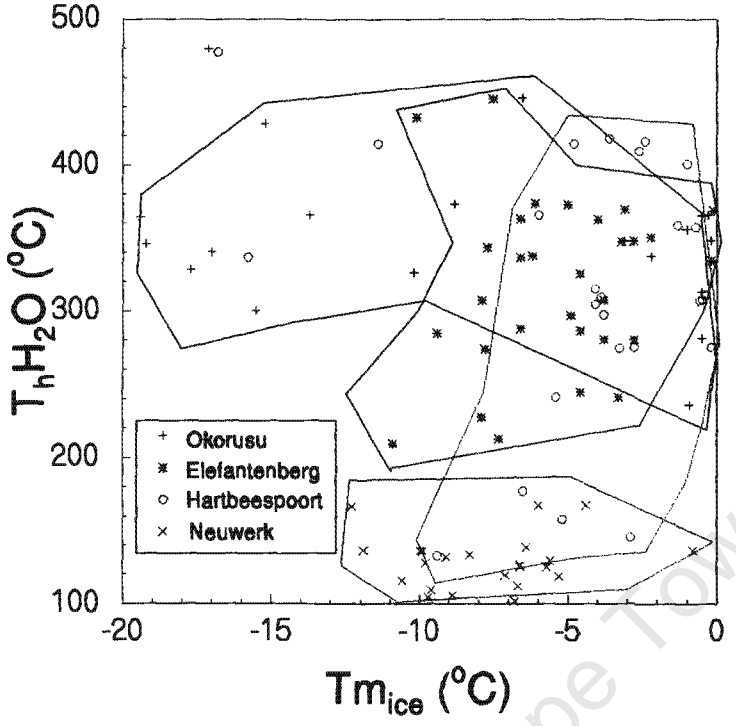

Figure 4.14 T_hH_2O versus Tm_{ice} values for aqueous inclusions in samples from the eastern dataset.

Distinctive fields can be outlined in the T_hH_2O versus Tm_{ice} plots for the eastern dataset sample areas (Figure 4.14). The samples from Okorusu/Gaidus are characterised by a high T_hH_2O and a range of Tm_{ice} values. The field defined by the samples from the farm Neuwerk also show a range of Tm_{ice} values but the T_hH_2O values are much lower. Samples from the farms Hartbeespoort and Elefantenberg show a similar range of Tm_{ice} and T_hH_2O values, with T_hH_2O values similar to the samples from Okorusu/Gaidus but a more restricted range of Tm_{ice} values.

4.2.3 Crush-Leach Analysis

4.2.3.1 Sample Selection and Analyses

Crush leach anaylses of the leachates from quartz subsamples from the quartz plugs and quartz veins from the western and eastern datasets were carried out. As in Chapter 3, the chemistry of the leachates was determined using HPIC (for anionic and cationic concentrations) and ICP-MS (exclusively for determining the Br^- concentration of these fluids).

4.2.3.2 Results

Ternary diagrams reflecting the bulk chemical composition of the fluid inclusion leachates from the samples areas which form the western and eastern datasets are presented in Figures 4.15 and 4.16. In the western dataset, the samples from Moselle, Omburu East and Karachas are dominated by Na^+ with subordinate Ca^{2+} and K^+. Leachates from samples from Bothashof, in contrast, are dominated by Ca^{2+} with subordinate K^+, Mg^{2+} and Na^+ (Figure 4.15). The leachates from the western dataset sample areas contain relatively small proportions of SO_4^{2-}, except for the sample from Karachas (Figure 4.16). The bromine concentrations in these leachates are variable and can be divided into samples with low Br^- (Moselle), intermediate Br^- (Omburu East) and high Br^- (Bothashof, Karachas). The CO_3^{2-} values used in Figure 4.16 are calculated values based the assumption that CO_3^{2-} is the only contributing anion on a charge deficit seen in the inclusion leachates. Clathrate-bearing inclusions and CO_2 inclusions encountered in the western dataset sample areas suggest that the presence of a carbonic anionic species in these fluids is likely. The leachates from Moselle and Omburu East presented in Figure 4.16 are therefore dominated by Cl^- and contain little CO_3^{2-}, while the leachates from Karachas and Bothashof have significant CO_3^{2-} contents.

The leachates from sample areas which form the eastern dataset are dominated by Ca^{2+} with subordinate Na^{+}, and very little K^{+} and Mg^{2+} (Figure 4.15). These leachates also show variable bromine contents, with two groupings being evident, a high-Br^{-} group (Hartbeespoort, Elefantenberg, Neuwerk) and a low-Br^{-} group (Kupferberg, Okorusu/Gaidus) (Figure 4.16). The samples from Okorusu/Gaidus and Kupferberg are characterised by significant CO_3^{2-} contents while the samples from Neuwerk, Elefantenberg and Hartbeespoort contain lower proportions of CO_3^{2-}, being slightly more Cl^{-}-rich.

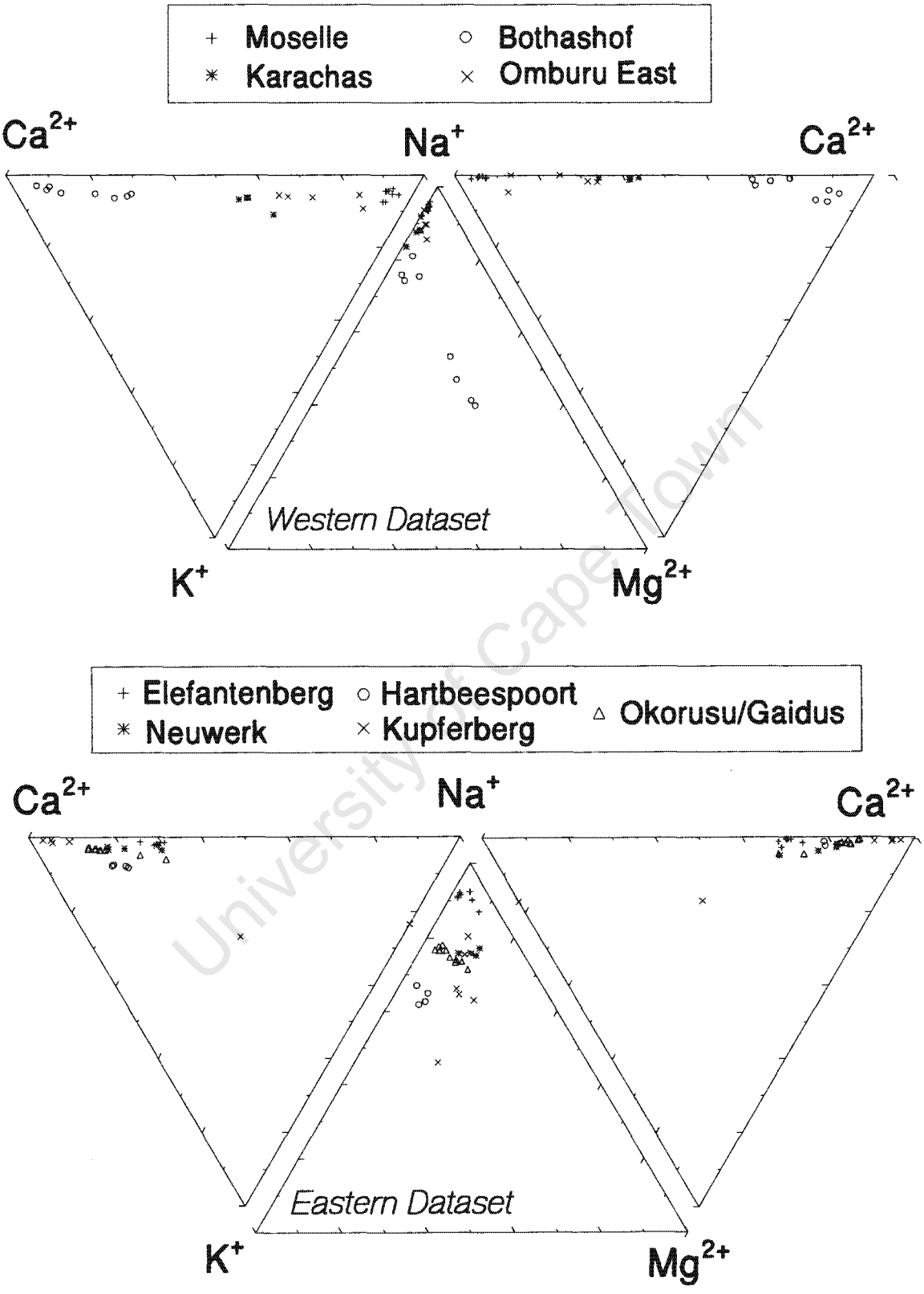

Figure 4.15 Compositional plot of the fluid inclusion leachates from the quartz plugs and veins from sample areas which form the western and eastern datasets, showing the variation in the molar proportions of cations in the fluid inclusion leachates.

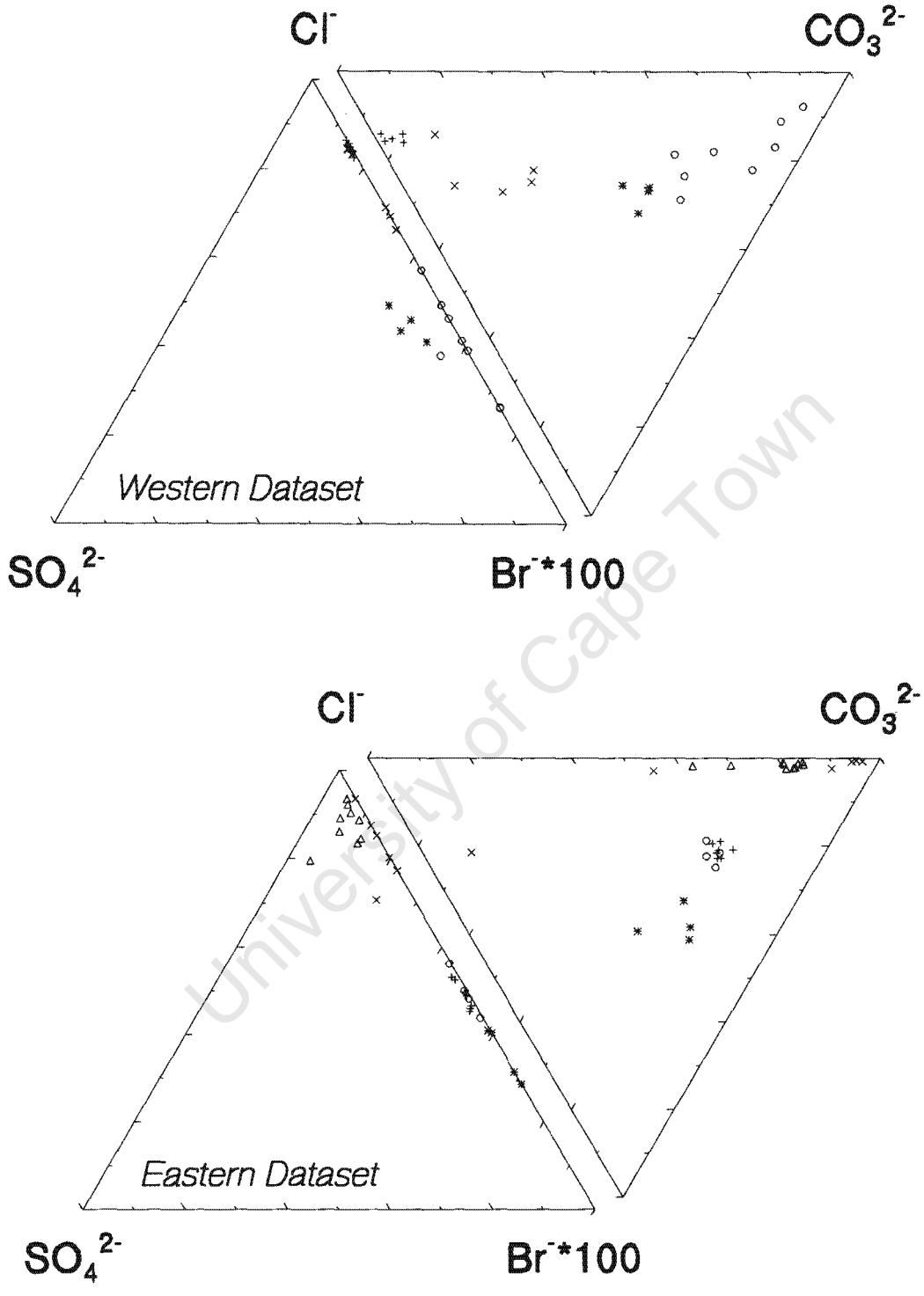

Figure 4.16 Ternary plots showing the molar proportions of anions in fluid inclusion leachates for sample areas which form the eastern and western datasets; for legend see Figure 4.15. The CO_3^{2-} contents of these inclusions represents a calculated concentration based on a charge imbalance seen in these inclusions.

4.2.3.3 Na-Br-Cl Systematics of Fluid inclusion leachates

The leachates from sample areas which form the western dataset lie on an evaporation trend in Na-Cl-Br space (Figure 4.17). The leachates from Bothashof and Karachas (Nosib Group) are characterised by very low Cl/Br and Na/Br ratios, while the Moselle leachates have Cl/Br and Na/Br ratios similar to sea water. The Omburu East leachates are variable in this respect showing a range of values which follow the sea water evaporation trend.

Leachates from Hartbeespoort, Elefantenberg and Neuwerk (eastern dataset) show a restricted range of Cl/Br and Na/Br ratios being characterised by very low ratios which plot on the sea water evaporation trend (Figure 4.18). The leachates from Kupferberg show a wide range of values which extend from low Cl/Br and Na/Br values (below that of sea water) to Cl/Br and Na/Br values higher than that of sea water, along the evaporation-halite dissolution trend. The samples from Okorusu/Gaidus are characterised by Cl/Br and Na/Br values that are all higher than that of sea water, plotting only on the halite dissolution trend.

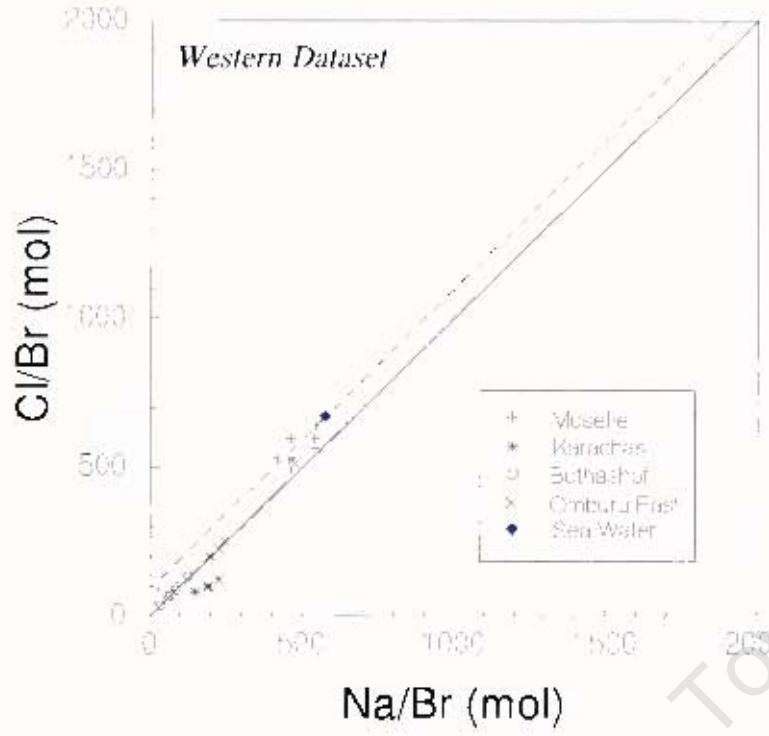

Figure 4.17 Na-Br-Cl systematics of fluid inclusion leachates from selected plug and vein samples from the western dataset using the composition of sea water as a reference. Sea water composition is quoted from Horita *et al* (1991).

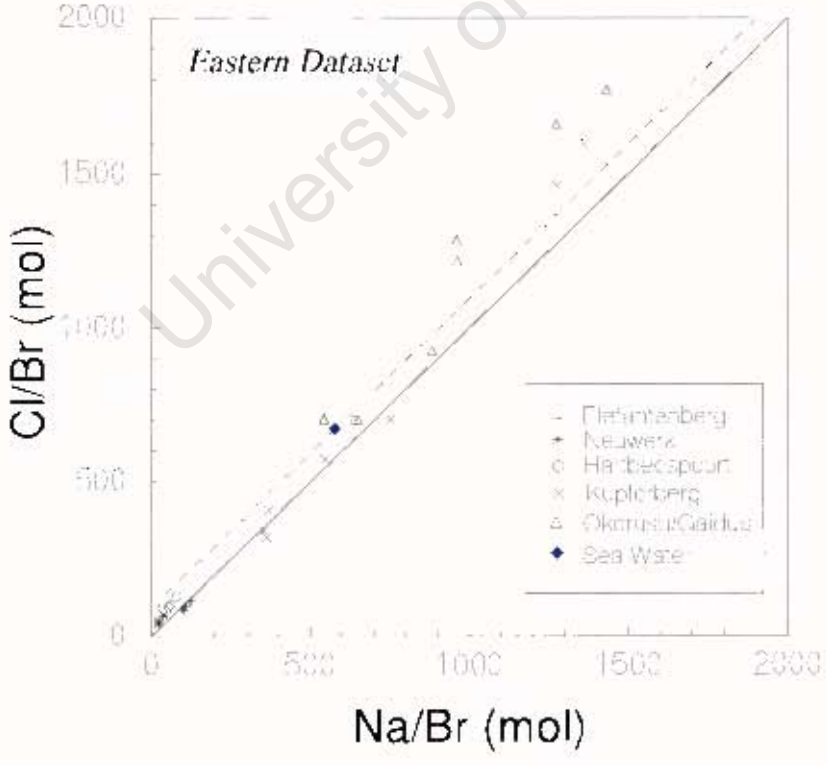

Figure 4.18 Na-Br-Cl systematics of fluid inclusion leachates from selected plug and vein samples from the eastern dataset using the composition of sea water as a reference. Sea water composition is quoted from Horita *et al* (1991).

4.3 Discussion – The Test Localities

4.3.1 Fluid Character and Composition

Western Dataset

The overlapping ranges of T_e, Tm_{ice} and T_hH_2O between the isolated and secondary fluid inclusions in the samples from Moselle and Omburu East indicates that the two types of fluid inclusions were formed by one fluid generation. The clear separation of T_hH_2O values in the sample from the farm Karachas, however, suggests that the isolated and secondary inclusions there represent two different fluid generations. In addition to this, it is clear on the basis of the lower Tm_{ice} and T_hH_2O ranges seen in the isolated and secondary inclusions from the Karachas samples, that the fluids preserved there are unrelated to the fluids preserved in the samples from the farms Omburu East, Moselle and Bothashof (Figure 4.11).

The minimum T_e values of –44.0°C and –40.0°C recorded in the samples from Bothashof and Omburu East indicates the presence of polyvalent cations in solution (Ca^{2+} and Mg^{2+}), in addition to Na^+ (Goldstein and Reynolds, 1984). The closeness of the T_e and Tm_{ice} ranges in the samples from Omburu East, Moselle and Bothashof reflects rapid melting which is indicative of the presence of K^+ (Davis *et al.*, 1990). The bulk chemical composition of the leachates from the sample areas which form the western dataset generally confirms these microthermometric observations. In the samples from Moselle, Omburu East and Karachas, the solutions contain Ca^{2+} with lower proportions of Mg^{2+} and K^+, in addition to Na^+. The samples from Bothashof are dominated by Ca^{2+}, with subordinate Na^+, resulting in the very low T_e values observed in these samples.

The predominance of Cl over CO_3^{2-} in the Omburu East and Moselle samples suggests that at least some of the Ca^{2+} and Mg^{2+} present in the leachates are in the form of dissolved salts of chlorides ($CaCl_2$ and $MgCl_2$) in addition to dissolved carbonate (Figure 4.19). The leachates from Bothashof and Karachas line lie on the 1:1 line in this plot suggesting that the Ca^{2+} and Mg^{2+} in these fluids are in the form of dissolved carbonates (Figure 4.19).

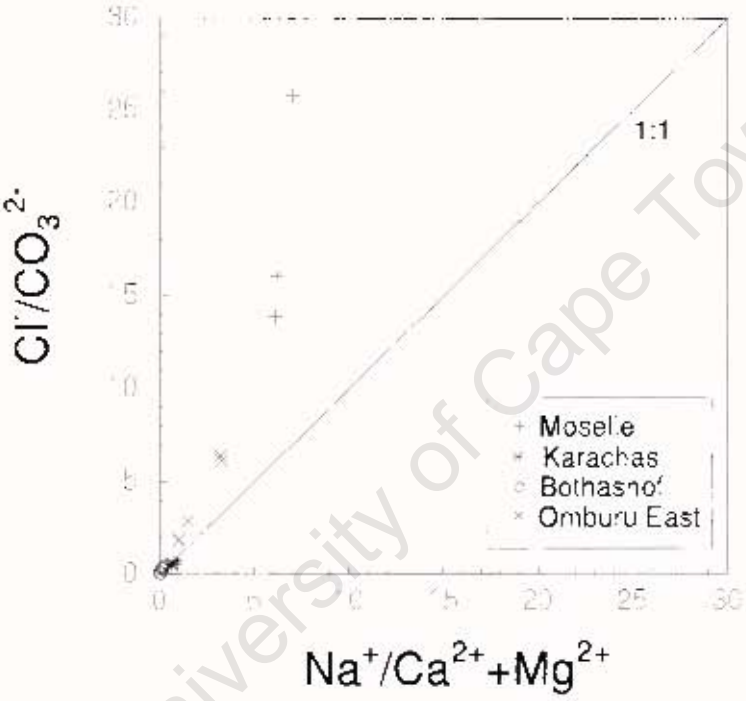

Figure 4.19 Cl^-/CO_3^{2-} versus $Na^+/Ca^{2+}+Mg^{2+}$ plot of fluid composition for samples from the western dataset) in terms of ratios of the dominant anionic and cationic species of these fluids. Samples plotting above the 1:1 line indicate a predominance of Cl over CO_3^{2-}.

The large range of Tm_{ice} values seen in the samples from Bothashof and Omburu East and the distribution of data in Figure 4.10 suggests the existence of two Tm_{ice} populations in the inclusions from these sample areas. Mixing between fluids of different salinities may be indicated by such a distribution and is therefore proposed as an explanation for such a signature in these two sample areas.

The large ranges of T_hH_2O values seen in the aqueous inclusions from Moselle, Omburu East and Bothashof suggests that necking of inclusions as well as the introduction of some CO_2 into the fluid might have played a role in their evolution. The presence of CO_2 inclusions as well as clathrate-bearing inclusions in some samples seems to support this contention. The sampled quartz plugs and veins are also hosted in carbonate units and are associated with carbonate precipitates and veins, lending further credence to the possibility of some CO_2 in the aqueous inclusions. An assessment of the CO_2 contents in the aqueous inclusions is presented in Figure 4.20. As in Part I, the solid lines in Figure 4.20 represent a fluid unmixing path of a NaCl-CO_2-H_2O fluid into its CO_2-rich and NaCl-H_2O-rich end members during cooling. The $X(CO_2)$ values measured in the Type IV inclusions from this dataset are in the range 50 to 62.5 % at T_hCO_2. This value was used to represent the CO_2-rich end member. Assuming that the clathrate-bearing inclusions and suspected clathrate-bearing inclusions in this dataset are related to the CO_2 inclusions and that the $X(CO_2)$ estimates are reasonably accurate, then an amount of between 10 and 15% CO_2 is estimated to be present in the NaCl-H_2O-rich clathrate-bearing end member (Figure 4.20). The total homogenisation temperatures of the clathrate-bearing inclusions are in the range 420°C to 500°C which conforms to well to the actual (higher) T_hH_2O ranges observed in the clathrate-bearing inclusions and suspected clathrate-bearing aqueous inclusions in this dataset. Variable CO_2 contents can therefore account for at least some of the higher T_hH_2O values recorded for the aqueous inclusions of the western dataset. An alternative explanation for the range of T_hH_2O values observed in the aqueous inclusions is a fluctuation in trapping pressure producing the range of T_hH_2O values observed. This is explored further in the next section (geothermobaromtery).

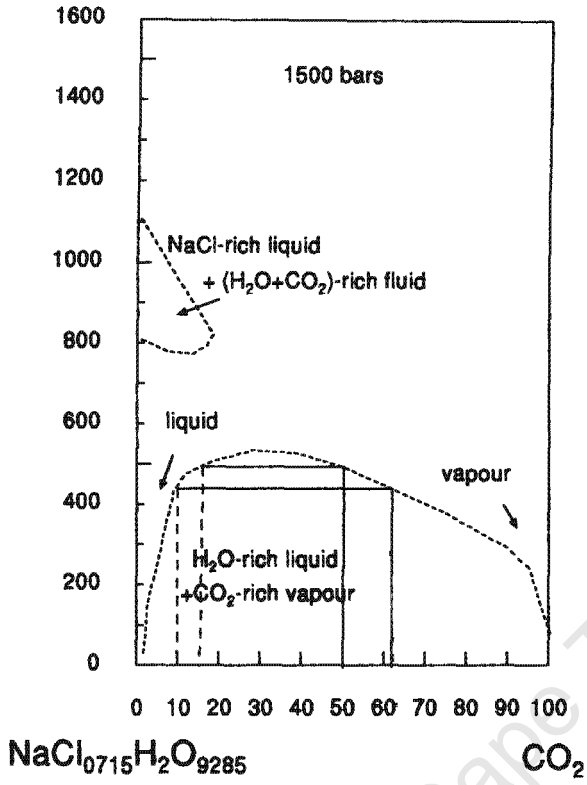

Figure 4.20 CO_2-NaCl-H_2O phase diagram assuming a salinity of 20 wt% $NaCl_{eq}$ and a pressure of 1500 bars (after Bowers and Helgeson, 1983).

Eastern Dataset

The microthermometric data seem to indicate the existence of at least three different fluid types in the sample areas which make up the eastern dataset (Figure 4.14). The leachates from Elefantenberg and Hartbeespoort form a low salinity, high T_hH_2O fluid type that shows a considerable degree of overlap in the two areas. The second fluid type is preserved within the quartz samples from the farm Neuwerk. These samples originate from the Nosib-Abenab transition zone and are characterised by low T_hH_2O values and a variable salinity (up to 16 wt% $NaCl_{eq}$). The third fluid type is preserved within the samples from the border of the farms Okorusu/Gaidus. There a fluid of variable salinity (up to 26 wt% $NaCl_{eq}$) with a consistent, high T_hH_2O occurs. Mixing between a fluid of high salinity and a fluid of low salinity is suggested as an explanation for the large range of salinities observed in the samples from this area

(two fluid generations, one of high salinity and the other of low salinity being suggested by the Tm_{ice} values recorded for this sample area).

Lower T_e values of down to –31.1°C seen in samples from Hartbeespoort and Elefantenberg indicates the presence of polyvalent cations (Ca^{2+} and Mg^{2+}) in addition to Na^+ in the fluids, in these areas. Eutectic temperatures bewteen -21.2°C and –30.0°C seen in samples from Neuwerk and Okorusu/Gaidus also indicate the presence of additional monovalent and polyvalent cations (in addition to Na^+) in solution in these areas (Goldstein and Reynolds, 1984). The bulk chemical compositions of the fluid inclusion leachates from the eastern dataset sample areas confirms the observations made on the T_e values. However, the large amount of Ca^{2+} in these fluids indicates that it may be the sole contributor to the low T_e values observed in the eastern dataset sample areas. The predominance of CO_3^{2-} over Cl^- in the leachates from Hartbeespoort and Neuwerk (and some samples from Okorusu/Gaidus) indicates that all of the Ca^{2+} and Mg^{2+}, as well as some Na^+ in these fluids is present in the form of dissolved carbonates (Figure 4.21). The Ca^{2+} and Mg^{2+} in the leachates from Elefantenberg, Kupferberg and the remaining samples from Okorusu/Gaidus, are most likely to be present in the form of dissolved carbonates, with Na^+ present as a dissolved chloride.

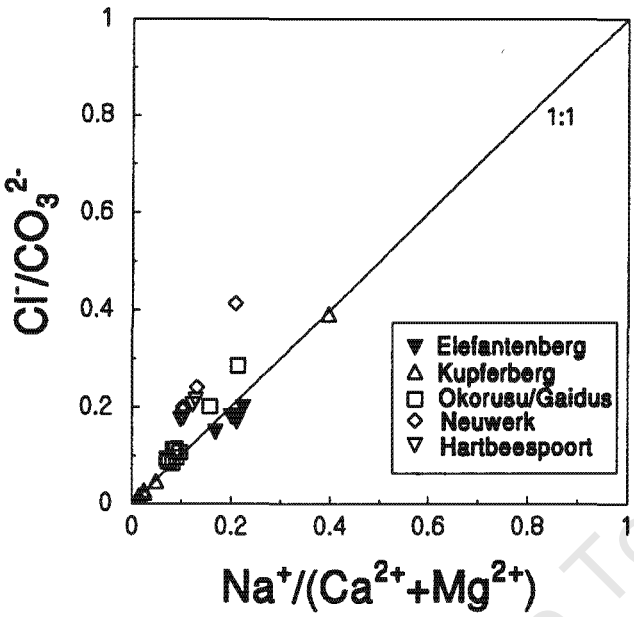

Figure 4.21 Cl^-/CO_3^{2-} versus $Na^+/(Ca^{2+}+Mg^{2+})$ plot of fluid composition for samples from the eastern dataset showing ratios of the dominant anionic and cationic species in these fluids. Samples plotting above the 1:1 line indicate a preedominance of Cl^- over CO_3^{2-}.

A large range of T_hH_2O is also recorded in the sample areas which make up the eastern dataset. The effect of necking of aqueous inclusions on the microthermometric data produced for the sample areas from the eastern dataset has not been evaluated due to the random distribution of inclusions commonly seen in these samples and it is suggested as one possible explanation for the range of T_hH_2O values observed. High T_hH_2O values of above 400°C suggests that the aqueous inclusions may contain some CO_2. The carbonate host rocks of these inclusion bearing veins and plugs as well as the associated calcite precipitates in these veins, along with the presence of CO_2 inclusions and clathrate-bearing inclusions in these samples, makes the possibility of a minor CO_2 content plausible. An similar assessment of the amount of CO_2 present in these inclusions was carried out as that outlined previously for the Western Dataset.

The $X(CO_2)$ range observed in the Type IV inclusions in the eastern dataset is similar to that seen in the western dataset, i.e., between 50 and 62.5 % resulting in a corresponding estimate of 10-15 % CO_2 in the suspected clathrate-bearing (aqueous) inclusions (Figure 4.22). Total homogenisation temperatures of between 420°C and 500°C for the inferred clathrate-bearing inclusions corresponds well with the observed high T_hH_2O range in the aqueous inclusions in the eastern dataset.

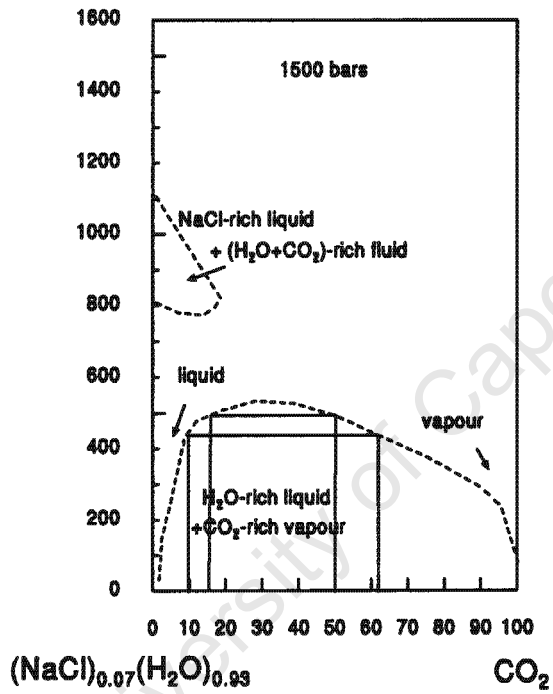

Figure 4.22 CO_2-NaCl-H_2O phase diagram assuming a salinity of 20 wt% $NaCl_{eq}$ and a pressure of 1500 bars (after Bowers and Helgeson, 1983).

Variation in Fluid Composition between the Eastern and Western datasets

The samples from lower down in the stratigraphy, i.e., Karachas (Nosib Group), Neuwerk (Nosib-Abenab transition), show quite different fluid compositions to those of the samples taken from higher stratigraphic levels. The samples from Elefantenberg and Hartbeespoort (in the Maieberg Formation) also show some degree of variation

The samples from Moselle, Okorusu/Gaidus, Bothashof and Omburu East all originate from a similar level in the stratigraphy, and these samples show the largest degree of overlap. With the exception of the samples from Moselle, all the samples from the remaining areas are characterised by a wide salinity range and high T_hH_2O. Four different fluids preserved in the sample areas are therefore indicated, i.e., that from (a) Okorusu/Gaidus, Moselle, Omburu East, Bothashof; (b) Hartbeespoort and Elefantenberg; (c) Neuwerk; (d) Karachas. Although the fluids from Karachas and Neuwerk are characterised by similar T_hH_2O ranges, they also show different salinities suggesting a different origin.

4.3.2 Geothermobarometry

The isochores produced Figure 4.23 are based on the microthermometric data from the eastern and western datasets and were generated using the FLINCOR software (Brown, 1989), an estimated composition of $NaCl\text{-}H_2O$, and the Brown and Lamb (1989) equation of state. The fluids from these two datasets are dominated by either Na^+ or Ca^{2+}. A simplified model system of $NaCl\text{-}H_2O$ was used as cotectic surfaces where ice melts for the systems $NaCl\text{-}H_2O$, $NaCl\text{-}CaCl_2\text{-}H_2O$, and $CaCl_2\text{-}H_2O$ lie essentially on top of each other with a only small deviation (Oakes *et al.*, 1990).

The isochores produced are based on the lowest and highest T_hH_2O values observed in isolated inclusions preserved in the eastern and western datasets (listed in Tables 4.1 and 4.2). The fluid densities indicated by the microthermometric data are as follows: Moselle (0.878 to 0.956 g/cm^{-3}); Omburu East (0.853 to 0.951 g/cm^{-3}); Bothashof (0.914 to 1.036 g/cm^{-3}); Okorusu/Gaidus (0.693 to 1.036 g/cm^{-3}); Hartbeespoort (0.702 to 0.994 g/cm^{-3}); Elefantenberg (0.688 to 0.969 g/cm^{-3}).

Bothashof (0.914 to 1.036 g/cm^{-3}); Okorusu/Gaidus (0.693 to 1.036 g/cm^{-3}); Hartbeespoort (0.702 to 0.994 g/cm^{-3}); Elefantenberg (0.688 to 0.969 g/cm^{-3}).

In the previous section it was found that the range of T_hH_2O that were observed in the inclusions preserved in the eastern and western datasets could not be adequately explained by CO_2 contents alone. An examination of the effect of hydrostatic versus lithostatic pressure on the trapping conditions of the fluids preserved, as was done in Chapter 3, was carried out for the samples from the eastern and western datasets.

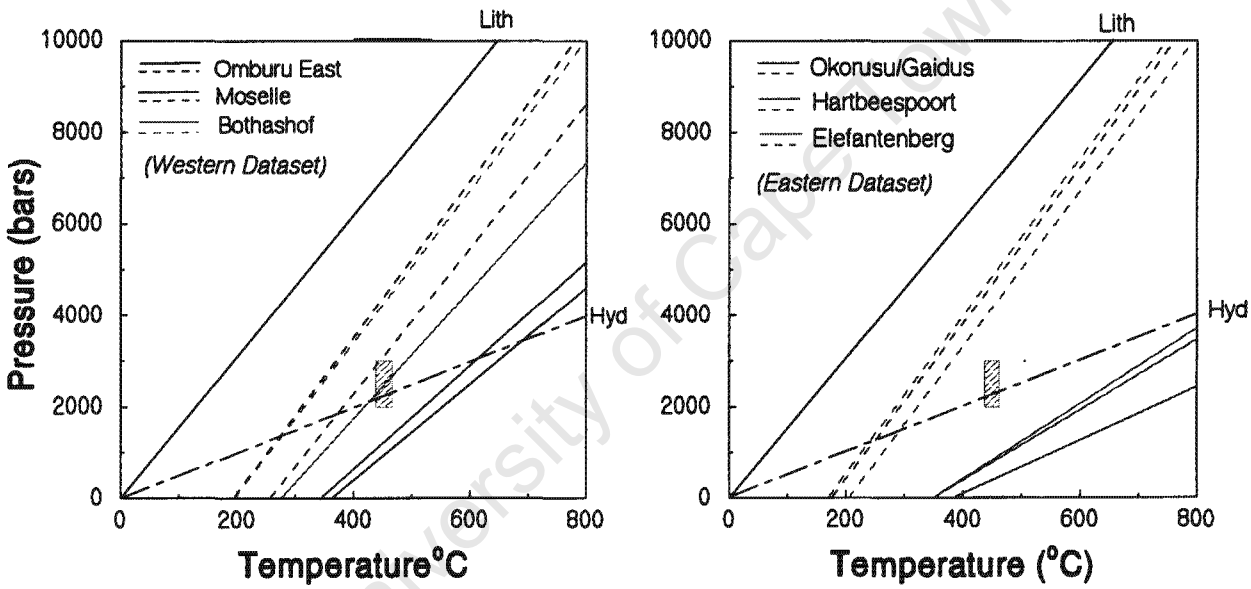

Figure 4.23 Geothermobarometry results based on the fluid inclusion data from the Eastern and Western Datasets. The dashed lines represent isochores for the lowest homogenisation temperatures and the solid lines represent the highest homogenisation temperatures recorded in these inclusions. The green field represents a peak metamorphic temperature and pressure estimate from Hoffer (1977). (Lith=lithostatic pressure; Hyd=hydrostatic pressure).

An independent estimate of pressure and temperature from a pelitic metamorphic assemblage in the eastern NZ in the range 430-450°C and 2-2.5 kbar (Hoffer, 1977) is represented as a field in Figure 4.23. Assuming peak metamorphic temperatures of between 430-450°C, the calculated isochores in Figure 4.23 indicate that the high T_hH_2O fluids preserved as inclusions in the western dataset were trapped under lower

(hydrostatic) pressures of between 1 and 2 kbars, while the lower temperature inclusions were trapped under high (lithostatic) pressures of between 3 and 4 kbars. Alternatively, a higher (amphibolite facies) trapping temperature for the high T_hH_2O fluids are indicated at pressures of 2-2.5 kbars, and low trapping temperatures of 300°C-350°C are indicated for the low T_hH_2O fluids.

Similarly, very low (hydrostatic) pressures of <1 kbar for the high T_hH_2O fluids in the inclusions from the eastern dataset and higher (lithostatic) pressures of between 4 and 4.5 kbar for the low T_hH_2O inclusions are indicated, if a peak metamorphic temperature of 430-450°C is assumed. A higher (amphibolite facies) trapping temperature for the high T_hH_2O fluids are indicated at pressures of 2-2.5 kbars, and low trapping temperatures of ~300°C are indicated for the low T_hH_2O fluids.

The peak metamorphic pressure calculated to be in operation in the eastern NZ by Hoffer (1977) was approximately 2,5 kbar. The higher pressures suggested by the lower temperature fluids preserved in both the eastern and western datasets are therefore considered unlikely. Similarly, the high trapping temperatures (>600°C) suggested by assuming a fixed pressure of 2- 2.5 kbar, for the high T_hH_2O fluids, seems unlikely as the grade of metamorphism in the sample areas (and in the NZ generally) is very low (greenschist facies). Necking of the aqueous fluid inclusions and variable CO_2 contents outlined in the previous sections are therefore suggested as the more likely cause for the spread of T_hH_2O data in the eastern and western datasets.

4.3.3 Fluid Source

Both evaporite-derived and retrograde fluids are considered likely candidates for generating high salinity, mineralising fluids (Chetty and Frimmel, 2000; Bennett and Barker, 1992). However, retrograde fluids were considered an unlikely source for the mineralising fluids sample areas selected in the NZ for the following reasons. The low to very low metamorphjc grade of the units in the sample areas in the NZ (and the eastern NZ in general) and the lack of any retrograde alteration effects in the sample areas, indicates that an origin for the fluids preserved as inclusions there, as a locally derived retrograde fluid, is unlikely. The Br^--rich composition of the fluids also argues against an origin as a retrograde fluid, the generation of the significant Br^- contents of the fluids by evaporitic concentration being considered more likely.

Other evidence which points to an evaporitic origin for the fluids in the NZ sample areas can be outlined as follows. The fluid inclusion leachates from the sample areas Moselle, Omburu East and Bothashof which form part of the western dataset lie on an evaporation trend in the Na/Br versus Cl/Br plot suggesting that these fluids are indeed evaporitic-derived (Figure 4.17). The samples from Karacahas, however, lie on a trend below the 1:1 line in these plots suggesting that a different anion (other than Cl^-) is dominant in these solutions, possibly a bicarbonate ion. The microthermometric data also indicate that the fluids preserved within the Karachas samples are of low salinity and are unrelated to the fluids from the other three sample areas which make up the western dataset. An evaporitic origin for this fluid is considered less likely.

these two sample areas. The xenoliths clearly show evidence of experiencing some degree of albitisation in their evolution (Figure 4.2, 4.3). The trends of the xenolith samples in the multi-element diagrams from these areas follow that shown by the albitised pelitic unit in the SMZ quite closely and in the case of the Omburu East sample, in the rare earth element plot as well (Figure 4.6). The Nosib Group samples, in contrast, show no relationship with the albitised sample trends indicating that they were not subject to a similar process in their evolution. The source of these xenolithic fragments present in the quartz plugs on the farm Moselle and in the siliceous dolomite present on the farm Omburu East, can therefore not be linked to the Nabis Formation (Nosib Group) in the NZ, on the basis of the data presented. However, the albitised nature of the xenolithic fragments and the albitisation trend shown by these units are quite similar to the those seen in the upper Nosib Group in the SMZ suggesting that the source of these xenoliths are possibly in the upper Nosib Group of the NZ.

The rare earth element trends also give an indication of the environment of formation of these units. The strong light rare earth element enrichment trends seen in the chondrite-normalised rare earth element plots along with the flattening of all the light rare earth element enrichment trends seen in the upper continental crust-normalised plots, suggests a strong continental influence. An origin within a continental rift graben for these units is therefore supported by the data presented and an origin within the NZ Nosib Group for these xenoliths is therefore possible. By implication, the source of the fluids preserved as inclusions in the sample areas Omburu East and Moselle is also within the NZ Nosib Group.

The leachates from the sample areas which make up the eastern dataset show some variability (Figure 4.18). The leachates in the samples from Okorusu/Gaidus and Kupferberg extend from the evaporation trend below the sea water marker onto the halite dissolution trend, indicating that some halite dissolution might have played a role in the evolution of these fluids. An alternate origin for the trend shown by the leachates from Okorusu/Gaidus was indicated by the microthermometric data for this sample area outlined previously. The wide range of salinities recorded at a consistent T_hH_2O values in the samples from Okorusu/Gaidus points to a mixing of a low salinity and high salinity fluid. The bimodal distribution of Tm_{ice} values in this sample area supports this contention (Figure 4.13). This could therefore explain the spread of data from the fluids from Okorusu/Gaidus in the Na/Br versus Cl/Br plots. An indication of the true character of the mineralising fluids in these areas can therefore be gained from the extreme end member compositions of these fluids in the Na-Br-Cl plots.

The leachates in the samples from Hartbeespoort, Elefantenberg and Neuwerk are characterised by very low Cl/Br and Na/Br ratios and lie parallel to the evaporation trend in Na-Cl-Br space, suggesting that they too are derived from evaporation. However, the low salinities of the fluids preserved as inclusions in these areas (indicated by the microthermometric data) seems inconsistent with such an origin and an evaporitic origin for the fluids from these three sample areas is considered unlikely. The leachates from these three sample areas also form a well defined field in Na-Br-Cl space, suggesting that fluid mixing in these areas was minimal. The fluids in operation in the eastern dataset sample areas are therefore quite variable. Only the fluids from Okorusu/Gaidus and Kuperberg are considered to be of an evaporitic

origin. These fluids have experienced some alteration of their geochemical signature due to mixing with a lower salinity fluid, probably meteoric water (suggested by the low Br^- content of the low salinity end member).

An examination of the Ca-excess versus Na-deficit in these fluids (as an assessment of the effect of alibitisation on fluid composition) is presented in Figure 4.24. Except for Bothashof, the leachates from the sample areas which form the western dataset show little variation in the Ca-excess, Na-deficit plot, plotting close to the origin. The effect of albitisation appears minimal on this dataset with only the Bothashof samples showing some evidence for dolomitisation.

The interpretation of the data from the eastern dataset is similar with little or no evidence seen for albitisation altering the fluid chemistry in these samples, and all leachates showing an enrichment in Ca which indicates dolomitisation or the addition of calcium into the system. The Ca-excess values seen in the eastern dataset sample areas and the samples from Bothashof therefore suggests that contamination by the host carbonates in these areas is likely enriching the fluids in Ca^{2+} and possibly CO_3^{2-}. The bulk chemistry of the leachates from these areas shows that they are indeed enriched in both Ca^{2+} and CO_3^{2-} (Figures 4.14 and 4.15). The Ca^{2+} and CO_3^{2-} contents of the fluids in Bothashof and the eastern dataset sample areas can therefore not be regarded as indicative of the original fluid composition.

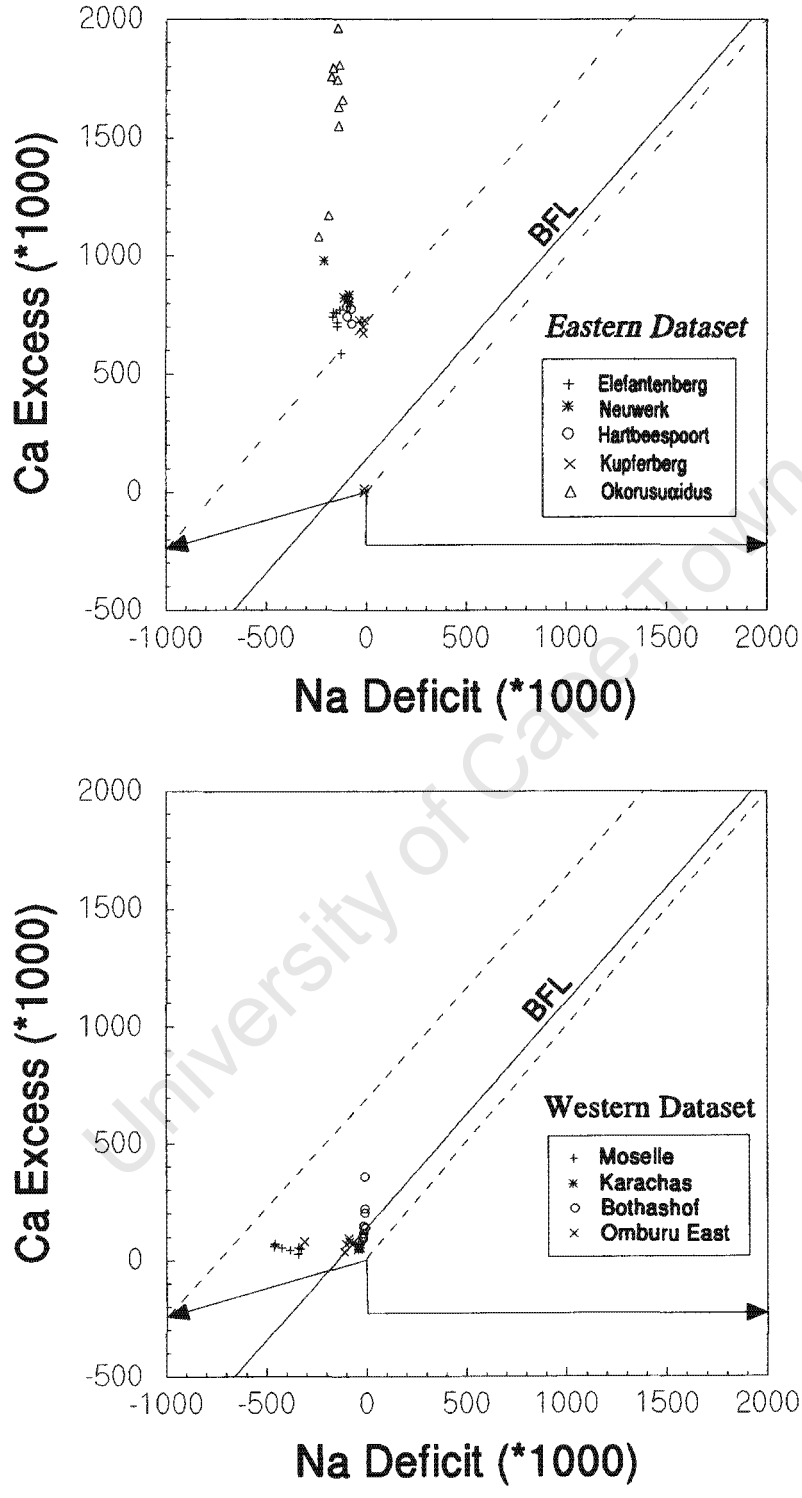

Figure 4.24 Ca Excess- Na Deficit plot for leachates of fluid inclusions from the sample areas within the eastern and western datasets. BFL = Basinal Fluid Line.

(5)

Assessment

5.1 Assessing the Test Localities

5.1.1 Comparison of data from NZ and SMZ

5.1.1.1 Fluid Source

The existence of evaporite-derived fluids in both the NZ and SMZ is indicated on the basis of their Na-Br-Cl contents and relatively high salinities. However, a slightly different fluid evolution in each of these areas is indicated by their fluid geochemistry. The fluids in the SMZ record the process of halite dissolution at some stage in their evolutionary history. The fluids from the NZ show little evidence for the process of halite dissolution and few halite oversaturated inclusions are encountered in the samples areas from the NZ . Although samples from Okorusu/Gaidus and Kupferberg do lie on the halite dissolution trend, the evidence presented previously argues for a process of mixing of fluids resulting in this fluid signature. The lack of halite dissolution playing a role in the evolution of these fluids is as would be expected. In the SMZ, the evaporitic fluids have not travelled far from their suspected source units (i.e. the evaporitic Duruchaus Formation) and some of the fluid could possibly have remained in contact with the primary evaporitic minerals that were precipitated from them. Halite dissolution in such an environment is quite likely (Kessler *et al.*, 1995). The fluids in the NZ have been removed from contact with their primary mineral precipitates and any dissolution of previously precipitated primary evaporitic minerals into this fluid would therefore not be possible. The fluids in Okorusu/Gaidus, Kupferberg, Bothashof, Moselle and Omburu East in the NZ are therefore also interpreted as being evaporite-derived but have experienced a different history when compared to the fluids from the SMZ.

There are also significant differences in salinity between the fluids from the NZ (up to 29 wt% $NaCl_{eq}$) and SMZ (up to 47 wt% $NaCl_{eq}$) which result due to the above processes. The halite dissolution seen in the SMZ is responsible for the generation of such large salinity values while the lack of a similar process in the NZ has resulted in halite undersaturated inclusions and the lower salinities recorded.

The xenoliths present with the quartz-dolomite and quartz plugs from the SMZ and from the sample areas Moselle and Omburu East (western dataset) in the NZ support an origin for the evaporitic fluids from within the Nosib Group. De-watering of the evaporites preserved within the Duruchaus Formation form a likely source for the highly saline fluids preserved as inclusions in the sample areas in the SMZ. The NZ Nosib Group represents a possible source region for the evaporitic fluids preserved in the NZ, the existence of evaporitic units similar to that seen in the Duruchaus Formation of the SMZ being supported by the presence of albitic and dolomitic xenoliths which show a similar whole rock chemistry to the *in situ* units of the Duruchaus Formation.

The source of the evaporitic fluids in the remaining sample areas can be speculated upon as follows. The samples from Okorusu/Gaidus and Bothashof were hosted in the upper Tsumeb and upper Swakop Groups. There are two possible evaporitic sources for these fluids, i.e., the Nosib Group of the NZ or alternatively the evaporitic units in the Hüttenberg Formation. Chetty and Frimmel (2000) suggest that that either of these evaporitic horizons could generate the types of fluid signatures seen in the NZ evaporitic fluids, i.e., relatively high salinities with low Na/Br and Cl/Br ratios.

5.1.2 Mineralising Potential

The preceding discussion focussed on geochemical trends shown by fluids derived from evaporites which were possibly formed in continental rifts (relected by the metasedimentary facies of the Nosib Group). Such environments have been found to show a clear general sequence in their evolution which contributes to the formation of metalliferous hydrothermal brines, i.e., (i) tectonism leads to high relief rift basins with rapid subsidence, high sedimentation rates, and high permeability and porosity, (ii) orographic effects promote high evaporation rates in hydrologically restricted rift basins, (iii) magmatism and high heat flow drive fluid flow and chemical reactions at shallow crustal levels (McKibben and Hardie, 1997). Once formed, the metalliferous brines formed in such environments must undergo focussed flow, and profound local thermal and chemical changes in order to induce concentrated deposition of their dissolved metals at economic grades (McKibben and Hardie, 1997). The rift systems which act as a source area for these brines are typically characterised by high rates of evaporation and the presence of significant evaporite beds. This results in fluids of high salinities which contain significant amounts of complexing ions available for base metal transport. Once these metalliferous brines are formed, fluid migration is facilitated when tectonic events generate or reopen vertical fractures that transgress the fluid interface. This allows more oxidised, less saline geothermal fluids to mix with deep, metalliferous, hypersaline brines resulting in eventual mineral precipitation (McKibben and Hardie, 1997). Mineral or ore precipitation may also be facilitated by simple cooling of the metalliferous brines or neutralising of the acidic ore fluids by reaction with carbonates in the sequence.

The fluids from Okorusu/Gaidus, Bothashof, Omburu East and Moselle are highly saline and all these fluids are therefore potential base metal carriers. The fluid

signature preserved in the Okorusu/Gaidus samples, however, also suggests that fluid mixing played a role in the fluid evolution in this area. The fluids from Okorusu/Gaidus therefore show a number of characteristics typical of mineralising brines preserved in ore localities (high salinity, evaporitic and the mixing of fluids at ore locality), and the samples from Okorusu are indeed associated with small scale base metal mineralisation. The small scale of the mineralisation is possibly due to a limited availability of metals in the sample area.

Closer examination of the geochemical trends shown by the fluids from Bothashof, Omburu East and Kupferberg suggests that a similar process of mixing of fluids may have been in operation there. The Tm_{ice} values observed in the samples from Bothashof and Omburu East suggests the existence of a mixed fluid signature in these areas (Figure 4.9) and the distribution of the Kupferberg leachates in Na-Br-Cl space mirroring the trend of the Okorusu/Gaidus samples suggests that fluid mixing played a role in the fluid evolution in this area as well (Figure 4.17). Base metal mineralisation has been reported in both Kupferberg and Bothashof (Schneider and Seeger, 1992).

Areas in the Test Localities which therefore show the most potential with regards to base metal mineralisation are: Okorusu/Gaidus, Bothashof, Omburu East and Kupferberg. Although the fluids from Moselle show a high salinity and an evaporitic signature, the lack of any evidence for fluid mixing in this area may preclude the formation of an ore deposit there.

(1983a). Positive Ce anomalies exhibited by the carbonates present in the sequence and the strong light rare earth enrichment trends shown by all the lithic units suggests a continental provenance for the Duruchaus Formation evaporites. No evidence for a marine sabkha deposit at the top of the Duruchaus Formation was found, though.

The microthermometric data from the inclusions preserved within the quartz-dolomite plugs of the Duruchaus Formation in the SMZ conform well with those reported by Schmidt-Mumm (1989). The data suggest that the Phase One generation of Schimdt-Mumm (1989) corresponds to the isolated inclusions measured in this study and that Schmidt-Mumm's Phase Two generation corresponds to the secondary inclusions (based on homogenisation temperatures and calculated salinities). Evidence for a higher CO_2 content in the Phase Two generation of Schimdt-Mumm (1989) was not found in the secondary inclusions, though, and the influence of Schmidt-Mumm's Phase Three fluid generation on this dataset appears minimal. A higher T_e temperature range was observed in this study when compared to Schmidt-Mumm (1989), and can possibly be explained by the subjectivity of this measurement. However, these data could also indicate that the T_e values (and hence the composition of the fluid) may be slightly different than that reported by Schimdt-Mumm (1989).

Based on the Na-Br-Cl contents of fluids examined in the NZ, the activity of evaporitic fluids in the NZ of the Damara Belt is also indicated, suggesting the presence of buried evaporitic units similar to those present in the Duruchaus Formation there. Evidence for the presence of buried evaporites in the western NZ is also seen in the form of xenoliths with a similar chemistry and morphology to the Duruchaus Formation evaporites.

The high temperatures and salinities of these evaporite-derived connate fluids make them potentially good base metal carriers. In the areas examined in the NZ, it is suggested that these fluids are, at least in part, the fluid source for the mineralising fluids which generated the base metal mineralisation seen.

5.2.1 Implications for Exploration

Evaporitic fluids are not always associated with ore mineralisation as a number of features have to coincide in order for an ore deposit of economic grade to be formed. While fluids of sufficient salinity and of evaporitic origin are present in some areas, e.g., Moselle, the conditions in the area of emplacement of these fluids may not support the formation of an ore deposit. A suitable source of metals is another factor which has to be considered, as even if all of the above factors coincide in a particular area, if there is no suitable source of metals then the formation of an ore deposit is unlikely. The presence of significant base metal mineral deposits in the northern part of the Damara Belt, however, indicates that a suitable source of metals was available there. The felsic volcanic units of the Nosib Group in the NZ and the mafic Grootfontein intrusive body southeast of the Otavi Mountainland represent two possible base metal sources in the NZ.

A fluid signature which combines an evaporitic origin with an environment of precipitation which shows some evidence for mixing of fluids is therefore thought be a good potential indicator for mineralisation in the areas investigated in this study and other potential prospect areas in the northern part of the Damara Belt.

6.References

Ahrendt H., Behr H.J., Clauer N., Hunziker J.C., Porada H. and Weber K. (1983). The Northern Branch: Depositional development and timing of the structural and metamorphic evolution within the framework of the Damara Orogen. *In*: Martin H. and Eder F.W. (Eds), *Intracontinental Fold Belts*, Springer-Verlag (Berlin), pp. 723-743.

Behr H.J., Ahrendt H., Porada H., Rohrs J. and Weber K. (1983a). Upper Proterozoic Playa and Sabkha Deposits in the Damara Orogen, SWA/Namibia. *In:* Miller R. McG. (Ed.), *Evolution of the Damara Orogen of South West Africa/Namibia.* Spec. Pub. No. **11**, Geol. Soc. S. Afr., pp. 1-20.

Behr H.J., Arendt H., Porada H., Rohrs J. and Weber K. (1983b). The Sole Dolomite at the Base of the Naukluft Nappe Complex. *In*: Miller R. McG. (Ed.), *Evolution of the Damara Orogen of South West Africa/Namibia.* Spec. Pub. No. **11**, Geol. Soc. S. Afr., pp. 185-197.

Behr H.J. and Schmidt-Mumm A. (1987). Fluid Inclusion Studies on Hydrothermal Mineralisation associated with the Duruchaus Formation: Genetic Aspects of large Quartz-Dolomite Bodies and Associated Alteration. *Communs Geol. Surv. SWA/Namibia*, **3**, pp. 111-117.

Bennett D.G. and Barker A.J. (1992). High salinity fluids: the result of retrograde metamorphism in thrust zones. Geochimica et Cosmochimica Acta, **56**, pp. 81-95.

Bodnar R.J. (1993). Revised equation and table for freezing point depressions of H_2O-NaCl solutions. *Geochim. Cosmochim. Acta*, **57**, pp. 683-684.

Botha B.J.V. (1960). *The arenaceous rocks and the pseudo-aplite of the Otavi Mountainland, South West Africa*. D.Sc. thesis, Univ. Pretoria, 133pp.

Bowers T.S. and Helgeson H.C. (1983). Calculation of the thermodynamic and geochemical consequences of nonideal mixing in the system H2O-CO2-NaCl on phase relations in geologic systems: Equation of state for H2O-CO2-NaCl fluids at high pressures and temperatures. *Geochimica et Cosmochimic Acta*, **47**, pp. 1247-1275.

Brown P.E. (1989). FLINCOR: A microcomputer program for the reduction and investigation of fluid inclusion data. *Am. Mineral.*, **74**, pp. 1390-1393.

Brown P.E. and Lamb W.M. (1989). P-V-T properties of fluids in the system H_2O-CO_2-NaCl: New graphical presentations and implications for fluid inclusion studies. *Geochim. et Cosmochim. Acta*, **53**, pp. 1209-1221.

Chetty D. (1998). *Geochemical Fingerprinting of Carbonate Wall Rock Alteration at Major Base Metal Sulphide Deposits in the Otavi Mountainland, Namibia.*Unpubl. Msc dissert., Department of Geological Sciences, University of Cape Town, 147pp.

Chetty D. and Frimmel H.E. (2000). The role of evaporites in the genesis of base metal sulphide mineralisation in the Northern Platform of the Pan African Damara Belt, Namibia: geochemical and fluid inclusion evidence from carbonate wall rock interaction. *Mineralium Deposita*, **35**, pp. 364-376.

Condie K.C. (1993). Chemical composition and evolution of the upper continental crust : Contrasting results from surface samples and shales, *Chemical Geology*, **104**, p. 1-37.

Cook N.D.J. and Ashley P.M. (1992). Meta-evaporite sequence, exhalative chemical sediments and associated rocks in the Proterozoic Willyama Supergroup, South Australia : Implications for Metallogenesis. *Precambrian Research*, **56**, pp. 211-226.

Davis D.W., Lowenstein T.K. and Spencer R.J. (1990). Melting behaviour of fluid inclusions in laboratory-grown halite crystals in the systems NaCl-H_2O, NaCl-KCl-H_2O, NaCl-$MgCl_2$-H_2O, and NaCl-$CaCl_2$-H_2O. *Geochimica et Cosmochimica Acta*, **54**, pp. 591-601.

Davisson M.L. and Criss R.E. (1996). Na-Ca-Cl relations in basinal fluids. *Geochimica et Cosmochimica Acta*, **60**, pp. 2743-2752.

Davisson M.L., Presser T.S. and Criss R.E. (1994). Geochemistry of tectonically expelled fluids from the northern Coast ranges, Rumsey Hills, California, USA. *Geochimica et Cosmochimica Acta*, **58**, pp. 1687-1699.

Dombrowski A., Hoernes S. and Okrusch M. (1996). Scapolitization in the Kuiseb Formation of the Damara Orogen: geochemical and stable isotope evidence for fluid infiltration along deep crustal shear zones. *Communs geol. Surv. Namibia*, **11**, pp.21-29.

Frimmel H.E., Deane J.G. and Chadwick P.J. (1996a). Pan-African tectonism and the genesis of base metal sulphide deposits in the Northern Foreland of the Damara Orogen, Namibia. *Society of Economic Geologists*, Special Publication **No. 4**, pp. 204-217.

Frimmel H.E., Klötzli U.S. and Siegfried P.R. (1996b). New Pb-Pb Single Zircon Age Constraints on the Timing of the Neoproterozoic Glaciation and Continental Breakup in Namibia. *The Journal of Geology*, **104**, pp. 459-469.

Frimmel H.E., Chetty D. and Board W.S. (1998). Tracing Neoproterozoic evaporites in southwestern Africa (abs.). *Journal of African Earth Sciences*, **Vol 27 (no. 1A)**, pp. 80-81.

Frimmel H.E. and Jiang S.Y. (~~in press~~ 2001) Marine evaporites from an oceanic island in the Neoproterozoic Adamastor Ocean. ~~*Chemical geology*~~ *Precamb. Res.*, 105, pp. 57-71.

Chetty D. (1998). *Geochemical Fingerprinting of Carbonate Wall Rock Alteration at Major Base Metal Sulphide Deposits in the Otavi Mountainland, Namibia.*Unpubl. Msc dissert., Department of Geological Sciences, University of Cape Town, 147pp.

Chetty D. and Frimmel H.E. (2000). The role of evaporites in the genesis of base metal sulphide mineralisation in the Northern Platform of the Pan African Damara Belt, Namibia: geochemical and fluid inclusion evidence from carbonate wall rock interaction. *Mineralium Deposita*, **35**, pp. 364-376.

Condie K.C. (1993). Chemical composition and evolution of the upper continental crust : Contrasting results from surface samples and shales, *Chemical Geology*, **104**, p. 1-37.

Cook N.D.J. and Ashley P.M. (1992). Meta-evaporite sequence, exhalative chemical sediments and associated rocks in the Proterozoic Willyama Supergroup, South Australia : Implications for Metallogenesis. *Precambrian Research*, **56**, pp. 211-226.

Davis D.W., Lowenstein T.K. and Spencer R.J. (1990). Melting behaviour of fluid inclusions in laboratory-grown halite crystals in the systems NaCl-H_2O, NaCl-KCl-H_2O, NaCl-$MgCl_2$-H_2O, and NaCl-$CaCl_2$-H_2O. *Geochimica et Cosmochimica Acta*, **54**, pp. 591-601.

Davisson M.L. and Criss R.E. (1996). Na-Ca-Cl relations in basinal fluids. *Geochimica et Cosmochimica Acta*, **60**, pp. 2743-2752.

Davisson M.L., Presser T.S. and Criss R.E. (1994). Geochemistry of tectonically expelled fluids from the northern Coast ranges, Rumsey Hills, California, USA. *Geochimica et Cosmochimica Acta*, **58**, pp. 1687-1699.

Dombrowski A., Hoernes S. and Okrusch M. (1996). Scapolitization in the Kuiseb Formation of the Damara Orogen: geochemical and stable isotope evidence for fluid infiltration along deep crustal shear zones. *Communs geol. Surv. Namibia*, **11**, pp.21-29.

Frimmel H.E., Deane J.G. and Chadwick P.J. (1996a). Pan-African tectonism and the genesis of base metal sulphide deposits in the Northern Foreland of the Damara Orogen, Namibia. *Society of Economic Geologists*, Special Publication **No. 4**, pp. 204-217.

Frimmel H.E., Klötzli U.S. and Siegfried P.R. (1996b). New Pb-Pb Single Zircon Age Constraints on the Timing of the Neoproterozoic Glaciation and Continental Breakup in Namibia. *The Journal of Geology*, **104**, pp. 459-469.

Frimmel H.E., Chetty D. and Board W.S. (1998). Tracing Neoproterozoic evaporites in southwestern Africa (abs.). *Journal of African Earth Sciences*, **Vol 27 (no. 1A)**, pp. 80-81.

Frimmel, H.E. and Jiang, S.-Y. (2001) Marine evaporites from an oceanic island in the Neoproterozoic Adamastor Ocean. *Precambrian Research*, **105**, pp. 57-71.

Goldstein R.H. and Reynolds T.J. (1994). *Systematics of Fluid Inclusions in Diaagenetic Minerals.* SEPM Short Course 31, 207pp.

Gunter C.J. (1970). *Die geologie van n gebied suid van Messum, Suid-Wes Afrika.* MSc. thesis (unpubl.), Univ. Free State, Bloemfontein, 116pp.

Glynn P.D., Reardon E.J., Plummer L.N. and Busenberg E. (1992). Comment on "Reaction paths and equilibrium end-points in solid-solution aqueous-solution systems". *Geochimica et Cosmochimica Acta*, **V.56**, pp. 2555-2557.

Hardie L.A., (1984). Evaporites: Marine or Non-Marine, *American Journal of Science*, **Vol 284**, pp. 193-240.

Hälbich I.W. (1970). *The geology of the western Windhoek and Rehoboth Districts, a stratigraphic-structural analysis of the Damara System.* DSc. thesis (unpubl.), Univ. Stellenbosch, 199 pp.

Hedberg R.M. (1979). Stratigraphy of the Ovamboland Basin, South West Africa. *Bull. Precambrian Research Unit, Univ. Cape Town*, **24**, 325pp.

Henderson I.H.C. and McCaig A.M. (1996). Fluid pressure and salinity variations in shear zone-related veins, central Pyrenees, France: Implications for the fault valve model. *Tectonophysics*, **262**, pp. 321-348.

Henry D.J and Dutrow B.L. (1996). Metamorphic Tourmaline and its Petrologic Applications. *In:* Grew E.S. and Anovitz L.M. (eds), Boron – Mineralogy, Petrology and Geochemistry, *Reviews in Mineralogy*, **V.33**, Mineralogical Society of America, Michigan, pp.505-557.

Henry D.J. and Guidotti C.V. (1985). Tourmaline as a petrogenetic indicator mineral: am example from staurolite-grade metapelites from NW Maine. *The American Mineralogist*, **70**, Mineralogical Society of America, pp. 1-15.

Hoernes S. and Hoffer E. (1979). Equilibrium relations of prograde metamorphic assemblages. A stable isotope study of rocks of the Damara Orogen, from Namibia. *Contributions to Mineralogy and Petrology*, **68**, pp. 377-389.

Hoffer E. (1977). *Petrologische Untersuchungen zur Regionlmetamorhpose Al-reicher Metapelite in sudlichen Damaran-Orogen, (Sudwest-Afrika).* Habilitationsschrift, Univ. Gottingen, 150pp.

Hoffer E. (1983). Compositional variations of minerals in metapelites involved in low to medium grade isograd reactions in the souther Damara Orogen, Namibia/SWA. *In*: Martin H. and Eder F.W. (Eds.) *Intracontinental Fold Belts*, Springer Verlag (Berlin), pp. 745-765.

Hoffman P.F., Hawkins D.P., Isachsen C.E. and Bowring S.A. (1996). Precise U-Pb zircon ages for the early Damaran magmatism in the Summas Mountains and Welwitschia inlier, northern Damara Belt, Namibia. *Communs geol. Survey Namibia*, **11**, pp. 47-52.

Hoffmann K.H. (1983). Lithostratigraphy and facies of the Swakop Group of the southern Damaran Belt, SWA/Namibia. *In*: Miller R. McG, *Evolution of the Damara Orogen of South West Africa/Namibia*, Spec. Publ. no. **11**, Geol. Soc. S. Afr., pp.43-63.

Hoffmann K.H. (1987). Stratigraphic subdivision and sedimentary facies of the Duruchaus Formation in the Geelkop Dome and Nauaspoort-Wortelpoort area north of Rehoboth, Southern Damara Belt, *Communs geol. Survey of S.W. Africa/Namibia*, **3**, pp. 9-18.

Hoffmann K.H. (1989). New aspects of the lithostratigraphic subdivision and correlation of the late Proterozoic to early Cambrian rocks of the southern Damara Belt and their correlation with the central and northern Damara Belt and the Gariep Belt. *Communs geol. Survey Namibia*, **5**, pp. 58-67.

Hoffmann K.H. and Prave A.R. (1996). A preliminary note on a revised subdivision and regional correlation of the Otavi Group based on glaciogenic diamictites and associated cap dolostones. *Communs. geol. Sur. Namibia*, **11**, pp.77-82.

Holser W.T. (1979). Mineralogy of Evaporites. *In:*Burns R.G. (ed.), Marine Minerals, *Reviews in Mineralogy,* **V.6**, Mineralogical Society of America, Michigan, pp.211-294.

Horita J., Friedman T.J., Lazar B. and Holland H.D. (1991). The composition of Permian seawater. *Geomchimica et Cosmochimica Acta*, **55**, pp. 417-432.

Kasch K.W. (1983a). Tectonothermal evolution of the southern Damara Orogen. *In:* Miller R. McG. (Ed.), *Evolution of the Damara Orogen of SWA/Namibia*, Spec. Publ. no. **11**, Geol soc. S. Afr., pp. 255-265.

Kasch K.W. (1983b). Regional P-T variations in the Damara Orogen with particular reference to early high pressure metamorphism along the southern margin. *In:* Miller R. McG. (Ed.), *Evolution of the Damara Orogen of SWA/Namibia*, Spec. Publ. no. **11**, Geol. soc. S. Afr., pp. 243-253.

Kasch K.W. (1983c). Folding and thrust tectonics in the south-eastern part of the Damara Orogen around Omitara, Namibia. *In:* Miller R. McG. (Ed.), *Evolution of the Damara Orogen of SWA/Namibia*, Spec. Publ. no. **11**, Geol. soc. S. Afr., pp. 175-184.

Kennedy M.J., Runnegar B., Prave A.R., Hoffmann K.H. and Arthur M.A. (1998). Two or four Neoproterozoic glaciations? *Geology*, **26**, pp. 1059-1063.

Kesler S.E., Appold M.S., Martini A.M., Walter L.M., Huston T.J. and Kyle J.R. (1995). Na-Cl-Br systematics of mineralising brines in Mississippi Valley-type deposits. *Geology*, **23**, pp. 641-644.

Kröner A. and Rankama K. (1972). Late Precambrian glaciogenic sedimentary rocks in southern Africa. *Bull. Precambrian Res. Unit, Univ. Cape Town*, **11**, 37pp.

Leach D.L. and Sangster D.F. (1993). Mississippi Valley-Type Lead-Zinc Deposits. *In:* Kirkham R.V., Sinclair W.D., Thorpe R.I., Duke J.M. (eds), *Mineral Deposit Modelling*, **40**, Geological Association of Canada, pp. 289-314.

Lombaard A.F., Gunzel A., Innes J. and Kruger T.L. (1986). The Tsumeb Lead-Copper-Zinc-Silver Deposit, South West Africa/Namibia, *In*: Anhaeusser C.R. and Maske S. (Eds.), *Mineral Deposits of Southern Africa, Vol. II*, Geological Society of South Africa, Johannesburg, pp. 1761-1788.

Martin H. (1965). *The Precambrian geology of South West Africa and Namaqualand.* Precambrian Research Unit, Univ. Cape Town, 159pp.

Martin, H. and Porada, H. (1977). The intracratonic arm of the Damara Orogen in South West Africa. I. Discussion of geodynamic models. II. Discussion of relationship with Pan African Mobile Belt system. *Precambrian Research*, **5**, pp. 311-338 and 339-357.

McKibben M.A. and Hardie L.A. (1997). Ore-forming brines in active continental rifts. *In:* Barnes H.L. (ed.), *Geochemistry of Hydrothermal Ore Deposits*, **3rd Edition**, John Wiley and Sons (New York), pp. 877-935.

Meert J.G. and van de Voo R. (1994). The Neoproterozoic (1000-540 Ma) glacial intervals: no more snowball earth? *Earth Planet. Sci. Lett.*, **123**, pp. 1-13.

Misiewicz J.E. (1988). *The geology and metallogeny of the Otavi Mountainland, Damara Orogen, SWA/Namibia, with particular reference to the Berg Aukas Zn-Pb-V deposit – a model of ore genesis.* Unpubl. MSc thesis, Rhodes Unversity, Grahamstown, 143 pp.

Miller R. McG. (1980). Geology of a part of central Damaraland, South West Africa/Namibia. *Mem. geol. Sur. S. Afr., S. W. Afr. Ser.*, **6**, 78pp.

Miller R. McG. (1983a). The Pan African Damara Orogen of South West Africa/Namibia. *In:* Miller R. McG. (Ed.), *Evolution of the Damara Orogen of SWA/Namibia*, Spec. Publ. no. **11**, Geol. soc. S. Afr., pp. 431-515.

Miller R. McG. (1983b). Economic implications of plate tectonic models of the Damara Orogen. *In:* Miller R. McG. (Ed.), *Evolution of the Damara Orogen of SWA/Namibia*, Spec. Publ. no. **11**, Geol. soc. S. Afr., pp. 385-395.

Möller P. and Bau M. (1993). Rare-earth patterns with a positive cerium anomaly in alkaline waters from Lake Van, Turkey. *Earth and Planetary Science Letters*, **117**, pp. 671-676.

Nesbitt H.W. and Young G.M. (1982). Early Proterozoic climates and plate motions inferred from major element chemistry of lutites. *Nature*, **Vol. 299**, pp.715-717.

Oakes C.S., Bodnar R.J. and Simonson J.M. (1990). The system NaCl-$CaCl_2$-H_2O: I. The ice liquidus at 1 atm total pressure. *Geochimica et Cosmochimica Acta*, **54**, pp. 603-610.

Porada H. and Wittig R. (1983). Turbidites and their significance for the geosynclinal evolution of the Damara Orogen, South West Africa/Namibia. *In:* Miller R. McG. (Ed.), *Evolution of the Damara Orogen of SWA/Namibia*, Spec. Publ. no. **11**, Geol. soc. S. Afr., pp. 21-36.

Pouchou J.L. and Pichoir F. (1984). A new model for quantitative X-ray microanalysis, *Rech. Aerosp.*, **3**, pp. 12-35.

Prave A.R. and Hoffmann K.H. (1995). Unequivocal evidence for two Neoproterozoic glaciations in the Damara succession of Namibia. *Geol. Soc. Am., Astr. with Program*, **27**, pp. 380.

Roedder E. (1984). Fluid inclusions. *Reviews in Mineralogy*, Vol. **12**, Mineralogical Society of America, Michigan, 644pp.

Rollinson H. (1993). *Using Geochemical Data : Evaluation, Presentation, Interpretation*, Longman Scientific and Technical, 352 pp.

Schermerhorn L.J.G. (1974). Late Precambrian mixtites: glacial and/or non-glacial? *American Journal of Science*, 274, pp. 673-824.

Schimdt-Mumm A. (1989). Die Entwicklung der Fluid-Systeme wahrend der oberproterozoischen Damara-Orogenese am Sudrand des Damara-Orogens, Namibia. *Gottinger Arbeiten zur Geologie und Panlaontologie*, **41**, 93 pp.

Schneider G.I.C. and Seeger K.G., (1992). Copper Occurances. *The Mineral Resources of Namibia*, Namibian Geological Survey/ Ministry of Mines and Energy, pp (2.3 : 1-118).

Siemann M.G. and Schramm M. (2000). Thermodynamic modelling of the Br partition between aqueous solutions and halite. *Geochimica et Cosmochimica Acta*, **V64 No.10**, pp. 1681-1693.

Slack J.F., Herriman N., Barnes R.G. and Plimer I.R. (1984). Stratiform tourmalinites in metamorphic terranes and their geologic significance. *Geology*, **12**, pp. 713-716.

Slack J.F., Palmer M.R. and Stevens B.P.J. (1989). Boron isotope evidence for involvement of non-marine evaporites in the origin of the Broken Hill ore deposits. *Nature,* **Vol. 342**, pp. 913-916.

Slack J.F., Palmer M.R., Stevens B.P. and Barnes R.G. (1993). Origin and significance of tourmaline-rich rocks in the Broken Hill District, Australia. *Economic Geology*, **88**, pp. 505-541.

South African Committee for Stratigraphy (SACS) (1980). Lithostratigraphy of the Republic of South Africa, South West Africa/Namibia and the republics of Boputhatswana, Transkei and Venda. Geological Survey of South Africa, *Handbook 8*, 633pp.

Sterner S.M., Hall D.L. and Bodnar R.J. (1988). Synthetic fluid inclusions. V. Solubility relations in the system NaCl-KCl-H_2O under vapour saturated conditions. *Geochimica et Cosmochemica Acta.* **V.46**, pp. 1327-1332.

Stewart J.I. (1994). The Role of Evaporitic Shale Sediment Packages in the Localisation of Copper-Gold Deposits:Copper Canyon Area, Cloncurry. *AusIMM Annual Conference Special Publication,* pp. 207-214.

Sun S.S. and McDonough W.F. (1989). *Chemical and isotopic systematics of ocean basalts: implications for mantle composition and processes,* Magmatism in Ocean Basins (Saunders A.D. and Norry M.J., eds), Geological Society Special Publication, **No. 42**, pp. 313-345.

Tankard A.J., Jackson M.P.A, Eriksson K.A., Hobday D.K., Hunter D.R. and Minter W.E.L. (1982). *Crustal Evolution of Southern Africa*, Springer-Verlag, New York, 523pp.

Taylor S.R. and McLennan S.M. (1981). The composition and evolution of the continental crust: rare earth element evidence from sedimentary rocks. *Phil. Trans. R. Soc.*, **A301**, pp. 381-399.

Taylor S.R. and McLennan S.M. (1985). *The Continental Crust: Its Composition and Evolution*, Blackwell, Cambridge, 312pp.

Walter L.M., Stueber A.M. and Huston T.J. (1990). Br-Cl-Na systematics in Illinois Basin fluids:Constraints on fluid origin and evolution. *Geology*, **v. 18**, pp. 315-318.

Weber K., Arendt H. and Hunziker J.C. (1983). Geodynamic aspects of Structural and Radiometric Investigations on the Northern and Southern Margins of the Damara Orogen, SWA/Namibia. *In:* Miller R. McG. (Ed.), *Evolution of the Damara Orogen of SWA/Namibia*, Spec. Publ. no. **11**, Geol. soc. S. Afr., pp. 307-319.

Appendices

Appendix I
Analytical Techniques

(AI.1) Fluid Inclusion Studies

(a) Fluid Inclusion Microthermometry

Sample Preparation

The sampled quartz crystals were cut and polished to thin (60-90μm) doubly polished sections or wafers. These wafers were then broken into chips of less than 1cm in diameter for microthermomteric analysis.

Analysis

A FLUID INC. adapted U.S.G.S. nitrogen gas flow heating-freezing stage was used to determine the temperatures at which phase changes occur in the quartz-hosted fluid inclusions, during heating and freezing of the prepared sample chips. The temperatures were measured by a thermocouple situated on the heating-freezing stage in direct contact with the sample chip (with the thermocouple tip being not more than 2mm from the inclusion measured). The system was calibrated using synthetic fluid inclusions in quartz produced by SYNFLINC. The three points of calibration were –56.6°C (CO_2 triple point), 0.0°C (H_2O triple point) and 374.1°C (H_2O critical point). Repeat analyses of the same inclusions were used to determine the precision of these microthermometric measurements. The precision of the calibration was determined to be within 0.2°C for –56.6°C, within 0.1°C for 0.0°C, and within 1.0°C for 374.1°C, for all of the heating-freezing runs. The accuracy for sample measurements made below 0°C is estimated to be within 0.5°C, and better than 1°C for measurements above this value. The microthemometric study was carried out according to the philosophy of conducting a fluid inclusion study outlined in Goldstein and Reynolds (1994).

Eutectic temperatures, final melting temperatures and homogenisation temperatures were measured for each of the phases (CO_2, H_2O) present in the inclusions. The microthermometric data so determined is presented in Table AIII.1. Eutectic and final melting temperatures were measured at heating rates of approximately 1°C/min and homogenisation temperatures were observed at heating rates of 1-5°C/min.

(b) Crush-Leach Analyses

The bulk chemistry of the fluids preserved as inclusions in the sampled quartz, dolomite and tourmaline mineral grains, was determined by a crush-leach analysis of these samples. HPIC was used to determine the cationic and anionic concentrations in the fluid inclusion leachates while ICP-MS was used to determine the Br^- concentration. A combination of these techniques was used due to the low Br^- concentrations in the samples analysed (below the detection limit of the HPIC) and due to the difficulties in measuring the Cl^- and Na^+ concentrations using the ICP-MS. Both techniques therefore needed to be employed to determine the Br^-, Na^+ and Cl^- character of the leachates from these samples.

(i) High Perfomance Ion Chromatography

Sample Preparation

.Samples of quartz, dolomite and tourmaline selected for the crush leach study were initially jaw-crushed to grains <5mm in size. The individual samples were then subdivided into 3 to 5 sub-samples depending on the availibility of sample material. In order to make sure that the sample surfaces were clean, the grains in each sub-sample were washed with acetone and doubly distilled, deionised water (DDW) before being placed in an ultrasonic bath for 15 minutes. This process was repeated

The Nalgene bottles used for sample collection were subjected to similar cleaning procedure prior to sample preparation. These bottles were cleaned using acetone and DDW aand then filled with DDW and placed in a shaker for 30 minutes. This process was repeated until the DDW in the bottles also showed insignificant concentrations of the elements under investigation.

500mg of each of the cleaned subsamples was weighed out into clean beakers and then washed into a (cleaned) boron-carbide mortar using 2.5 to 3.5ml of DDW. These sub-samples were then crushed while submerged under the DDW until a fine powder was obtained. The resulting leachate was drawn up into a syringe and then filtered into the cleaned Nalgene bottles. Two crushes of each subsample was carried out to bring up the volume of each leachate to 6ml.

(i) High Perfomance Ion Chromatography

Analysis

The bulk chemistry of these leachates was determined using a DIONEX DX300 system operating on a DIONEX Gradient Ion Chromatograph. The instrumental set-up for anions and cations was as follows:

Anions:

Eluent: 3.5 mM Na_2CO_3/ 1.0 mM $NaHCO_3$

Flow Rate: 1.2 ml/min

Injection Volume: 50µl

Guard Column: AG4A

Separator Column: AS14 (4mm)

Cations:

Eluent: 22mM MSA (methane sulphonic acid)

Flow Rate: 1 ml/min

Injection Volume: 25µl

Guard Column: CG12A

Separator Column: CS12A (4x250mm)

The instruments were standardised daily for anions and cations using a set of standards prepared from a stock solution. The reproducibility of results on the HPIC was tested using these standards (Table AI.1 and AI.2). The precision was found to be within 2% for Na^+ and K^+, within 4% for Ca^{2+} and better than 1% for Cl^-. The accuracy of the analyses was tested by randomly running a standard as an unknown.

During the sample runs, blanks were run between samples to test and prevent inter-sample contamination (flooding of the column by eg. chloride ions, sometimes left a residue that was removed by these blanks). This also gave an indication of the background provided by the DDW. The samples were analysed for Li^+, Na^+, K^+, NH_4^+, Mg^{2+}, Ca^{2+} (cations) and F^-, Cl^-, NO_2^-, Br^-, NO_3^-, PO_4^{3-}, SO_4^{2-} (anions). The chromatograms produced were automatically integrated and the resultant concentrations were presented as parts per million (ppm) values. The dominant anions and cations in these fluids and their respective concentrations are presented in Table AIII.2.

Table A1.1 Precision of cation analyses on the HPIC. Concentrations are in ppm.

Standard	Na^+	K^+	Ca^{2+}	mean	SD
AK2	6.38	1.36	6.84	6.28	0.08
	6.22	1.33	6.79		
	6.25	1.32	6.81		
AK3	12.72	2.60	12.43	12.70	0.02
	12.69	2.55	12.35		
	12.68	2.55	12.37		
AK4	25.53	5.17	25.23	25.50	0.08
	25.41	5.15	25.10		
	25.57	5.18	25.25		

Table A1.2 Precision of anion analyses on the HPIC. Concentrations are in ppm.

Standard	Cl^-	mean	SD
AN2	4.48	4.44	0.04
	4.39		
	4.45		
AN4	18.35	18.31	0.03
	18.29		
	18.29		
AN5	38.05	37.97	0.08
	37.95		
	37.90		

(ii) Inductively-Coupled Plasma Mass Spectrometry

Sample Preparation

Part of the volume of the leachates prepared for HPIC analyses were used in an ICP-MS study (without additional dilution) to determine the Br^- concentration of the leachates. The leachates were prepared for ICP-MS analyses as follows. 1.5ml of the leachate was first transferred into a 15ml centrifuge tube. 13.5ml of a 2% HNO_3 solution was then added to the mixture along with 50µl of a 10ppb ^{89}Y internal standard. The sample solution was then shaken and left to stand before analysis.

Analysis

The Br^- analyses were carried out on a Perkin Elmer/SCIEX ELAN 6000 inductively-coupled, argon plasma, quadrupole mass spectrometer. The typical instrumental settings for Br^- analyses are presented in Table AI.3. The lower limits of detection for this instrument are presented in Table AI.4a. The reproducibility of the Br^- analyses was tested using three bromine standards (Table AI.4b). The absolute standard deviation for all repeat analyses was found to be 9.76ppb (relative S.D. = 20.6%).

Table AI.3 Typical instrumental settings for bromine analyses using the ICP-MS.

Nebuliser Gas Flow:	0.86 L/min	
Main Gas Flow:	15 L/min	
Auxillary Gas Flow:	0.75 L/min	
ICP RF Forward Power:	1100W	
Instrument Sensitivity:	300 000 cps	(10 ppb Rh)
Autolens Setting		
Lens Voltage	^{9}Be 7.6 V	
	^{59}Co 8.2 V	
	^{115}I 9.0 V	
Analyses:		
Analytical time per sample:	21s (50 sweeps/4 replicates)	
Dwell Time:	50 milliseconds	
Internal Standard:	^{89}Y	

Table AI.4a Lower limits of detection for the ICP-MS technique.

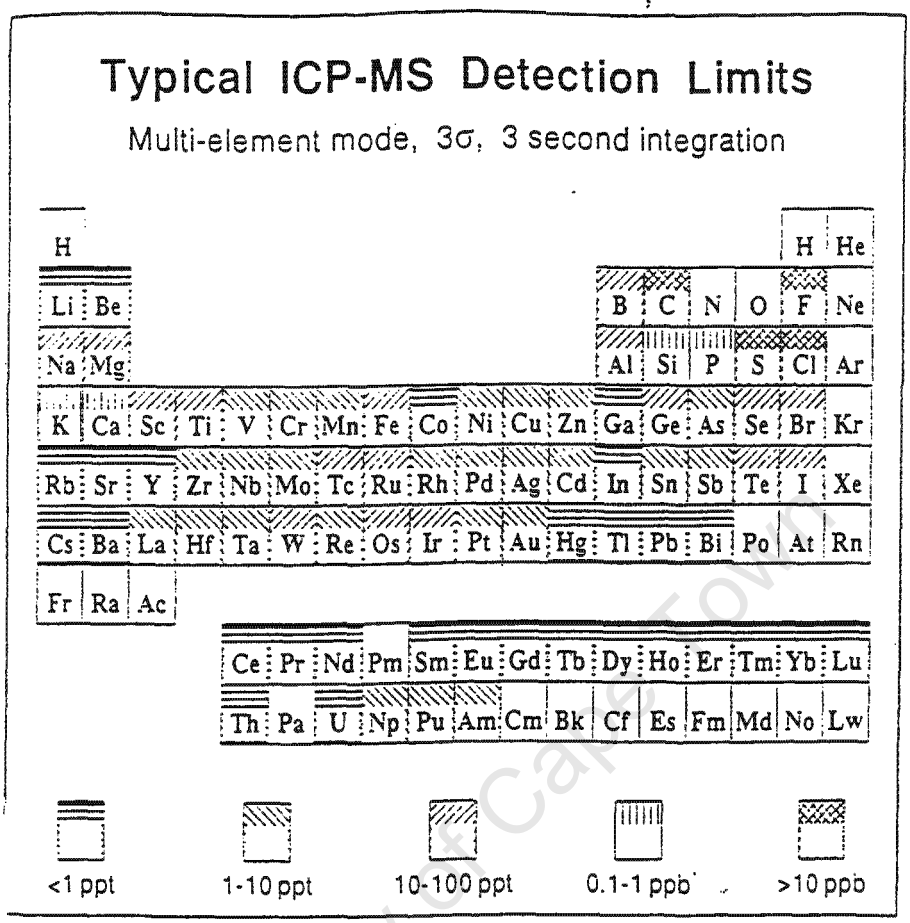

Table AI.4b Precision of analyses on ICP-MS. Concentrations are in ppb.

Standard	Concentration	Mean	Standard Deviation
1	19.49 19.57 19.54	19.54	0.04
2	50.57 50.58 50.54	50.56	0.02
3	99.72 99.32 99.69	99.58	0.23

(AI.2) Whole Rock Chemistry

(a) X-Ray Flourescence Analyses

Sample Preparation

Whole rock samples were prepared for analysis by initially splitting the rock samples into 1-2cm blocks using a hydraulic splitter and crushing the resultant fragments in a jaw crusher. The crushed sample was then coned and divided into two sub-samples. 80g of each sub-sample was then milled to approximately –200 mesh in a carbon steel mortar placed within a Sieb Techniek mill run for two minutes. The apparatus were pre-contaminated with the sample to minimise inter-sample contamination.

The sample powders were then roasted in an oven to remove molecular and surface water before being combined with a LiT (lithium tetraborate)-LiM (lithium metaborate) flux (57:43) in the proportion 0.7g of sample to 6g of flux. A few drops of LiBr was also added to act as a releasing agent. The mixture was then fused into a glass disc using a Claisse fusion machine.

Analysis

The analysis was carried out on a Phillips PW1480 wavelength dispersive X-Ray spectrometer with a dual target Mo/Sc X-Ray tube. All measurements were made with the tube at 50 kV and 50 mA. The analytical conditions for the major elements are given in the Table AI.5.

The samples were analysed for the following major element oxides: SiO_2, TiO_2, Al_2O_3, Fe_2O_3, MnO, MgO, CaO, Na_2O, K_2O, P_2O_5, SO_3, NiO and Cr_2O_3. Duplicates were randomly inserted into the run to test the precision of the analysis.

Table AI.5 XRF instrumental set-up for major element analytical runs at UCT.

Element /line	Collimator	Crystal	Detector	PHS LWL	PHS UPL	Counting time (s)	Concentration range **	RMS	Lower limits of determination*	No. of standards
NiKα	F	LiF(220)	FS	22	70	100	0 - 0.48	0.003	0.004	11
FeKα	F	LiF(220)	FL	16	68	100	0 - 17	0.069	0.019	20
MnKα	F	LiF(220)	FL	15	66	100	0 - 0.27	0.004	0.014	22
CrKα	F	LiF(220)	FL	14	70	100	0 - 3.5	0.011	0.008	11
TiKα	F	LiF(200)	FL	32	68	100	0 - 3.9	0.022	0.023	22
CaKα	F	LiF(200)	FL	30	76	50	0 - 77	0.102	0.004	21
K Kα	F	LiF(200)	FL	32	74	100	0 - 15.5	0.037	0.003	21
S Kα	C	GE(111)	FL	32	74	100	0 - 53.5	0.112	0.100	11
P Kα	C	GE(111)	FL	34	74	100	0 - 3.4	0.011	0.008	16
SiKα	C	PE(002)	FL	26	80	100	0 - 100	0.215	0.052	20
AlKα	C	PE(002)	FL	26	80	100	0 - 100	0.084	0.074	21
MgKα	F	PX-1	FL	36	68	100	0 - 85	0.141	0.102	20
NaKα	F	PX-1	FL	30	78	100	0 - 9.1	0.065	0.17	12

** all concentrations expressed as wt% oxide; S as SO_3

* = 10 × lower limit of detection, expressed as wt% oxide

$$RMS = \sqrt{\frac{1}{n - k} \sum \left(Conc_{given} - Conc_{calc} \right)}$$

where

n = no. of standards

k = no. of calibration coefficients, *i.e.* 2, the slope and intercept of the calibration line.

$Conc_{given}$ = recommended concentration for an element in a standard

$Conc_{calc}$ = concentration of an element calculated from the best-fit calibration line

(b) Inductively-Coupled Plasma Mass Spectrometry

Sample Preparation

50mg of each sample powder (preparation described in (a)) was first placed in a teflon beaker with approximately 4ml of HF/HNO_3 stock solution (4:1). The lids on the beakers were then closed and the samples were left to stand for 48 hours on a hot plate set at 50-60°C. The samples were then allowed to evaporate to complete dryness, before 2ml of 2-bottled HNO_3 was added to them. The sample solutions were then returned to the hotplate and allowed to evaporate to complete dryness at approximately 75°C. Another 2ml of HNO_3 was then added to the samples and the lids were returned to the beakers and the samples were allowed to dissolve overnight. Finally, the samples were allowed to evaporate to complete dryness at 75°C for a second time.

The dry sample was dissolved in 4ml of an internal standard stock solution (5% HNO_3 + 10ppb In, Re, Rh, Bi). The dissolved sample was then transferred to a 50ml centrifuge tube and the volume was made up to 50ml with the internal standard stock solution. Once mixed this solution represented a 1000-fold dilution of the original solid sample and this was used in the analysis. Further dilutions were carried out in samples where elemental concentrations were too high.

Analysis

The trace element and rare earth element contents of the samples were determined on a Perkin Elmer/SCIEX ELAN 6000 inductively-coupled, argon plasma, quadrupole mass spectrometer, with the instrumental settings listed in Table AI.6. The lower limits of detection for this instrument are presented in Table AI.4. The trace element and rare earth element contents of the samples are presented in Table (AIII 3.2).

Table AI.6 Typical instrumental settings for trace element analyses using the ICP-MS

Nebuliser Gas Flow:	0.86 L/min	
Main Gas Flow:	15 L/min	
Auxillary Gas Flow:	0.75 L/min	
ICP RF Forward Power:	1100W	
Instrument Sensitivity:	300 000 cps	(10 ppb Rh)
Autolens Setting		
Lens Voltage	^{9}Be 7.6 V	
	^{59}Co 8.2 V	
	^{115}I 9.0 V	
Analyses:		
Analytical time per sample:	50s (20 sweeps/3 replicates)	
Dwell Time:	35-50 milliseconds	
Internal Standard:	^{115}I, ^{187}Re	

(AI.3) Mineral Chemistry

(a) Electron Microprobe Analysis

Sample Preparation

Doubly-polished microprobe sections (45-50μm) were prepared of the tourmaline samples encountered in the field. These sections were then coated with a layer of carbon to minimise charging effects.

Analysis

Mineral analyses were carried out using a Cameca Camebax Electron Microprobe. Instrumental settings were as follows:

Acceleration Potential	15kV
Beam Current	40nA
Beam Diameter	1μm

The machine was calibrated using the standards listed in Table AI.7. Both core and rim analyses were carried out on grains which showed some indication of core-rim variation in composition. Between 10 and 20 analyses were carried out on each sample. The data was reduced using an on-line PAP correction procedure (Pouchou and Pichoir, 1984), and the major element concentrations thus corrected (expressed as weight percent oxides), appear in Appendix III. The iron in these samples has been recalculated to FeO and Fe_2O_3, and B_2O_3 has been iteratively calculated and is presented along with the data from the electron microprobe analyses in Appendix III.

Table AI.7 Standards used in the calibration of the electron microprobe along with LLD values and 1σ errors for tourmaline analyses.

Element	Standard	Analysing Crystal	LLD	1σ
Si	K-H	TAP	0.055	0.2
Ti	Rut	PET	0.039	0.06
Al	K-H	TAP	0.044	0.11
Fe	K-H	LIF	0.077	0.19
Mn	Rhod	LIF	0.061	0.03
Mg	K-H	TAP	0.029	0.09
Ca	K-H	PET	0.027	0.10
Na	K-H	TAP	0.033	0.06
K	K-H	PET	0.019	0.02

Appendix II
(Petrographic Descriptions)

(XPL=cross polarised light; PPL=plane polarised light)

Sample No.	Hand Specimen	Petrography	Rock Texture	Rock Name
Duruchaus Formation Samples				
NP003	Red-brown, fine grained specimen - appears fresh - within quartz plug	**Dolomite** - Subhedral-anhedral grains 0-2mm *(85%)* **Quartz** - Anhedral-subhedral grains (0.5-1mm) *(15%)* **Opaques** - haematite (opaque with reddish rims)	Granoblastic	Dolomitic Marble
NP010	Fine-grained micaeous phyllite, weathers grey-black, adjacent to quartz plug 2 (Hilton)	**Biotite** - Pleochroic (straw brown - clear), subhedral anhedral (0-2mm) laths, associated with albite, well developed cleavage (15%) **Albite** - Subhedral-euhedral crystals (0-1mm), low interference colours, simple twins *(50%)* **Sillimanite** - Fibrous aggregate, associated with biotite, anhedral laths - only mineral without strong preffered orientation implies late origin? pseudomorphing larger grains - andalusite? *(10%)* **Dolomite** - high interference colours, anhedral grains (0-1mm) *(5%)* **Quartz** - anhedral grains (0-1mm), undulose extinction *(20%)* **Opaques/Haematite** - Subhedral grains (1-2mm), red grains *(tr.)*	Lepidoblastic	Phyllite (micaeous)
NP012	Fine-grained albitite - albitised NP010	**Quartz** - <1mm subhedral grains *(20%)* **Albite** - subhedral crystals (<1mm in diameter), simple twins, low interference colours *(60%)* **Dolomite** - subhedral grains 1-2mm, show well developed twin lamellae *(10%)* **Muscovite** - Well developed cleavage, subhedral grains showing stippled extinction, minor constituent *(tr.)* **Haematite/Rutile** - red grains, slightly pleochroic to brown-yellow 1-2mm euhedral crystals *(10%)* **Sphene** - yellow-brown, anhedral grains present in trace amounts	Granoblastic (polygonal)	Albitite
NP016	Ilmenite albite crystals in Fe-dolomite matrix	**Albite** - Poikiloblastic porphyroblasts of albite present, anhedral grains (6-8mm), grains contain inclusions of the other phases - *(30%)* **Opaques** - Anhedral grains (0-1mm), main component of matrix - *(30%)* **Biotite** - Subhedral/anhedral grains (0-1mm), well developed cleavage pleochroic - straw yellow/brown, stippled extinction *(10%)* **Dolomite** - Anhedral grains (<1mm), occur in clusters/aggregates and as part of matrix *(20%)* **Quartz** - subhedral/anhedral grains *(10%)*	Porphyritic, Poikiloblastic	Fe-dolomite

Sample No.	Hand Specimen	Petrography	Rock Texture	Rock Name
NP019	Silicified Breccia, brown-weathering, finely laminated.	**Dolomite** - Anhedral grains up to 2mm long, some grains contain feldspar inclusions *(50%)* **Quartz** - Forms large poikiloblastic grains up to 4mm, talc/muscovite inclusions, grains are subhedral and show undulose extinction Smaller anhedral/subheral (<0.5mm) grains make up the matrix *(20%)* **Albite**: Forms subhedral grains <0.5mm, lamellae twins *(10%)* **Opaque** - red-brown grains; anhedral and up to 1mm long, haematite? *-10%* **Talc** - Subhedral/anhedral grains (~1mm), stippled extinction, almost parallel extinction *(10%)* **Sphene** - anhedral yellow-brown grains, <0.25mm	Seriate	Siliceous Dolomite
NP020	Silicified breccia in pellitic/psammtic sequence	**Quartz** - Large porphyroblastic grains 2-4mm, undulose extinction, anhedral grains (25%) **Albite** - Smaller 0-1mm subhedral grains, simple twins and lamellae twins - *(35%)* **Dolomite** - anhedral 0-1mm grains *(35%)* **Opaque/Haematite** - suhedral, anhedral grains (0-1mm), pleochroic yellow-brown/red-brown, parallel extinction *(5%)*	Porphyroblastic	Siliceous Marble
NP022	Albitite fragments in albitised dolomitic matrix Breccia unit 1	**Dolomite** - Forms large anhedral porphyroblasts, 0-5mm *(40%)* **Albite** - Forms fine grained matrix - 0-1mm, subhedral simple twins and lamellae twins *(35%)* **Quartz** - subhedral (0-1mm) grains, undulose extinction, forms porphyroblasts and part of the matrix *(10%)* **Opaques** - form *5%* of matrix, anhedral grains <0.25mm **Sphene** - present in trace amounts, grey anhedral grains	Seriate	Breccia
NP025	Dolomite bearing albite pseudmorphs in finely laminated dolomitic, albitised? matrix	**Albite** - Form porphyroblasts, lamellae twins, anhedral grains (1-2mm) *(30%)* **Quartz** - anhedral grains (1-2mm), forms porphyroblasts and matrix (<1mm) *(45%)* **Dolomite** - <1mm subhedral grains - form part of the matrix *(25%)* **Opaques** - minor, some showing reddish rims (hematite?) **Muscovite** - minor	Subidioblastic	Sandy Dolomite

Sample No.	Hand Specimen	Petrography	Rock Texture	Rock Name
NP028	Fine grained, recrystallised? unit, appears massive, albitite (pink-white)	**Quartz** - Rock mainly consists of quartz, <1mm grains subhedral/anhedral grains *(80%)* **Dolomite** - Anhedral grains also <1mm *(20%)* **Sphene** - Rounded anhedral grains, showing parallel extinction, (0-1mm) *(tr.)* **Albite** - Minor constituent, lamellae twins, <1mm grains *(tr.)* Minor **muscovite**	Granoblastic	Quartzite
NP030	Fine-grained pink albitite with small albite pseudomorphs	**Quartz** - subhedral/anhedral grains (0-1mm), undulose extinction, matrix constituent and also forms porphyroblasts *(70%)* **Albite** - subhedral/anhedral (0-1mm) grains, lamellae twinning seen, as with quartz - matrix & porphyroblasts *(10%)* **Dolomite** - Anhedral grains (0-1mm), mainly interstitial *(10%)* **Sphene/Rutile** - Anhedral grains (<1mm), slightly pleochroic (red-brown/yellow-brown), parallel extinction *(10%)*	Granoblastic	Feldspathic quartzite
NP031	Pink-white albitite, massive crystalline rock	**Quartz** - Coarse grains averaging ~1mm; as well as matrix grains <0.5mm; anhedral grains showing undulose extinction *(40%)* **Albite** - Similar grain sizes to quartz (coarse 1mm grains and matrix grains ~0.5mm); anhedral; lamellae twins *(40%)* **Dolomite** - Anhedral grains ~0.25mm *(20%)* Minor **muscovite** (euhedral laths <0.25mm); and **rutile/sphene** (anhedral grains, pleochroic red-brown/yellow brown)	Subidioblastic	Feldspathic Quartzite
NP032	Green-grey micaceous metapelite	**Biotite** - Subhedral/anhedral laths (~0.25mm), Pleochroic - red-brown, straw-yellow; well developed cleavage, stippled extinction, strong preffered orientation of laths with some randomly orientated large later grains *(33%)* **Muscovite** - Similar orientation to biotite, subhedral/anhedral laths (0-0.5mm); clear, well developed cleavage, stippled extinction *(33%)* **Quartz** - Subhedral grains up to 0.5mm; grains show fractures and undulose extinction *(34%)* **Haematite** - Present in trace amounts; reddish grains almost opaque; <0.5mm, anhedral grains **Tourmaline** - Also present in trace amounts; rounded grains, pleochroic (emerald green/clear); <0.5mm	Lepidoblastic	Quartz-mica Schist

Sample No.	Hand Specimen	Petrography	Rock Texture	Rock Name
NP033	Blue-grey, medium-grained psammitic unit	**Quartz** - Dominant mineral phase; Matrix : Anhedral <0.25mm Grains : Subhedral 0-0.5mm Undulose extinction *(70%)* **Biotite** - Pleochroic (brown-green/clear); 0-0.5mm *(10%)* **Muscovite** - Subhedral (<0,25mm) clear grains *(10%)* **Dolomite** - Minor component; anhedral grains (0-0.5mm) **Opaques** - Rounded grains <0.25mm; anhedral grains, hematite *(10%)* - elongate grains also present - ilmenite?	Granoblastic	Phyllite
NP034	Blue-grey, fine-grained, finely laminated pelite	**Quartz** - Anhedral grains 0-0.5mm *(40%)* **Biotite** - Subhedral/euhedral grains 0-0.25mm; pleochroic (brown-clear) *(10%)* **Muscovite** - Subhedral/euhdral grains 0-0.25mm; clear, well cleaved grains *(10%)* **Sillimanite** - Aggregates pseudomorphing larger elongate grains, pleochroic (grey-white); fibrous; low interference colours *(40%)* **Opaques** - Anhedral grains <0,25mm; hematite? *(tr.)* Minor amounts of **albite** as well	Subidioblastic/lepidoblastic	Pelite
NP035	Pseudomorph-bearing mudstone, green-grey fine grained mudstone	**Feldspar/quartz aggregates** - Anhedral clusters of interlocked grains (<1mm), show undulose extinction and low interference colours, feldspars occur as both simple and lamellae twins, Clusters are pseudomorphs of a larger phase - scapolite? *(20%)* **Biotite** - Anhedral/subhedral grains (<0.5mm), well developed cleavage, pleochroic (brown-yellow/straw yellow) *(20%)* **Dolomite** - Subhedral/anhedral grains, *(40%)* **Opaques** - Anhedral grains (0.5mm) *(10%)* **Tourmaline** - Only present in certain pseudomorphs (ie. reflects compositional variation in precursors - B-bearing phases?) subhedral grains (<0.5mm), pleochroic - emerald green to clear *(tr.)*	Subidioblastic	Pelite
NP036	Similar to NP030 - Sandy dolomite?	**Albite** - Important matrix constituent, euhedral/subhedral grains (<1mm), simple and lamellae twins seen *(35%)* **Quartz** - Forms porphyroblasts (1-2mm), anhedral/subhedral grains *(30%)* **Dolomite** - 2 generations?, large anhedral porphyroblasts (0-2mm) subhedral/anhedral matrix constit (<1mm) - *(30%)* Minor **muscovite** **Sphene + Haematite** grains also present *(5%)*	Subidioblastic	Sandy Dolomite (Siliceous dolomite)

Sample No.	Hand Specimen	Petrography	Rock Texture	Rock Name
NP037	Massive, recrystallised?, pink rock, brown weathering, fine grained - albitite	**Quartz** - anhedral (0-1mm) grains, *(40%)* **Albite** - Anhedral grains (<1mm), forms the large part of matrix (untwinned and lamellae twins) *(40%)* **Dolomite** - Isolated grains, anhedral (<1mm) grains, mainly interstitial *(15%)* **Sphene** - Anhedral grains (<0.5mm), yellow-brown pleochroism parallel extinction *(5%)*	Granoblastic	Felspathic quartzite (Albitite)
NP038	Pink-white breccia - angular albite? fragments in silicified matrix	Fragments : **Quartzite fragments** - 0-2mm quartz grains, subhedral, undulose ext as well as anhedral dolomite grains **Quartz-feldspar aggregates** - clusters of quartz/feldspar grains (pseudomorphs?) ~2-3mm **Dolomite** - Anhedral dolomite grains (0-1mm); quartz inclusions common; larger grains associated with quartzite Matrix : Consists of **dolomite** *(35%)*, **quartz** *(40%)* grains as well as **albite** (lamellae and simple twins) *(20%)* Trace amounts of **sphene** *(5%)* and **zircon** present	Seriate	Breccia
NP039	Crystalline silicified? Pink-white unit Sandy Dolomite? Albitite ?	**Albite** - Arguably the dominant mineral phase, simple&lamellae twinning seer <0.5mm anhedral grains; low interference colours *(40%)* **Quartz** - Minor mineral phase *(10%)* **Dolomite** - Anhedral grains ~0.5mm *(30%)* Minor **muscovite** (subhedral grains <0.25mm) and **sphene** (anhedral grains <0.25mm); Trace **zircon**	Granoblastic; seriate	Albitite
NP040	Medium-grained massive grey quartzite	**Quartz** - Anhedral grains (0.25mm); anhedral porphyroblasts ~0.25 undulose extinction; triple junctions? *(60%)* **Albite** - Anhedral grains form part of the matrix (<0.25mm); Lamellae twinning seen *(20%)* **Dolomite** - 0.5mm grains; anhedral *(10%)* Minor **opaques** *(10%)*; Trace amounts of **zircon, sphene**	Granoblastic seriate	Quartzite
NP041	Felspathic quartz arenite	**Quartz** - occurs as both matrix constituent and also forms larger porphyroblasts (1-2mm) *(65%)* **Albite** - Also occurs as both matrix constituent and porphyroblasts, lamellae twins common (1-2mm) *(25%)* **Dolomite** - also minor matrix constituent *(5%)* **Sphene/Rutile** - High relief, brown-red, anhedral mineral grains *(5%)* Trace **zircon**	Granoblastic	Feldspathic Quartzite (Albitite)

Sample No.	Hand Specimen	Petrography	Rock Texture	Rock Name
NP042	Finely and coarsely laminated albitic units	**Quartz** - Subhedral/anhedral grains (0-1mm), main matrix constituent *(75%)* **Albite** - minor matrix constituent, anhedral grains (0-1mm) lamellae twins, low relief *(10%)* **Dolomite** - Minor matrix constituent, well developed twin lamellae, anhedral grains (0-1mm) *(10%)* **Haematite** - Reddish-brown , pleochroic (brown-yellow), anhedral grains (<0.5mm) *(Tr.)* **Sphene** - yellow-brown grains, anhedral <0.25mm *(5%)* Trace amounts of **zircon, (&talc?)**	Granoblastic	Felspathic quartzite
NP043	Coarse carbonate unit	**Dolomite** - Well developed twin lamellae, subhedral/anhedral grains (~1mm) *(50%)* **Albite** - Subhedral/anhedral grains (0-1mm), simple twins and untwinned grains *(30%)* **Quartz** - subhedral/anhedral grains (0-1mm) *(20%)* Traces amounts of : **Hematite** - Anhedral reddish-brown grains, almost opaque grains (<0.5mm) **Talc** - subhedral grains <0.5mm **Sphene** - Yellow-brown, anhedral grains	Granoblastic	Siliceous marble
NP045	Fe-stained quartz sandstone - granular/pebbly soft rock	**Quartz** - Subhedral/anhedral (0-1mm) grains *(30%)* **Albite** - Individual and simple twinned subhedral/anhedral grains (0-1mm), undulose extinction, well developed triple junctions seen - *(40%)* **K-spar** - Anhedral grains (0-1mm), tartan twins *(20%)* **Biotite** - pleochroic (brown/yellow), anhedral *(10%)* Trace amounts of : **Muscovite, haematite, tourmaline** and **sphene**	Subidioblastic	Arkosic sandstone (immature)
NP046	blue grey arenaceous unit	**Quartz** - anhedral (<0.5mm) grains *(20%)* **Biotite** - Anhedral (<1mm) grains, pleochroic (brown-yellow/ straw yellow) *(20%)* **Dolomite** - form anhedral grains (0.25mm) *(20%)* **Albite** - Forms isolated aggregates, (<0.5mm) grains, simple & lamellae twins - *(30%)* **Opaques** - Anhedral grains (<0.5mm) *(10%)*	Subidioblastic	Felspathic quartzite

Sample No.	Hand Specimen	Petrography	Rock Texture	Rock Name
NP047	Coarsely recrystallised? talc-bearing dolomitic marble	**Dolomite** - Subhedral recrystallised grains up to 2mm; well developed triple junctions *(85%)* **Quartz** - Minor component; anhedral grains (<0.5mm); undulose extinction *(5%)* **Talc** - Anhedral/subhedral grains ~1mm; well developed cleaved *(10%)*	Polygonal Granoblastic	Dolomitic Marble
NP048	Yellow-white porphyroblastic rock, talc porphyroblasts, coarse dolomite matrix	**Dolomite** - Forms dominant mineral phase, anhedral grains up to 2mm long along the long axis *(75%)* **Talc** - Large porphyroblasts up to 2mm long; stippled extinction subhedral/anhedral grains *(20%)* **Tremolite?** - Anhedral aggregates of grains (<1mm), undulose extinction, low interference colours, form fibrous aggregates Trace amounts of **rutile** (red-brown subhedral grains 0.25mm) *(5%)* Vermiform breakdown/growth of dolomite grains - poikiloblastic	Seriate	Dolomitic Marble
NP049	Coarsely crystalline Fe-dolomite breccia	**Dolomite** - Anhedral grains up to 2mm *(70%)* **Quartz** - Grains 0-1mm; anhedral; undulose extinction *(10%)* **Talc** - Subhedral laths up to 2mm; undulose extinction; deformed kinked grains *(20%)* Similar to NP050	Decussate	Dolomitic Marble
NP050	Silicified Fe-dolomite?	**Dolomite** - Anhedral grains (~1.5mm); dominant mineral phase *(70%)* **Quartz** - Also form anhedral grains (~1.5mm); lower proportion; undulose extinction, contain rutile inclusions *(20%)* **Talc** - Kinked grains (up to 0.5mm); well developed cleavage; stippled extinction *(minor)* **Haematite** - Anhedral aggregates commonly less than 0.5mm; some up to 1mm; red-brown; almost opaque, form needle-like inclusions in quartz grains *(10%)*	Seriate (ameboid)	Dolomite Marble
NP055	Arenaceous unit; fine grained, green-grey	**Quartz** - Subhedral grains ~0.5mm; undulose extinction; *(80%)* **Muscovite** - Minor interstitial phase; Subhedral grains <0.25mm *-(10%)* **Plagioclase** - Also minor phase (0-0.5mm); anhedral grains; lamellae twins; *(10%)* Trace amounts of **biotite, sphene and opaques**	Granoblastic	Quartzite

Sample No.	Hand Specimen	Petrography	Rock Texture	Rock Name
NP056	Fine-grained quartz sandstone, weathers red-brown	**Quartz** - Subhedral grains ~0.25mm; undulose extinction; interlocking grains *(75%)* **Plagioclase** - Anhedral grains (<0.5mm); lamellae twinning seen; - *(10%)* **K-feldspar** - Tartan twinning seen; anhedral grains <0.25mm; microcline? *(10%)* Minor **muscovite** (subhedral <0.25mm) and **opaques** Rhombic, yellow-brown **sphenes** also present	Granoblastic	Quartzite
NP057	Fine-grained pellitic metasediments, tightly isoclinally folded	**Quartz** - Large (~1mm) subhedral grains as well as finer matrix constituents; undulose extinction *(50%)* **Hematite** - Subhedral/euhedral grains (~0.5mm); reddish-brown grains with some more anhedral grains associated with mica *(10%)* **Biotite** - Up to 2mm long pleochroic laths; brown-green/yellow-white - *(20%)* **Muscovite** - Also form large laths, show consistent alignment similar to biotite; *(20%)* Minor **plagioclase** also present *Microscale isoclinal folding outlined by the micas especially, clearly seen in thin section.*	Mylonitic?	Pelite
NP058	Fe-carbonate unit weathering brown-black	**Dolomite** - Subhedral grains (0-1.5mm); grains are rounded *(60%)* **Quartz** - Subhedral rounded grains (also 0-1.5mm); undulose extinction *(30%)* **Plagioclase** - More minor phase; Anhedral grains (<0.5mm); lamellae twinning seen *(10%)* Minor **hematite** - anhedral aggregates	Seriate	Dolomitic Marble
NP026/65	Sandy dolomite unit with albite pseudomorphs	**Quartz** - Subhedral/anhedral grains <0.25mm; interlocking crystals, triple junctions *(45%)* **Dolomite** - Anhedral grains <0.1mm; mainly forms a matrix component *(45%)* **Rutile/sphene** - scattered anhedral grains; yellow-brown/red brown grains; ; (10%) Rare lamellae-twinned **plagioclase** and **zircon**	Equigranular, granoblastic	Feldspathic quartzite

Sample No.	Hand Specimen	Petrography	Rock Texture	Rock Name
NP067	Siliceous breccia	***Clasts:*** **Dolomite** - forms large anhedral grains up to 10mm across, well developed twin lamellae *(40%)* **Quartz** - Often integrated with dolomite grains, also anhedral but smaller ~2mm across but grainsup to 5mm also seen; undulose extinction *-20%* **Albite** - Lamellae twinned anhedral to subhedral grains; generally ~1mm in length; commonly included in dolomite-quartz grains *(20%)* ***Matrix:*** Composed of a fine-grained aggregate (<0.25mm) aggregate of intergrown quartz/feldspar grains *(20%)* *Rutile&Zircon are randomly scattered over the clasts and matrix -> late?* **Sphene/Rutile** - yellow-brown to red brown interference colours - weakly pleochroic; anhedral; 0.5mm **Zircon** - clear but fractured grains; high relief; anhedral ~0.5mm	Seriate	Breccia
NP071	Breccia unit - clasts of albitites?, silicified matrix	***Matrix:*** Consist of quartz-feldspar aggregates, anhedral, <0.1mm; pseudomorphing other grains? ***Clasts:*** **Quartz** - Large anhedral grains, ~1mm across *(40%)* **Dolomite** - also anhedral ~1mm across; but some partially replaced? by opaque veins *(10%)* **Albite** - Large amount of lamellae twinned anhedral grains ~0.25mm laths show a random decussate orientation *(40%)* **Sphene** - Commonly associated with above grains; anhedral, up to 0.25mm *(5%)* **Opaques** - very irregular grains, late? *(5%)*	Seriate	Breccia - silicified
NP075	Fe-dolomite unit - brown-black weathering, fine grained and pink on fresh surface	**Quartzite** - Anhedral grains <0.25mm *(45%)* **Dolomite** - Anhedral grains; up to 1.5mm *(45%)* **Muscovite** - Subhedral/anhedral laths; ~0.5mm *(2%)* **Haematite** - opaque cores with reddish rims ; indicative of oxidisation?; <0.25mm *(1%)* **Sphene** - Anhedral yellow-brown grains, anhedral, <0.25mm; same interf colours in XPL and PPL *(2%)* **Albite** - Rare lamellae twins present in matrix, anhedral grains <0.25mm *-5%*	Granoblastic, equigranular	Siliceous dolomite?

Sample No.	Hand Specimen	Petrography	Rock Texture	Rock Name
NP082	Pebbly sandstone unit - soft, pebbly unit, yellow-white in fresh exposure,	**Quartz** - Coarsely recrystallised quartz grains (subhedral) approximately 0.5mm on average; triple junctions present *(80%)* **Biotite/Muscovite** - occupy interstices; ~0.25mm; subhedral; well cleaved; stippled extinction; (biotite - brown-yellow/yellow pleochroism) *(20%)* **Opaques** - Scattered through matrix; anhedral < 0.25mm Rare lamellae-twinned **plagioclase** grains present as well	Quartzite	Granoblastic polygonal
NP088	Red stained, soft weathering sandstone	**Quartzite** - Recrystallised quartz grains, polygonal grains, triple junctions common *(90%)* **Biotite** - Pleochroic grains (yellow-brown/straw-yellow); subhedral (<0.25mm) but larger than muscovite which is present as small subhedral laths *(5%)* **Opaques** - Anhedral grains up to 0.25mm *(5%)* Rare **plagioclase, rutile/sphene** and **zircon**	Granoblastic polygonal	Quartzite
NP096	Blue-grey weathering, micaceous sandstone	**Quartz** - Again a coarsely crystalline quartz fabric; anhedral ~0.5mm; low interference colours; undulose extinction *(80%)* **Dolomite** - Also present as part of matrix but subordinate to quartz; appear extremely altered with opaque inclusions; anhedral up to 0.5mm *(10%)* **Muscovite** - Clear laths, commonly <0.25mm but grains up to 1mm present well developed cleavage; stippled extinction *(5%)* **Chlorite** - present randomly in the matrix; blue-green to clear pleochroism; anomalous interference colours *(tr)* **Plagioclase** - Minor component of matrix; anhedral grains ~0.5mm; lamellae twins present, usually altered *(5%)* Trace amounts of **zircon, rutile/sphene** also present	Granoblastic seriate	Quartzite
NP101	Breccia unit - clasts of albitites?, silicified	***Clasts:*** **Quartz** - Anhedral grains ~0.5mm *(35%)* **Dolomite** - Subhedral/anhedral grains up to 2-3mm; well developed twin lamellae *(25%)* **Albite** - Lamellae twinned grains; ~0.5mm, subhedral grains *(35%)* **Opaques** - Anhedral grains, <0.25mm **Sphene** - anhedral yellow-brown grains; <0.25mm *(5%)* ***Matrix:*** consists of quartz-feldspar aggregate, coarse grained sphene and zircon and dolomite (euhedral crystals) also present; all grains except dolomite <0.25mm (dolomite - ~1mm)	Seriate	Silicified breccia

Sample No.	Hand Specimen	Petrography	Rock Texture	Rock Name
NP103	Dolomitic lens in southern part of dome	**Quartz** - Recrystallised quartz grains; commonly <0.25mm; subhedral -20% **Dolomite** - Anhedral grains form matrix along wwith quartz crystals; appear somewhat altered (<0.25mm) *(60%)* **Muscovite** - Subhedral/anhedral grains <0.25mm; parallel bird's eye extinct. rare **biotite** (green-clear pleochroism) also present *(10%)* **Haematite** - Present as scattered anhedral grains in matrix - opaques cores surrounded by reddish borders; anhedral grains around 0.25mm *(5%)* **Sphene/Rutile** - Yellow-brown anhedral grains scattered through matrix; <0.25mm *(5%)*	Lattice-preferred orientation	Siliceous marble/dolomite
NP114	Soft, red-stained quartz sandstone	**Quartz** - Interlocking subhedral grains dominate this rock; numerous triple junctions and penetration twins seen; low int colours; ~0.5mm undulose extinction *(80%)* **Microcline** - Subhedral/anhedral grains are interlocked with the quartz grains; typical tartan twinning seen; grains also ~0.5mm *(14%)* **Muscovite** - Forms a subordinate phase occupying spaces between above 2 minerals; forms small laths <0.5mm and aggregtes; parallel/bird's eye extinction *(5%)* **Opaques** - irregular, anhedral grains, associated with sphene/rutile **Rutile/sphene** - almost opaque; anhedral grains<0.5mm *(1%)* **Zircon** - Also trace constituent; high relief, small anhedral grains up to 0.25mm *(tr.)*	Recrystallised, granoblastic	Quartzite
NP115	Soft, red-stained quartz sandstone	**Quartz** - Interlocking subhedral grains dominate this rock; numerous triple junctions and penetration twins seen; low int colours; ~0.5mm undulose extinction *(80%)* **Microcline** - Subhedral/anhedral grains are interlocked with the quartz grains; typical tartan twinning seen; grains also ~0.5mm *(14%)* **Muscovite** - Forms a subordinate phase occupying spaces bet above 2 minerals; forms small laths <0.5mm and aggregtes; parallel/bird's eye extinction *(5%)* **Biotite** - pleochroic red-brown/ yellow-brown; 0.5mm, anhedral grains ; well developed cleavage; detrital?; slightly altered to chlorite *(1%)* Rare **zircon, sphene/rutile, opaques**	Recrystallised, granoblastic	Quartzite

Sample No.	Hand Specimen	Petrography	Rock Texture	Rock Name
NP116	Soft, red-stained quartz sandstone	**Quartz** - Interlocking subhedral grains dominate this rock; numerous triple junctions and penetration twins seen; grains ~0.5mm undulose extinction *(80%)* **Microcline** - Subhedral/anhedral grains are interlocked with the quartz grains; typical tartan twinning seen; grains also ~0.5mm *(14%)* **Muscovite** - Forms forms small laths <0.5mm and aggregates *(5%)* **Rare Biotite** - pleochroic red-brown/ yellow-brown; <0.5mm, anhedral *(tr.)* **Opaques** - irregular, anhedral grains, associated with sphene/rutile **Rutile/sphene** - grey-white grains showing the same interference colours in PPL and XPL; anhedral grains <0.5mm *(1%)* **Zircon** - Also trace constituent; high relief, small anhedral grains up to 0.25mm *(tr.)*	Granoblastic	Quartzite
NP118	Brown-weathering carbonate unit	**Dolomite** - Large and small grains; matrix - fg dolomite <0.25mm; anhedral *(80%)* clasts - ~1mm; anhedral grains **Quartz** - Large clasts up to 0.5mm; anhedral grains; zircon/apatite? inclusions *(10%)* **Feldspars** - lots of albite clasts in the matrix, associated with quartz/ dolomite clasts; simple and lamellas twins seen; ~0.25mm; subhedral/anhedral *-10%* **Rutile/sphene** - dark reddish brown elongate grains scattered randomly in the matrix; show same colours in XPL and PPL; <0.25mm subhedral/anhedral more likely rutile from colour *(tr.)* **Biotite** - rare grains, green-white pleochroism; parallel extinction	Seriate	Siliceous Dolomite/Marble
NP119	Soft, red-stained quartz sandstone	**Quartz** - Rock is dominated by recrystallised quartz (<0.25mm); usually anhedral grains with undulose extinction *(85%)* **Muscovite** - Occupies interstices; forms aggregates of laths <0.25mm; anhedral grains; stippled extinction *(10%)* **Biotite** - Also occupies interstices but unlike muscovite grains are singular and larger (~0.2mm); pleochroic - red-brown/yellow-brown; well cleaved *-5%* Rare **plagioclase**, and **opaques** associated with **sphene/rutile**	Granoblastic polygonal	Quartzite
NP123	Quartz sandstone, brown weathering	**Quartz** - interlocked, recrystallised grains, subhedral ~0.25mm *(65%)* **Dolomite** - Interstitial grains, anhedral; 0.25-0.5 mm *(20%)* **Biotite** - Green to clear pleochroism, subhedral laths ~0.25mm, scattered in matrix *(5%)* **Muscovite** - also subhedral laths ~0.25mm, scattered in matrix, clear *(5%)* **Opaques** - anhedral grains associated with sphene *(5 %)* Rare **sphene** and **plagioclase** seen	Seriate with some kinking	Quartzite

Sample No.	Hand Specimen	Petrography	Rock Texture	Rock Name
NP125	Schistose unit - blue grey weathering, mica-rich, finely laminated	**Quartz** - Again the dominant mineral phase in the rock; forms interlocked subhedral to anhedral grains (<0.25mm); triple junctions common *(65%)* **Dolomite** - Appears intersitital subordinte to the quartz; grains irregular anhedral (<0.25mm) *(10%)* **Biotite** - Green? biotite; laths show blue-green/clear pleochroism; grains are subhedral to anhedral and up to 0.5mm long **Muscovite** - same as biotite except clear and non-pleochroic and less frequent *Combined, the micas form 10% of the matrix and show a clear kinked texture - folded/refolded texture* **Chlorite** - Interstitial fibrous aggregates present showing anomalous extinction and blue green/clear pleochroism *(5%)* **Sphene** - Small, fractured brown-grey grains; anhedral, same intereference colours in XPL and PPL *(3%)* **Epidote** - Present as large grains - up to 1mm across; highly fractured/ deformed; show an anomalous blue extinction; high relief and interference colours; some grains show allanite? cores *(10%)* **Opaques** - Subhedral grains <0.25mm *(2%)*	Recrystallised, kinked	Psammite/quartzite
NP127	Brown-weathering carbonate unit	**Quartz** - Along with dolomite, forms the dominant mineral assemblage; anhedral/subhedral grains (<0.25mm); interlocking texture; some mica inclusions *(40%)* **Dolomite** - Forms anhedral grains interlocking with quartz forming the matrix; size varies from 0.25mm to 0.5mm; some grains show well developed twin lamellae *(50%)* **Biotite** - Occurs as well developed laths (late overprint?); brown-green to clear pleochroism; grains are euhedral/subhedral ~0.25mm; stippled ext. with noticable lack of cleavage; minor muscovite as well *(10%)* **Rutile/Sphene** - present scattered through the matrix; yellow to red-brown grains; anhedral <0.1mm; same colour in XPL and PPL *(tr.)*	Granoblastic polygonal	Siliceous marble/dolomite
NP132	Grey-white soft weathering sandstone, hematite cubes present in matrix	**Quartz** - Dominant mineral phase forming polygonal matrix crystals; anhedral to subhedral grains ~0.25mm; low interference colours *(80%)* **Biotite** - Subhedral/anhedral grains ~0.5mm; pleochroic (red-brown/yellow brown); well developed cleavage; stippled extinction *(5%)* **Muscovite** - Subhedral interstitial grains; stippled extinction; smaller than biotite ~0.25mm; form laths *(10%)* **Zircon** - Scattered grains present in matrix, high relief, anhedral, high interference colours *(2%)* **Haematite** - Some large grains - with reddish borders; up to 2mm ; *(2%)* **Sphene** - Some brown-grey grains (<0.25mm) *(1%)* Micas show strong preferred orientation	Granoblastic polygonal lepidoblastic	Quartzite

Sample No.	Hand Specimen	Petrography	Rock Texture	Rock Name
NP133	Iron-carbonate unit - brown weathering, pink on fresh surfaces	**Dolomite** - Matrix : Anhedral rounded grains <0.25mm Veins : Anhedral grains, larger than matrix grains (~1mm) *(80%)* **Quartz** - Smaller component - present in veins mainly but also small part of matrix; ~1mm anhedral grains *(15%)* **Feldspar** - Lamellae twinned plagioclase also present in veins *(5%)*	Seriate	Siliceous marble/dolomite
Omburu East Samples				
HFD80	Dolomitic shale	**Quartz** - Grains are anhedral (~0.5mm), poikiloblastic with feldspar inlcusions, undulose extinction, *(10%)* **K-feldspar** - Anhedral grains <1mm, tartan twinning seen - microcline? -10% **Plagioclase** - Lamellae twnning common, grains are anhedral (<1mm) **Muscovite** - Anhedral grains (<0.5mm), form matrix grains, parallel stippled extinction *(40%)* **Dolomite** - Grains are of similar habit and size, also matrix components *(40%)* Minor **rutile/sphene & hematite**	Seriate	Quartz-dolomite Schist
HFD82	Grey, dolomitic shale (associated with breccia alteration in the area - host rock)	**Dolomite** - Subhedral/anhedral grains (~1mm on average), dominant mineral loblastic/Lattice preferred orien show a strong preferred orientation of grains *(90%)* **Opaques** - Form large euhedral grains (2.5mm in diameter), late stage grains - haematite? *(10%)* Minor amounts of **quartz** and **albite** present (anhedral grains ~ 1mm)		Dolomitic Marble
HFD83	Coarse replacement of HFD82	**Dolomite** - Subhedral/euhedral grains ~2mm, well developed twin lamellae - recrystallised? *(80%)* **Quartz** - Subhedral grains commonly with muscovite inclusions undulose extinction, grain size ~0.5mm but up to 1mm *(10%)* **Opaques** - Anhedral remnants commonly <0.5mm *(10%)* Minor **muscovite** - subhedral grains <0.5mm, well cleaved, stippled extinction	Recrystallised/ Granoblastic	Sparry Dolomitic Marble
HFD 84	dolomite	**Dolomite** - Euhedral/subhedral grains ~0.5mm; *(80%)* **Quartz** - Subhedral grains ~0.5 mm; low int colours; undulose extinction; forms veins? in matrix *(20%)* **Hematite** - Minor phase, anhedral reddish grains (in PPL); commonly associated with quartz	Seriate	Dolomitic Marble

Sample No.	Hand Specimen	Petrography	Rock Texture	Rock Name
HFD87	Massive, pink-white, crystalline unit	**Quartz** - Anhedral grains <0.5mm; undulose extinction; *(65%)* **Albite** - Simple&lamellae twinned grains <0.5mm *(30%)* **Sphene/Rutile** - Anhedral grains <0.25mm; dark red in PPL *(5%)* Minor **muscovite** and **zircon** also present	Granoblastic	Feldspathic quartzite (Albitite)
HFD90	Psammitic unit - host to breccia bodies in north	**Biotite** - Anhedral grains (~0.25mm), pleochroic (red-brown/straw-yellow), stippled extinction, well developed cleavage *(40%)* **Quartz** - Anhedral grains (~0.5mm) & matrix grains (<0.25mm), low interference colours, undulose extinction *(40%)* **Plagioclase** - Minor anhedral plagioclase grains (~0.25mm), lamellae twinning seen *(10%)* **Haematite** - Anhedral grains (<0.25mm), reddish-brown *(tr.)* **Sphene** - Yellow-brown/grey-brown anhedral grains <0.25mm *(10%)* Minor **muscovite**	Seriate	Psammite
HFD91	Dolomitic breccia in dolomitised matrix	**Quartz-feldspar-dolomite aggregates** - rounded aggregates up to 5mm and 10mm; made up of finely crystallised phases quartz-feldspar-dolomite pseudomorphing larger phases **Dolomite** - Large anhedral grains up to 4mm; contain inclusions of quartz and feldspar *(30%)* **Quartz** - Form large anhedral-subhedral grains 1-2mm; also part of matrix; undulose extinction; some feldspar inclusions *(30%)* Matrix largely made up of feldspar: **Albite** - Form subhedral grains <0.5mm; simple & lamellae twins *(35%)* Some larger grains also present **Hematite** - Dark red grains, anhedral/subhedral grains up to 1mm - *(5%)*	Seriate	Siliceous dolomite breccia
HFD92	Siliceous Breccia	**Dolomite** - Large anhedral grains up to 4mm, contains feldspar and quartz inclusions, *(30%)* **Quartz** - Forms large subhedral/anhedral laths ~1mm, low int colours & undulose extinction *(20%)* **Sphene/Rutile** - Anhedral grains up to 1mm, reddish brown (almost opaque) - *(10%)* **Albite** - simple and lamellae twins up to 1mm, subhedral/anhedral grains *(20%)* **Feldspar/Quartz/Dolomite aggregates** : Forms clusters 2-3mm in diameter, made up of albite grains, quartz, and less commonly dolomite (grains <0.25mm in size) *(20%)*	Seriate	Siliceous Breccia

Sample No.	Hand Specimen	Petrography	Rock Texture	Rock Name
HFD97	Siliceous Fe-rich dolomite	**Dolomite** - 2 generations : (1) Forms large subhedral grain clusters grains ~2mm (2) Forms matrix; anhedral grains 0-0.5m - *(80%)* **Talc** - 0-1mm subhedral laths; stippled extinction *(15%)* Minor **haematite** *(5%)* and **quartz** also present	Porphyroblastic	Dolomitic marble
HFD 98	Siliceous talc-dolomite	**Dolomite** - Anhedral/subhedral grains (0-1mm); *(75%)* **Quartz** - Minor constituent; anhedral grains <0.5mm; undulose extinction *(5%)* **Talc** - Stippled extinction; grains on average ~0.5mm *(20%)*	Granoblastic	Talc-dolomite marble
HFD101	Siliceous talc-dolomite	**Dolomite** - Coarse anhedral grains up to 2mm, stippled extinction, *(70%)* **Talc** - Subhedral/anhedral laths up to 2mm, stippled extinction, forms secondary veins, cleavage not as well developed as micas *(30%)*	Decussate	Talc-Dolomite Marble
Moselle Samples				
NPD004 NPD005 NPD013(2)	Feldspathic quartzite, medium grained, pink weathering	**Quartz** - Variety of grain sizes (some rounded, some angular) 0.5-4 mm, anhedral, some grains - undulose extinction, some poikiloblasts replacing plagioclase grains. *(60%)* **Plagioclase** - also variety of grain sizes (0.5-4mm), anhedral, lamellae twins, poikiloblastic grains common, some sericitization - mica replacing plagioclase grains. *(20%)* **Biotite** - Rare green/brown to clear grains, anhedral (~0.5mm), stippled extinction, well developed cleavage *(10%)* **Dolomite** - Anhedral grains forming part of the matrix, interstitial grains *(10%)* **Zircon** - Rare grains, high relief, high interference colours, subhedral, <0.5mm *(tr.)* **Rutile** - Black-red grains, anhedral, sometimes opaque, grains up to 1mm *(tr.)* **Sphene** - Rare grains also present, yellow-brown, subhedral, low interference colours *(tr.)*	Seriate	Feldspathic Quartz Sandstone
NPD009	Brown-grey dolomite, siliceous	Anhedral aggregate of **Dolomite**, **Quartz** and **Plagioclase** in equal proportions. Trace components include **rutile**, **zircon** and **opaques** occuring as inclusions in larger grains.	Seriate Poikiloblastic	Siliceous Dolomite

Sample No.	Hand Specimen	Petrography	Rock Texture	Rock Name
Nosib Group Samples(NZ)				
NPD020	Medium grained feldspathic quarzite, pink weathering	**Quartz** - Matrix is dominated by equigranular quartz (~1mm), frequent triple junctions imply the matrix is recrystallised, subhedral grains *(80%)* **K-spar** - Cross-hatch, tartan twinning is seen in subhedral/anhedral grains, also ~1mm, show some mica inclusions *(10%)* **Muscovite** - Rare grains appear as interstitial grains, show stippled extinction and well developed cleavage *(5%)* **Rutile** - Form almost opaque, subhedral grains, <1mm *(5%)* **Sphene** - Rare, yellow-brown grains occur associated with opaques *(tr.)* **Zircon** - Rare high relief grains occur showing high interference colours and parallel extinction *(tr.)*	Polygonal-Equigranular	Feldspathic quartzite
NPD021	Medium grained feldspathic quartzite, with mica and carbonate blebs in matrix	**Quartz** - Recrystallised quartz grains ~1mm in diameter form matrix triple junctions, subhedral grains common *(80%)* **K-Spar** - Anhedral grains, ~1mm, also forms part of matrix, tartan twinning seen *(10%)* **Muscovite** - Rare laths occur, 0-2mm, form interstitial grains in matrix anhedral grains, stippled extinction *(5%)* **Carbonate** - Altered carbonate grains also occur as interstitial grains in the matrix *(5%)* **Sphene&Rutile** - Subhedral grains, dark grey to opaque grains form an accessory phase *(tr.)*	Polygonal	Feldspathic Quartzite

Appendix III
Analytical Data

(AIII.1) Microthermometric Data (Temperatures in °C; Salinity = wt% NaCleq)

Duruchaus Formation Dataset (All data from quartz-hosted inclusions)

Isolated Inclusions (all data) (NB - a T_h of 400°C represents a value of >400°C)

Sample	Chip	Type	Tm(CO2)	Te	Tm(ice)	Tm(clath.)	Th (CO2)	Th (H2O)	Salinity
Plugs									
Hakos Group									
NP001	1	I		-21.1		9.6			
		I		-20.5		12.8		351	
	2	I		-13.9		11.3		246	34
	3	II				14.1		250	35
		I		-19.9		7.3		382	45
		I		-19.0		21.9		400	38
NP008	1	I			-15.4			400	38
		II				11.0		400	
		IV	-60.1	-19.1				400	37
		II		-24.4		14.5		400	
		IV	-60.1	-26.7		9.5		382	46
		IV	-60.5			6.9		400	47
		II		-23.4	-21.7			327	40
NP006	1	II			-17.8			400	47
		II		-22.2	-16.8			269	
		II			-21.7			324	
		I				14.1		336	41
		III			-17.9			263	
	2	I				6.6		400	40
		I				27.8		373	
		II		-27.4	-21.7			297	
		I				25.2		346	38
		I				29.3		305	37
Duruchaus Formation									
NP014	3	III		-21.7	-7.5			400	
	4	IV	-56.9	-15.5	-14.5			400	
		I		-23.1		1.0		403	
NP017	1	I				9.8		313	
		III			-22.4			400	
		I				6.6		310	47
	3	II			-12.2			133	
		III			-18.8			147	
		II			-35.5			137	
NP081	2	II			-22.9			332	
		II			-20.2			334	
		II			-22.5			282	41
		IV	-56.6				-19.1		

Sample	Chip	Type	Tm(CO2)	Te	Tm(ice)	Tm(clath.)	Th (CO2)	Th (H2O)	Salinity
		I				9.8		232	
		I			-25.5	9.5		280	34
	3	II			-1.5			240	31
NP079	1	I		-25.5		6.1		182	29
		I		-28.1	-2.1	8.7		156	31
		I				6.7		148	30
		I				8.1		167	30
		IV	-57.6			7.5	19.5		30
		I				8.8			
		I				8.2			
		I				8.3		181	
		I				7.8		169	34
		II			-2.7			164	30
		I				29.9		189	
		I				9.9		179	
		I				8.2		172	34
		I				8.4		173	33
		I				7.5		190	34
		I				5.5		174	34
	2	I			-24.8	9.8		191	31
		II			-2.0			186	31
		I			-25.1	6.4		172	31
		I			-23.6	4.3		177	31
		I			-25.6	6.7		203	
		II			-31.1			273	46
	3	I				2.4		273	36
		I			-27.1	8.6		170	36
									30
Veins									
Duruchaus Formation									
NP072	1	II			-9.2			359	
		II			-23.4			371	32
		I		-20.2		18.6		334	
		I				11.4		235	34
	2	I		-26.0		12.9		366	44
		I				9.7		270	
	3	I				6.7		363	44
		I				6.3		320	47
		I				7.8		288	36
		I				6.9		333	41
		I		-16.0		6.6		276	36
		I				19.8		288	33
NP060	1	IV	-57.6				8.4		
		IV	-57.4				10.4		
		IV	-57.6				9.8		
		IV	-57.4				10.2		
		IV	-57.7				13		
		I				7.6		331	
		IV	-57.8				16.3	26	
		IV	-57.8				17.3	24	
		IV	-57.6				14.9	24	
		IV	-57.7				15	24	

Sample	Chip	Type	Tm(CO2)	Te	Tm(ice)	Tm(clath.)	Th (CO2)	Th (H2O)	Salinity
		IV	-57.5				12.9	21	
		II	]		-15.3			290	
		II	] early t	-21.3	-13.3			265	
		II	]	-21.0	-11.1			258	
		II	}early t		-4.0			248	
		II	}		-2.5			282	

Duruchaus Formation - Secondary Inclusions (all data)

Sample	Chip	Type	Tm(CO2)	Te	Tm(ice)	Tm(clath.)	Th (CO2)	Th (H2O)	Salinity
Plugs									
Hakos Group									
NP001	2	II		-34.2	-22.8			116	24
		II		-36.2	-22.6			114	24
		II		-30.1	-19.5			193	22
	3	II		-22.6	-12.1			214	16
		II		-30.3	-22.1			217	24
	4	II			-25.3			376	26
		II			-23.6			400	25
		II			-25.6			369	26
NP008	1	II		-31.3	-22.3			140	24
		II		-23.0	-19.3			174	22
		IV	-68		-24.2			400	25
		IV	-56.7	-22.0	-10.7			400	15
	2	IV	-67		-14.0			400	18
		II		-23.2	-14.1			181	18
	3	IV	-56.6		-27.0			120	27
NP006	1	II			-18.1			400	21
		II			-22.2			400	24
		II			-21.1			317	23
		II				15.1		329	
	2	I				8.1		130	4
		I							
Duruchaus Formation									
NP014	2	II		-33.7	-8.9				13
		II		-25.1	-23.8			172	25
		II			-10.1			196	14
		II			-5.3			93	8
		II			-3.0			221	5
		II			-3.0			232	5
		II		-18.1	-4.4			279	7
		II			-2.8			217	5
	3	II		-22.7	-19.3			204	22
		II		-22.2	-16.9			136	20
		II		-25.1	-18.2			300	21
	4	II			-22.3			210	24
NP073	1	II		-28.0	-22.0			256	24
		I		-41.6	-23.6			153	25
		I			-23.0			167	24
		I			-22.8			176	24
		I			-19.0			301	22
		I			-17.1			285	20
	2	I		-37.8	-23.3			267	25
		I		-27.0	-23.3			235	25
		I		-28.1	-22.9			225	24
		II		-26.0	-22.2			347	24

Sample	Chip	Type	Tm(CO2)	Te	Tm(ice)	Tm(clath.)	Th (CO2)	Th (H2O)	Salinity
	3	II			-18.0			275	21
		II			-10.4			371	14
NP017	1	II			-22.4			154	24
	2	II			-21.4			127	23
		II			-19.0			161	22
	3	II			-17.9			174	21
		II			-31.6			69	30
		II		-24.1	-23.1			131	24
		II		-44.7	-34.1			148	31
		II		-37.1	-36.7			169	33
		II			-35.8			170	33
		II		-38.1	-31.7			127	30
NP081	1	II		-17.7	-7.7			27	11
	2	II			-17.7			197	21
		II			-19.0			265	22
		II			-20.1			287	22
		II		-30.7	-28.5			221	28
		II			-19.1			113	22
		II			-23.6			262	25
		II			-10.9			238	15
		II			-12.6			270	17
		I			-23.3	9.6		184	1
		I				9.8		160	0
		I				11.0		229	
	3	I				10.1	18?	206	
		I		-23.2		30.7		4	
NP079	1	I				8.1		190	4
		I				8.6		175	3
	2	I			-22.4	7.4		172	5
Veins									
Duruchaus Formation									
NP072	1	II			-22.4			195	24
		II			-1.0			361	2
	3	II			-22.1			240	24
NP060	1	IV	-57.7				-20.7	21	
		IV	-56.9				12.6	25	
		IV	-57.1				19.4	24	
		IV	-57				9.6	21	
		IV	-57.1				18	23	
		IV	-57.4				19.3	24	
		III			-49.8			144	48
		III		-51.8	-45.6			145	42
		III			-40.2			218	36
		III			-23.2			148	24
		III			-48.1			245	45
		III			-19.8			245	22

Eastern Dataset (All data from quartz-hosted inclusions)

Isolated Inclusions

Sample	Chip	Type	Tm(CO2)	Te	Tm(ice)	Tm(clath.)	Th (CO2)	Th (H2O)	Salinity
Okorusu/Gaidus									
NPD46(1)	1	III		-26.8	-15.5			300	19
		II			-10.2			327	14
		III			-17.1			479	20
		I				15.2		462	
		III		-24.3	-15.2			428	19
NPD46(2)	1	III			-0.9			236	2
		III			-0.5			313	1
		III			-0.2			348	0
		III			-17.0			340	20
		III			-19.4			364	22
		II		-30.1	-13.7			366	18
		III			-0.5			282	1
		III		-26.7	-19.1			178	22
	2	III		-28.3	-8.8			374	13
		III		-17.8	-0.3			366	1
		III		-25.1	-17.7			328	21
		III		-30.1	-2.2			338	4
		III		-31.2	-3.1			348	5
		III			-0.5			365	1
		III		-25.2	-19.2			346	22
	3	I		-27.4	-25.2	12.7		223	26
		I			-13.5	8.7		280	17
		III		-17.4	-1.0			356	2
		I		-19.4		29.0		399	
		III			-6.5			446	10
Elefantenberg									
NPD 49	1	III		-23.1	-7.3			213	11
		II		-21.1	-7.9			228	12
		III			-3.8			307	6
		III		-19.3	-6.6			363	10
		III			-7.5			445	11
		III		-19.5	-7.8			274	11
		III			-9.4			285	13
		III			-7.9			307	12
		III			-7.7			344	11
		III			-2.8			348	5
		III			-4.6			326	7
		III			-5.0			373	8
		II			-3.2			348	5
		III		-22.2	-4.9			297	8
		III		-16.0	-6.1			374	9
		II		-21.0	-6.6			288	10
		III		-19.1	-3.1			370	5
		III			-0.1			369	0
		III			-0.2			335	0
	2	III		-22.1	-4.6			287	7

Sample	Chip	Type	Tm(CO2)	Te	Tm(ice)	Tm(clath.)	Th (CO2)	Th (H2O)	Salinity
		II		-21.4	-4.6			245	7
		III		-21.1	-3.3			241	5
		III		-31.0	-3.8			280	6
		III		-21.3	-6.6			337	10
		III		-22.7	-2.2			351	4
		I				3.7		375	
		III			-4.0			363	6
		III		-17.3	-6.2			338	9
		III		-22.9	-10.1			433	14
		III		-22.3	-10.9			209	15
Hartbeespoort									
NPD37	1	III			-3.8			297	6
		IV	-58.6			14.6			
		III			-2.8			275	5
		III			-2.9			146	5
		III		-22.0	-0.7			358	1
		III			-6.5			177	10
		III		-21.1	-15.8			337	19
		III		-21.1	-3.9			310	6
	2	III		-20.9	-16.8			477	20
		III		-23.5	-11.4			414	15
		III		-22.2	-1.3			359	2
		III			-9.4			133	13
		III		-24.6	-6.0			366	9
		III	-57	-23.4	-1.0			400	2
		III		-23.5	-2.6			410	4
		III		-23.3	-2.4			416	4
		I		-22.3		8.8		367	
		III			-3.6			418	6
	3	III		-24.5	-0.2			275	0
		III		-25.2	-4.1			315	7
		III		-22.5	-0.5			308	1
		III		-23.2	-0.6			307	1
		III		-23.2	-0.4			311	1
		III		-22.2	-5.2			158	8
		III		-23.5				327	
		III		-22.1	-3.3			275	5
		III		-22.5	-16.8			154	20
		III			-4.8			415	8
Neuwerk									
NPD32	1	III		-23.3	-12.3			167	16
		III		-20.2	-9.8			128	14
		III		-24.4	-10.0			136	14
		III		-16.0	-9.7			105	14
		I				3.2		108	0
		III		-18.0	-11.9			137	16
		III		-16.4	-9.9			136	14
		III		-24.2	-10.6			116	15
		III		-22.2	-6.7			112	10
		III		-23.2	-6.6			126	10
		III		-23.0	-4.4			168	7

Sample	Chip	Type	Tm(CO2)	Te	Tm(ice)	Tm(clath.)	Th (CO2)	Th (H2O)	Salinity
		III		-22.1	-7.1			120	11
		III		-22.5	-8.3			134	12
		III		-11.3	-6.6			127	10
		II		-11.7	-5.7			125	9
		III		-19.0	-6.0			168	9
		III		-12.7	-9.6			109	14
		II		-20.3	-9.1			132	13
		III		-16.0	-8.9			106	13
		III			-5.3			119	8
		III		-14.3	-0.8			137	1
		III		-23.0	-5.6			130	9

Western Dataset (All data from quartz-hosted inclusions)

Isolated Inclusions

Sample	Chip	Type	Tm(CO2)	Te	Tm(ice)	Tm(clath.)	Th (CO2)	Th (H2O)	Salinity
Omburu East									
HFD95	1	I				28.5		356	
		I				29.1		320	
		I				0.4		331	15
		III			-22.1			385	24
		I				0.1		348	15
		III			-2.1			337	4
	2	III			-0.2			363	0
		III			-5.5			274	9
		III			-1.5			226	3
		III			-4.2			311	7
		II			-1.0			262	2
HFD102	1	III			-21.7			413	24
		III			-8.4			388	12
		III		-26.2	-22.9			240	24
		III			-30.4			225	29
		III			-20.7			348	23
		III		-24.2	-22.0			211	24
		II			-21.7			394	24
		III			-22.0			456	24
		III		-24.6	-18.0			245	21
		III		-26.2	-24.1			287	25
		III			-0.2			218	0
		II		-22.7	-12.6			225	17
		III		-19.6	-6.6			191	10
		III			-22.2			268	24
		III		-12.2	-3.5			152	6
		III		-21.9	-2.1			192	4
		III		-40	-1.2			294	2
HFD85	1	III		-24	-21.3			324	23
		III		-25.3	-22.8			310	24
		III			-21.1			267	23
		III			-23.9			272	25
		III		-26	-22.7			375	24
		III		-27.9	-21.9			440	24
		III			-18.9			153	22
		III		-24.2	-22.4			200	24
		III		-26.2	-22.5			272	24
Moselle									
NPD002	1	III			-21.3			279	23
		III		-23.3	-14.1			249	18
		II		-23.8	-22.3			427	24
		III			-22.8			420	24
		I			-23.2	16.4		383	24
		III		-22.2	-21.2			364	23

Sample	Chip	Type	Tm(CO2)	Te	Tm(ice)	Tm(clath.)	Th (CO2)	Th (H2O)	Salinity
		III		-23.3	-22.4			315	24
		III		-24.6	-21.5			319	23
		III			-22.5			455	24
		III			-22.1			392	24
		III		-29.4	-21.2			129	23
		III		-25.4	-22.4			437	24
		III		-24.2	-21.4			395	23
		III		-27	-23.0			317	24
NPD016	1	III		-25.2	-18.4			276	21
		I				28.7		332	
		III		-29	-23.7			302	25
		III			-16.7			336	20
		I		-27.3	-23.4	23.9		364	25
		I			-22.3	11.4		254	24
		I		-28.7	-23.7	28.4		363	25
		III			-22.2			377	24
		I				29.3		450	
		I			-22.7	13.5		464	24
	2	III			-21.3			254	23
		I		-24.2	-22.2	29.3		346	24
		I			-23.0	29.6		322	24
		III			-17.5			262	21
		III			-22.4			328	24
		I			-23.5	27.2		309	25
	3	I			-21.5	29.2		374	23
		III			-22.3			282	24
		III			-24.2			333	25
		I	-59.7	-21.5	-16.5	24.2		438	20
		I			-15.4	27.8		400	19
Karachas									
NPD018	1	III			-6.8			119	10
		III			-7.4			109	11
		III			-0.6			136	1
		III		-21.7	-5.4			150	8
		III		-20.7	-6.3			111	10
		III		-26.5	-4.6			203	7
		III		-20.8	-6.2			178	9
		III		-21.3	-6.4			137	10
		III			-2.9			109	5
		III			-0.6			108	1
		III		-20.1	-5.4			278	8
		III		-22.8	-2.2			127	4
		III			-6.0			124	9
Bothashof									
NPD43	1	III		-26	-6.6			159	10
		III		-24.3	-11.3			220	15
		III			-11.9			254	16
		III			-0.1			254	0
		III			-11.2			244	15
		III			-11.5			276	15
		III			-7.1			239	11
		III		-32	-14.6			401	18

Sample	Chip	Type	Tm(CO2)	Te	Tm(ice)	Tm(clath.)	Th (CO2)	Th (H2O)	Salinity
		III		-21.2	-13.5			312	17
		III		-22.4	-16.8			217	20
		III		-24.3	-13.2			227	17
		III		-44	-23.3			210	25
		III			-23.8			270	25
		III			-18.0			193	21
		III			-21.4			214	23
		III			-22.7			211	24
		III			-22.7			211	24
		III			-21.1			211	23
		III		-29.9	-21.9			333	24
		III		-22.8	-11.1			366	15
		III		-21.9	-11.1			223	15
		III		-31.1	-18.3			254	21
		III		-31.1	-18.3			254	21
		III		-22.7	-17.1			221	20
		III		-22.4	-19.4			244	22
		III			-21.0			152	23
		III			-22.8			234	24
		III			-22.9			233	24
		III		-33.3	-22.4			384	24
		III		-37	-19.5			227	22

Western Dataset

Secondary inclusions

Sample	Chip	Type	Tm(CO2)	Te	Tm(ice)	Tm(clath.)	Th (CO2)	Th (H2O)	Salinity
Omburu East									
HFD 95	1	III			-3.8			135	6
		III			-7.3			306	11
		I				0.4		331	15
		I				0.7		371	15
		III			-7.4			369	11
		I				0.4		139	15
		I				0.9		145	15
HFD102	1	III		-20.1	-2.2			100	4
		III			-2.6			98	4
		III			-3.0			221	5
		III			-5.0			222	8
		III			-6.2			202	9
HFD85	1	III		-21.9				219	
		III		-23.9	-22.2			236	24
		III			-22.2			148	24
		III			-20.4			130	23
		III			-24.6			254	25
		III			-23.5			290	25
		III			-23.6			283	25
		III		-28.5	-22.6			278	24
		III		-26.5	-22.7			265	24
		III			-21.0			210	23
		III			-21.0			176	23
		III		-22.1	-20.7			185	23
Moselle									
NPD002	1	III			-21.4			184	23
		III		-29.1	-24.2			357	25
		III			-25.2			232	26
		III			-24.4			267	25
		III			-25.6			263	26
		III			-22.7			288	24
		III		-24.3	-23.4			312	25
		III			-23.1			263	24
		III		-25.3	-22.7			302	24
		III							
NPD016	2	III			-8.0			236	12
		III			-6.0			307	9
Karachas									
NPD018	1	III			0.0			250	
		III		-24.5	-3.6			257	6
		III		-24.1	-5.4			211	8
		III			-6.5			272	10

Sample	Chip	Type	Tm(CO2)	Te	Tm(ice)	Tm(clath.)	Th (CO2)	Th (H2O)	Salinity
		III		-22.6	-6.9			308	10
		III		-20.1	-5.8			315	9
		III			-4.5			248	7
		III			-5.8			305	9
		III			-5.6			307	9

(AIII.2) Crush-Leach Data

(n.d.= not detected) - All element concentrations except Br^- and CO_3^{2-} were determined by HPIC
Br^- concentrations were determined by ICP-MS analyses; CO_3^{2-} concentrations are based on observed charge imbalances
(Samples with the prefix "D" and "T" are the dolomite and tourmaline samples respectively)

Sample	Cl^-	SO_4^{2-}	Br-	CO_3^{2-}	Na^+	K^+	Mg^{2+}	Ca^{2+}	Cl/Br	Na/Br
	ppm	*ppm*	*ppb*	*ppm*	*ppm*	*ppm*	*ppm*	*ppm*	*mol*	*mol*
SMZ Samples										
Plugs										
Swakop Group										
NP001.1	12.75	3.47	15.24		5.28	3.30	0.17	0.71	1886	1204
NP001.3	10.15	3.65	12.76		2.93	1.89	0.15	0.51	1793	798
NP001.4	8.98	14.13	14.87		3.14	1.89	0.61	0.68	1361	734
NP001.5	4.86	3.71	9.33	0.90	3.73	1.83	0.12	0.51	1174	1389
NP001.1	14.86	0.62	9.15		4.67	3.29	0.21	1.39	3659	1774
NP001.2	13.02	0.51	11.70		4.15	2.79	0.08	1.10	2509	1233
NP001.4	13.96	0.62	33.80		4.11	3.13	0.08	0.94	931	423
NP008.1	28.16	n.d.	37.05		13.20	2.48	0.10	0.61	1713	1238
NP008.2	26.08	n.d.	42.75		12.24	2.36	0.24	0.83	1375	995
NP008.4	27.90	n.d.	32.30		13.32	2.33	0.15	0.80	1947	1433
NP008.5	34.24	n.d.	35.20		18.58	3.16	0.10	0.87	2192	1835
NP008.1	15.94	2.06	18.20	2.26	11.03	1.70	0.16	0.92	1974	2106
NP008.2	22.93	2.26	19.40		11.15	1.84	0.16	0.90	2663	1998
NP008.3	23.00	2.25	18.20		11.13	1.81	0.12	0.70	2848	2125
NP008.5	20.41	1.94	19.10		9.18	1.77	0.06	0.78	2408	1670
NP006.1	25.31	2.32	21.25		13.03	1.54	0.57	1.60	2684	2131
NP006.2	24.26	1.28	29.55		12.32	1.44	0.23	1.35	1850	1449
NP006.4	23.04	0.86	17.85		11.91	1.31	0.18	1.63	2909	2319
NP006.1	18.15	0.69	12.90		10.16	0.35	0.06	0.65	3171	2737
NP006.2	19.75	0.70	15.20		10.97	0.42	0.11	1.15	2929	2508
NP006.3	13.16	0.46	11.50		7.66	0.30	0.10	0.63	2579	2315
NP006.4	14.77	0.45	10.10		8.44	0.31	0.09	0.81	3295	2904
DNP002.1	6.25	0.17			2.02	0.83	15.79	10.43		
DNP002.2	6.91	0.26	10.22	50.05	2.31	0.94	15.45	10.29	1524	786
Duruchaus Formation										
NP014.1	8.16	1.26	33.70	4.44	4.20	1.48	0.82	3.10	546	433
NP014.2	0.70	0.62	31.90	3.49	0.40	0.23	0.32	2.05	50	44
NP014.3	9.18	1.13	31.10	3.23	4.55	1.53	0.76	3.06	665	508
NP073.1	15.07	2.56	19.75		5.62	2.04	0.53	1.38	1720	989
NP073.2	13.57	1.97	22.80		4.92	1.83	0.55	0.97	1341	750
NP073.3	10.49	1.53	12.25		3.68	1.44	0.55	0.82	1931	1044
NP073.4	11.73	4.61	14.00		3.90	1.52	2.24	1.99	1888	968
NP0017.1	7.77	0.76	13.75	1.43	2.85	1.24	0.66	2.25	1273	720
NP0017.2	8.22	2.79	18.80	4.71	4.39	1.04	0.75	4.53	985	812
NP0017.3	6.35	0.99	17.40	1.15	3.26	0.74	0.20	2.13	822	651

Sample	Cl^-	$SO4^{2-}$	Br^-	Na^+	K^+	Mg^{2+}	Ca^{2+}	Cl/Br	Na/Br
	ppm	*ppm*	*ppm*	*ppm*	*ppm*	*ppm*	*ppm*	*mol*	*mol*
NP077.1	40.97	0.80	0.05	19.41	4.52	0.06	0.84	1944	1420
NP077.2	19.42	0.44	0.02	10.31	2.73	0.02	1.07	1894	1551
NP077.3	23.95	0.68	0.03	10.21	2.74	0.03	0.96	1935	1272
NP077.4	27.60	0.37	0.03	12.12	3.00	0.03	0.93	2007	1359
NP079.1	24.02	0.60	0.03	11.77	1.01	0.22	1.48	1990	1504
NP079.2	13.62	0.32	0.02	7.12	0.62	0.24	1.02	2047	1650
NP079.3	14.71	0.34	0.02	7.64	0.67	0.24	1.39	1842	1475
NP079.4	19.09	0.40	0.02	9.59	0.91	0.19	1.26	2151	1667
NP081.1	19.31	0.72	0.01	9.88	0.81	0.17	0.83	2941	2320
NP081.2	19.65	0.84	0.02	9.90	0.80	0.06	0.82	2821	2192
NP081.3	13.04	1.62	0.02	7.42	1.13	0.41	0.35	1580	1387
NP081.4	12.85	0.54	0.01	7.36	1.09	0.12	0.29	2084	1840
NP059.1	0.95	n.d.	0.02	0.65	0.44	0.31	0.67	117	124
NP059.2	2.04	n.d.	0.03	1.27	1.04	0.21	0.73	154	148
NP059.3	2.48	n.d.	0.02	1.53	1.62	0.33	1.26	265	253
NP059.4	1.34	n.d.	0.02	1.65	0.65	0.13	1.06	198	377
NP059(T)1	0.25	0.32	0.27	1.44	0.17	1.14	0.34	2	18
NP059(T)2	0.15	0.00	0.00	1.39	0.09	1.37	0.30	203	2982
NP059(T)3	0.16	0.09	0.01	0.96	0.12	0.55	0.21	63	606
NP085.1	1.86	0.98	0.01	0.16	0.27	0.16	1.46	326	43
NP085.2	1.36	0.69	0.01	1.05	0.99	0.28	2.53	358	425
NP085.3	1.54	0.60	0.01	1.23	1.13	0.28	2.37	283	349
NP085.4	1.42	0.72	0.01	1.13	0.95	0.21	1.89	258	317
NP021.1	2.42	0.32	0.01	2.90	6.32	3.27	6.33	578	1070
NP021.2	1.55	0.47	0.00	2.85	3.18	3.88	7.71	1079	3068
NP021.3	2.21	0.43	0.01	2.96	2.09	4.02	8.28	674	1395
NP085T(1)	0.15	n.d.	0.01	0.42	13.55	0.61	3.46	31	132
NP085T(2)	0.19	0.10	0.00	0.36	10.16	0.82	2.62	92	267
NP085T(3)	0.14	n.d.	0.00	0.30	9.54	1.01	3.91	989	3244
NP086.1	9.76	0.43	0.09	5.75	2.13	0.26	1.78	248	225
NP086.2	7.46	0.26	0.01	4.41	1.70	0.06	1.61	1430	1303
NP086.3	8.19	0.37	0.02	4.81	1.66	0.09	1.38	1215	1101
NP086.4	7.37	0.25	0.02	4.32	1.60	0.10	1.73	1101	995
NP099.1	2.12	0.79	0.00	1.97	0.95	0.03	0.95	998	1428
NP099.2	1.49	0.58	0.01	1.34	0.72	0.12	0.95	496	686
NP099.3	1.34	0.54	0.00	1.27	0.61	0.02	0.71	627	915
NP099.4	1.42	0.56	0.01	1.50	0.61	0.02	1.63	598	976

Sample	Cl^- ppm	$SO4^{2-}$ ppm	Br^- ppm	Na^+ ppm	K^+ ppm	Mg^{2+} ppm	Ca^{2+} ppm	Cl/Br mol	Na/Br mol
Veins									
Duruchaus Formation									
NP072.1	27.83	1.23	0.03	11.96	3.78	0.22	2.43	2323	1540
NP072.2	23.44	1.15	0.03	8.81	3.43	0.18	2.39	1957	1134
NP072.3	20.41	1.67	0.02	7.24	3.03	0.42	4.10	1870	1023
NP072.4	17.76	0.81	0.02	6.28	2.59	0.25	4.76	1775	968
NP060.1	3.20	0.58	0.02	1.76	0.49	0.22	11.88	367	312
NP060.2	1.83	0.14	0.02	0.99	0.32	0.09	10.24	202	168
NP060.3	2.62	0.21	0.02	1.32	0.38	0.15	10.18	342	266
NP060.4	2.99	0.19	0.02	1.63	0.44	0.11	11.88	319	268
Western Dataset									
Moselle									
NPD2.1	12.68	0.09	0.05	7.85	0.66	0.05	1.08	568	542
NPD2.2	17.18	0.37	0.08	10.56	0.89	0.10	1.41	489	464
NPD2.3	12.99	n.d.	0.05	7.61	0.62	0.01	0.95	599	541
NPD2.4	17.59	0.12	0.06	9.77	0.67	0.02	1.05	639	548
NPD16.1	17.63	0.22	0.07	8.86	0.88	0.06	0.87	598	463
NPD16.2	15.42	n.d.	0.07	7.87	0.79	0.10	0.50	530	418
NPD16.3	18.87	0.09	0.08	10.64	1.54	0.01	1.17	524	456
NPD16.4	18.48	0.08	0.08	10.58	1.56	0.01	1.31	535	472
Karachas									
NPD18.1	0.84	0.48	0.02	1.01	0.32	0.01	0.92	122	226
NPD18.2	0.71	0.33	0.02	0.87	0.17	0.02	1.08	79	149
NPD18.3	0.62	0.28	0.01	0.77	0.17	0.01	1.05	99	190
NPD18.4	0.79	0.53	0.02	1.02	0.20	0.02	1.28	95	191
Bothashof									
NPD42(1)	0.40	0.16	0.01	0.26	0.23	0.25	7.14	68	68
NPD42(2)	0.30	n.d.	0.02	0.20	0.16	0.14	2.77	36	37
NPD42(3)	0.36	n.d.	0.01	0.23	0.15	0.12	4.06	70	70
NPD42(4)	0.34	n.d.	0.02	0.22	0.20	0.23	4.41	36	36
NPD43(1)	0.69	n.d.	0.02	0.45	0.17	0.05	2.05	86	87
NPD43(2)	0.70	n.d.	0.02	0.42	0.20	0.03	2.29	64	60
NPD43(3)	0.70	n.d.	0.02	0.41	0.19	0.02	2.91	97	87
NPD43(4)	0.71	n.d.	0.01	0.43	0.14	0.02	1.85	133	125
Omburu East									
HFD85.2	16.81	0.48	0.07	1.02	0.25	0.09	0.31	566	53
HFD85.3	11.94	0.28	0.05	7.14	1.39	0.41	1.55	515	475
HFD95.1	4.03	n.d.	0.04	2.59	0.30	n.d.	0.70	248	246
HFD95.2	3.67	0.07	0.04	2.34	0.35	n.d.	1.37	198	195
HFD95.3	2.99	0.06	0.03	1.98	0.31	0.05	1.59	199	203
HFD95.4	3.21	n.d.	0.03	2.08	0.31	0.06	1.85	226	226

Sample	Cl^- ppm	$SO4^{2-}$ ppm	Br^- ppm	Na^+ ppm	K^+ ppm	Mg^{2+} ppm	Ca^{2+} ppm	Cl/Br mol	Na/Br mol
Eastern Dataset									
Neuwerk									
NPD 32(1)	13.15	0.34	0.43	4.86	1.00	0.90	19.60	70	40
NPD 32(2)	6.77	n.d.	0.23	2.55	0.64	0.49	16.51	68	39
NPD 32(3)	5.43	n.d.	0.27	1.93	0.65	0.25	16.12	46	25
NPD 32(4)	5.52	n.d.	0.31	2.01	0.54	0.34	16.75	40	23
Hartbeespoort									
NPD37(1)	5.65	0.16	0.13	2.26	1.63	0.28	15.74	101	62
NPD37(2)	4.40	0.14	0.13	1.70	1.35	0.23	14.28	79	47
NPD37(3)	5.52	0.08	0.10	2.22	1.63	0.14	14.91	129	80
NPD37(4)	4.73	0.17	0.11	1.78	1.52	0.21	15.54	94	55
Elefantenberg									
NPD49(1)1	4.87	0.51	0.13	3.78	0.33	0.39	15.28	86	103
NPD49(1)2	5.40	0.37	0.10	3.88	0.28	0.17	14.90	117	130
NPD49(1)3	4.19	0.33	0.11	3.03	0.26	0.19	15.47	87	98
NPD49(2)1	4.57	0.24	0.12	3.36	0.39	0.08	14.08	89	101
NPD49(2)2	4.96	0.25	0.10	3.49	0.49	0.07	15.22	113	123
NPD49(2)3	3.90	0.16	0.09	2.84	0.39	0.05	11.77	97	108
NPD49(2)4	4.70	0.15	0.11	3.38	0.39	0.06	14.40	100	111
Kupferberg									
NPD23(2)A	0.56	n.d.	0.00	0.39	0.12	0.06	13.49	701	753
NPD23(2)B	0.43	n.d.	0.00	0.25	0.12	0.08	14.55	410	370
NPD23(2)C	1.22	n.d.	0.01	0.82	0.18	0.10	14.59	341	355
NPD23(2)D	0.66	n.d.	0.00	0.41	0.22	0.10	14.05	573	546
NPD23(3)A	0.31	0.09	0.00	0.23	0.12	0.05	0.00	320	362
NPD23(3)B	0.32	n.d.	0.00	0.18	0.23	0.08	0.33	1463	1277
Okorusu/Gaidus									
NPD46(1)A	5.47	0.83	0.02	2.73	1.20	0.13	33.28	704	542
NPD46(1)B	5.57	0.90	0.01	3.06	1.17	0.19	36.21	1596	1353
NPD46(1)C	6.34	1.39	0.01	3.24	1.32	0.17	39.33	1221	962
NPD46(1)D	6.07	3.28	0.01	3.19	1.34	0.20	31.07	1768	1432
NPD46(2)A	6.50	0.50	0.01	3.15	1.19	0.43	32.71	1285	960
NPD46(2)B	5.35	0.30	0.01	3.30	1.29	0.47	35.00	927	882
NPD46(2)C	6.26	0.70	0.02	3.76	1.50	0.42	35.97	702	650
NPD46(2)D	6.75	0.77	0.02	3.97	1.54	0.33	35.22	704	639
NPD46(3)A	8.75	n.d.	0.01	4.36	1.56	0.88	23.46	1658	1273
NPD46(3)B	11.31	n.d.	0.01	5.49	1.94	0.89	21.64	2007	1502

(AIII.3.1) XRF Analyses (Whole Rock Chemistry)

Duruchaus Formation (Weight percent oxides)

	SiO_2	TiO_2	Al_2O_3	Fe_2O_3	MnO	MgO	CaO	Na_2O	K_2O	P_2O_5	SO_3	NiO	CR_2O_3	H_2O-	LOI	TOTAL
NP10	71.83	0.55	12.49	1.93	0.01	5.99	0.92	2.90	3.23	0.14	-0.01	0.00	0.01	0.00	0.02	100.01
NP11	60.33	0.50	11.38	1.95	0.05	7.40	11.21	6.59	0.13	0.13	0.25	0.00	0.00	0.00	0.15	100.06
NP71	59.60	0.75	14.16	2.18	0.04	5.83	9.01	8.41	0.09	0.18	-0.01	0.00	0.01	0.00	0.12	100.37
NP22(1)	32.94	0.46	6.54	5.75	0.10	19.14	29.22	3.63	0.05	0.07	-0.01	0.00	0.01	0.00	0.31	98.20
NP22(2)	33.64	0.46	6.80	5.50	0.09	17.44	27.29	3.92	0.05	0.07	-0.02	0.00	0.01	0.00	0.30	95.55
NP25(1)	56.29	0.69	10.99	2.27	0.07	8.59	14.27	6.39	0.10	0.20	-0.01	0.00	0.01	0.00	0.17	100.02
NP25(2)	56.64	0.65	10.96	2.27	0.07	8.64	14.45	6.44	0.10	0.20	-0.01	0.00	0.01	0.00	0.17	100.60
NP35	53.79	0.71	13.14	4.88	0.06	10.00	9.43	5.62	1.86	0.14	-0.02	0.01	0.01	0.00	0.13	99.76
NP35(2)	53.95	0.73	13.34	4.94	0.07	9.98	9.08	5.67	1.92	0.14	-0.02	0.01	0.01	0.00	0.13	99.95
NP41	72.56	0.82	13.48	0.53	0.01	1.97	3.46	8.04	0.05	0.18	-0.04	0.00	0.01	0.00	0.05	101.14
NP41(2)	73.47	0.86	13.71	0.56	0.01	2.01	3.42	7.97	0.06	0.19	-0.03	0.00	0.01	0.00	0.05	102.28
NP42	82.54	0.50	9.83	0.75	0.02	0.62	1.26	5.61	0.14	0.17	-0.02	0.00	0.01	0.01	0.02	101.44
NP45	85.04	0.13	8.89	0.96	0.01	0.27	0.09	2.15	3.67	0.04	-0.03	0.00	0.00	0.00	0.00	101.23
NP45(2)	86.39	0.13	8.97	0.93	0.01	0.25	0.10	2.16	3.72	0.04	-0.03	0.00	0.00	0.00	0.00	102.68
NP56	92.39	0.10	5.13	1.16	0.01	0.13	0.17	-0.06	2.66	0.11	-0.01	0.00	0.00	0.00	0.01	101.81
NP57	66.82	0.52	13.26	7.84	0.02	4.14	0.28	4.38	3.05	0.14	-0.01	0.00	0.01	0.00	0.02	100.46
NP58	36.29	0.26	5.87	2.55	0.49	3.70	45.00	3.04	0.11	0.24	0.00	0.00	0.01	0.00	0.28	97.86
NP26	59.07	0.65	11.67	1.84	0.04	7.51	12.41	6.79	0.06	0.20	-0.02	0.00	0.00	0.00	0.15	100.38
NP69	58.54	0.71	11.43	3.07	0.08	5.58	14.36	6.43	0.12	0.19	0.01	0.00	0.01	0.00	0.15	100.68
NP71	61.00	0.79	14.47	2.01	0.04	5.69	8.80	8.39	0.09	0.19	-0.01	0.00	0.01	0.00	0.11	101.58
NP75	54.51	0.27	6.11	1.74	0.37	0.85	32.57	2.76	0.27	0.08	0.06	0.00	0.00	0.00	0.21	99.80
NP82	91.94	0.22	4.77	1.72	0.01	0.21	0.13	0.57	1.96	0.04	-0.01	0.00	0.00	0.00	0.01	101.58
NP116	92.47	0.29	5.43	2.06	0.01	0.39	0.02	-0.12	2.28	0.02	-0.01	0.00	0.00	0.00	0.01	102.86
NP118	16.67	0.11	2.96	3.36	0.38	1.05	68.50	1.28	0.02	0.09	0.35	0.004	0.00	0.00	0.37	95.14
NP119	91.86	0.21	6.43	1.85	0.01	0.27	0.07	0.82	1.03	0.10	-0.01	0.00	0.00	0.00	0.01	102.65
NP123	62.09	0.56	8.80	3.19	0.13	1.32	20.58	2.32	1.27	0.16	0.01	0.00	0.01	0.00	0.15	100.57
NP125	63.91	0.56	11.38	4.13	0.08	3.50	11.37	2.33	2.99	0.17	0.00	0.01	0.01	0.00	0.09	100.51
NP127	41.98	0.37	6.53	2.86	0.16	6.27	37.62	1.98	0.75	0.15	-0.01	0.00	0.01	0.00	0.26	98.93
NP132	86.42	0.55	7.28	3.74	0.02	0.58	0.27	-0.08	3.47	0.21	-0.02	0.00	0.00	0.00	0.01	102.47
NP133	14.00	0.09	2.62	6.13	0.61	23.40	41.66	1.26	0.04	0.10	0.34	0.00	0.00	0.00	0.39	90.64
NP103	37.92	0.34	8.38	5.27	0.30	1.45	39.29	3.85	0.37	0.23	0.03	0.00	0.00	0.00	0.25	97.66
NP088	85.24	0.24	7.81	1.75	0.03	0.08	0.13	1.09	4.30	0.07	-0.01	0.00	0.00	0.00	0.00	100.73
NP115	92.07	0.24	4.97	1.81	0.01	0.21	0.06	-0.05	1.93	0.01	-0.01	0.00	0.00	0.00	0.01	101.26
NP100	56.42	0.72	12.79	3.06	0.11	6.91	11.49	7.60	0.09	0.20	0.00	0.00	0.01	0.00	0.14	99.53
NP101	62.85	0.56	11.94	1.40	0.03	6.03	9.58	6.86	0.07	0.15	-0.02	0.00	0.01	0.00	0.12	99.58

(AIII.3.2)ICP-MS Analyses (Whole Rock Chemistry)

Trace and REE Data (all values in ppm)

Duruchaus Formation

	NP 055	NP 056	NP 057	NP 058	NP 116	NP 115	NP 114	NP 118	NP 119	NP 127	NP 125	NP 123	NP 082	NP 096	NP 133
Li	3.39	5.43	65.46	0.65	14.80	11.63	7.74	0.28	17.87	11.80	51.47	19.11	4.79	6.03	0.23
Sc	1.55	1.45	10.88	4.79	3.09	2.61	2.16	2.52	4.88	5.82	8.74	6.53	2.56	4.04	7.75
V	22.72	12.76	101.63	31.67	22.23	17.67	20.74	12.53	37.65	28.54	66.69	41.86	24.93	30.34	8.68
Cr	31.45	24.71	59.61	31.01	29.05	25.37	32.02	9.09	27.62	29.56	55.51	44.04	27.30	35.97	8.74
Co	1.84	0.96	34.60	4.17	2.21	1.59	1.55	4.55	3.37	5.18	11.17	6.51	1.88	3.94	15.28
Ni	8.75	9.02	36.50	14.72	10.24	9.68	9.88	12.08	13.74	15.40	26.82	15.84	10.12	13.66	15.76
Cu	6.83	6.10	100.81	33.49	12.19	7.86	7.61	5.22	13.27	2.92	4.54	23.61	6.48	59.80	7.69
Rb	13.12	50.23	122.78	2.18	54.00	38.88	39.13	0.21	36.89	24.88	114.70	46.10	42.83	3.08	0.27
Sr	19.14	22.31	227.21	204.51	31.20	14.29	24.31	285.85	25.38		255.90	689.84	31.81	76.12	489.98
Y	11.04	7.76	27.05	40.81	13.23	11.69	12.01	52.37	14.66	24.31	31.68	39.36	11.96	9.82	31.64
Zr	43.96	41.54	111.13	65.52	113.52	65.00	66.43	27.77	85.63	62.85	119.59	123.64	76.91	57.00	31.43
Nb	5.34	2.49	11.25	9.57	5.85	4.40	3.31	2.19	3.72	6.09	13.12	12.46	4.81	18.45	3.61
Cs	0.55	0.85	7.03	0.05	2.71	1.13	0.95	0.01	2.19	1.50	5.70	2.02	1.18	0.23	0.01
Ba	395.08	495.76	295.60	102.00	522.10	320.60	451.85	8.74	283.28	123.91	544.83	244.53	414.11	62.68	2617.20
La	10.35	10.66	52.29	18.65	14.75	13.17	10.86	23.31	13.49	15.14	29.04	27.48	17.24	9.85	16.65
Ce	25.77	18.78	104.37	38.60	28.92	27.07	16.55	27.22	25.37	33.06	61.15	58.89	34.58	27.91	33.98
Pr	3.00	2.42	11.73	4.57	3.81	3.89	2.97	5.07	3.47	3.93	7.27	7.09	4.68	3.03	4.30
Nd	12.18	9.00	44.95	18.06	15.10	15.44	12.06	23.40	14.00	15.95	28.45	28.67	18.21	13.00	19.97
Sm	2.39	1.56	7.99	3.96	2.87	3.02	2.49	5.99	3.05	3.56	5.50	6.24	3.40	2.91	5.73
Eu	0.47	0.34	1.26	1.00	0.59	0.63	0.58	1.41	0.65	0.89	0.94	1.33	0.64	0.56	1.45
Gd	2.12	1.35	5.93	4.67	2.36	2.53	2.22	8.77	2.86	3.76	4.58	6.75	2.56	2.56	6.81
Tb	0.34	0.21	0.83	0.85	0.36	0.38	0.35	1.28	0.47	0.60	0.73	1.07	0.38	0.39	1.02
Dy	2.11	1.34	4.73	5.73	2.30	2.29	2.24	7.71	2.97	3.80	4.76	6.60	2.24	2.33	5.95
Ho	0.42	0.27	0.91	1.16	0.47	0.43	0.44	1.41	0.56	0.77	1.01	1.26	0.43	0.43	1.09
Er	1.29	0.81	2.70	3.45	1.43	1.27	1.33	3.57	1.60	2.30	3.21	3.63	1.27	1.24	3.07
Tm	0.19	0.12	0.38	0.48	0.21	0.18	0.20	0.41	0.23	0.33	0.47	0.50	0.19	0.18	0.43
Yb	1.33	0.84	2.53	3.15	1.49	1.30	1.36	2.42	1.49	2.21	3.26	3.32	1.27	1.19	2.92
Lu	0.20	0.12	0.37	0.43	0.23	0.19	0.20	0.34	0.22	0.32	0.48	0.48	0.19	0.17	0.45
Hf	3.06	1.27	3.26	1.52	3.36	2.14	2.15	0.66	2.31	1.74	3.31	3.32	2.29	1.74	0.69
Ta	0.31	0.21	0.99	0.32	0.40	0.32	0.29	0.15	0.29	0.35	0.87	0.59	0.42	0.78	0.18
Pb	6.33	17.21	13.18	87.97	13.08	7.15	10.86	31.44	17.09	24.71	16.69	16.85	5.12	9.92	291.22
Th	6.12	3.16	12.83	4.04	4.58	4.64	3.70	7.49	5.84	4.91	9.79	8.15	5.39	3.95	8.79
U	0.62	0.42	5.68	1.17	0.68	0.60	0.55	3.25	0.58	8.42	1.62	3.60	0.73	0.84	1.52

Duruchaus Formation

	NP132	NP 103	NP 088	NP 025	NP 026	NP 069	NP 035	NP 041	NP 042	NP 075	NP 045
Li	12.48	1.82	6.95	0.71	0.65	0.64	11.37	0.73	1.40	0.82	1.61
Sc	4.95	7.40	3.07	3.21	10.98	9.76	16.52	5.94	3.62	12.74	1.48
V	55.30	17.33	25.98	22.69	21.09	68.82	100.38	42.22	32.01	44.65	21.95
Cr	43.67	27.92	31.41	21.19	43.79	60.09	72.61	68.65	39.42	53.81	16.57
Co	8.30	5.98	3.48	8.78	4.62	13.42	12.67	1.16	1.87	5.51	4.65
Ni	13.94	19.06	11.27	9.85	18.97	18.48	39.53	6.76	8.05	17.50	6.62
Cu	24.68	4.81	16.81	2.31	4.21	5.44	3.91	4.59	3.76	3.80	19.07
Rb	98.61	5.61	75.95	4.57	1.87	2.50	103.34	0.85	1.77	3.88	69.32
Sr	11.00	182.25	95.42	292.19	66.52	75.10	71.01	27.02	10.39	82.40	51.01
Y	24.13	39.29	19.61	27.72	31.53	32.93	24.47	21.30	14.55	28.25	6.21
Zr	168.60	55.58	80.03	63.88	67.99	71.81	131.79	167.28	134.62	159.51	50.69
Nb	10.92	5.29	5.08	4.15	12.08	8.78	19.45	14.15	9.03	12.00	3.71
Cs	0.87	0.10	0.65	0.07	0.09	0.08	4.75	0.02	0.04	0.12	0.52
Ba	518.37	270.35	1324.81	68.16	13.73	15.74	28.68	8.29	14.28	11.27	821.09
La	25.06	16.42	19.35	17.92	6.20	8.52	23.20	8.56	33.41	5.55	10.82
Ce	50.75	36.43	33.20	50.86	18.33	19.05	49.72	21.15	76.71	15.36	24.21
Pr	6.76	4.07	4.72	4.59	2.61	2.41	5.82	2.66	8.89	2.14	3.07
Nd	27.36	16.23	19.30	18.89	12.88	11.67	23.16	11.26	33.44	10.61	12.24
Sm	5.76	3.45	3.96	4.36	3.78	3.50	4.89	2.76	5.63	3.12	2.45
Eu	1.14	0.78	0.94	1.36	0.78	0.64	1.03	0.51	0.79	0.58	0.55
Gd	5.04	3.96	3.58	4.55	4.51	4.13	4.73	3.00	4.08	3.74	1.71
Tb	0.76	0.72	0.53	0.78	0.77	0.73	0.73	0.53	0.56	0.64	0.24
Dy	4.48	5.30	3.23	5.05	5.03	4.95	4.26	3.58	3.05	4.32	1.39
Ho	0.85	1.19	0.65	1.00	1.02	1.05	0.80	0.75	0.57	0.93	0.27
Er	2.48	3.89	1.98	2.89	3.04	3.39	2.24	2.32	1.59	2.94	0.83
Tm	0.35	0.58	0.28	0.38	0.41	0.52	0.31	0.33	0.21	0.44	0.12
Yb	2.40	4.07	1.93	2.29	2.72	3.79	2.16	2.27	1.49	3.05	0.87
Lu	0.36	0.59	0.29	0.29	0.38	0.56	0.33	0.34	0.23	0.46	0.13
Hf	4.96	1.56	2.36	1.53	2.76	3.59	3.55	6.19	3.96	4.08	1.41
Ta	0.76	0.33	0.40	0.31	0.91	0.75	1.36	1.08	0.63	0.87	0.36
Pb	3.05	21.94	12.42	0.61	0.26	1.11	0.49	0.51	0.73	0.49	6.98
Th	9.01	4.69	5.04	5.88	3.73	3.76	9.26	6.35	10.37	4.78	3.03
U	2.72	3.84	0.83	1.94	1.44	2.35	2.28	1.24	1.56	2.32	0.77

	Duruchaus Formation *Breccias*			*Dolomite Xenolith*	*Swakop - Alteration Vein*	
	NP 022	**NP071**	**NP 101**	**NP 100**	**NP 010**	**NP 011**
Li	1.30	0.27	0.48	0.32	5.77	0.34
Sc	38.53	8.19	13.19	11.18	9.95	6.62
V	85.54	30.36	30.51	92.50	72.56	34.61
Cr	44.82	49.16	62.29	55.13	56.47	35.87
Co	6.16	5.15	3.20	6.02	2.65	8.59
Ni	17.46	20.74	11.39	22.79	17.12	11.79
Cu	2.55	6.07	4.33	5.75	10.52	5.56
Rb	1.49	0.73	1.20	1.51	123.09	3.82
Sr	136.47	76.89	66.51	53.60	34.93	73.87
Y	77.03	21.85	31.73	23.64	20.54	22.83
Zr	75.25	115.82	139.04	114.69	173.56	118.16
Nb	9.75	15.19	13.74	13.43	13.13	11.97
Cs	0.21	0.03	0.04	0.06	3.08	0.03
Ba	2.74	6.20	4.47	11.99	402.82	11.32
La	32.54	11.34	10.07	10.25	36.80	53.51
Ce	71.95	28.26	24.97	26.34	79.64	116.68
Pr	9.14	3.47	3.20	3.33	9.20	13.86
Nd	38.22	14.91	14.06	14.72	36.16	52.82
Sm	9.12	3.45	3.44	3.59	6.75	9.18
Eu	2.00	0.68	0.62	0.69	0.97	1.40
Gd	10.11	3.49	3.76	3.91	5.05	6.82
Tb	1.81	0.60	0.68	0.64	0.69	0.89
Dy	12.35	3.94	4.77	4.01	3.84	4.55
Ho	2.69	0.81	1.03	0.78	0.71	0.79
Er	8.80	2.46	3.31	2.20	2.06	2.17
Tm	1.33	0.35	0.49	0.30	0.29	0.29
Yb	9.53	2.46	3.48	1.97	2.04	1.94
Lu	1.41	0.36	0.52	0.30	0.30	0.28
Hf	2.09	3.31	3.86	3.72	4.68	3.29
Ta	0.86	1.09	0.84	0.98	1.02	0.83
Pb	0.59	0.64	0.50	0.96	0.98	1.72
Th	9.23	7.07	4.24	5.11	12.91	18.95
U	0.94	1.59	1.42	2.58	2.37	1.91

	Xenoliths in NZ								Nosib Group (NZ)		
	Omburu East			Moselle					Karachas		
	HFD87	HFD91	HFD92	NPD 001	NPD 004	NPD 005	NPD 009	NPD 13.2	NPD 17	NPD 20	NPD 22
Li											
Sc	5.63	14.3	17.6	4.58	5.89	9.30	16.3	9.78	2.83	3.27	1.57
V	57	36.3	37.6	23.1	49.4	49.8	206	56.4	9.05	7.46	5.06
Cr	33.2	29	28.8	12.3	30.8	36.8	19.2	36.9	9.06	8.21	7.73
Co	1.57	19.8	13.8	10.4	5.33	7.99	3.22	7.70	1.44	0.99	1.47
Ni	10.9	40.6	35.3	20.4	11.1	22.1	12.4	23.0	8.68	5.72	5.36
Cu	6.35	3.65	3.53	5.85	6.05	6.28	18.3	5.56	5.35	3.39	3.92
Rb	2.69	0.57	0.98	11.6	1.64	16.3	7.76	14.9	92.1	90.8	97.7
Sr	60.2	113	114	162	62.7	55.3	96.6	58.4	42.8	32.8	60.2
Y	13.6	23.7	24.7	9.02	15.0	22.3	27.1	23.8	6.73	6.38	5.24
Zr	220	98.5	126	33.8	193	202	152	219	37.9	54.4	33.1
Nb	13.4	18.7	14.7	3.26	14.1	13.0	34.2	12.7	2.87	3.30	1.73
Cs	0.16	0.051	0.054	1.01	0.072	0.88	0.27	0.82	0.53	0.45	0.49
Ba	12.4	11	11.5	88.8	21.7	56.1	70.3	52.0	557	497	851
La	38.4	9.38	15.5	8.93	10.0	30.1	11.4	29.2	14.8	16.6	16.7
Ce	80.3	29.4	36.5	13.3	23.1	64.5	26.4	65.4	30.1	33.0	32.7
Pr	9.36	4.78	4.9	2.11	2.74	7.52	3.60	7.44	3.94	4.43	4.55
Nd	35.4	24.7	21.4	8.95	11.3	28.7	16.1	28.3	14.7	16.7	17.3
Sm	6.31	7.32	5.18	1.86	2.67	5.63	4.28	5.68	2.57	3.08	3.00
Eu	0.75	1.39	1.1	0.40	0.50	0.97	1.39	0.98	0.48	0.56	0.55
Gd	4.34	6.92	4.81	1.79	2.77	4.80	4.86	4.99	1.67	1.99	1.79
Tb	0.57	1	0.76	0.26	0.45	0.73	0.82	0.77	0.23	0.26	0.24
Dy	2.82	5.11	4.45	1.48	2.64	4.09	4.93	4.47	1.27	1.36	1.16
Ho	0.51	0.83	0.87	0.29	0.52	0.81	0.99	0.89	0.25	0.25	0.21
Er	1.41	1.9	2.35	0.79	1.51	2.31	2.77	2.56	0.70	0.67	0.54
Tm	0.2	0.23	0.31	0.11	0.22	0.34	0.39	0.37	0.10	0.10	0.077
Yb	1.43	1.32	1.97	0.74	1.56	2.31	2.55	2.57	0.71	0.66	0.52
Lu	0.22	0.19	0.29	0.12	0.24	0.36	0.38	0.39	0.11	0.10	0.076
Hf	6.03	2.43	3.19	0.88	5.15	5.35	3.73	6.03	1.13	1.58	0.97
Ta	1.07	0.94	0.87	0.25	0.94	0.94	1.87	0.92	0.21	0.24	0.13
Pb	1.86	0.99	0.85	1.67	1.23	1.48	0.63	1.34	5.76	6.00	5.55
Th	12.1	7.77	8.4	3.12	9.67	12.6	2.73	11.6	4.85	6.06	4.18
U	2.6	2.36	2.47	1.04	2.98	3.44	2.02	3.11	0.62	0.68	0.46

(AIII.4)Electron Microprobe Anayises of Tourmaline Grains

Iron has been recalculated into FeO and Fe_2O_3; B_2O_3 has been iteratively estimated; C=Core, R=Rim

NP059

Oxide	NP59T5(C)	NP59T5(R)	NP59T6(C)	NP59T6(R)	NP59T7(C)	NP59T7(R)	NP59T8(C)	NP59T8(R)	NP59T9(C)	NP59T9(R)	NP59T10(C)	NP59T10(R)	NP59T11(C)	NP59T11(R)
SiO2	34.78	35.56	35.81	36.05	35.65	36.55	34.42	34.82	36.42	36.04	36.18	36.05	35.79	36.12
Al2O3	32.14	31.37	31.62	31.64	31.42	31.10	31.01	31.75	30.21	30.97	32.97	32.20	32.39	31.24
TiO2	0.65	0.39	0.45	0.60	0.54	0.64	0.58	0.61	0.69	0.48	0.26	0.37	0.28	0.52
FeO	8.37	7.05	6.84	8.09	6.65	8.23	6.56	7.91	6.19	7.33	6.86	7.17	7.00	8.62
Fe2O3	0.00	0.51	0.82	0.84	1.37	0.79	1.82	0.51	2.78	1.12	0.00	0.00	0.00	0.42
MnO	0.00	0.01	0.05	0.03	0.05	0.01	0.04	0.02	0.05	0.07	0.03	0.05	0.00	0.07
MgO	7.45	8.33	8.45	7.71	8.43	7.44	8.39	7.72	8.31	8.03	7.98	7.95	8.47	7.21
CaO	0.06	0.24	0.23	0.04	0.31	0.04	0.47	0.05	0.74	0.22	0.02	0.05	0.19	0.03
Na2O	2.77	2.61	2.80	2.86	2.84	2.77	2.66	2.87	2.57	2.66	2.52	2.62	2.64	2.84
K2O	0.05	0.04	0.04	0.04	0.04	0.03	0.02	0.05	0.04	0.05	0.02	0.03	0.03	0.04
B2O3	10.52	10.56	10.67	10.72	10.67	10.69	10.47	10.52	10.73	10.63	10.73	10.65	10.68	10.61
Total	96.78	96.67	97.77	98.64	97.98	98.29	96.43	96.84	98.72	97.60	97.56	97.15	97.47	97.73

Oxide	NP59T12(C)	NP59T12(R)	NP59T13(C)	NP59T13(R)	NP59T14(C)	NP59T14(R)	NP59T15(C)	NP59T15(R)	NP059T19(C)
SiO2	35.90	35.76	35.72	35.67	35.00	35.55	35.49	35.15	36.76
Al2O3	30.13	30.08	31.84	31.64	29.73	30.17	29.77	30.82	29.64
TiO2	0.58	0.54	0.45	0.30	0.69	0.55	0.46	0.57	0.31
FeO	6.02	8.10	7.75	8.69	8.50	8.79	6.46	7.43	5.31
Fe2O3	2.31	1.65	0.09	0.00	1.91	0.96	2.08	0.42	1.89
MnO	0.00	0.02	0.04	0.05	0.04	0.03	0.06	0.01	0.03
MgO	8.53	7.25	7.97	7.21	6.86	6.89	8.20	7.66	8.39
CaO	0.51	0.21	0.07	0.09	0.10	0.06	0.35	0.06	0.03
Na2O	2.57	2.80	2.78	2.52	2.77	2.65	2.66	2.80	2.99
K2O	0.04	0.05	0.03	0.04	0.04	0.04	0.03	0.04	0.03
B2O3	10.59	10.49	10.62	10.53	10.35	10.40	10.44	10.40	10.53
Total	97.17	96.95	97.35	96.75	95.99	96.08	96.00	95.37	95.89

NP035

Oxide	NP035T1(C)	NP035T2(C)	NP035T2(R)	NP035T3(C)	NP035T4(C)	NP035T4(R)	NP035T5	NP035T6	NP035T8	NP035T9	NP035T10	NP035T11
SiO2	37.62	36.91	37.46	36.89	36.02	35.68	35.90	35.76	35.14	36.06	35.10	35.59
Al2O3	30.36	29.43	30.50	27.77	31.42	30.66	31.60	29.23	29.46	30.57	30.18	30.38
TiO2	0.32	0.61	0.25	0.71	0.16	0.27	0.15	0.34	0.28	0.23	0.72	0.30
FeO	4.78	4.28	4.96	3.72	5.03	4.67	4.74	3.74	3.94	4.57	4.19	4.42
Fe2O3	2.34	3.30	1.73	5.47	0.76	1.84	0.71	3.48	2.48	1.68	3.73	2.37
MnO	0.00	0.02	0.00	0.00	0.02	0.00	0.01	0.04	0.00	0.00	0.01	0.02
MgO	9.69	9.84	9.25	9.47	9.80	9.72	9.99	10.00	9.68	9.51	9.76	9.63
CaO	0.76	0.69	0.56	0.55	0.39	0.63	0.38	0.70	0.73	0.58	0.85	0.62
Na2O	2.06	1.82	2.44	2.60	2.39	2.39	2.49	2.31	2.44	2.81	2.26	2.74
K2O	0.03	0.03	0.02	0.02	0.02	0.02	0.03	0.02	0.02	0.03	0.05	0.02
B2O3	10.88	10.72	10.79	10.66	10.68	10.60	10.68	10.54	10.38	10.62	10.63	10.59
Total	98.84	97.64	97.95	97.86	96.70	96.49	96.69	96.15	94.54	96.66	97.47	96.69

Oxide	NP035T12	NP035T13	NP035T14	NP035T14(R)	NP035T15
SiO2	35.87	35.88	35.69	36.02	36.07
Al2O3	30.64	31.65	30.84	30.96	30.27
TiO2	0.30	0.20	0.22	0.20	0.23
FeO	4.69	5.30	4.86	4.54	4.90
Fe2O3	2.66	1.22	1.97	1.54	1.87
MnO	0.00	0.01	0.01	0.02	0.00
MgO	9.88	9.66	9.57	9.77	9.54
CaO	0.85	0.59	0.60	0.53	0.64
Na2O	2.19	2.50	2.74	2.71	2.30
K2O	0.01	0.03	0.03	0.02	0.02
B2O3	10.71	10.73	10.64	10.67	10.59
Total	97.79	97.77	97.17	96.98	96.45

NP021

Oxide	NP021T3(C)	NP021T18(C	NP021T1(C)	NP021T1(R)	NP021T2(C)	NP021T2(R)	NP021T3(C)	NP021T3(R)	NP021T4(C)	NP021T4(R)	NP021T5(C)	NP021T5(R)	NP021T6(C)	NP021T6(R)
SiO2	36.42	35.24	35.08	35.07	35.96	35.98	35.48	35.15	36.47	35.10	35.76	36.03	36.18	35.78
Al2O3	31.16	28.88	28.24	28.61	30.98	31.02	30.09	31.19	31.95	29.57	31.50	31.05	28.72	31.05
TiO2	0.11	0.65	0.43	0.45	0.30	0.48	0.26	0.29	0.24	0.45	0.14	0.35	0.67	0.31
FeO	7.31	9.35	6.81	7.58	7.85	8.98	8.22	9.72	8.51	7.50	8.17	8.85	7.58	9.49
Fe2O3	1.52	2.41	2.70	2.51	0.77	0.91	0.67	0.87	0.02	2.17	0.45	1.05	3.14	0.01
MnO	0.01	0.04	0.02	0.01	0.02	0.01	0.03	0.01	0.03	0.01	0.01	0.02	0.00	0.06
MgO	8.57	5.83	7.44	7.08	7.80	6.87	7.29	6.72	7.73	7.61	7.99	7.10	7.12	6.69
CaO	0.40	0.80	0.93	0.80	0.81	0.83	0.82	0.87	0.71	0.92	0.62	0.82	1.10	0.90
Na2O	2.62	2.55	2.18	2.37	2.12	2.34	1.94	2.26	2.17	2.00	2.19	2.38	2.04	1.96
K2O	0.02	0.04	0.04	0.03	0.01	0.03	0.05	0.04	0.03	0.03	0.04	0.04	0.03	0.03
B2O3	10.76	10.30	10.20	10.23	10.58	10.61	10.35	10.51	10.74	10.36	10.61	10.63	10.48	10.49
Total	98.89	96.10	94.06	94.75	97.19	98.06	95.20	97.62	98.60	95.71	97.48	98.33	97.06	96.77

Oxide	NP021T7(C)	NP021T7(R)	NP021T8(C)	NP021T8(R)	NP021T9(C)	NP021T9(R)	NP021T10(C	NP021T10	NP021T11	NP021T11(R)	NP021T12	NP021T12
SiO2	36.71	36.62	37.11	36.54	36.77	36.27	36.85	36.48	36.61	36.87	36.81	37.30
Al2O3	28.84	29.20	29.85	30.04	30.32	29.81	30.90	29.51	28.40	31.34	31.64	31.11
TiO2	0.31	0.30	0.19	0.29	0.18	0.23	0.12	0.33	0.54	0.43	0.20	0.10
FeO	6.68	6.54	5.56	7.09	6.98	8.73	8.07	7.11	5.93	8.29	9.44	8.23
Fe2O3	2.89	2.65	2.05	1.68	1.20	1.69	0.14	1.96	4.14	0.66	0.03	0.71
MnO	0.00	0.00	0.03	0.01	0.01	0.02	0.02	0.03	0.02	0.00	0.04	0.00
MgO	7.32	7.92	8.66	8.04	8.18	7.04	7.44	7.50	8.07	7.47	7.09	7.87
CaO	0.92	0.78	0.45	0.78	0.60	0.85	0.48	0.87	1.22	0.72	0.73	0.67
Na2O	2.11	2.30	2.34	2.26	2.18	2.22	2.11	2.16	2.21	2.37	2.19	2.01
K2O	0.04	0.04	0.03	0.03	0.04	0.04	0.04	0.04	0.02	0.04	0.04	0.03
B2O3	10.47	10.54	10.63	10.60	10.61	10.52	10.58	10.50	10.59	10.76	10.74	10.78
Total	96.29	96.91	96.89	97.33	97.07	97.41	96.74	96.50	97.76	98.96	98.96	98.82

I hereby declare that the data and interpretations presented in this dissertation are my own.

Signed: ..... ***Date:*** 10/07/2000

N. Pillay